

**Role of Copper, Zinc-Superoxide Dismutase in *S*-Nitrosation and  
Denitrosation of Cysteine Residues**

Mengwei Ye

A Thesis

In

The Department

Of

Chemistry and Biochemistry

Presented in Partial Fulfillment of the Requirements

for the Degree of Doctor of Philosophy at

Concordia University

Montreal, Quebec, Canada

October 2007

© Mengwei Ye, 2007



Library and  
Archives Canada

Bibliothèque et  
Archives Canada

Published Heritage  
Branch

Direction du  
Patrimoine de l'édition

395 Wellington Street  
Ottawa ON K1A 0N4  
Canada

395, rue Wellington  
Ottawa ON K1A 0N4  
Canada

*Your file    Votre référence*

*ISBN: 978-0-494-37725-3*

*Our file    Notre référence*

*ISBN: 978-0-494-37725-3*

#### NOTICE:

The author has granted a non-exclusive license allowing Library and Archives Canada to reproduce, publish, archive, preserve, conserve, communicate to the public by telecommunication or on the Internet, loan, distribute and sell theses worldwide, for commercial or non-commercial purposes, in microform, paper, electronic and/or any other formats.

The author retains copyright ownership and moral rights in this thesis. Neither the thesis nor substantial extracts from it may be printed or otherwise reproduced without the author's permission.

#### AVIS:

L'auteur a accordé une licence non exclusive permettant à la Bibliothèque et Archives Canada de reproduire, publier, archiver, sauvegarder, conserver, transmettre au public par télécommunication ou par l'Internet, prêter, distribuer et vendre des thèses partout dans le monde, à des fins commerciales ou autres, sur support microforme, papier, électronique et/ou autres formats.

L'auteur conserve la propriété du droit d'auteur et des droits moraux qui protègent cette thèse. Ni la thèse ni des extraits substantiels de celle-ci ne doivent être imprimés ou autrement reproduits sans son autorisation.

---

In compliance with the Canadian Privacy Act some supporting forms may have been removed from this thesis.

Conformément à la loi canadienne sur la protection de la vie privée, quelques formulaires secondaires ont été enlevés de cette thèse.

While these forms may be included in the document page count, their removal does not represent any loss of content from the thesis.

Bien que ces formulaires aient inclus dans la pagination, il n'y aura aucun contenu manquant.

  
**Canada**

## Abstract

### Role of Copper, Zinc-Superoxide Dismutase in *S*-Nitrosation and Denitrosation of Cysteine Residues

Mengwei Ye, Ph.D.

Concordia University, 2007

Selective inhibition of the *S*-nitroso-*L*-glutathione (GSNO) reductase activity but not the superoxide dismutase (SOD) activity of Cu,Zn-superoxide dismutase (CuZnSOD) by the commonly used polyaminocarboxylate metal-ion chelators, EDTA and DTPA, is systematically investigated here. The effects of EDTA and DTPA on the Cu<sup>II</sup> *d-d* absorption of Cu<sup>II</sup>ZnSOD at 680-nm, on the reduction of Cu<sup>II</sup>ZnSOD by GSH, on the metal-loading of the enzyme, on the chemical modification of catalytic Arg141, and on the SOD and GSNO-reductase activities were studied. Binding to the enzyme was probed by measuring heat changes with ITC on titration of CuZnSOD and the metal-free EESOD with the chelators. The results reveal that EDTA and DTPA bind to the solvent-exposed active-site copper of one subunit without removing the metal. This induces a conformational change at the second active site that inhibits the GSNO-reductase but not the SOD activity of the enzyme.

The effects of the copper colorimetric reagents, neocuproine (neo), diethyldithiocarbamate (DDC), and cuprizone (cup), on the GSNO-reductase and the SOD activities of CuZnSOD were also examined. These chelators alter the Cu<sup>II</sup> *d-d*

absorption of Cu<sup>II</sup>ZnSOD at 680 nm and give the absorption characteristic of their CuL<sub>2</sub> complexes. The GSNO-reductase activity of CuZnSOD was inhibited by the three colorimetric reagents in the order: DDC > neo > cup which mirrors the extent of CuL<sub>2</sub> formation. Incubation of CuZnSOD with 5 mM DDC also resulted in 90% loss of its SOD activity due to removal of ~73% of the active-site copper. No loss of SOD activity resulted from CuZnSOD exposure to neo or cup. These results indicate that removal of the active-site copper is necessary for loss of SOD activity whereas association of the chelators with the active-site copper is sufficient for loss of GSNO-reductase activity.

Chemical modification at pH 8.0 of Arg- and Cys-containing peptides and CuZnSOD by phenylglyoxal (PGO), an arginine specific reagent, was re-evaluated. ESI-MS analysis shows that doubly PGO-labelled Arg and Cys residues were formed in the peptides but only singly PGO-labelled Arg residues formed in CuZnSOD. Loss of SOD activity of PGO-modified CuZnSOD was observed due to derivatization of its Arg residues by PGO. Labelling of multiple Arg residues in the enzyme is in disagreement with previous reports that Arg141, which is essential for SOD activity, was selectively PGO-modified.

Two to four free Cys residues per tetramer of commercial rat hemoglobin (Hb) from Sigma and of Hb isolated from rat red blood cells (RBCs) were determined by 5,5'-dithiolbis(2-nitrobenzoic acid) (DTNB) titration and by ESI mass spectrometry using *N*-ethylmaleimide (NEM). Both Cysβ125 and Cysβ93 in rat RBC oxyHb were *S*-nitrosated and *S*-glutathiolated in GSNO/oxyHb (10:1) incubations with and without 20 μM bovine CuZnSOD indicating that this enzyme is not essential for *S*-nitrosation of rat Hb under the conditions used here. Based on the Saville assay, NO release from rat Hb-SNO in the



presence of GSH was catalyzed by free copper ions and by CuZnSOD. As observed for the GSNO-reductase activity of CuZnSOD, Hb-SNO denitrosation was inhibited by the metal chelators confirming a catalytic role for copper. Combining the results presented in thesis with those obtained from the literature helps us understand the role of CuZnSOD in the formation of Hb-SNO and the release of NO from Hb-SNO.

## **Acknowledgements**

First of all, I would like to deeply thank my research supervisor, Dr. Ann English, for giving me the opportunity to carry out research in such an interesting area, for her support and guidance, and for her encouragement and patience throughout the duration of my stay at Concordia University.

I would like to thank my committee members, Dr. Cameron Skinner and Dr. Justin Powlowski, for their time and expertise.

I would like to thank my colleagues who, during my years at Concordia University, gave me useful and helpful advice. Heng Jiang and Songping Zhao provided me with help in getting started in cell and molecular biology; Biao Shen gave me his invaluable help at the beginning and over the years; Pascal Turcotte was always willing to offer his kind assistance in the lab; Hasnain Jaffer's encouragement, Georgia Kremmydiotis' friendship, and help from Limei Tao, Andrea Romeo, David Yeung, and too many more to list here who supported me to get through the difficulties and finish my program.

Finally, I would like to thank my entire extended family for all their love, support, and many other contributions. Without their encouragement, my research would likely have remained incomplete and unfinished.

## **Dedications**

To my mother,

Jinping Zhang

For her love, support, and longterm belief in me;

To the memories of my father and my elder brother,

Jingzhe Ye and Beijia Ye

I will love you forever;

To my son,

Yifeng Yan

For giving me the greatest pleasure in life;

To my husband,

Xiaowang Yan

For his support throughout the years

## Table of Contents

List of Figures	xix
List of Tables	xxv
List of Abbreviations	xxvii
1.0 Introduction	1
1.1 Nitric oxide (NO) – An important signaling molecule	1
1.2 RSNOs – a NO reservoir <i>in vivo</i>	3
1.3 S-Nitrosoglutathione (GSNO) and the mechanism of NO release	5
1.4 Copper,zinc-superoxide dismutase (CuZnSOD)	7
1.4.1 Superoxide dismutase (SOD) activity of CuZnSOD	7
1.4.2 GSNO-reductase activity of CuZnSOD	8
1.4.3 Modulators of the SOD and GSNO-reductase activities of CuZnSOD	8
1.4.4 Comparison of human, bovine and rat CuZnSODs	11
1.5 Hemoglobin (Hb)	12
1.5.1 Reactions of NO with deoxy and oxyHb	13
1.5.2 The proposed action of Hb-SNO <i>in vivo</i>	14
1.5.3 Mechanism of Hb S-nitrosation	14
1.5.4 Reactivity of cysteine residues in rat vs human Hb	17
1.5.5 S-Nitrosation of rat vs human Hb	18

1.5.6	Hb-SNO denitrosation and possible regulators	19
1.6	Hypotheses, scope and organization of thesis	22
1.7	Contributions of colleagues	23
2.0	Binding of polyaminocarboxylate chelators to the active-site copper inhibits the GSNO-reductase activity but not the superoxide dismutase activity of Cu,Zn-superoxide dismutase	25
2.1	Abstract	25
2.2	Introduction	26
2.3	Materials and methods	28
2.3.1	Materials	28
2.3.2	Methods	29
2.3.2.1	Effects of chelators on CuZnSOD 680-nm absorption	29
2.3.2.2	CuZnSOD modification by PGO	29
2.3.2.3	Xanthine oxidase-cytc <sup>III</sup> assay for SOD activity	30
2.3.2.4	GSNO-reductase activity of CuZnSOD	31
2.3.2.5	ICP-MS determination of metal-ion content of CuZnSOD	31
2.3.2.6	Preparation of EESOD	32
2.3.2.7	ITC analysis of CuZnSOD-chelator and EESOD-chelator association	32

2.4	Results	33
2.4.1	Effects of chelators on CuZnSOD 680-nm absorption	33
2.4.2	Effects of chelators on metal-ion content of CuZnSOD	33
2.4.3	Effects of chelators on Cu <sup>II</sup> ZnSOD reduction	36
2.4.4	Effects of chelators and GSH on SOD activity	36
2.4.5	Effects of chelators on PGO-inactivation of SOD activity	37
2.4.6	Effects of chelators and GSH on the GSNO-reductase activity of CuZnSOD	38
2.4.7	Thermodynamic parameters for EDTA and DTPA association with CuZnSOD	40
2.5	Discussion	44
2.6	Conclusions	49
2.7	Acknowledgements	50
Appendix 1.0	Supplementary Experimental Data for Chapter 2.0	51
A1.1	UV-Vis absorption spectrum of EESOD	51
A1.2	UV-Vis absorption spectrum of EESOD/DDC incubation	51
A1.3	SOD activity of EESOD	53
A1.4	ESI-ToF mass spectrum of EESOD	53
3.0	Effects of copper colorimetric reagents on the GSNO- reductase and SOD activity of CuZnSOD	55

3.1	Abstract	55
3.2	Introduction	56
3.3	Materials and Methods	62
3.3.1	Materials	62
3.3.2	Methods	62
3.3.2.1	Visible spectra of CuZnSOD/chelator incubations	62
3.3.2.2	Pyrogallol autooxidation assay of SOD activity	63
3.3.2.3	GSNO-reductase activity of CuZnSOD	64
3.4	Results	65
3.4.1	CuL <sub>2</sub> absorption grows in spectra of the CuZnSOD/chelator incubations	65
3.4.2	Effects of preincubation with the chelators and GSH on SOD activity	67
3.4.3	Effects of the chelators on the GSNO-reductase activity of CuZnSOD	70
3.5	Discussion	70
3.6	Conclusions	78
4.0	Reevaluation based on mass spectrometric analysis of phenylglyoxal as an arginine-specific reagent: Characterization of phenylglyoxal-modified peptides and	80

## Cu,Zn-superoxide dismutase

4.1	Abstract	80
4.2	Introduction	81
4.3	Materials and methods	86
4.3.1	Materials	86
4.3.2	Methods	87
4.3.2.1	PGO modification reactions	87
4.3.2.2	NEM and Sulfo-NHS acetate modification reactions	88
4.3.2.3	Tryptic digestion of BCuZnSOD	88
4.3.2.4	ESI-MS and ESI-MS/MS analysis	89
4.3.2.5	MALDI-ToF-MS analysis	89
4.3.2.6	SOD activity assay	90
4.4	Results	90
4.4.1	Modification of MRF by PGO and sulfo-NHS acetate	90
4.4.2	Modification of porcine renin substrate (PRS) by PGO	94
4.4.3	Modification of ACTH by PGO and sulfo-NHS acetate	95
4.4.4	Modification of glutathione (GSH) by PGO	96
4.4.5	Modification of BCuZnSOD by PGO and NEM	100
4.4.6	Modification of BCuZnSOD by sulfo-NHS acetate	106
4.4.7	SOD activity of PGO-modified BCuZnSOD	110
4.5	Discussion	112
4.5.1	PGO modification of small peptides	112



4.5.2	PGO modification of BCuZnSOD	115
4.6	Conclusions	118
4.7	Acknowledgements	120
Appendix 2.0 Supplementary Experimental Data for Chapter 4.0		121
A2.1	Characterization of PGO dimer in solution by ESI-MS	121
A2.2	Characterization of the thermal- and pH-stabilities of the PGO derivatives in BCuZnSOD by ESI-MS	123
A2.3	Mass spectrometric analysis of the NEM labelling of the buried free cysteine residue in BCuZnSOD	128
A2.4	Supplementary mass spectra of PGO-modified peptides	128
5.0	Construction, expression and purification of human Cu,Zn-superoxide dismutase (hSOD1) in yeast and <i>E. coli</i> hosts	132
5.1	Introduction	132
5.2	Experimental procedures	133
5.2.1	Materials	133
5.2.2	Plasmids and strains	134
5.2.3	Transformation of YEp351 and pET-22b(+) plasmid DNA into the non-expression host	135
5.2.4	Sub-cloning the hSOD1 gene into the pET-22b(+) vector	135
5.2.5	Transformation of plasmids containing the hSOD1 gene	137

into the expression hosts	
5.2.5.1 Transformation of YEp351-hSOD1 wild type and R143E plasmids into <i>S. cerevisiae</i> strain BY4742	137
5.2.5.2 Transformation of pET-hSOD1 wild type plasmid into <i>E. coli</i> strain BL21(DE3)	139
5.2.6 Expression of recombinant hSOD1	139
5.2.6.1 Expression of recombinant hSOD1 (wild type) in yeast	139
5.2.6.2 Expression of recombinant hSOD1 (wild type) in <i>E. coli</i>	140
5.2.7 Purification of recombinant hSOD1 from yeast and <i>E. coli</i> hosts	143
5.2.7.1 Ammonium sulfate protein precipitation from Yeast	143
5.2.7.2 Gel-filtration chromatography	143
5.2.7.3 Anion-exchange chromatography	144
5.2.7.4 Heat precipitation of yeast proteins	144
5.2.8 Gel electrophoresis	144
5.2.8.1 Agarose gel electrophoresis	145
5.2.8.2 SDS-polyacrylamide gel electrophoresis (SDS-PAGE)	145
5.2.8.3 Western blot analysis of hSOD1	146

5.2.9	Determination of SOD activity	146
5.2.10	Spectrophotometric analysis	147
5.2.11	Mass spectrometry	147
5.3	Results	147
5.3.1	Overexpression and purification of hSOD1 (wild type) in yeast	147
5.3.1.1	Analysis of the YEp351-hSOD1 vector	147
5.3.1.2	Expression of hSOD1 in yeast	149
5.3.1.3	Purification of hSOD1 from yeast	151
5.3.1.4	Purification of hSOD1 from yeast after heat shock treatment	154
5.3.1.5	Yield of hSOD1 from yeast and specific activity of fractions	155
5.3.1.6	UV absorption spectrum of reconstituted hSOD1	156
5.3.1.7	ESI-mass spectrum of recombinant hSOD1 from yeast	157
5.3.2	Overexpression of hSOD1 in <i>E. coli</i>	158
5.3.2.1	Transfer of hSOD1 from YEp351-hSOD1 to pET-22b(+)	158
5.3.2.2	Expression of hSOD1 in BL21(DE3)	162
5.3.2.3	Optimization hSOD1 expression in <i>E. coli</i>	162
5.4	Discussion	165
5.5	Acknowledgements	169

Appendix 3.0	DNA sequences of human CuZnSOD (wild type, R143A, R143E, R143I and R143K) inserts in the YEp351 and pET-22b(+) plasmids	170
A3.1	YEp351-hSOD1(wild type)	170
A3.2	YEp351-hSOD1(R143E)	172
A3.3	YEp351-hSOD1(R143K)	173
A3.4	YEp351-hSOD1(R143A)	175
A3.5	YEp351-hSOD1(R143I)	177
A3.6	pET-hSOD1(wild type)	178
6.0	The role of CuZnSOD in <i>S</i> -nitrosation and denitrosation of cysteine residues in rat Hb	181
6.1	Abstract	181
6.2	Introduction	182
6.3	Materials and methods	184
6.3.1	Materials	185
6.3.2	Methods	185
6.3.2.1	oxyHb preparation from Sigma rat Hb	185
6.3.2.2	oxyHb preparation from rat RBCs	186
6.3.2.3	CuZnSOD-free Hb preparation	186
6.3.2.4	Hb-SNO Preparation	186
6.3.2.5	Hb-NEM preparation	187

6.3.2.6	Preparation of copper-free CuZnSOD (EZnSOD)	187
6.3.2.7	Extraction of CuZnSOD from rat RBCs	188
6.3.2.8	Spectrophotometric determination of free Cys residues using DTNB	189
6.3.2.9	Mass spectrometric determination of free Cys residues using NEM	190
6.3.2.10	Tryptic and Glu-C digestion of protein samples	191
6.3.2.11	ESI-ToF-MS analysis	191
6.3.2.12	MALDI-ToF-MS analysis	192
6.3.2.13	Determination of the <i>S</i> -nitrosothiol content of rat Hb (Sigma) by the Saville assay	192
6.4	Results	194
6.4.1	CuZnSOD in rat RBCs	194
6.4.2	Reactive Cys residues in rat Hb	198
6.4.3	<i>S</i> -Nitrosation and <i>S</i> -thiolation of Hb from rat RBCs	203
6.4.4	Identification of the sites of rat Hb <i>S</i> -nitrosation and <i>S</i> -thiolation by MALDI-ToF-MS	209
6.4.5	Determination of NO release from Sigma rat Hb-SNO	214
6.5	Discussion	215
6.5.1	Comparison of Cys reactivity in rat and human Hbs	215
6.5.2	<i>S</i> -Nitrosation of rat vs human Hbs	218
6.5.3	Role of CuZnSOD	219

6.5.4	<i>Trans</i> -S-nitrosation and S-thiolation of rat RBC Hb	220
6.5.5	Hb-SNO denitrosation	222
6.6	Conclusions	223
7.0	Conclusions and Suggestions for Future Work	225
7.1	Chapter 2 and 3	225
7.2	Chapter 4	227
7.3	Chapter 5	228
7.4	Chapter 6	229
7.5	Suggestions for Future Work	230
8.0	References	232

## List of Figures

<b>Figure 1.1</b>	Nitric oxide and cGMP signaling in smooth muscle cells	2
<b>Figure 1.2</b>	Structure of GSNO	5
<b>Figure 1.3</b>	GSSG acts as a Cu <sup>II</sup> chelator	6
<b>Figure 1.4</b>	(A) X-ray structure of the metal binding region, and (B) the copper active-site channel of one subunit of bovine CuZnSOD	9
<b>Figure 1.5</b>	X-ray structure of human oxyHb	12
<b>Figure 1.6</b>	NO in the human respiratory cycle	15
<b>Figure 2.1</b>	Cu <sup>II</sup> <i>d-d</i> absorption at 680 nm vs time in incubates of 200 μM CuZnSOD with EDTA, DTPA or GSSG	34
<b>Figure 2.2</b>	Cu <sup>II</sup> <i>d-d</i> absorption at 680 nm vs time of CuZnSOD/GSH incubates with and without EDTA or DTPA	34
<b>Figure 2.3</b>	Effects of preincubation with chelators, GSSG or GSH on SOD activity of CuZnSOD	37
<b>Figure 2.4</b>	Effects of preincubation with PGO without or with EDTA or DTPA on SOD activity of CuZnSOD	38
<b>Figure 2.5</b>	Effects of EDTA and DTPA on the GSNO-reductase activity of CuZnSOD with GSH as a donor substrate	39
<b>Figure 2.6</b>	OxyMb assay of effects of metal chelators on NO release from GSNO	40
<b>Figure 2.7</b>	ITC analysis of EDTA and DTPA binding to CuZnSOD	41
<b>Figure 2.8</b>	ITC analysis of EDTA and DTPA binding to EESOD	42
<b>Figure 2.9</b>	Docking of EDTA into the active-site channel of bovine	44

## CuZnSOD

<b>Figure A1.1</b>	Absorption spectrum of BCuZnSOD in metal-free (A) and native (B) forms	52
<b>Figure A1.2</b>	Absorption spectrum vs time of the EESOD/DDC incubation	52
<b>Figure A1.3</b>	ESI mass spectrometric analysis of EESOD	54
<b>Figure 3.1</b>	Visible absorption spectrum of $\text{Cu}^{\text{II}}(\text{DDC})_2$ and calibration curve for the colorimetric determination of copper	57
<b>Figure 3.2</b>	Visible absorption spectrum of $\text{Cu}^{\text{I}}(\text{neo})_2$ at RT	59
<b>Figure 3.3</b>	Visible absorption spectrum of $\text{Cu}^{\text{II}}(\text{cup})_2$ and calibration curve for the colorimetric determination of copper	60
<b>Figure 3.4</b>	$\text{Cu}^{\text{II}}(\text{DDC})_2$ absorption vs time of the CuZnSOD/DDC incubation	65
<b>Figure 3.5</b>	$\text{Cu}^{\text{II}}(\text{cup})_2$ absorption vs time of the CuZnSOD/cup incubation	66
<b>Figure 3.6</b>	$[\text{Cu}^{\text{I}}(\text{neo})_2]^+$ absorption vs time of CuZnSOD/GSH/neo incubation	67
<b>Figure 3.7</b>	Inhibition calibration curve for the pyrogallol autooxidation assay for SOD activity	68
<b>Figure 3.8</b>	Effects of preincubation with the chelators $\pm$ GSH on the SOD activity of CuZnSOD	69
<b>Figure 3.9</b>	Metal binding site of the CuZnSOD monomer	71
<b>Figure 4.1</b>	ESI and MALDI mass spectra of PGO-modified MRF peptide	92
<b>Figure 4.2</b>	ESI MS/MS analysis of doubly PGO-labeled MRF peptide	93
<b>Figure 4.3</b>	Acetylation of untreated and PGO-labeled MRF	94
<b>Figure 4.4</b>	Mass spectrometric analysis of PGO-modified porcine renin substrate (PRS)	98



<b>Figure 4.5</b>	Mass spectrometric analysis of PGO-modified ACTH	99
<b>Figure 4.6</b>	Acetylation of untreated and PGO-labeled ACTH	100
<b>Figure 4.7</b>	Mass spectrometric analysis of PGO-modified GSH	103
<b>Figure 4.8</b>	PGO-concentration-dependence of BCuZnSOD modification	106
<b>Figure 4.9</b>	Time-dependence of BCuZnSOD modification by 40-fold excess PGO	107
<b>Figure 4.10</b>	Thiol alkylation of native and PGO-modified BCuZnSOD	108
<b>Figure 4.11</b>	Acetylation of native and PGO-modified BCuZnSOD	110
<b>Figure 4.12</b>	Effect of preincubation with PGO on the SOD activity of BCuZnSOD	111
<b>Figure A2.1</b>	Mass spectrometric analysis of PGO	123
<b>Figure A2.2</b>	Mass spectrometric analysis of stability of PGO-modified BCuZnSOD	124
<b>Figure A2.3</b>	Mass spectrometric analysis of thermostability of PGO-modified BCuZnSOD	126
<b>Figure A2.4</b>	Reactivity of Cys6 in BCuZnSOD with NEM	127
<b>Figure A2.5</b>	MALDI mass spectrometric analysis of PGO-modified PRS	129
<b>Figure A2.6</b>	MALDI mass spectrometric analysis of PGO-modified ACTH	130
<b>Figure A2.7</b>	ESI mass spectrometric analysis of PGO derivatives in an equimolar GSH and MRF incubation	130
<b>Figure 5.1</b>	Schematic description of plasmid YEp351-hSOD1	148
<b>Figure 5.2</b>	Restriction enzyme analysis of plasmid YEp351-hSOD1	149
<b>Figure 5.3</b>	(A) SDS-PAGE (15%) and (B) Western blot (10%) analysis of	150

## hSOD1 expression in *sodI*<sup>-</sup> BY4742 Cells

<b>Figure 5.4</b>	hSOD1 purification by gel filtration and anion-exchange Chromatography	151
<b>Figure 5.5</b>	SDS-PAGE (15%) analysis hSOD1 purification from yeast cells	152
<b>Figure 5.6</b>	SDS-PAGE (15%) analysis hSOD1 present in yeast cells after heat shock	153
<b>Figure 5.7</b>	SOD activity in the yeast-cells extracts	154
<b>Figure 5.8</b>	Comparison of UV absorbance spectra of reconstituted hSOD1 produced in yeast with apo- and reconstituted hSOD1 produced in <i>E. coli</i>	156
<b>Figure 5.9</b>	Absorbance spectra of reconstituted hSOD1 following DDC addition	157
<b>Figure 5.10</b>	ESI-mass spectrum of recombinant hSOD1 from yeast	158
<b>Figure 5.11</b>	Construction of pET-hSOD1 plasmid	159
<b>Figure 5.12</b>	Restriction digestion analysis of the YEp351-hSOD1 and pET-22b(+) plasmids	160
<b>Figure 5.13</b>	Restriction digestion analysis of the pET-hSOD1(wild type) vector	160 161
<b>Figure 5.14</b>	SDS-PAGE (15%) analysis of hSOD1 expression in BL21(DE3) cells	
<b>Figure 5.15</b>	SDS-PAGE (15%) analysis of hSOD1 localization BL21(DE3) cells	161
<b>Figure 5.16</b>	SDS-PAGE (15%) analysis of hSOD1 in the (A) cell-lysate	163

	supernatants and (B) growth medium under (C) different BL21(DE3) growth conditions	
<b>Figure 5.17</b>	(A) SDS-PAGE (12%) and (B) Western blot (12%) analysis of hSOD1 expression in BL21(DE3) cells	164
<b>Figure 6.1</b>	10% SDS-PAGE analysis of CuZnSOD extracted from rat RBCs	195
<b>Figure 6.2</b>	Deconvolved ESI mass spectra of rat, human, and bovine CuZnSOD	196
<b>Figure 6.3</b>	Inhibition calibration curve for the determination of CuZnSOD concentration	197
<b>Figure 6.4</b>	Plots of 412-nm and 450-nm absorbance vs <i>L</i> -cysteine concentration in the presence of DTNB	198
<b>Figure 6.5</b>	Plots of 450-nm absorption vs time in the DTNB titration of Cys residues in oxyHb from rat RBCs and its Hb-SNO derivative	199
<b>Figure 6.6</b>	Plot of 450-nm absorption vs time in the DTNB titration of Cys residues in native and denatured Sigma rat Hb	200
<b>Figure 6.7</b>	ESI-MS analysis of reactive Cys residues in RBC rat oxyHb.	201
<b>Figure 6.8</b>	ESI-MS analysis of reactive Cys residues in Sigma rat oxyHb	203
<b>Figure 6.9</b>	UV-Vis spectra of rat oxyHb	204
<b>Figure 6.10</b>	LC-ESI-MS analysis of the RBC rat oxyHb/GSNO incubation in (A) the absence and (B) the presence of BCuZnSOD	205
<b>Figure 6.11</b>	UV-Vis spectra of Sigma rat oxyHb and Hb-SNO derivative	206
<b>Figure 6.12</b>	ESI-MS analysis of GSNO and NEM-modified RBC rat oxyHb	207
<b>Figure 6.13</b>	Effects of GSH, chelators, CuSO <sub>4</sub> , and BCuZnSOD on NO	213

release from Sigma rat methHb-SNO

**Figure 6.14** Effects of EDTA, DTPA, and neocuproine on (A) BCuZnSOD- 214  
and (B) CuSO<sub>4</sub>-catalyzed NO release from Sigma rat methHb-  
SNO

## List of Tables

<b>Table 1.1</b>	Comparison of sequences of human, bovine, and rat erythrocyte CuZnSODs	10
<b>Table 1.2</b>	SOD activity and quantities in human, bovine, and rat erythrocytes	11
<b>Table 1.3</b>	Cysteine residues in rat Hb and human HbA	17
<b>Table 1.4</b>	Endogenous levels of Hb-SNO and Hb-NO	19
<b>Table 1.5</b>	Rate constants ( $M^{-1}s^{-1}$ ) for <i>S</i> -nitrosation and <i>S</i> -thiolation of rat Hb and human HbA	20
<b>Table 2.1</b>	Cu and Zn concentrations of CuZnSOD samples determined by ICP-MS	35
<b>Table 2.2</b>	SOD activity of CuZnSOD in the presence of EDTA and DTPA	35
<b>Table 2.3</b>	Thermodynamic parameters from the titration of CuZnSOD with EDTA and DTPA	43
<b>Table A1.1</b>	SOD activity of EESOD vs native BCuZnSOD	53
<b>Table 3.1</b>	Literature data on the CuZnSOD- and CuSO <sub>4</sub> -induced GSNO decomposition of GSNO in the presence of GSH, neo, and cup	61
<b>Table 3.2</b>	Effects of cup, DDC and neo on the GSNO-reductase activity of CuZnSOD with GSH as a donor substrate	70
<b>Table 3.3</b>	Millimolar absorptivity ( $\epsilon$ ) of copper-chelator complex	73
<b>Table 4.1</b>	Assignment of peaks in the derivatized MRF, PRS, and ACTH peptides	102
<b>Table 4.2</b>	Assignment of peaks in PGO-derivatized GSH	104
<b>Table 4.3</b>	Assignment of peaks in PGO- and/or NEM-derivatized	105

## BCuZnSOD

<b>Table 4.4</b>	Arg-containing tryptic peptides from PGO-modified BCuZnSOD	107
<b>Table 4.5</b>	Assignment of peaks in PGO- and/or sulfo-NHS acetate-derivatized BCuZnSOD	109
<b>Table A2.1</b>	Concentration of glyoxal monomer vs total glyoxal concentration in aqueous solution	122
<b>Table A2.2</b>	Assignment of PGO peaks in water	123
<b>Table A2.3</b>	Assignment of peaks in PGO- or NEM-derivatized BCuZnSOD	125
<b>Table A2.4</b>	Assignment of peaks in the MALDI mass spectra of PGO-derivatized PRS, ACTH, and the ESI mass spectra of the MRF/GSH mixture	129
<b>Table 5.1</b>	Purification of recombinant hSOD1 from yeast cells	155
<b>Table 5.2</b>	Literature values for enzyme activity and metal content of hSOD1 preparations	166
<b>Table 6.1</b>	Estimation of CuZnSOD concentration in rat RBCs	197
<b>Table 6.2</b>	Amino acid sequences of the major and minor isoforms of rat Hb	202
<b>Table 6.3</b>	S-Nitrosation of Sigma rat oxyHb as determined by Saville assay	206
<b>Table 6.4</b>	Tryptic peptides of the two isoforms of rat Hb	208
<b>Table 6.5</b>	Glu-C peptides of the two isoforms of rat Hb	209
<b>Table 6.6</b>	MALDI-MS analysis of Cys-containing tryptic peptides of rat Hb-NEM and (Hb-SNO)-NEM	211
<b>Table 6.7</b>	MALDI-MS analysis of the Cys-containing Glu-C peptides from rat oxyHb and its derivatives	212

## List of Abbreviations

ACN	acetonitrile
ACTH	Adrenocorticotrophic hormone fragment 18-39
$\alpha$ -CHCA	$\alpha$ -cyanohydroxycinnamic acid
AGEs	advanced glycation end-products
BCuZnSOD	bovine copper,zinc-superoxide dismutase
BSA	bovine serum albumin
CID	collision-induced dissociation
CNBr	cyanogen bromide
Cup	cuprizone; <i>bis</i> -cyclohexanone oxaldihydrazone
CuZnSOD	copper,zinc-superoxide dismutase
CysNO	<i>S</i> -niytrosocysteine
cyt <sup>c</sup> <sup>III</sup>	ferricytochrome <i>c</i>
DDC	diethyldithiocarbamate, sodium salt
DEAE	diethylaminoethyl
DeoxyHb	HbFe <sup>II</sup>
2,5-DHB	2,5-dihydroxybenzoic acid
DTNB	5,5'-dithiolbis(2-nitrobenzoic acid)
DTPA	diethylenetriamine- <i>N,N,N',N',N''</i> -pentaacetic acid
EDRF	endothelium-derived relaxing factor
EDTA	ethylenediaminetetracetic acid
EESOD	metal-free CuZnSOD
ESI-MS	electrospray ionization mass spectrometry

G25/G75	G-type of dextran gel (Sephadex)
GSH	glutathione; <i>N</i> -( <i>N</i> - <i>L</i> - $\gamma$ -glutamyl- <i>L</i> -cysteinyl)glycine
GSNO	<i>S</i> -Nitrosoglutathione; <i>N</i> -( <i>N</i> - <i>L</i> - $\gamma$ -glutamyl- <i>S</i> -nitroso- <i>L</i> -cysteinyl)glycine
GSSG	glutathione disulfide; <i>N</i> -( <i>N</i> - <i>L</i> - $\gamma$ -glutamyl- <i>S</i> -nitroso- <i>L</i> -cysteinyl)glycine disulfide
Hb	hemoglobin
Hb-SNO	<i>S</i> -nitrosated Hb
HPLC	high-performance liquid chromatography
hSOD1	human copper,zinc-superoxide dismutase
ICP-MS	inductively coupled plasma mass spectrometry
IPTG	isopropyl $\beta$ - <i>D</i> -thiogalactoside
ITC	isothermal titration calorimetry
MALDI	matrix-assisted laser desorption ionization
Mb	myoglobin
MCS	multi-cloning site
MetHb	HbFe <sup>III</sup>
MRF	H-Met-Arg-Phe-OH
MS	mass spectrometry
MS/MS	tandem MS
NEDA	<i>N</i> -(1-naphthyl)ethylenediamine dihydrochloride
NEM	<i>N</i> -ethylmaleimide
Neo	neocuproine; 2,9-dimethyl-1,10-phenanthroline

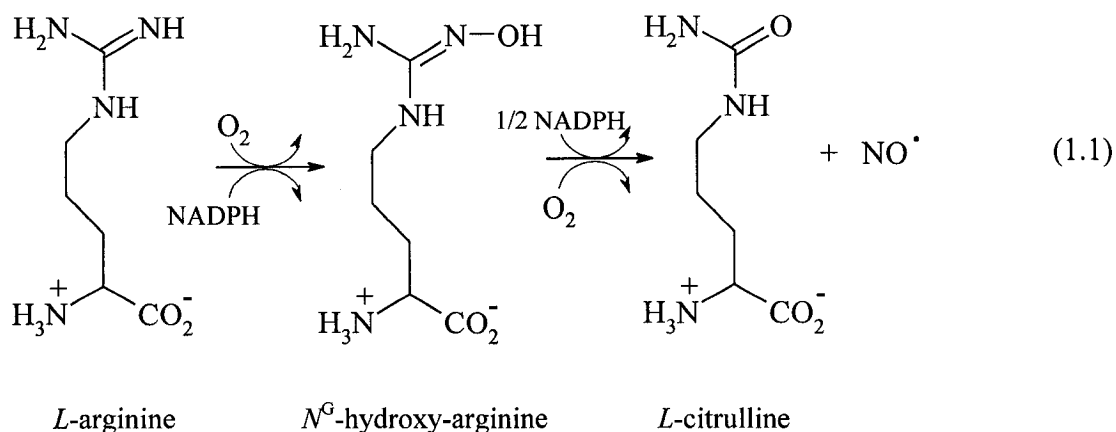


nitrosylHb	HbFe <sup>II</sup> NO
NO	nitric oxide
HNO/NO <sup>-</sup>	nitroxyl
NO <sup>+</sup>	nitrosonium cation
NOS	NO synthase
O <sub>2</sub> <sup>•-</sup>	superoxide radical
oxyHb	HbFe <sup>II</sup> O <sub>2</sub>
PAGE	polyacrylamide gel electrophoresis
PGO	phenylglyoxal hydrate
PRS	porcine rennin substrate tetradecapeptide
PVDF	polyvinylidene difluoride
Py	pyrogallol; 1, 2, 3-trihydroxybenzene
Py <sub>ox</sub>	oxidized Py
Q-ToF2	quadrupole time-of-flight
RBC	red blood cell
RSNO	<i>S</i> -nitrosothiol
SDS	sodium dodecyl sulfate
TEMED	<i>N,N,N',N'</i> -tetramethylethylene diamine
TFA	trifluoroacetic acid
TMB	3,3',5,5'-tetramethyl benzidine
TNB <sup>2-</sup>	5-thio-2-thiobenzoate anion

## 1.0 Introduction

### 1.1 Nitric oxide (NO) – an important signaling molecule

NO is a free radical that can transmit signals in cells. Endogenous NO is synthesized from L-arginine by NO synthases (NOSs), an enzyme family present in endothelial cells and in a variety of other mammalian tissues (Reaction 1.1). NO is about 70 times more soluble in hydrophobic solvents than in water (1), which allows it to easily diffuse among cellular compartments and transmit information to its targets.



The major effect of NO is the activation of soluble guanylate cyclase (sGC), which catalyzes the conversion of guanosine triphosphate (GTP) to 3',5'-cyclic guanosine monophosphate (cGMP). cGMP is a second messenger molecule that activates a number of proteins including protein kinases (PKG), phosphodiesterases (PDE), and ion channels. One important function of NO is the mediation of smooth muscle relaxation shown in Figure 1.1. In response to circulatory signals, NOS can be stimulated to produce high levels of NO (up to  $5 \mu\text{M}$ ) in arterial endothelial cells (2). The gas then

diffuses into adjacent smooth muscle cells, activates sGC, and triggers a cascade of metabolic events that culminate in smooth muscle relaxation (3, 4). NO, as an endothelium-derived relaxing factor (EDRF), regulates blood vessel tone and blood flow by inhibiting smooth muscle contraction and platelet aggregation. A wide range of other functions in bioregulation include roles in inflammation, immunity, programmed cell death, and neurotransmission (2). To regulate these diverse and important processes in biological systems, NO has to function not only at its site of generation but also its bioactivity has to be transported to distant targets.

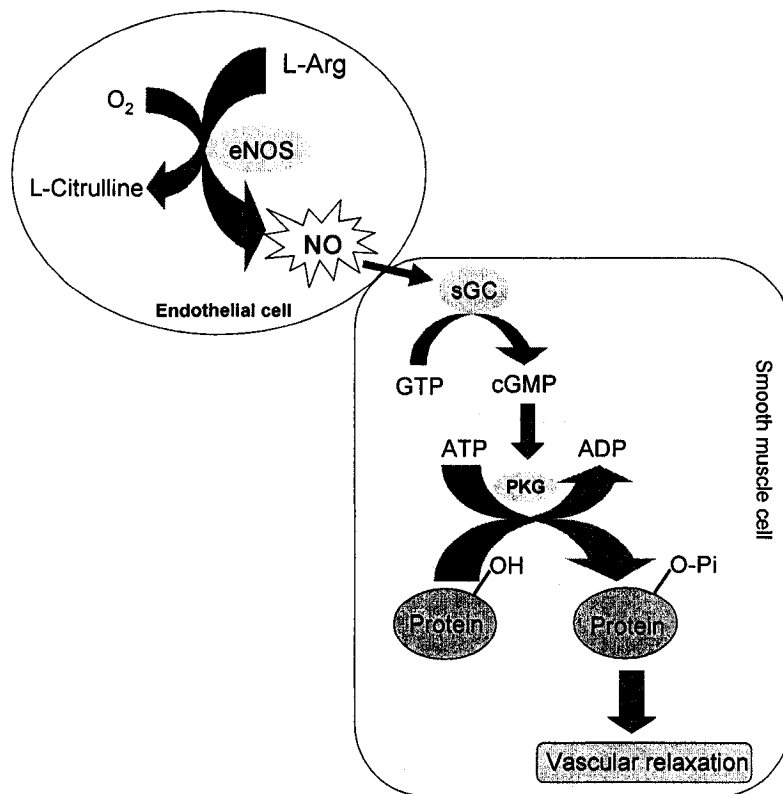


Figure 1.1 Nitric oxide and cGMP signaling in smooth muscle cells. [Adapted from [http://www.biomedicale.univ-paris5.fr/umr747/presentation\\_equipe4\\_eng.html](http://www.biomedicale.univ-paris5.fr/umr747/presentation_equipe4_eng.html) and Ref (5)]

The estimated half-life of NO ranges from 0.05 to 1.8 ms due to its reaction with molecular oxygen (6-8). The diffusion rate of NO is  $50 \mu\text{ms}^{-1}$  in a single direction in biological systems (9). These properties require that free NO exert its effects within a few microns from its site of generation. The hypothesis that NO is stabilized by a carrier molecule that prolongs its half-life and preserves its biological activity has been proposed (10) and has been demonstrated (11, 12). *S*-nitrosothiols (RSNOs) have been shown to be potent smooth muscle relaxants and inhibitors of platelet aggregation and are currently the best candidates for the endogenous storage and transport of NO (13-18). For example, experiments from Rassaf and coworkers (11) have demonstrated that intra-arterially applied NO can be transported in a bioactive form for significant distances along the vascular bed, and most of the systemic effects of NO administered intravenously are mediated by its conversion into plasma RSNOs (12).

## **1.2 RSNOs – a NO reservoir *in vivo***

RSNOs are considered to play important roles in storing, transporting, and releasing NO *in vivo* (13, 19). Some RSNOs, such as *S*-nitrosoalbumin (Alb-SNO) (14), *S*-nitroso-*L*-cysteine (CysNO) (20), and *S*-nitrosoglutathione (GSNO) (10, 19, 21, 22) have been detected *in vivo*. Stamler *et al.* (14) reported that NO circulates in the plasma of healthy humans primarily as Alb-SNO, suggesting that Alb-SNO may be a physiological reservoir of NO. The levels of RSNOs reported in rat and human plasma vary from micromolar to nanomolar depending on the measurement methodology (23).

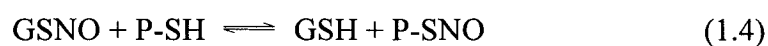
The mechanism of RSNO formation *in vivo* is not clear. It is unlikely to involve the direct reaction of NO with free thiol groups as this is actually a very slow oxidation

that yields thiol disulfide and nitroxyl ( $2\text{NO} + 2\text{RSH} \rightarrow \text{RSSR} + 2\text{HNO}$ ) (24, 25). The production of RSNOs in oxygenated buffers (5) is probably due to oxidation of NO to dinitrogen trioxide ( $\text{N}_2\text{O}_3$ ), a potent nitrosating agent that reacts with thiols to yield RSNOs and nitrate (16):



Several other routes of RSNOs formation have been proposed. For example, the reaction of thiols with peroxynitrite ( $\text{ONOO}^-$ ) or with the nitrosonium cation ( $\text{NO}^+$ ) formed on the oxidation of NO by transition metals (5, 26-28).

RSNOs regulate physiological functions by donating  $\text{NO}^+$ , NO, and HNO. These properties make RSNOs EDRF-like in their activity (20). Low-molecular-weight RSNOs are generally less stable than *S*-nitrosoproteins (23), and *trans*-*S*-nitrosation reactions are possible such as that between GSNO and a protein thiol (P-SH):



This exchange of an  $\text{NO}^+$  moiety provides further pathways for NO metabolism and action (29). Thus, as NO reservoirs *in vivo*, RSNOs act as physiological mediators, intermediates in the excretion of NO and as storage forms of NO (29, 30). Despite their biological importance, it is still uncertain how small thiols and protein thiols (P-SH) are initially *S*-nitrosated as mentioned above, or how RSNOs are involved in multiple *trans*-*S*-nitrosations.

### 1.3 *S*-Nitrosoglutathione (GSNO) and the mechanism of NO release

GSNO (Figure 1.2) is the most important low-molecular-weight RSNO found *in vivo* (10, 19, 31, 32), and is a relatively stable compound in aqueous media in the dark (33-35). Previous results indicate that GSNO is a potent nitrovasodilator, an inhibitor of platelet aggregation (36-38), and provides significant protection to the ischemic myocardium (39, 40).

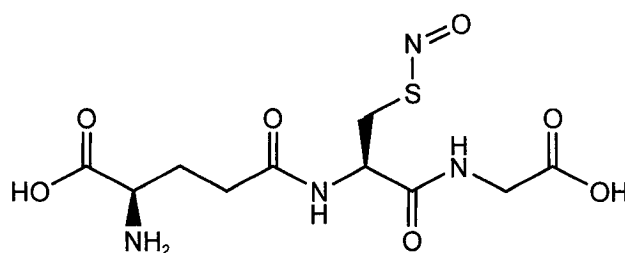
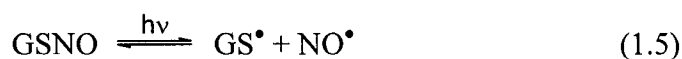
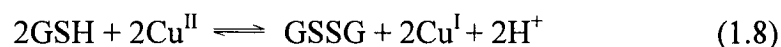
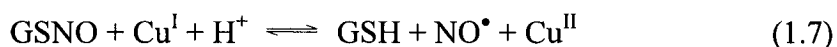


Figure 1.2 **Structure of GSNO.** Reproduced from [www.cambridgesoft.com](http://www.cambridgesoft.com).

The factors affecting GSNO decomposition in solution include light, temperature, pH, and contaminating transition metal ions. As GSNO has the most EDRF-like activity (23), NO release should be related to its biological activity. Efficient homolytic cleavage of the S-NO bond (Reactions 1.5 and 1.6) only happens *via* photolysis at physiological temperatures (33):



GSNO reductive decomposition with NO release is accelerated by contaminating or exogenously added copper ions (33-35):



The chelation of copper by GSH and the GSSG product (Figure 1.3) complicates the kinetics of this process (34, 41). Since  $\text{Cu}^{\text{I}}$  is the active species in GSNO decomposition, reducing agents such as GSH and ascorbate accelerate copper-catalyzed GSNO breakdown by chemical reduction of the metal (Reaction 1.8) (42, 43). Interestingly, no  $\text{GS}^\bullet$  radical formation was detected during copper-catalyzed GSNO breakdown (33), suggesting that the reaction intermediates are copper-bound species. Heterolytic cleavage of RSNO to  $\text{NO}^+$  or  $\text{NO}^-$  was also reported since in some cases RSNOs mediate their biological actions independent of NO generation (26, 44-46).

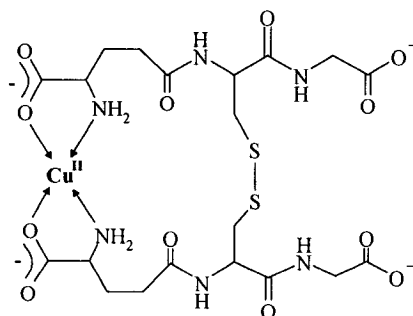


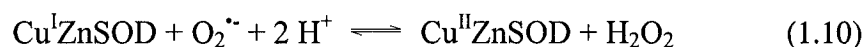
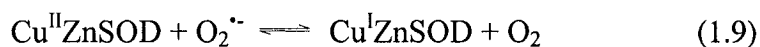
Figure 1.3 GSSG acts as a  $\text{Cu}^{\text{II}}$  chelator. Reproduced from Ref (34).

## 1.4 Copper,zinc-superoxide dismutase (CuZnSOD)

CuZnSOD is a homodimer with molecular weight of ~32 kDa and an isoelectric point of 4.8 (47-49). There is one copper and one zinc in each subunit, and the imidazole rings of His44, 46, 61, and 118 are ligated to the Cu<sup>II</sup> ion. Zn<sup>II</sup> lies 6 Å from the copper and is ligated to the imidazoles of His61 (which ligates both metals giving rise to an imidazolate bridge), 69, and 78, and to the carboxylate of Asp81 (Figure 1.4A). A total of 10 lysine and 4 arginine residues are present in each subunit of bovine erythrocyte CuZnSOD (50). Arg141, Lys120, and Lys134, are 5, 12 and 13 Å from the copper, respectively, forming a positively charged access channel to the active site (Figure 1.4B) (50).

### 1.4.1 Superoxide dismutase (SOD) activity of CuZnSOD

The primary function *in vivo* of CuZnSOD is proposed to be the efficient catalysis of superoxide (O<sub>2</sub><sup>•-</sup>) dismutation (47, 51). Rapid removal of the O<sub>2</sub><sup>•-</sup> radical is important in antioxidant defence. The rate constant for enzyme-catalyzed O<sub>2</sub><sup>•-</sup> dismutation is  $2 \times 10^9 \text{ M}^{-1} \text{ s}^{-1}$  at pH 7.0 and 20-25°C (52, 53). The mechanism involves Reaction 1.9 and 1.10:



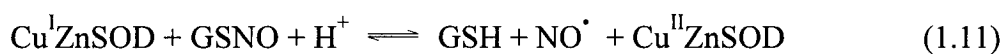
The reduction of the enzyme by O<sub>2</sub><sup>•-</sup> (Reaction 1.9) is the rate-limiting step (53), and the site of reactivity for O<sub>2</sub><sup>•-</sup> is the copper ion. This metal functions in catalysis by alternate reduction (Reaction 1.9) and reoxidation (Reaction 1.10) during successive



encounters with  $O_2^{\cdot-}$  (52, 54). In the oxidized enzyme, His61 ligates copper and zinc to form an imidazolate bridge, but during the process of copper reduction by  $O_2^{\cdot-}$ , the imidazolate bridge is protonated and does not ligate the copper. The proton is released upon copper oxidation and the imidazolate bridge reforms. The positively charged side chains of Arg141, Lys120, and Lys134 (Figure 1.4B) are responsible for the electrostatic guidance of  $O_2^{\cdot-}$  to the active site (50, 55).

#### 1.4.2 GSNO-reductase activity of CuZnSOD

In the presence of an electron donor such as GSH, CuZnSOD catalyzes the reductive decomposition of RSNOs such as GSNO (Reactions 1.11 and 1.12) (56, 57):



This mechanism also involves alternate reduction (Reaction 1.12) and reoxidation (Reaction 1.11) of the active-site copper. It has been demonstrated that the  $GS^{\cdot}$  radicals formed in Reaction 1.12 dimerize to yield GSSG rather than reform GSNO by reacting with NO (57). The GSSG product may function as an inhibitor of the GSNO-reductase activity of CuZnSOD as it attenuates the  $Cu^{II}$ -catalyzed NO release from GSNO due to its strong chelation of copper ions (34).

#### 1.4.3 Modulators of the SOD and GSNO-reductase activities of CuZnSOD

Both the SOD and GSNO-reductase activity of CuZnSOD require redox turnover of the active-site copper. Thus, factors that could inhibit or attenuate catalysis by CuZnSOD include: (i) removal of copper from the active site; (ii) alteration of the  $Cu^{II/I}$

reduction potential; (iii) prevention of substrate access to the active site; and (iv) neutralisation of the positively charged side chains of Arg141, Lys120, or Lys134. Metal

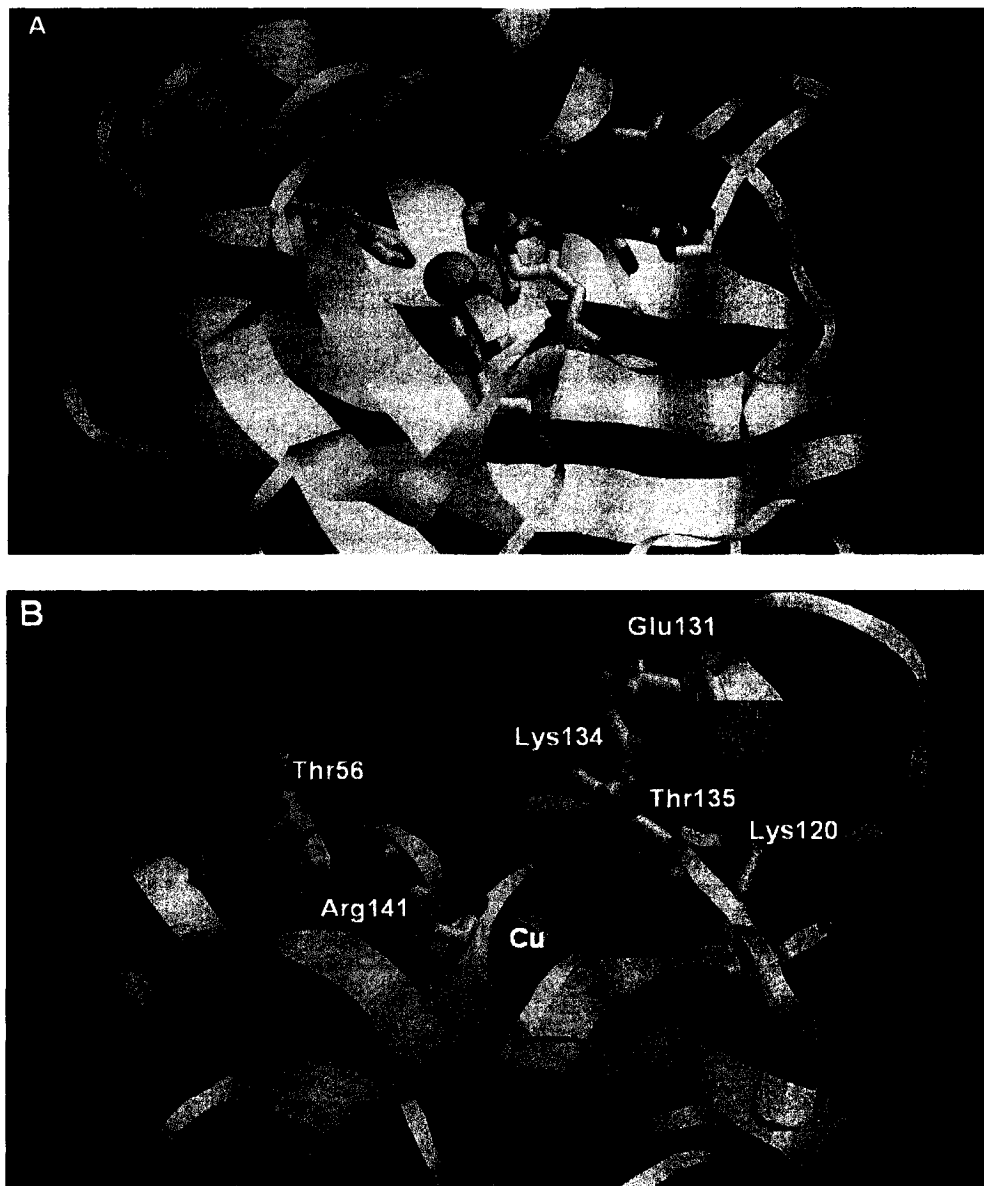


Figure 1.4 (A) X-ray structure of the metal binding region, and (B) the copper active-site channel of one subunit of bovine CuZnSOD. Structure drawn using RasMol V2.6 (<http://www.umass.edu/microbio/rasmol/>) and the PDB file 1CBJ from the published x-ray structure in the Research Collaboratory for Structural Bioinformatics (RCSB).

chelators, such as EDTA, DTPA, DDC, cuprizone, and neocuproine could be potential modulations of CuZnSOD activity. Possible physiological modulators include redox-active species such as GSH and GSSG, and anions such as phosphate (58), 2,3-diphosphoglycerate (2,3-DPG), and inositol hexaphosphate (IHP).

**Table 1.1 Comparison of sequences of human, bovine, and rat erythrocyte CuZnSODs<sup>a</sup>**

human	ATKAVCVLKG	DGPVQGIINF	EQKESNGPVK	VWGSIKGLTE	GLHGF <b>HV</b> HEF50
bovine	ATKAVCVLKG	DGPVQGTIHF	EAK--GDTVV	VTGSITGLTE	GDHGF <b>HV</b> HQF48
	*****	*****	* * * *	* * * *	* * * *
rat	AMKAVCVLKG	DGPVQGVHIF	EQKASGEPVV	VSGQITGLTE	GEHGF <b>HV</b> HQY50
	* * * * *	*****	* * * *	* * * *	* * * *
human	GDNTAGCTSA	GPHFNPLSRK	<b>HGGPKDEERH</b>	VGDLGNVTAD	KDGVADVSIE100
bovine	GDNTQGCTSA	GPHFNPLSKK	<b>HGGPKDEERH</b>	VGDLGNVTAD	KNGVAIVDIV98
	****	*****	*****	*****	* * * *
rat	GDNTQGCTTA	GPHFNPHSKK	<b>HGGPADEERH</b>	VGDLGNVAAG	KDGVANVSIE100
	****	*****	*****	*****	*****
human	DSVISLSGDH	CIIGRTLIV <b>H</b>	<b>EK</b> ADDLGKGG	NEEST <b>KT</b> GNA	GS <b>RL</b> ACGVIG150
bovine	DPLISLSGEY	SIIGRTMV <b>VH</b>	<b>EKP</b> DDLGRGG	NEEST <b>KT</b> GNA	GS <b>RL</b> ACGVIG148
	* * * * *	*****	* * * * *	*****	*****
rat	DRVISLSGEH	SIIGRTMV <b>VH</b>	<b>EKQ</b> DDLGRGG	NEEST <b>KT</b> GNA	GS <b>RL</b> ACGVIG150
	* * * * *	*****	* * * * *	*****	*****
human	IAQ153				
bovine	IAK151				
	**				
rat	IAQ153				
	***				

<sup>a</sup>Sequences from NP\_000445 (human), 1CBB (bovine) and NP\_058746 (rat) (<http://www.ncbi.nlm.nih.gov/>). The amino acids forming the metal binding regions and the positively charged side chains located in the active-site channel in the three enzymes are in bold font. The identical sequences in bovine and rat vs human are presented by “\*” symbols. SIM (<http://www.expasy.ch/tools/sim-prot.html>) was used to align the protein sequences.

#### 1.4.4 Comparison of human, bovine, and rat CuZnSODs

The sequences and SOD activities of human, bovine and rat erythrocyte CuZnSOD are compared in Tables 1.1 and 1.2, respectively. Human and rat CuZnSOD exhibit 83% sequence identity, and human and bovine CuZnSOD exhibit 81% sequence identity. In the three proteins, the positively charged side chains of Arg143, Lys122, and Lys136 in the human and rat enzyme (Arg141, Lys120, and Lys134 in the bovine enzyme; Figure 1.4) and the metal binding residues are conserved (Table 1.1 residues in bold font). Higher SOD activity was measured in rat (59) as compared to human erythrocytes (Table 1.2).

Table 1.2 SOD activity and quantities in human, bovine, and rat erythrocytes

Species	SOD activity <sup>a</sup>	Assay method (ref)	[copper] in erythrocyte (ref)
Human	~91 units /mL extracted sample	Increased autoxidation of BXT-01050 (59)	5–10 $\mu$ M (60)
Rat	~123 units/mL extracted sample	Increased autoxidation of BXT-01050 (59)	Not reported
Bovine	90 units/mL whole blood	decreased cytochrome c reduction (47)	~10 $\mu$ M (60)

<sup>a</sup>The extracted sample was prepared by resuspending the erythrocyte pellet from at least 200  $\mu$ L of whole blood in four times its volume of ice-cold water. After centrifugation, 250  $\mu$ L of the lysate supernatant was mixed with 400  $\mu$ L of ice-cold chloroform/ethanol (37.5/62.5, v/v) for at least 30 s, centrifuged at 4°C and 2500 g for 10 min, and the resulting supernatant was stored between 2–8°C for SOD activity assay (59).

## 1.5 Hemoglobin (Hb)

Hb is a tetrameric protein (~64 kDa) which is composed of 2 $\alpha$  and 2 $\beta$  chains that each contains a heme prosthetic group. The  $\alpha$  and  $\beta$  chains combine to form stable  $\alpha\beta$  dimers, and the dimers associate to form the Hb tetramer (Figure 1.5). The best characterized physiological function of Hb in red blood cells (RBCs) is the transport of O<sub>2</sub> by its heme iron for tissue respiration. The transport capacity is governed by a cycle of allosteric transitions in which Hb assumes the R state (relaxed, high O<sub>2</sub> affinity or oxyHb) to bind O<sub>2</sub> in the lungs and, on partial deoxygenation, the T state (tense, low O<sub>2</sub> affinity or deoxyHb) to efficiently deliver O<sub>2</sub> to tissues.



Figure 1.5 **X-ray structure of human oxyHb.** The four polypeptide chains and hemes (red with iron in yellow) are indicated. This structure was drawn using RasMol V2.6 and the PDB file 2DN2 from Research Collaboratory for Structural Bioinformatics (RCSB).

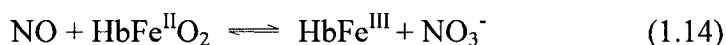
Cysteine residues in Hb from different species are not identical except for the highly conserved cysteine on the  $\beta$  chain at position 93 (Cys $\beta$ 93) (Table 1.3, Section 1.5.4). The R–T transition also controls the reactivity of Cys $\beta$ 93 such that the thiol can react with an NO donor to form *S*-nitrosohemoglobin (Hb-SNO) in the R state, and unload NO from the sulfhydryl group in the T state (19, 61-66). As NO is also captured by heme (Section 1.5.1), there is considerable debate over the nature and chemistry of the interaction between NO and RBCs, in particular, whether Hb consumes or conserves NO bioactivity (67-69).

### 1.5.1 Reactions of NO with deoxy and oxyHb

A model (19) has been proposed by Stamler and coworkers suggesting that NO is transported by Hb on binding to the highly conserved Cys $\beta$ 93 residue, forming Hb-SNO. The heme group in deoxyHb is an efficient scavenger of free NO (64, 70), and forms a stable heme-NO complex ( $K_d \approx 4$  pM) (68) to give nitrosylHb (HbFe<sup>II</sup>NO or Hb-NO). Binding of NO to the deoxy heme is rapid ( $2.6 \times 10^7$  M<sup>-1</sup>s<sup>-1</sup>, Reaction 1.13) (64):



Alternatively, NO can convert oxyHb to metHb with its parallel oxidation to nitrate ( $3.7 \times 10^7$  M<sup>-1</sup>s<sup>-1</sup>, Reaction 1.14) (64, 71):



Given the presence of a highly conserved sulfhydryl group at position  $\beta$ 93, it was proposed that human Hb undergoes NO exchange (*trans*-*S*-nitrosation) with low-molecular-weight *S*-nitrosothiols such as GSNO *in vivo* (19, 72).

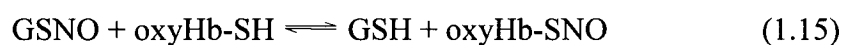
### 1.5.2 The proposed action of Hb-SNO *in vivo*

The well-known physiological actions of NO in the blood stream are vasodilatation and inhibition of platelet aggregation (23). The endogenous levels and corresponding half-lives of high-molecular-weight RSNOs, such as Alb-SNO and Hb-SNO may be much higher than the concentration of free NO (0.1–100 nM) produced by eNOS (23, 69, 73). Interest in these protein RSNOs is intense since they elicit physiological responses similar to those evoked by NO including vasodilation and platelet inhibition (16, 74, 75). Regulation of vascular tone by Hb-SNO *via* the delivery and release of NO has been reported (63). A model (61) of Hb *S*-nitrosation and denitrosation that promotes NO transport and control of blood flow is shown in Figure 1.6. As described in Section 1.1, NO is a vasodilator that increases the diameter of blood vessels and hence blood flow by relaxing vascular smooth muscle cells. In the human respiratory cycle, NO binds to Cys $\beta$ 93 of adult Hb (HbA) in regions of high O<sub>2</sub> concentration (*e.g.*, lungs) to form Hb-SNO. On O<sub>2</sub> release from the heme, NO is released from Cys $\beta$ 93, which relaxes the vessels and aids in O<sub>2</sub> delivery to tissues (61). In contrast, in T-state Hb (low O<sub>2</sub> pressure) extra NO is picked up by the heme to form Hb-NO to mitigate the cytotoxic effects of NO (Figure 1.6). This model is discussed further in Section 1.5.5.

### 1.5.3 Mechanism of Hb *S*-nitrosation

Different mechanisms have been proposed for Hb *S*-nitrosation. These include:

(i) *Trans-S*-nitrosation involving direct NO<sup>+</sup> transfer from an NO donor (such as GSNO) to Cys $\beta$ 93 of oxyHb:



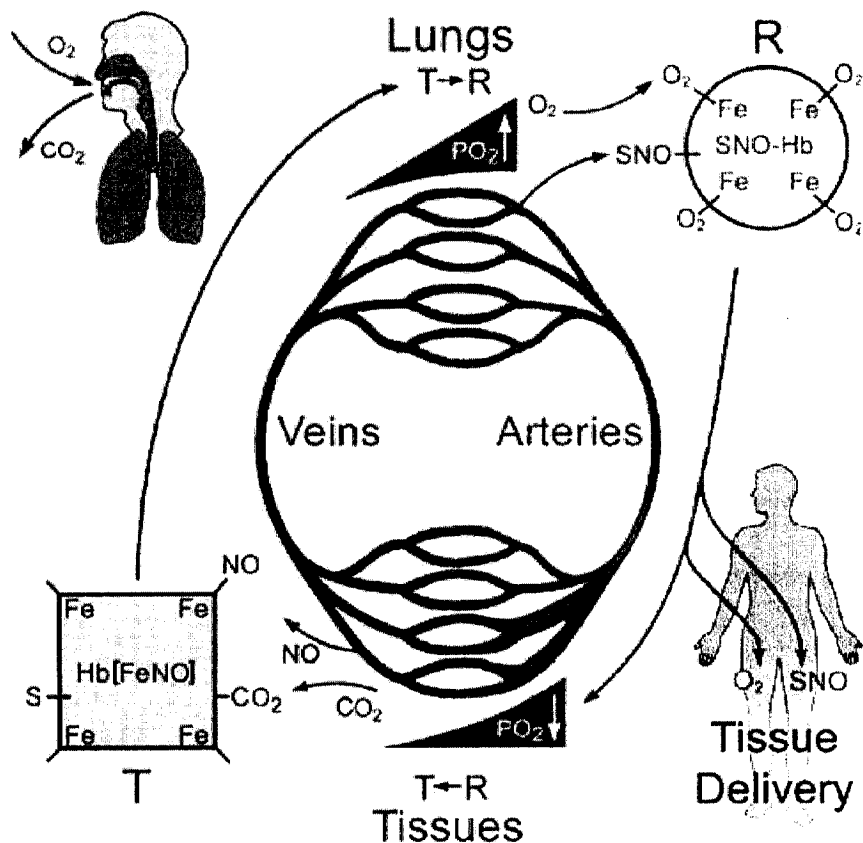
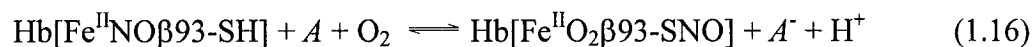


Figure 1.6 NO in the human respiratory cycle. Cited from Ref (61).

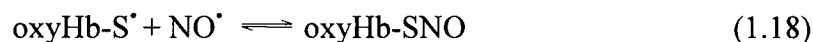
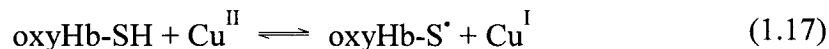
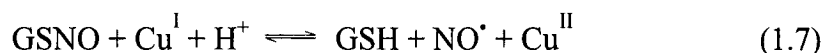
(ii) Intramolecular transfer of NO from the heme of deoxyHb to Cys $\beta$ 93 in the presence of  $O_2$ . Recent evidence indicates that nitrosylHb is formed *via* the nitrite-reductase activity of deoxyHb ( $2HbFe^{II} + NO_2^- + H^+ \rightarrow HbFe^{III} + HbFe^{II}NO + OH^-$ ) (76-80). Under high  $O_2$  pressures,  $O_2$  displaces NO from the heme to form oxyHb, and the released NO moves to the relatively exposed sulfhydryl groups of Cys $\beta$ 93 (78, 81):





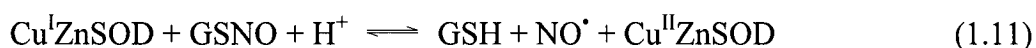
where  $A$  is an electron acceptor such as an oxidized heme, another metal ion, oxygen, or other organic acceptors (81).

(iii) Copper-catalyzed Hb *S*-nitrosation involving the following reactions:



$\text{Cu}^{\text{I}}$  catalyzes breakdown of GSNO (Reaction 1.7) and NO reacts directly with the nascent Cys $\beta$ 93 radical formed in Reaction 1.17.

(iv) CuZnSOD-catalyzed *S*-nitrosation. We have demonstrated that CuZnSOD possesses NO-transferase activity (57, 82), and based on our observation that thiols in calbindin D<sub>28K</sub> (P-SH) reduce the  $\text{Cu}^{\text{II}}$  center in  $\text{Cu}^{\text{II}}$ ZnSOD, the following mechanism was proposed (82):



Furthermore, we proposed (57) that erythrocyte CuZnSOD plays a critical role in preserving the biological activity of NO by targeting it from GSNO to Cys $\beta$ 93 of human oxyHb. Cys $\beta$ 93 was fully *S*-nitrosated when oxyHbA containing CuZnSOD was incubated with GSNO (Cys $\beta$ 93/GSNO = 1) at physiological concentrations of the

proteins (5 mM Hb, 10  $\mu$ M CuZnSOD). In contrast, removal of CuZnSOD by anion-exchange chromatography or dilution of Hb to micromolar concentrations resulted in metHb formation (57). These results revealed that the NO from CuZnSOD-catalyzed GSNO decomposition is likely channeled to Cys $\beta$ 93 within an oxyHb-CuZnSOD encounter complex. The formation of this complex *in vivo* may allow Cys $\beta$ 93 in oxyHb to compete with GSH (present in human RBCs at >5 mM) as an electron donor to Cu<sup>II</sup>ZnSOD (Reaction 1.19). The thiyl radical formed on Cys $\beta$ 93 acts as an efficient scavenger of the released NO to preserve its bioactivity.

**Table 1.3 Cysteine residues in rat Hb and human HbA<sup>a</sup>**

Human HbA	Rat Hb	
	Major form	Minor form
Cys $\beta$ 93	Cys $\beta$ 93	Cys $\beta$ 93
Cys $\beta$ 112	Cys $\beta$ 125	--
--	Cys $\alpha$ 13	Cys $\alpha$ 13
Cys $\alpha$ 104	Cys $\alpha$ 104	Cys $\alpha$ 104
--	Cys $\alpha$ 111	Cys $\alpha$ 111

<sup>a</sup>From the sequences of rat (Accession #: P02091, AAA41308, S00840 ) and human (Accession #: P01922 and P02023) Hb in the NCBI protein database (<http://www.ncbi.nlm.nih.gov>).

#### **1.5.4 Reactivity of cysteine residues in rat vs human Hb**

The major isoform of rat Hb has ten cysteine residues per tetramer (Table 1.3) and six of these are reactive with DTNB (29). The two Cys $\beta$ 125 residues are 100-times more reactive than GSH and the half-life ( $t_{1/2}$ ) for their reaction with excess DTNB (0.5

mM) under pseudo-first-order conditions is  $< 100$  ms. The other two families of reactive thiols, Cys $\beta$ 93 and Cys $\alpha$ 13, are slow reacting ( $t_{1/2} = 30 - 50$  s) (83). HbA has six cysteine residues per tetramer (Table 1.3) and only Cys $\beta$ 93 is reactive with DTNB with a  $t_{1/2}$  of  $\sim 30$  s (0.5 mM DTNB) (83), corresponding to the slow reacting thiols in rat Hb.

### 1.5.5 *S*-Nitrosation of rat vs human Hb

The fast-reacting thiols in rat blood will likely influence the pharmacokinetics, toxicity, and action of NO donors. To fully understand differences in the *S*-nitrosation/denitrosation of rat Hb compared to human HbA is critical since a rat model is frequently used in studies of NO biochemistry (19, 72).

The allosteric model of human Hb *S*-nitrosation was first proposed by Stamler's group (19, 63, 65). They suggested that the rates of *S*-nitrosation/denitrosation of Hb were markedly dependent on its conformational state. The dynamic cycle in which Hb is *S*-nitrosated in the lungs and the NO group is released during arterial-venous transit (Figure 1.6) was based on endogenous levels of Hb-SNO and Hb-NO in arterial and venous rat blood (19). However, data from humans reported by Gladwin *et al.* (84-86) weaken the suggested allosteric-regulated model of NO/O<sub>2</sub> delivery since no significant differences between arterial and venous Hb-SNO levels in human blood were revealed in their measurements (Table 1.4).

*S*-Nitrosation of Cys $\beta$ 93 of human HbA only occurs in the oxy form (65, 87, 88), but the reactivity of Cys $\beta$ 125 in rat Hb is independent of quaternary structure (Table 1.5) (29). Rossi *et al.* (83) proposed that, because of its low  $pK_a$  ( $\sim 6.9$ , the cysteinyl anion being stabilized by hydrogen bond donation from Ser $\beta$ 123) and large surface exposure (as estimated by computer analysis of a model of the molecular surface of rat Hb),

Cys $\beta$ 125 in rat erythrocytes is the kinetically preferred site of *S*-conjugation. Only the slow-reacting thiols in rat Hb, Cys $\beta$ 93 and Cys $\alpha$ 13, became more reactive in the presence of O<sub>2</sub>, like Cys $\beta$ 93 in human Hb (29).

Table 1.4 **Endogenous levels of Hb-SNO and Hb-NO**

Hb form	Arterial	Venous	Blood	Refs
Hb-SNO	311 nM	32 nM	Rat	(19)
Hb-NO	536 nM	894 nM		Stamler & coworkers
Hb-SNO	2.5 $\mu$ M	0.8 $\mu$ M	Human	(61)
Hb-NO	2.5 $\mu$ M	5 $\mu$ M		Stamler & coworkers
Hb-SNO	161 nM	142 nM	Human	(85, 86)
Hb-NO	150 nM	160 nM		Gladwin & coworkers
Hb-SNO	46 nM	69 nM	Human	(84) Gladwin & coworkers

### 1.5.6 Hb-SNO denitrosation and possible regulators

Preservation of the bioactivity of NO and delivery of NO to distant targets are proposed functions of Hb-SNO *in vivo*. Investigation of NO release from Hb-SNO (denitrosation) is thus another key step in fully understanding how Hb-SNO behaves like NO in the regulation of blood vessel tone and in inhibiting aggregation of platelets.

Hb-SNO bioactivity is promoted by low *p*O<sub>2</sub>, thiols, and heme oxidation (16, 19, 62). Jia *et al.* found that during arterial-venous transit in rat blood (Table 1.4) (19), NO release from deoxyHb-SNO is favored. Hb-SNO is less stable in the T structure since Cys $\beta$ 93-NO is solvent exposed but it is located in a protected pocket in the R conformation (62).

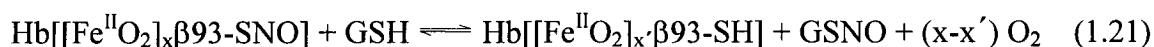
**Table 1.5 Rate constants ( $M^{-1}s^{-1}$ ) for *S*-nitrosation and *S*-thiolation of rat Hb and human HbA**

Reaction	<i>S</i> -nitrosation <sup>a</sup> (29)						<i>S</i> -thiolation <sup>b</sup> (83)	
	$\beta 93$		$\beta 125$		$\alpha 13$		$\beta 125$	
O <sub>2</sub>	+	-	+	-	+	-	+	-
Rat	0.304	0.093	112	116	2.04	0.97	$2.94 \times 10^4$	$2.91 \times 10^4$
Human	0.365	0.101	—	—	—	—	—	—

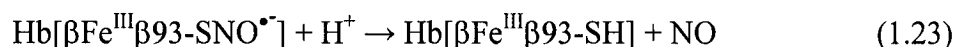
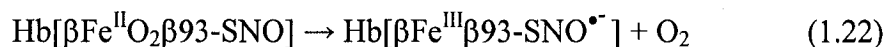
<sup>a</sup>The *S*-nitrosating reagent was 400  $\mu M$  GSNO and the reaction was carried out using 10–50  $\mu M$  Hb in 100 mM phosphate buffer/2 mM DTPA (pH 7.4) prepared from human or rat blood. Kinetics of Hb-SNO formation in the presence and absence of oxygen by *trans*-*S*-nitrosation was determined by three methods: spectrophotometric assay, the Saville assay, and spectral deconvolution as described in (29). The rate constants were determined by fitting the experimental data to exponential growth curves for Hb-SNO (29).

<sup>b</sup>The *S*-thiolating reagent was 340  $\mu M$  DTNB (Reaction 6.2, Section 6.3.2.8) and its reaction with 6.8  $\mu M$  Hb (in heme) in 100 mM phosphate buffer (pH 7) at 20°C was monitored at 450 nm ( $\epsilon = 7.0 \text{ mM}^{-1}\text{cm}^{-1}$ ) following mixing of the reagents in a stopped-flow apparatus.

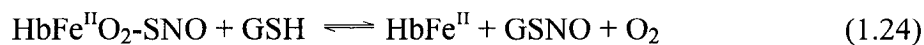
McMahon *et al.* (65) demonstrated allosteric regulation of NO release from Hb-SNO by observing NO group transfer between Hb-SNO and GSH. They showed that Hb-SNO was stable in its R state in the presence of GSH, but decomposed upon deoxygenation (Reaction 1.21). Allosteric modulators that shift the position of the R/T equilibrium toward the T state would increase NO transfer to GSH and thereby increase the bioactivity of Hb-SNO (Reaction 1.21).



$\beta$ -SNO is also less stable when the hemes in Hb-SNO are oxidized to the met form (89-91). Reactions 1.22 and 1.23 describe coupling between heme deoxygenation and  $\beta$ heme/SNO redox chemistry that could lead to liberation of NO from a nascent SNO anion radical (92):



Free thiols also facilitate NO release from Hb-SNO (65, 72). Results from Woltz *et al.* revealed that Hb-SNO decays within 30 min in the presence of GSH or L-cysteine vs <5% decomposition over 4 h at 25° and 37°C in phosphate-buffered saline (72). Furthermore, they demonstrated that Hb-SNO-induced relaxation was dependent entirely on the availability of GSH and cysteine but not GSSG or bovine serum albumin (72). One explanation is that high concentrations of GSH could shift the R/T equilibrium in favor of the deoxy structure (19, 93). This is supported by the observations that at millimolar GSH, the Hb-SNO/GSNO equilibrium shifts toward GSNO regardless of the Hb quaternary structure (Reaction 1.24) (65). Thus, in the presence of GSH relaxation caused by Hb-SNO in hypoxia is comparable to that seen in normoxia (65), which may be due to the enhancement of vasodilation by GSNO.



In agreement with free-thiol-mediated decomposition of Hb-SNO, Gladwin *et al.* (84) proposed that Hb-SNO undergoes reductive decomposition in erythrocytes rather

than allosterically-linked NO release. Reductive decomposition could be a concomitant pathway in the modulation of Hb-SNO bioactivity *in vivo* since GSH, ascorbate, and other naturally occurring reductants are abundant in the RBC (94, 95).

CuZnSOD as a catalyst of GSNO reductive decomposition has been confirmed (56). However, data obtained by Jourdain *et al.* show that it does not catalyze the decomposition of *S*-nitrosoproteins such as AlbNO (56). The effects of CuZnSOD as a regulator of NO release from Hb-SNO will be investigated here.

## **1.6 Hypotheses, scope and organization of thesis**

The objectives of the research conducted for this thesis were to fully understand the effects of various copper chelators on the GSNO-reductase activity of CuZnSOD, and to establish the role of CuZnSOD in the *S*-nitrosation/denitrosation of human and rat Hb.

CuZnSOD is the major intracellular copper binding protein accounting for ~95% of the copper in RBCs (60). Its function as a GSNO-reductase in reductive decomposition of GSNO has been proposed (56). Experiments were carried out to determine how chelators decrease the GSNO-reductase activity of CuZnSOD. Binding to the active-site copper of CuZnSOD was examined by UV-Vis absorption, ICP-MS, enzyme activity assay, and isothermal titration calorimetry (Chapters 2 and 3). The interactions proposed from the experimental data involve Arg141, a key residue in bovine CuZnSOD that affects its SOD activity. To explore the role of Arg141 in the GSNO-reductase activity of CuZnSOD, the arginine-specific agent, phenylglyoxal, was employed, coupled with mass spectrometry, to characterize the modification of arginine-containing peptides and CuZnSOD (Chapter 4). In order to specifically modify the human enzyme at Arg143

(corresponding to Arg141 of bovine CuZnSOD) expression of wild-type and site-directed mutants of human CuZnSOD was also attempted (Chapter 5). CuZnSOD has been proposed to function as a GSNO-transferase in *S*-nitrosation of Cys $\beta$ 93 of human Hb (57). The role of CuZnSOD in the formation of Hb-SNO and in NO release from rat Hb-SNO was investigated using the Saville assay, UV-Vis absorption, and mass spectrometry (Chapter 6). Possible differences in how CuZnSOD might function in NO signalling in rat and in human blood are also discussed in Chapter 6.

## **1.7 Contributions of colleagues**

Chapter 2 was published in *Biochemistry* [Ye M., and English A. M. (2006), *Biochemistry* 45 (42), 12723-12732] and is reproduced with the permission of the journal. All abbreviations, citations, figures and table numbering systems in the published work were changed to the format of this thesis. I carried out all the work reported in this publication and prepared the first draft of the manuscript. Megan Marshall helped with the ICP-MS measurements, and Figure 2.9 was prepared by Dr. Qadir Timerghazin. A. M. English provided intellectual support and edited the manuscript.

Chapter 3 extends the chelator work to non-anionic compounds. I carried out all the experimental work. This chapter is being prepared for publication in *The Journal of Inorganic Biochemistry*.

Chapter 4 is also being prepared for publication. I carried out all the work reported in this chapter and wrote the first draft of the manuscript. A. M. English provided intellectual support and edited the manuscript.



The work in Chapter 5 was carried out with the help of Dr. Heng Jiang. I carried out all the experimental work except Figure 5.17 was prepared by Lily Zhang.

Chapter 6 is currently being prepared for the publication. I carried out all the experimental work and wrote the manuscript.

## **2.0 Binding of polyaminocarboxylate chelators to the active-site copper inhibits the GSNO-reductase activity but not the superoxide dismutase activity of Cu,Zn-superoxide dismutase**

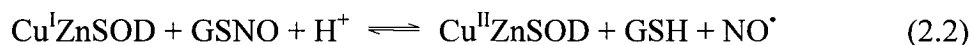
### **2.1 Abstract**

In addition to its superoxide dismutase (SOD) activity, Cu,Zn-superoxide dismutase (CuZnSOD) catalyzes the reductive decomposition of *S*-nitroso-*L*-glutathione (GSNO) in the presence of thiols such as *L*-glutathione (GSH). The GSNO-reductase activity but not the SOD activity of CuZnSOD is inhibited by the commonly used polyaminocarboxylate metal-ion chelators, EDTA and DTPA. The basis for this selective inhibition is systematically investigated here. Incubation with EDTA or DTPA caused a time-dependent decrease in the 680-nm *d-d* absorption of Cu<sup>II</sup>ZnSOD but no loss in SOD activity or in metal-loading of the enzyme as determined by ICP-MS. The chelators also protected the SOD activity against inhibition by the arginine-specific reagent, phenylglyoxal. Measurements of both the time course of SNO absorption decay at 333 nm and oxymyoglobin scavenging of the NO that is released confirmed that the chelators inhibit CuZnSOD catalysis of GSNO reductive decomposition by GSH. The decreased GSNO-reductase activity is correlated with decreased rates of Cu<sup>II</sup>ZnSOD reduction by GSH in the presence of the chelators as monitored spectrophotometrically at 680 nm. The aggregate data suggest binding of the chelators to CuZnSOD, which was detected by isothermal titration calorimetry (ITC). Dissociation constants of  $0.08 \pm 0.02$   $\mu\text{M}$  and  $8.3 \pm 0.2$   $\mu\text{M}$  were calculated from the ITC thermograms for the binding of a single EDTA and DTPA, respectively, to the CuZnSOD homodimer. No association was detected

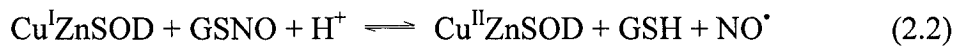
under the same conditions with the metal-free enzyme (EESOD). Thus, EDTA and DTPA must bind to the solvent-exposed active-site copper of one subunit without removing the metal. This induces a conformational change at the second active site that inhibits the GSNO-reductase but not the SOD activity of the enzyme.

## 2.2 Introduction

Trace copper impurities found in aqueous buffers catalyze the reductive decomposition of *S*-nitrosothiols (RSNOs) (27, 33-35, 96, 97). Recently, Dicks *et al.* demonstrated that NO generation from RSNOs was also catalyzed by peptide- and protein-bound copper (98) providing a mechanism for intracellular RSNO breakdown (99) since cells harbour no free copper (100). Jourde'heuil *et al.* reported that CuZnSOD exhibits GSNO-reductase activity yielding free NO in the presence of GSH (56):

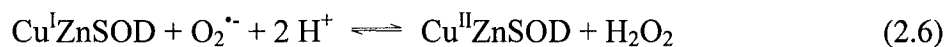


We previously demonstrated that CuZnSOD is an efficient catalyst of NO transfer between *S*-nitrosoglutathione (GSNO) and Cys $\beta$ 93 of oxyhemoglobin (oxyHb) (57) and cysteine residues in calbindin D<sub>28K</sub> (82) at physiological concentrations of the proteins. We observed that both GSH and calbindin reduce Cu<sup>II</sup>ZnSOD (82) and proposed the following mechanism for CuZnSOD-catalyzed *S*-nitrosation of the protein-based thiols (P-SH) in calbindin (82) and oxyHb (57) by GSNO:



Unlike  $\text{GS}^{\bullet}$  (Reaction 2.3) (82, 101), dimerization of  $\text{P-S}^{\bullet}$  is suppressed by steric bulk allowing efficient protein *S*-nitrosation by combination of  $\text{P-S}^{\bullet}$  radicals with  $\text{NO}^{\bullet}$  (Reaction 2.4) (57, 82). We further hypothesised (57) that the GSNO-derived NO is channelled to oxyHb Cys $\beta$ 93 within a CuZnSOD/oxyHb encounter complex to prevent its scavenging by oxyheme ( $\text{Fe}^{\text{II}}\text{O}_2$ ).

The SOD activity of CuZnSOD (Reactions 2.5, 2.6) also requires redox turnover of the active-site copper(47, 102, 103):



Jourd'heuil *et al.* reported that 1 mM neocuproine, a  $\text{Cu}^{\text{I}}$ -specific chelator, had no effect on the SOD activity of CuZnSOD (Reactions 2.5, 2.6) but inhibited its GSNO-reductase activity (Reactions 2.1, 2.2). Inhibition of the latter activity by the  $\text{Cu}^{\text{II}}$ -specific chelators, EDTA and DTPA, was also reported (56) but no data or mechanism were provided. Since EDTA and DTPA are used routinely in SOD assays (47, 104, 105) and in RSNO investigations (19, 101, 106), the purpose of this study is to explore the mechanism by which these anionic polyaminocarboxylate metal chelators selectively inhibit the GSNO-reductase activity of CuZnSOD.

The effects of EDTA and DTPA on (i) the *d-d* absorption of Cu<sup>II</sup>ZnSOD, (ii) the reduction of Cu<sup>II</sup>ZnSOD by GSH, (iii) the metal-ion content of the enzyme and its (iv) SOD and (v) GSNO-reductase activities were investigated here. The ability of EDTA and DTPA to protect the SOD activity of CuZnSOD from phenylglyoxal-induced inactivation was also evaluated. Arg141 at 5 Å from the catalytic copper (107) is critical for SOD activity (49, 50, 55, 58, 107-112), which is lost on modification of Arg141 with the arginine-specific reagent, phenylglyoxal (PGO) (50, 55, 112). Finally, isothermal titration calorimetry (ITC) was used to directly probe association of EDTA and DTPA with CuZnSOD and its metal-free form, EESOD (47, 113-115).

Reaction 2.2 is likely a key common step in the *S*-nitrosation of protein thiols (P-SH) by GSNO, the most physiologically relevant NO donor identified to date (36, 44, 116-118). Thus, the GSNO-reductase activity of CuZnSOD may play a vital role in NO signaling *in vivo*, and the data presented here provide critical information on how the polyaminocarboxylate chelators modulate this activity *in vitro*, and suggest possible mechanisms for its *in vivo* modulation.

## **2.3 Materials and methods**

### **2.3.1 Materials**

Bovine erythrocyte CuZnSOD (Roche Molecular Biochemicals) was used without further purification except where indicated. All reagents were of analytical grade or higher. GSNO [glycine *N*-(*N*-*L*- $\gamma$ -glutamyl-*S*-nitroso-*L*-cysteinyl)] was obtained from Cayman. Horse heart myoglobin, horse heart cytochrome *c* (type III), xanthine, xanthine oxidase, PGO (phenylglyoxal hydrate), EDTA (ethylenediamine-*N,N,N',N'*-tetraacetic

acid, disodium salt), DDC (diethyldithiocarbamate, sodium salt), neocuproine (2,9-dimethyl-1,10-phenanthroline hydrochloride), DTPA (diethylenetriamine-*N,N,N',N'',N'''*-pentaacetic acid), GSH (glutathione, reduced form), GSSG (glutathione, oxidized form) were purchased from Sigma and ultra high purity concentrated HNO<sub>3</sub> was from EM Science. H<sub>2</sub>O<sub>2</sub> (30%), 1000 ppm standard solutions (Cu and Zn) were purchased from ACP Chemicals Inc, Montreal. Nanopure water (specific resistance 18 MΩ-cm) obtained from a Millipore Simplicity water purification system was used to prepare all solutions. The sodium phosphate buffers used in the SOD activity assay and ITC measurements were treated with Chelex-100 resin (Bio-Rad) prior to use to remove trace metal ions.

### **2.3.2 Methods**

#### **2.3.2.1 Effects of chelators on CuZnSOD 680-nm absorption**

The concentration of CuZnSOD dissolved in 50 mM sodium phosphate buffer (pH 7.2) was determined spectrophotometrically ( $\epsilon_{258} = 10,300 \text{ M}^{-1} \text{ cm}^{-1}$  per dimer) (47). Changes in the Cu<sup>II</sup> *d-d* absorption of 200  $\mu\text{M}$  enzyme at 680 nm ( $\epsilon_{680} = 300 \text{ M}^{-1} \text{ cm}^{-1}$  per dimer) (47) vs time were monitored at 37°C in the presence of 5–10 mM EDTA, DTPA, GSH and GSSG. All absorbance readings were carried out in 1-cm cells on an Agilent 8453 UV-visible diode-array or a Beckman DU 650 spectrophotometer equipped with thermostated cell compartments.

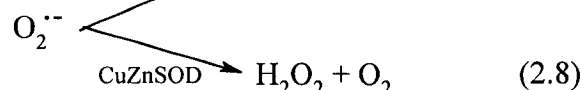
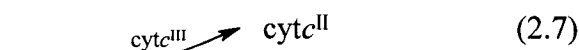
#### **2.3.2.2 CuZnSOD modification by PGO**

Modification of the arginine residues in CuZnSOD by PGO was carried out as described previously (55, 119). Briefly, 105  $\mu\text{M}$  CuZnSOD with and without 1 mM EDTA or DTPA or neocuproine was incubated with 4.2 mM PGO in 250 mM sodium bicarbonate (pH 8.0) with gentle shaking at RT for 6 h. Aliquots were removed from the

reaction vials every hour and the SOD activity was determined by the cytochrome *c* reduction assay as described below.

### 2.3.2.3 Xanthine oxidase-cytc<sup>III</sup> assay for SOD activity

The SOD activity was determined from the competition between CuZnSOD and ferricytochrome *c* (cytc<sup>III</sup>) for O<sub>2</sub><sup>•-</sup>, which decreases the rate of cytc<sup>III</sup> reduction (47):



Cytc<sup>III</sup> reduction was initiated by adding xanthine oxidase to assay solutions containing 10 μM cytc<sup>III</sup>, 50 μM xanthine and 3.3 nM CuZnSOD in 50 mM sodium phosphate buffer (pH 7.8) at 25°C. The xanthine oxidase concentration was adjusted to produce an initial ΔA<sub>550</sub> of 0.025 ± 0.003 absorbance unit/min in a 1-cm pathlength cuvette, and A<sub>550</sub> was read every 15 s over 3 min to monitor cytc<sup>III</sup> reduction. SOD activities were determined from the percent inhibition (%*I*, Eq 2.9) of cytc<sup>III</sup> reduction calculated from the initial slopes of A<sub>550</sub> vs time plots generated in the absence (Slope<sub>cytc<sup>III</sup></sub>) and presence of CuZnSOD (Slope<sub>s</sub>). The relative SOD activities (Eq 2.10) are the ratios of %*I*<sub>c</sub> for the control (untreated CuZnSOD) and %*I*<sub>s</sub> for the samples (CuZnSOD exposed to PGO or a chelator):

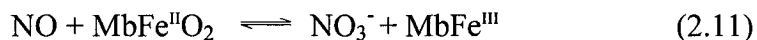
$$\%I = \frac{(\text{Slope}_{\text{cytc}^{\text{III}}} - \text{Slope}_s)}{\text{Slope}_{\text{cytc}^{\text{III}}}} \times 100 \quad (2.9)$$

$$\% \text{ relative SOD activity} = \frac{\%I_s}{\%I_c} \times 100 \quad (2.10)$$

#### 2.3.2.4 GSNO-reductase activity of CuZnSOD

Solutions containing GSNO, GSH, CuZnSOD and EDTA or DTPA were incubated at 37°C for 30 min to establish the extent of chelator inhibition of the GSNO-reductase activity of CuZnSOD (Reactions 2.1–2.3). The decrease in the GSNO concentration was determined spectrophotometrically at the S-NO absorption band ( $\epsilon_{333} = 0.767 \text{ mM}^{-1} \text{ cm}^{-1}$ ) (25).

Free NO is rapidly scavenged by oxymyoglobin (oxyMb,  $\text{MbFe}^{\text{II}}\text{O}_2$ ), which is the basis of the oxyMb assay (82) used to monitor NO release from GSNO:



OxyMb was added to GSNO/GSH/ $\pm$ CuZnSOD/ $\pm$ chelator incubates and the spectral changes on oxyMb conversion to metMb were monitored vs time.

#### 2.3.2.5 ICP-MS determination of metal-ion content of CuZnSOD

The copper and zinc loading of CuZnSOD following incubation with the chelators was determined by inductively coupled plasma mass spectrometry (ICP-MS). CuZnSOD was incubated with 5 mM EDTA, DTPA or DDC at 37°C for 30 min. Since DDC is known to remove copper at neutral pH (120), the DDC/CuZnSOD incubate was included with the controls (CuZnSOD without chelators and the chelators alone). Acetone (1.0 mL) was added to 100- $\mu$ L aliquots of the incubates and after standing at –20°C for 30 min, the precipitated protein was washed twice with cold acetone. The SOD



activity was measured before and after acetone treatment to ensure complete enzyme precipitation, and after centrifugation at 12000×g for 7 min, the supernatant was removed with a micropipette and the precipitate was dried on a Speed Vac (SC 110, Savant). The residue was transferred quantitatively to a 10-mL beaker, digested at 90°C with 1 mL of concentrated HNO<sub>3</sub> plus 100 µL of 30% H<sub>2</sub>O<sub>2</sub>, and diluted to a final volume of 10.0 mL with deionized water. Samples were introduced into the torch of a PE Sciex Elan 6000 ICP-MS *via* a cross-flow nebuliser/Scott-type spray chamber system. The RF power was 1000 W and the argon flow 0.85 L/min, which gave the best sensitivity as determined by the recommended optimization procedure. The optimum lens voltage was determined by maximizing rhodium sensitivity, and data were acquired in the pulse-count mode (121).

#### **2.3.2.6 Preparation of EESOD**

The metal-free enzyme was prepared by 24-h dialysis at 4°C of CuZnSOD against 50 mM sodium acetate buffer (pH 3.8) containing 10 mM EDTA (47). EDTA-free EESOD was obtained as described (113) by 24-h dialysis against 3 changes of 50 mM sodium acetate buffer (pH 5), 24-h dialysis against 2 changes of 0.1 M NaClO<sub>4</sub> in 50 mM sodium phosphate buffer (pH 7.4), followed by 24-h dialysis against 3 changes of 50 mM sodium phosphate buffer (pH 7.4).

#### **2.3.2.7 ITC analysis of CuZnSOD-chelator and EESOD-chelator association**

Protein samples were prepared by overnight dialysis against Chelex-treated 50 mM sodium phosphate buffer (pH 7.4). EDTA (a 50.1-mM standard solution, Aldrich) and DTPA (powder with > 99% purity, Sigma) were added to the dialysis buffer and the pH was adjusted to pH 7.4 using ultra pure NaOH (Fluka) to ensure minimal background from buffer mismatch. A known concentration of protein determined

spectrophotometrically [ $\epsilon_{258} = 10,300 \text{ M}^{-1} \text{ cm}^{-1}$  (CuZnSOD dimer) and  $\epsilon_{258} = 2920 \text{ M}^{-1} \text{ cm}^{-1}$  (EESOD dimer)(47, 113)] was added to the cell of a VP-ITC MicroCalorimeter (MicroCal) following degassing the protein and chelator solutions using the ThermoVac (MicroCal). The chelator was injected with 300-rpm stirring at discrete intervals into the cell and the heat per injection was measured. The observed heats were corrected for heat of dilution of the chelator by performing control titrations in the absence of protein, and the resulting thermograms were analyzed using the Origin software for ITC supplied by MicroCal (Microcal).

## **2.4 Results**

### **2.4.1 Effects of chelators on CuZnSOD 680-nm absorption**

Cu<sup>II</sup>ZnSOD exhibits a weak Cu<sup>II</sup> *d-d* absorption band at 680 nm ( $\epsilon = 300 \text{ M}^{-1} \text{ cm}^{-1}$  per dimer) (47). This band is sensitive to changes in Cu<sup>II</sup> ligation and geometry, and is lost on reduction of the enzyme to Cu<sup>I</sup>ZnSOD (47, 122, 123). As we reported previously (82), a 30-min incubation at 37°C of Cu<sup>II</sup>ZnSOD alone or with GSSG resulted in negligible loss of 680-nm absorbance, but addition of DTPA and EDTA decreased the absorbance at 680-nm by ~20% (Figure 2.1). This loss could be caused by copper reduction, removal and/or by conformational changes induced by the presence of the chelators.

### **2.4.2 Effects of chelators on metal-ion content of CuZnSOD**

The ICP-MS results in Table 2.1 reveal that within experimental error there is no loss of copper or zinc from CuZnSOD following preincubation with EDTA or DTPA. Consistent with the spectrophotometric data (Figure 3.4, Section 3.4.1), DDC removed

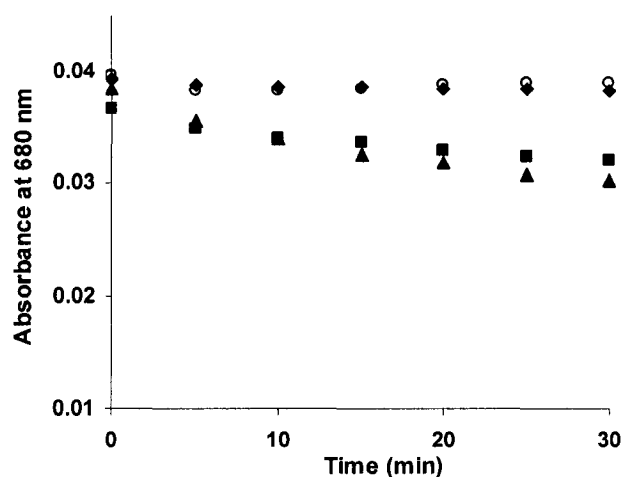


Figure 2.1  $\text{Cu}^{\text{II}}$  *d-d* absorption at 680 nm vs time in incubates of 200  $\mu\text{M}$  CuZnSOD with EDTA, DTPA or GSSG. CuZnSOD only (diamonds), CuZnSOD with 10 mM DTPA (squares), 10 mM EDTA (triangles), and 5 mM GSSG (open circles). Samples were in 50 mM sodium phosphate buffer (pH 7.2), and absorbance at 680 nm was recorded at 5-min intervals after EDTA, DTPA or GSSG addition to  $\text{Cu}^{\text{II}}$ ZnSOD at 37°C.

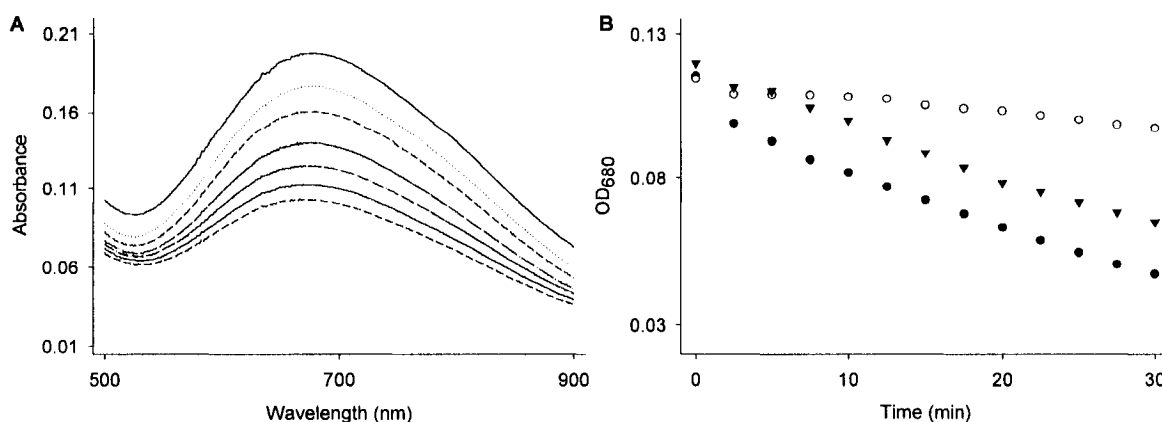


Figure 2.2  $\text{Cu}^{\text{II}}$  *d-d* absorption at 680 nm vs time of CuZnSOD/GSH incubates with and without EDTA or DTPA. (A) Spectrum of 690  $\mu\text{M}$  CuZnSOD plus 5 mM GSH at  $t = 0, 2.5, 5, 10, 15, 20,$  and 30 min. (B) Data points are the absorbance at 680 nm vs time of samples containing 400  $\mu\text{M}$  CuZnSOD plus 3.3 mM GSH (closed circles) and 3.3 mM EDTA (triangles) or 3.3 mM DTPA (open circles). Absorbances of samples in 50 mM sodium phosphate buffer (pH 7.2) were recorded in a 1-cm cuvette at 37°C immediately after GSH, DTPA or EDTA addition to CuZnSOD ( $t = 0$  min) and at 2.5-min intervals over 30 min.

**Table 2.1 Cu and Zn concentrations of CuZnSOD samples determined by ICP-MS**

Sample <sup>a</sup>	Cu (μM) ± SD <sup>b</sup>	Zn (μM) ±SD <sup>b</sup>
0.6 μM CuZnSOD	1.41 ± 0.326	1.28 ± 0.233
50 μM EDTA	0.19 ± 0.036	0.42 ± 0.052
50 μM DTPA	0.24 ± 0.036	0.06 ± 0.044
50 μM DDC	0.21 ± 0.005	0.35 ± 0.043
0.6 μM CuZnSOD + EDTA	1.40 ± 0.085	1.14 ± 0.198
0.6 μM CuZnSOD + DTPA	1.42 ± 0.230	1.11 ± 0.087
0.6 μM CuZnSOD + DDC	0.33 ± 0.027	0.71 ± 0.154

<sup>a</sup>CuZnSOD (60 μM) in PBS (pH 7.4) was incubated with 5 mM EDTA, DTPA or DDC at 37°C for 30 min and precipitated with acetone. The precipitates were acid digested and diluted 10<sup>3</sup>-fold for the ICP-MS analysis (see text). <sup>b</sup>Values are the averages of three separate trials.

**Table 2.2 SOD activity of CuZnSOD in the presence of EDTA and DTPA**

[chelator] <sup>b</sup> (mM)		% inhibition ± SD <sup>c</sup>	% Rel SOD activity <sup>d</sup>
	0	49.01 ± 0.39	100
EDTA	0.1	49.02 ± 1.45	100
EDTA	2.0	49.17 ± 0.94	100
DTPA	0.1	48.25 ± 0.58	98.4
DTPA	2.0	48.59 ± 0.45	99.1

<sup>a</sup>Assay solutions contained 10 μM cytc<sup>III</sup>, 3.3 nM CuZnSOD, 50 μM xanthine ± chelator in Chelex-100-treated 50 mM sodium phosphate buffer (pH 7.8). The assay was triggered by the addition of ~3.5 units/L xanthine oxidase. <sup>b</sup>Concentration of the chelator in assay solution. <sup>c</sup>CuZnSOD inhibition of cytc<sup>III</sup> reduction by O<sub>2</sub><sup>•-</sup> as calculated using Eq 2.9. Values given are the averages of three measurements. <sup>d</sup>The SOD activity of 3.3 nM CuZnSOD in the absence of chelator was taken as 100%.

77% of the Cu from CuZnSOD as well as 44% of the Zn (Table 2.1). Unlike EDTA, DDC is known to remove copper from the enzyme at neutral pH (120, 124).

#### **2.4.3 Effects of chelators on Cu<sup>II</sup>ZnSOD reduction**

Figure 2.2A shows the decrease in the 680-nm band over 30 min after adding 5 mM GSH to Cu<sup>II</sup>ZnSOD, which can be readily reduced ( $E_{\text{Cu}^{\text{II/I}}}^0 = 0.28\text{--}0.42\text{ V}$ ) (123, 125). Addition of 3.3 mM EDTA or DTPA significantly inhibited reduction of the active-site Cu<sup>II</sup> (Figure 2.2B), indicating that the chelators interfere with electron transfer from GSH to the copper possibly by interacting with CuZnSOD close to its active-site channel.

#### **2.4.4 Effects of chelators and GSH on SOD activity**

Using the xanthine oxidase-cyt<sup>c</sup><sup>III</sup> assay (Reactions 2.8, 2.9) (47, 105, 126), SOD activity was found to be linear in CuZnSOD concentration up to 6 nM enzyme (data not shown) as reported (127). To avoid interference from trace metal contaminants 0.1–1 mM EDTA or DTPA is routinely added to SOD activity assays (47, 105, 128). As shown in Table 2.2, negligible SOD activity changes were observed in the presence of 0.1–2 mM EDTA or DTPA as reported for the pyrogallol autoxidation assay (105).

Figure 2.3 shows that CuZnSOD preincubation at pH 7.2 and 37°C for 0–60 min with 2 mM EDTA, DTPA, GSSG or 5 mM GSH had no effect on its SOD activity. Since thiols interfere with the xanthine oxidase-cyt<sup>c</sup><sup>III</sup> assay by reducing cyt<sup>c</sup><sup>III</sup> (127), 5 mM GSH was added to the assay solution just prior to triggering the measurement. The activity of the control (CuZnSOD that was not preincubated with GSH) was also measured in the presence of thiol. The results reveal that although GSH reduces Cu<sup>II</sup>ZnSOD (Figure 2.2A), this does not interfere with its SOD activity (Figure 2.3). Consistent with previous reports (120, 124), 20 min CuZnSOD preincubation with DDC

at pH 7.2 resulted in > 90% SOD activity loss, which is attributed to Cu removal from the enzyme (Table 2.1).

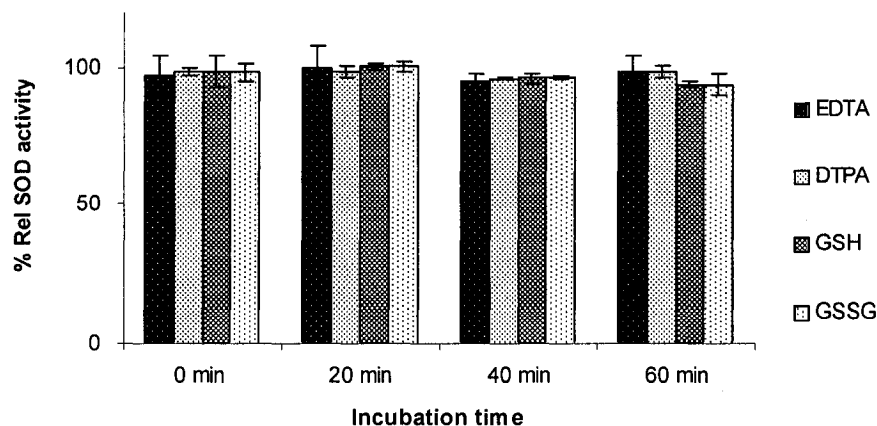


**Figure 2.3 Effects of preincubation with chelators, GSSG or GSH on SOD activity of CuZnSOD.** CuZnSOD (20  $\mu$ M) was preincubated with 2 mM EDTA, DTPA, GSSG or 5 mM GSH in 50 mM sodium phosphate buffer (pH 7.2) at 37°C for 60 min. Aliquots were removed every 20 min and assayed for SOD activity. Assay solutions contained 10  $\mu$ M cytc<sup>III</sup>, 50  $\mu$ M xanthine and 3.3 nM CuZnSOD in 50 mM sodium phosphate buffer/0.1 mM EDTA (pH 7.8). Where indicated, 2 mM chelator or GSSG was also present in the assay solution. To trigger the assay, ~3.5 units/L xanthine oxidase was added (as well as 5 mM GSH to the assay containing this reagent). The relative SOD activity of untreated CuZnSOD was taken as 100%.

#### 2.4.5 Effects of chelators on PGO-inactivation of SOD activity

Aliquots removed from the PGO incubates were diluted  $\sim 10^3$ -fold into the SOD assay solution. After 6 h preincubation with 40-fold molar excess of PGO, CuZnSOD exhibited  $\sim 25\%$  SOD activity (Figure 2.4), consistent with reports that PGO modification of Arg141 resulted in loss of 80–97% of SOD activity (55, 58, 108). Addition of EDTA or DTPA to the incubates increased the SOD activity remaining after 6 h to  $\sim 43\%$  (Figure 2.4), suggesting that these chelators had a protective effect on Arg141. In contrast, the uncharged copper chelator, neocuproine, offered CuZnSOD no protection against PGO inactivation (Figure 2.4).

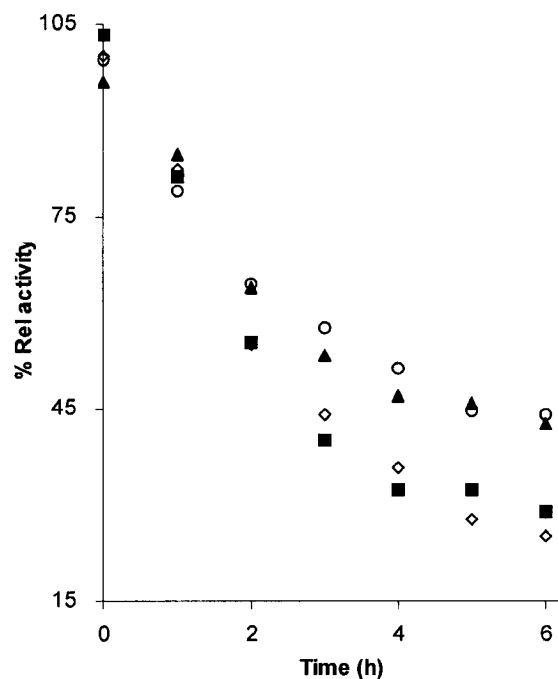
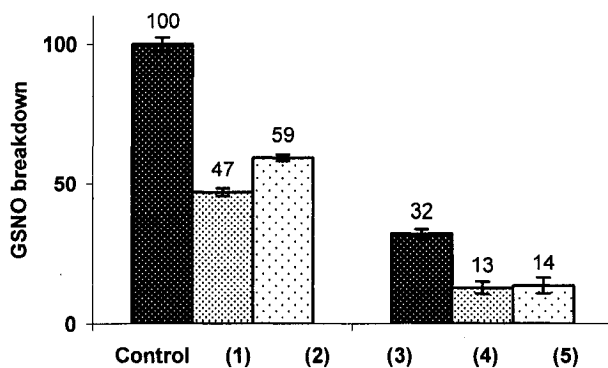


Figure 2.4 **Effects of preincubation with PGO without or with EDTA or DTPA on SOD activity of CuZnSOD.** CuZnSOD plus PGO only (open diamonds), and in the presence of 1 mM EDTA (triangles), 1 mM DTPA (open circles) or 1 mM neocuproine (squares). Experimental: 105  $\mu$ M CuZnSOD was incubated with 4.2 mM PGO in 250 mM  $\text{Na}_2\text{CO}_3$  (pH 8.0)  $\pm$  1 mM chelators with gentle shaking at RT for 6 h. Aliquots were removed, diluted 70-fold and 10  $\mu$ L was added to 3-mL of 50 mM sodium phosphate/0.1 mM EDTA (pH 7.8) and assayed for SOD activity as described in the Experimental Section. The relative SOD activity of CuZnSOD from <1 min incubates was taken as 100%.

#### 2.4.6 Effects of chelators and GSH on the GSNO-reductase activity of CuZnSOD

In the presence of 30  $\mu$ M CuZnSOD and 5 mM GSH,  $\sim$ 170  $\mu$ M GSNO decomposed in 30 min at 37°C. Addition of 2 mM DTPA or EDTA decreased GSNO decomposition to 47% and 59%, respectively (Figure 2.5), consistent with the chelators' inhibition of  $\text{Cu}^{\text{II}}$ ZnSOD reduction by GSH (Figure 2.2B). The data in Figure 2.5 also show that GSNO is decomposed by trace copper impurities in the samples but this is only 32% of GSNO decomposed in the presence of the enzyme. Thus, free copper is a less effective catalyst of GSNO reductive cleavage by GSH than CuZnSOD-bound copper as

we reported previously using P-SH in calbindin (82) and oxyhemoglobin (57) as reductants. Not surprisingly, the chelators also inhibited GSNO decomposition by free copper (Figure 2.5).



**Figure 2.5 Effects of EDTA and DTPA on the GSNO-reductase activity of CuZnSOD with GSH as a donor substrate.** Samples: (Control) GSNO/GSH/CuZnSOD, (1) GSNO/GSH/CuZnSOD/DTPA, (2) GSNO/GSH/CuZnSOD/EDTA, (3) GSNO/GSH, (4) GSNO/GSH/DTPA and (5) GSNO/GSH/EDTA. Experimental: solutions containing 470  $\mu$ M GSNO, 5 mM GSH, 30  $\mu$ M CuZnSOD, 2 mM DTPA, 2 mM EDTA where indicated were incubated in 50 mM sodium phosphate buffer (pH 7.2) at 37°C for 30 min. The GSNO remaining was determined spectrophotometrically ( $\epsilon_{333} = 0.76 \text{ mM}^{-1} \text{ cm}^{-1}$ ) and the decomposition of 170  $\mu$ M GSNO in the control was normalized to 100%. Each bar represents the mean  $\pm$  SD of triplicates.

Release of NO from GSNO (Reaction 2.2) was confirmed using oxyMb as a scavenger (Reaction 2.11). In the presence of GSNO alone  $\sim 5 \mu$ M oxyMb was converted to metMb over 20 min (Figure 2.6A) consistent with the decomposition of  $\sim 5 \mu$ M GSNO over 30 min in buffer only (data not shown). Addition of CuZnSOD plus GSH to the oxyMb/GSNO incubate resulted in the conversion of the limiting (25  $\mu$ M) oxyMb present to metMb in  $< 4$  min (Figure 2.6B), and release of NO was retarded on addition of DTPA or EDTA since oxyMb peaks are still clearly visible in the spectra after 20 min (Figures 2.6C,D).



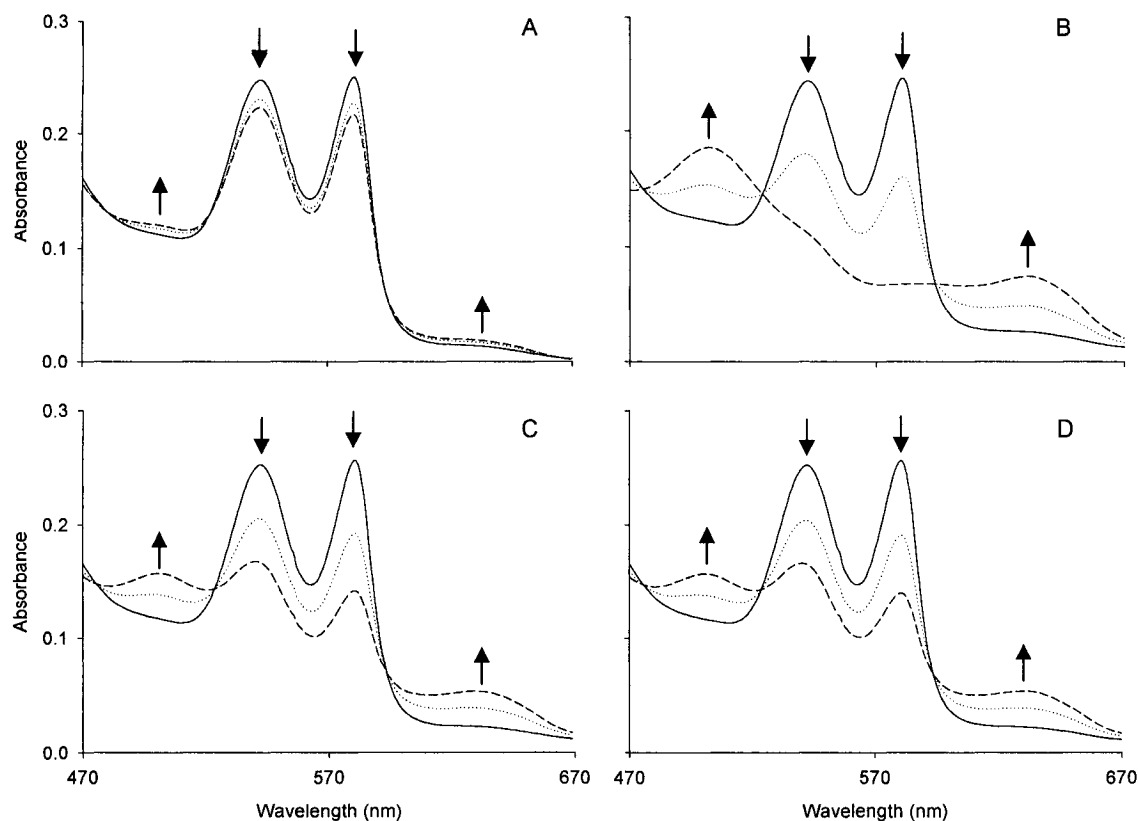
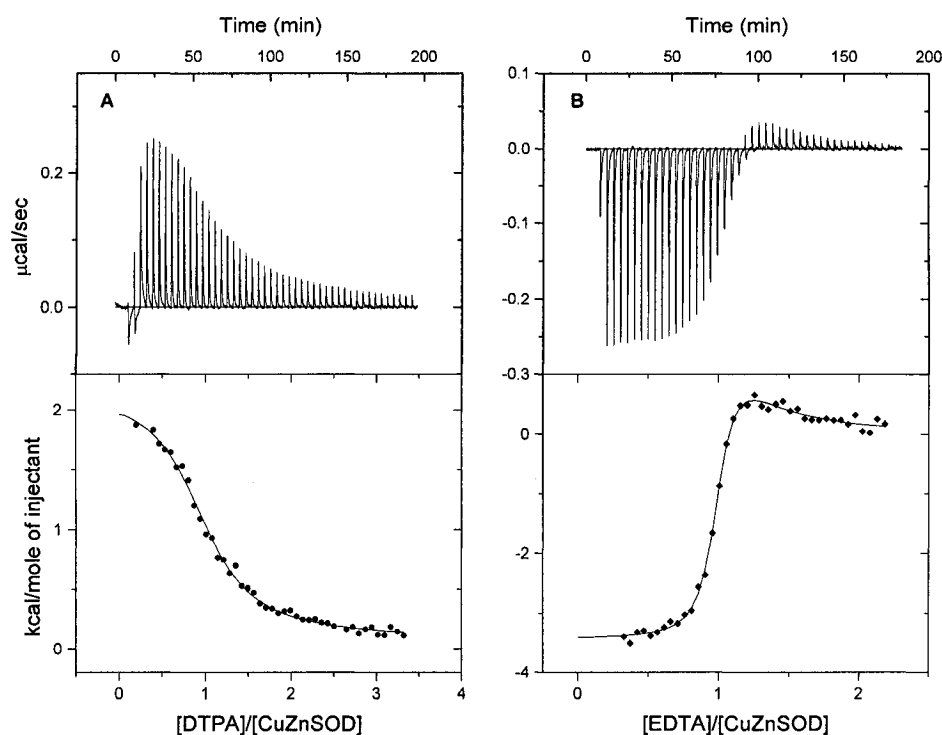


Figure 2.6 **OxyMb assay of effects of metal chelators on NO release from GSNO.** Incubates: (A) oxyMb/GSNO, (B) oxyMb/GSNO/GSH/CuZnSOD, (C) oxyMb/GSNO/GSH/CuZnSOD/EDTA, and (D) oxyMb/GSNO/GSH/CuZnSOD/DTPA. Experimental conditions: 25  $\mu$ M oxyMb and 145  $\mu$ M GSNO were incubated with 1 mM GSH, 20  $\mu$ M CuZnSOD and 1 mM chelator (where indicated) in 50 mM sodium phosphate buffer (pH 7.2) at 37°C for 20 min. Spectra in (A) were recorded in a 1-cm cuvette at  $t = 0, 12$  and 20 min; in (B) at  $t = 0, 2$  and 4 min; in (C) and (D) at  $t = 0, 12$  and 20 min. The down arrows at 542 and 580 nm indicate oxyMb decay, and the up arrows at 502 and 632 nm indicate metMb growth.

#### 2.4.7 Thermodynamic parameters for EDTA and DTPA association with CuZnSOD

ITC was employed to examine the association of EDTA and DTPA with CuZnSOD and EESOD. The heat change upon ligand binding to a protein is given by  $\Delta H_b = \Delta H_{ITC} - \Delta H_{blank}$ , where  $\Delta H_{ITC}$  is the apparent heat of binding measured by ITC and  $\Delta H_{blank}$  corrects for ligand dilution into the buffer only. The raw data obtained in the

titration of CuZnSOD with the chelators as ligands (Figure 2.7, top panels) reveal that DTPA binding is an endothermic process while EDTA binding is largely exothermic. The thermograms corresponding to integrated heat vs chelator/CuZnSOD-dimer molar ratio are displayed in the lower panels. Origin software provides three curve-fitting models involving one or two sets of binding sites and sequential binding sites (129). Best fits were obtained using one set of binding sites for DTPA and two sets of sites for EDTA (Figure 2.7, bottom panels).



**Figure 2.7 ITC analysis of DTPA and EDTA binding to CuZnSOD.** (A) 5- $\mu$ L aliquots of 806  $\mu$ M DTPA were injected into the 1.5-mL ITC cell containing CuZnSOD at an initial concentration of 41.0  $\mu$ M at 37°C. (B) 5- $\mu$ L aliquots of 501  $\mu$ M EDTA were injected into the 1.5-mL ITC cell containing CuZnSOD at an initial concentration of 36.1  $\mu$ M at 25°C. Both protein and chelators were in 50 mM phosphate buffer (pH 7.4). Top panels show the raw data for 45–48 injections of chelator into the CuZnSOD solution at 4-min intervals. The data points in the bottom panels are the integrated heats of binding ( $\Delta H_b$ ) after subtraction of blank ( $\Delta H_{\text{blank}}$ ). The solid lines correspond to the best fits of the data to (A) one set of binding sites and (B) two sets of binding sites using Origin Software.

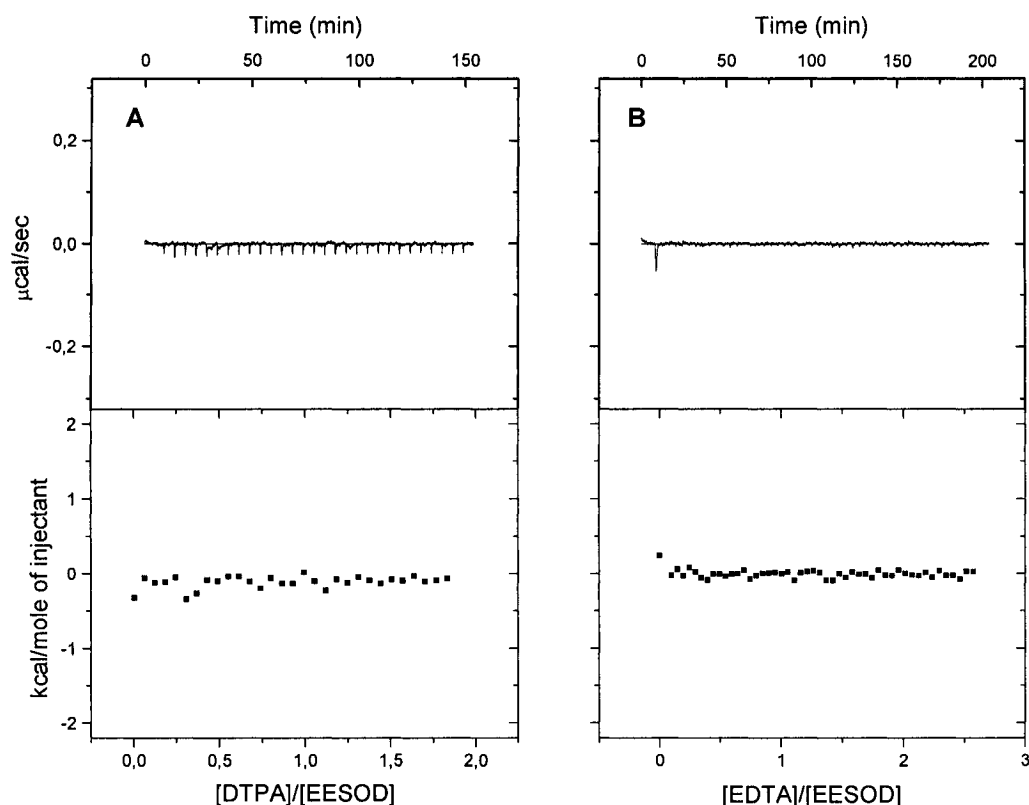


Figure 2.8 ITC analysis of EDTA and DTPA binding to EESOD. 5- $\mu\text{L}$  aliquots of 1 mM DTPA (A) or 806  $\mu\text{M}$  EDTA (B) were injected into the 1.5-mL ITC cell containing EESOD at an initial concentration of 55.4  $\mu\text{M}$  at 37°C, respectively. Both protein and chelators were in 50 mM phosphate buffer (pH 7.4). Top panels show the raw data for 30–50 injections of chelator into the EESOD solution at 4-min intervals. The data points in the bottom panels show the integrated heats.

The apparent number of chelator binding sites ( $n$ ) per CuZnSOD dimer and the thermodynamic parameters, including the dissociation constant ( $K_d$ ), the enthalpy ( $\Delta H$ ) and the entropy ( $\Delta S$ ) of binding are listed in Table 2.3. One EDTA molecule per CuZnSOD dimer binds to the high-affinity site with a  $K_d$  of  $\sim 80$  nM. Thus, a single EDTA molecule interacts with both monomers or EDTA binding to one monomer inhibits binding of a second EDTA molecule binding to the dimer. The stoichiometry of the EDTA low-affinity site  $K_d$  ( $\sim 4$  micromolar) is 0.2–0.4 chelator molecules per dimer,

which suggests that binding of EDTA to the high-affinity site inhibits binding of a second EDTA. Based on the  $K_d$  values (Table 2.3), DTPA affinity for the CuZnSOD dimer is two orders of magnitude lower than that for EDTA at 25°C. Furthermore, the negative  $\Delta H_b$  and positive  $\Delta S_b$  values reveal that EDTA binding to CuZnSOD is both enthalpically and entropically favourable whereas both  $\Delta H_b$  and  $\Delta S_b$  values are positive for DTPA indicating that DTPA binding is entropically driven. Significantly, binding to the low-affinity EDTA site exhibits binding parameters similar to those obtained for DTPA especially at 37°C. Also, since the 25°C and 37°C enthalpy and entropy values vary, the chelator/CuZnSOD complexes may undergo temperature-dependent rearrangement.

**Table 2.3 Thermodynamic parameters from the titration of CuZnSOD with EDTA and DTPA<sup>a</sup>**

Chelator <sup>b</sup> ( <i>T</i> )	<i>n</i> <sup>c</sup>	$K_d$ ( $\mu\text{M}$ )	$\Delta H_b$ (kcal/mol)	$\Delta S_b$ (cal/K·mol)
EDTA <sup>(1)</sup> (25°C)	1.09 ± 0.16	0.08 ± 0.02	−3.42 ± 0.02	21.05 ± 0.7
(37°C)	0.83 ± 0.16	0.03 ± 0.02	−2.59 ± 0.41	24.29 ± 4.9
EDTA <sup>(2)</sup> (25°C)	0.23 ± 0.01	4.25 ± 11.1	3.65 ± 0.07	36.39 ± 2.1
(37°C)	0.38 ± 0.03	3.25 ± 3.12	2.21 ± 0.28	32.24 ± 1.8
DTPA (25°C)	0.97 ± 0.04	8.26 ± 0.20	1.19 ± 0.24	27.23 ± 0.8
(37°C)	1.04 ± 0.02	7.58 ± 0.99	2.43 ± 0.20	31.25 ± 0.4

<sup>a</sup>Data were fit to two binding sites (EDTA) and one binding site (DTPA) models using Origin Software. The binding parameters given are the average of three measurements. <sup>b</sup>The experimental conditions are given in the legend of Figure 2.7. EDTA<sup>(1)</sup> and EDTA<sup>(2)</sup> refer to the two binding sites detected and the ITC experiments were performed at the temperatures indicated (*T*). <sup>c</sup>The stoichiometry of binding is the chelator/CuZnSOD dimer molar ratio.

Chelator association with metal-free EESOD was also examined. Contrary to expectation, the same heat changes were recorded on titration of the buffer ( $\Delta H_{blank}$ ) (data not shown) and EESOD with both EDTA and DTPA ( $\Delta H_{ITC}$ ) (Figure 2.8). Thus, the EESOD thermograms show no heat changes revealing that the metals promote the association of the chelators with CuZnSOD.

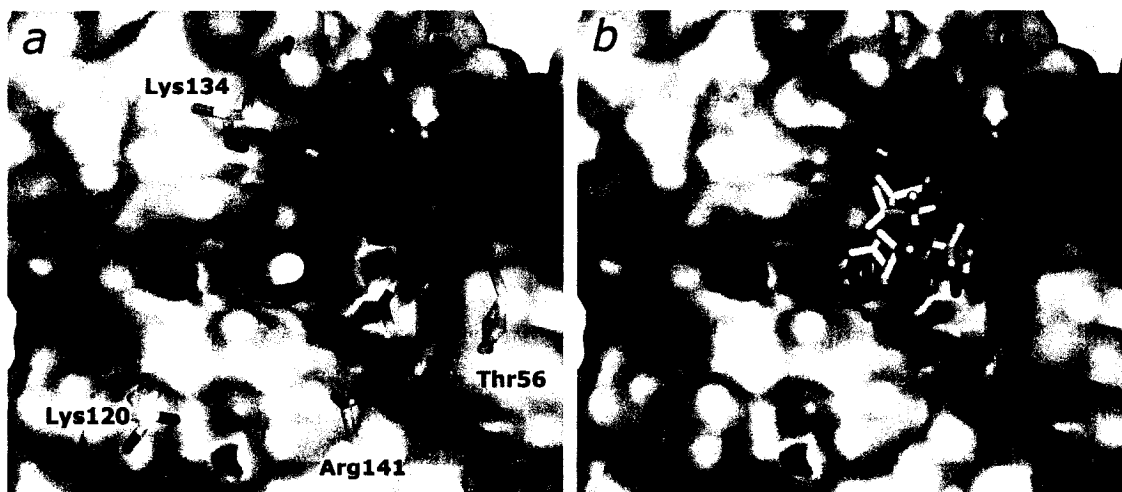


Figure 2.9 **Docking of EDTA into the active-site channel of bovine CuZnSOD.** (A) Molecular surface and electrostatic potential map of the active-site channel of CuZnSOD. Thr56 and Glu131 form the opening of the active-site cavity. An electrostatic loop consisting of the positively charged side chains of Arg141, Lys120 and Lys134 guides the anionic superoxide substrate to the copper center. Arg141 with Thr135 act as a ‘bottleneck’ for the active site, limiting the access of bulky anions to the copper shown as a yellow sphere at the bottom of the active-site channel (130). (B) Docking of the EDTA molecule into the active-site channel demonstrates that a carboxylic group of EDTA can access the active-site copper. The electrostatic potential surface of CuZnSOD was obtained using the reported crystal structure (131), which was pre-processed with PDB2PQR program (132), and the electrostatic potential was calculated by the APBS package (133) and visualized with PyMOL (134).

## 2.5 Discussion

The ITC data summarized in Table 2.3 reveal that the CuZnSOD homodimer binds a single polyaminocarboxylate chelator.  $K_d$  values of 0.08  $\mu\text{M}$  and 8.3  $\mu\text{M}$ ,

respectively, at 25°C, where obtained for EDTA and DTPA association with the enzyme and a second low-affinity EDTA site was also detected but with low binding stoichiometry (Table 2.2). Since it was previously reported that Arg141 is a phosphate binding site in CuZnSOD (58) and EESOD binds EDTA (113), we presumed that the chelator binding site included Arg141 and possibly Lys134 and/or Lys120 (Figure 2.9A). However, no evidence for association of the chelators with metal-free EESOD was obtained by ITC (Figure 2.8), indicating that the active-site copper is necessary for the high-affinity binding observed here.

The x-ray structure shows that active-site cavity of bovine CuZnSOD is ~15-Å deep, 12-Å wide near the protein surface and narrows to ~3 Å at the catalytic copper, which has a solvent exposed surface of ~5 Å<sup>2</sup>. The copper is coordinated by His44, His46, His61 and His118 and a weakly bound water molecule which occupies the axial position of a distorted square pyramid and is directed towards the cavity opening. Strong ligands such as CN<sup>-</sup> and N<sub>3</sub><sup>-</sup> bind to Cu<sup>II</sup>ZnSOD and cause a weakening of the Cu-His46 bond (135). The zinc, which is completely buried in the protein, is bridged to the copper by the imidazolate side-chain of His61. Since the only access to the copper is from the active-site cavity, the chelators must enter *via* the channel. This interaction would be promoted by the positive residues lining the channel such as Arg141, Lys120 and Lys134 (Figure 2.9A). In fact, it has been suggested that phosphate bridges Arg141 and cobalt in the CoZnSOD metalloderivative leading to cleavage of the imidazolate bridge and movement of the tetrahedral cobalt towards the cavity (136). A similar situation can be envisaged whereby the copper moves towards an oxygen donor atom of the chelator but remains bound to the polypeptide, which has a high affinity for the metal ( $K_d = 6$  fM)

(100). Consistent with this proposal, the  $\text{Cu}^{\text{II}}\text{ZnSOD}$ -chelator complexes are  $>10^{11}$ -fold lower in stability than the  $\text{Cu}(\text{EDTA})^{2-}$  and  $\text{Cu}(\text{DTPA})^{3-}$  complexes with  $\log K_a$  values of 18.8 and 21.1, respectively (137). The ICP-MS analysis (Table 2.1) confirmed that EDTA or DTPA do not sequester any metal from  $\text{CuZnSOD}$  at pH 7.4. In contrast, incubation with DDC, which is known to remove copper from the enzyme at neutral pH (120, 138), led to significant demetallation (Table 2.1), and EESOD was formed in EDTA incubates at pH 3.8 (47, 113, 114) with loss of SOD activity (see Appendix 1).

A network of well-ordered water molecules is found in the active-site cavity of  $\text{CuZnSOD}$ . This network extends from the bottom of the cavity in two directions and connects the copper-bound water to the solvent. The large favourable entropies for chelator binding (21–36 eu, Table 2.3) are consistent with release of water from the cavity to the bulk solvent as well as dissociation of the aquo and histidyl ligands from the copper. The latter bond cleavages are expected to be enthalpically unfavourable and would contribute to the low binding enthalpies observed for the chelators. In particular, the positive binding enthalpy for DTPA suggests that there is negative compensation between bond making and breaking in the  $\text{CuZnSOD}/\text{DTPA}$  complex. Ionization of the chelators, which are hexaprotic (EDTA) and octaprotic (DTPA) acids, may also contribute to the observed heats of binding.

The data in Figures 2.1, 2 and 4 provide additional support for the binding of the chelators in the active-site channel. The loss of the 680-nm *d-d* absorption (Figure 2.1) may be due to direct  $\text{Cu}^{\text{II}}$ -EDTA and  $\text{Cu}^{\text{II}}$ -DTPA binding as well as to additional interaction with Arg141 since modification of this residue is known to alter the *d-d* absorption (55). GSH is a poorer reductant of  $\text{Cu}^{\text{II}}\text{ZnSOD}$  in the presence of the chelators

(Figure 2.2B), which could reflect decreased GSH accessibility to the copper in the enzyme-chelator complexes. Less SOD activity was lost in CuZnSOD/PGO incubates containing EDTA or DTPA (Figure 2.4), suggesting that the chelators decreased PGO access to Arg141 at  $\sim 5$  Å from the copper. Based on NMR data (139), binding of formate *via* H-bonding of its oxygens to the N $^{\epsilon}$  and NH $_2$  atoms of the Arg141 side chain was proposed. The formate carboxylate carbon, also at a distance of  $\sim 5$  Å from the copper, did not displace the coordinated water (139). However, the additional carboxylate groups in the polyaminocarboxylate chelators would allow them to bind the active-site copper as well as Arg141, which would explain their  $10^4$ – $10^6$ -fold higher affinity for the protein ( $K_d = 0.08$ – $8$   $\mu$ M, Table 2.3) compared to formate ( $K_d = 0.24$  M).

Relevant to the 2:1 Cu<sup>II</sup>/chelator stoichiometry observed here (Table 2.3), it was found that both Fe(CN) $_6^{3-}$  and IrCl $_6^{2-}$  bound preferentially to a single CuZnSOD subunit rendering one of the Cu<sup>II</sup> non-titratable (125). The iridium complex was used to form a heavy-atom derivatives of CuZnSOD and the major IrCl $_6^{2-}$  binding site involves Arg141 (140). Thus, binding of a large anion in the active-site cavity of one subunit appears to induce conformational change at the other active site although the copper atoms are 34 Å apart (140).

Coordination of EDTA with the active site copper was visualized by manually docking EDTA into the active-site channel with PyMol software (Figure 2.9B). Docking the chelator into the static enzyme molecule demonstrates that, contrary to expectation, one of EDTA's carboxylate groups can coordinate to the active-site copper without reorganization of groups in the active-site cavity. Furthermore, the concentration of positive electrostatic potential (blue) around the cavity (Figure 2.9) should promote



binding of anionic ligands in the cavity. Nonetheless, copper binding has also been observed for uncharged ligands, which underscores its accessibility and reactivity. For example, addition of DDC and neocuproine to Cu<sup>II</sup>ZnSOD gave rise to new absorption bands at 450 nm and 454 nm, respectively, but on dilution of the enzyme into the assay buffer no loss of SOD activity was observed (56, 124).

Why do the chelators selectively inhibit the GSNO reductase activity of CuZnSOD? The inhibitory effect of DTPA and EDTA on the GSNO-reductase activity of CuZnSOD (Reactions 2.1, 2.2) is demonstrated in Figures 2.5 and 6. Since Cu<sup>I</sup>-catalyzed GSNO breakdown is rapid (35), the rate-limiting step in GSNO turnover by CuZnSOD/GSH is assumed to be formation of the cuprous enzyme (Reaction 2.1). As shown here, the chelators retard Cu<sup>II</sup>ZnSOD reduction by GSH (Figure 2.2B). Additionally, the GSSG oxidation product, known to chelate Cu<sup>II</sup> and inhibit free-copper-catalyzed GSNO decomposition (27, 34), likely inhibits Cu<sup>II</sup>ZnSOD reduction by GSH since the enzyme is not fully reduced even in the presence of a large excess of this thiol (82). Also, Jourdeuil observed 90% decomposition of 10  $\mu$ M GSNO by CuZnSOD in the presence of 50  $\mu$ M GSH whereas we observed only 36% decomposition of 470  $\mu$ M GSNO in the presence of 5 mM GSH, which is consistent with product inhibition by the GSSG generated in GSNO turnover (Reaction 2.3). However, as we reported previously (82), addition of 5 mM GSSG did not alter the 680-nm absorption of CuZnSOD (Figure 2.1) nor its SOD activity (Figure 2.3).

An electrostatic loop consisting of the positively charged side chains of Arg141, Lys120 and Lys134 (Figure 2.9A) are located at 5, 12 and 13 Å, respectively, from the copper (58, 107). These residues promote access of superoxide, small anionic inhibitors

such as cyanide and water to the copper (50, 109-111, 141). The reported bimolecular rate constant for reduction of Cu<sup>II</sup>ZnSOD by O<sub>2</sub><sup>•-</sup>, which involves direct O<sub>2</sub><sup>•-</sup> binding to Cu<sup>II</sup>, is  $\sim 2 \times 10^9 \text{ M}^{-1} \text{ s}^{-1}$  at 25°C (47, 103, 142). Binding of superoxide to the enzyme is the rate-limiting step in SOD catalysis (52, 143) and saturation is not observed in assays carried out at low superoxide concentrations such as those used here. Since neither EDTA nor DTPA binding alters the SOD activity (Table 2.2), the chelators must not alter the overall rate of Cu<sup>II</sup> reduction by O<sub>2</sub><sup>•-</sup>. CuZnSOD binds one chelator per homodimer (Table 2.3), so it is likely that only one copper is active in O<sub>2</sub><sup>•-</sup> turnover in the CuZnSOD-chelator complex. Thus, chelator binding to one copper must increase the SOD activity and decrease the GSNO-reductase activity at the second copper. The latter observation is in fact consistent with the negative cooperativity in the association of the chelators, as well as Fe(CN)<sub>6</sub><sup>3-</sup> and IrCl<sub>6</sub><sup>2-</sup>, with CuZnSOD. Since the homodimer does not bind two large ligands, it is not surprising that large substrates such as GSH and GSNO have decreased access to the second copper in the CuZnSOD-chelator complexes. Alternatively, CuZnSOD may exhibit half-site reactivity in both its free and chelator-bound forms, with both forms possessing the same SOD activity but only the free form possessing GSNO-reductase activity. Half-site reactivity has been demonstrated for enzymes composed of identical subunits such as the tyrosyl-tRNA synthase homodimer (144).

## 2.6 Conclusions

CuZnSOD, abundant in the red blood cell and many other cell types, likely mediates NO metabolism by “moonlighting” as a GSNO reductase. Given its high

affinity for a single EDTA or DTPA ligand, negatively charged metabolites such as 2,3-diphosphoglycerate found in red blood cells (145) may bind to CuZnSOD *in vivo* and modulate NO signalling by altering its GSNO-reductase (Reactions 2.1, 2.2) or NO-transferase (Reactions 2.1', 2.2 and 2.4) activities. CuZnSOD exhibits negative cooperativity in binding large anions, which may serve to prevent nonproductive GSH turnover *in vivo* and also control GSNO turnover. The conformational changes in the homodimer resulting in negative cooperativity would have to double  $O_2^{\bullet -}$  turnover at the single active site in the CuZnSOD-chelator complexes unless the free enzyme exhibits half-site reactivity. Irrespective of the mechanistic details, it is essential to consider the effects of polyaminocarboxylate chelators on the GSNO-reductase activity of CuZnSOD in studies on GSNO and NO biochemistry.

## **2.7 Acknowledgements**

This research was supported by the Canadian Institutes for Health Research (CIHR) and Natural Sciences and Engineering Research Council of Canada (NSERC) to A. M. E. We would like to thank Professor Eric Salin and Megan Marshall from the Department of Chemistry, McGill University (Montreal) for help with the ICP-MS measurements, and Dr Qadir Timerghazin for preparing Figure 2.9.

## Appendix 1.0 Supplementary Experimental Data for Chapter 2.0

### A1.1 UV-Vis absorption spectrum of EESOD

Metal- and EDTA-free SOD (EESOD) was prepared as described by McCord and Fridovich (47, 113) (see Section 2.3.2.6). The UV-Vis spectrum of EESOD (solid line in Figure A1.1) was recorded on Beckman DU800 spectrophotometer. Obvious absorbance differences were observed between the spectra of native BCuZnSOD and its apo form (Figure A1.1B vs A)). As reported in literature (47), BCuZnSOD exhibits a unique ultraviolet spectrum with fine structure in 250–270 nm region due to its phenylalanine residues, and maximum absorption at 258 nm ( $\epsilon = 10.300 \text{ mM}^{-1}\text{cm}^{-1}$ ) (Figure A1.1B). In addition, the  $\text{Cu}^{\text{II}}$ ZnSOD form has a broad, weak visible band at 680 nm ( $\epsilon = 300 \text{ M}^{-1}\text{cm}^{-1}$ ) which is attributed to copper *d-d* transitions (Figure A1.1B, insert). The spectrum of the metal-free form is consistent with that reported by Fee with fine structure in the 250–280-nm region, an extinction coefficient at 258 nm of  $2.92 \text{ mM}^{-1}\text{cm}^{-1}$  (146), and loss of the *d-d* absorption band (insert in Figure A1.1A vs 1B) confirming removal of copper from the active-site.

### A1.2 UV-Vis absorption spectrum of the EESOD/DDC incubation

As described in Section 3.4.1, the 452-nm absorption band of  $\text{Cu}^{\text{II}}(\text{DDC})_2$  grows in the spectrum of the CuZnSOD/DDC incubation (Figure 3.4) indicating that DDC coordinates the active-site copper (120, 124). EESOD (55.4  $\mu\text{M}$ ) was also incubated with 1 mM DDC at RT over 10 min. As can be seen from Figure A1.2, the 452-nm absorption

of the  $\text{Cu}^{\text{II}}(\text{DDC})_2$  complex was not observed confirming that copper was removed from the active-site.

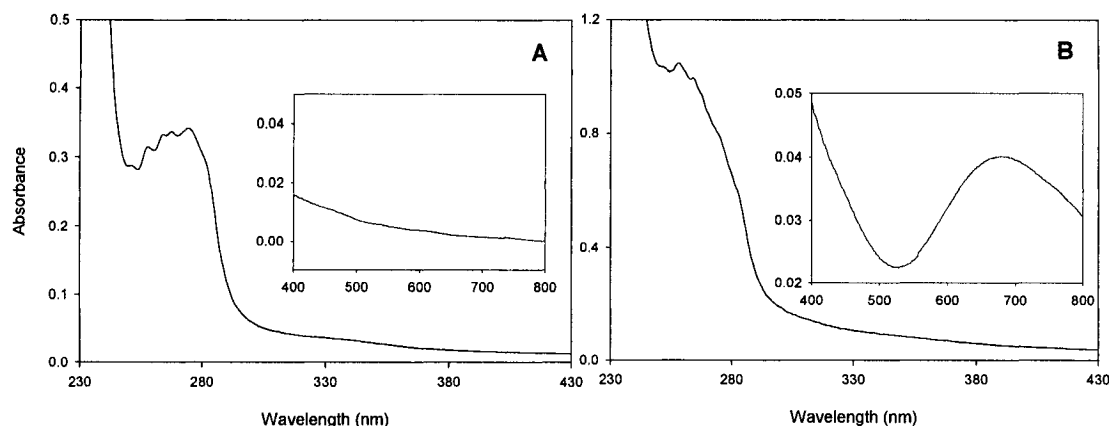


**Figure A1.1 Absorption spectrum of BCuZnSOD in its metal-free (A) and native (B) forms.** EESOD was prepared from  $\sim 120 \mu\text{M}$  native BCuZnSOD as described in Section 2.3.2.6. Spectra of  $\sim 120 \mu\text{M}$  protein in 50 mM sodium phosphate buffer (pH 7.4) were recorded in a 1-cm quartz cuvette at RT. Inserts in (A) and (B) are the spectra in *d-d* absorption region expanded 5- and 20-fold, respectively.

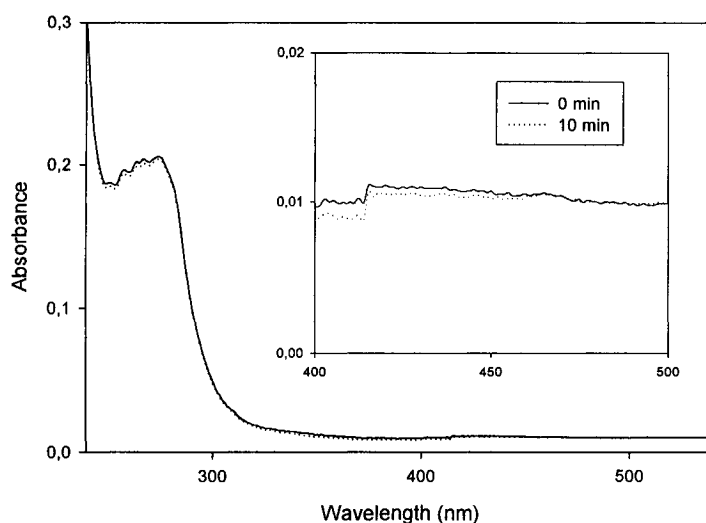


**Figure A1.2 Absorption spectrum vs time of the EESOD/DDC incubation.** Spectrum at  $t = 0$  min (solid line) and  $t = 10$  min (dashed line) of  $55.4 \mu\text{M}$  EESOD with 1 mM DDC in 50 mM sodium phosphate buffer (pH 7.4) at RT. The absorbance was recorded immediately in a 1-cm quartz cuvette after DDC addition to EESOD and after a 10-min interval. The inset shows the spectrum in the region of the  $\text{Cu}^{\text{II}}(\text{DDC})_2$  visible absorption band expanded 10-fold.

### A1.3 SOD activity of EESOD

The SOD activity of the metal-free and native enzymes was compared using the xanthine oxidase-cytc<sup>III</sup> reduction assay (see Section 2.3.2.3). The residual SOD activity of EESOD was  $(6.4 \pm 0.28)\%$  that of the holoenzyme (Table A1.1) suggesting that the active-site copper was almost completely removed by dialysis against EDTA at pH 3.8.

Table A1.1 SOD activity of EESOD vs native BCuZnSOD<sup>a</sup>

4.2 nM Enzyme	% inhibition $\pm$ SD <sup>b</sup>	% Rel SOD activity
CuZnSOD	$57.89 \pm 1.61$	100
EESOD	$3.72 \pm 0.16$	$6.42 \pm 0.28$

<sup>a</sup>Assay solutions contained 10  $\mu$ M cytc<sup>III</sup>, 4.2 nM CuZnSOD, 50  $\mu$ M xanthine in 50 mM sodium phosphate buffer/0.1 mM EDTA (pH 7.8). The assay was triggered by the addition of  $\sim 3.5$  units/L xanthine oxidase.

<sup>b</sup>CuZnSOD inhibition of cytc<sup>III</sup> reduction by O<sub>2</sub><sup>•−</sup> as calculated using Eq 2.9 in Section 2.3.2.3. Values given are the averages of three measurements.

### A1.4 ESI-ToF mass spectrum of EESOD

Figure A1.3 shows the deconvolved ESI-mass spectrum recorded for  $\sim 5$   $\mu$ M EESOD in 60% ACN/0.1% TFA. The measured mass of 15,591 u matches the calculated mass of 15,551 u based on protein's sequence plus an additional 42 u due to *N*-terminal acetylation minus 2 u due to disulfide bond between Cys33 and Cys144 (Section 4.4.5).

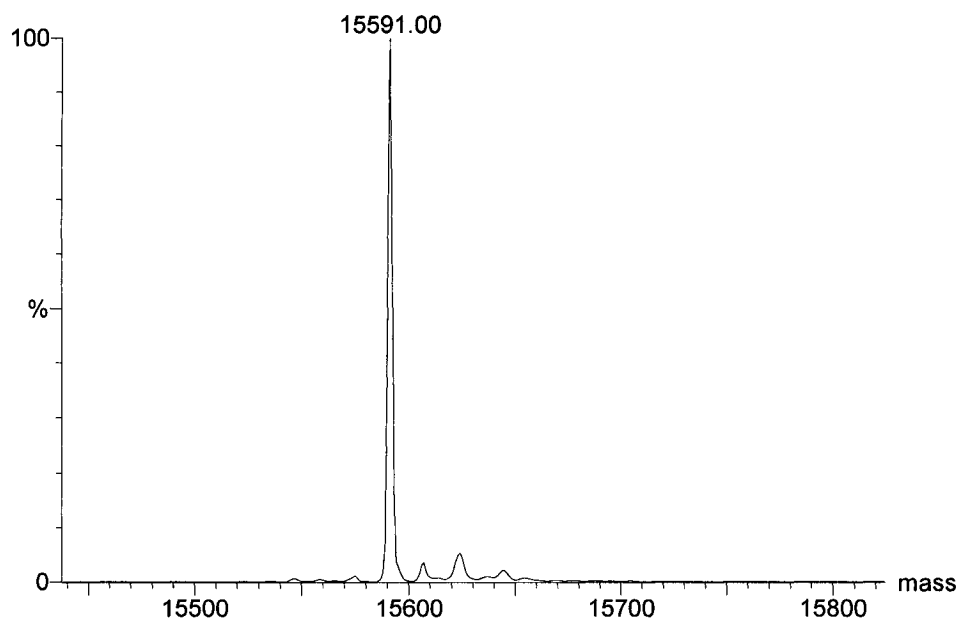


**Figure A1.3 ESI mass spectrometric analysis of EESOD.** EESOD was prepared as described in Section 2.3.2.6 and the protein concentration was measured using the Bio-Rad assay. A 50- $\mu$ L aliquot of 1% TFA was added to a 8- $\mu$ L aliquot of 55  $\mu$ M EESOD in 50 mM sodium phosphate buffer (pH 7.4) to decrease the pH to 3–4. The sample was desalted on a ZipTipC<sub>18</sub>, eluted from the tip into 50  $\mu$ L of 60% ACN/0.1% TFA, and directly infused at a flow rate of 2  $\mu$ L/min into the Z-spray ion source of the mass spectrometer. The mass spectrometric parameters are given in the legend of Figure 4.1.

### 3.0 Effects of copper colorimetric reagents on the GSNO-reductase and SOD activities of CuZnSOD

#### 3.1 Abstract

The effects of the copper colorimetric reagents, neocuproine (neo), diethyldithiocarbamate (DDC) and cuprizone (cup), on GSNO-reductase and SOD activity of bovin CuZnSOD (BCuZnSOD) were examined. Incubation with these chelators alters the  $\text{Cu}^{\text{II}}$  *d-d* absorption of BCu<sup>II</sup>ZnSOD at 680 nm and gives absorption characteristic of the  $\text{CuL}_2$  complexes suggesting that the chelators bind to the active-site copper. Growth of  $\text{Cu}^{\text{I}}(\text{neo})_2$  absorption at 454 nm accompanied the decrease of the 680-nm  $\text{Cu}^{\text{II}}$  *d-d* absorption when 95  $\mu\text{M}$   $\text{Cu}^{\text{II}}$ ZnSOD was incubated with 380  $\mu\text{M}$  neo in the presence of 190  $\mu\text{M}$  GSH at 37°C for 25 min. The extent of copper removal as  $\text{Cu}^{\text{I}}(\text{neo})_2$  on extraction of the complex into isoamyl alcohol was only ~6% of total copper in BCuZnSOD dimer. No significant SOD activity change was detected following BCuZnSOD/neo incubation, supporting negligible removal of the active-site copper. Also, unlike EDTA and DTPA (Chapter 2), neo did not protect BCuZnSOD from phenylglyoxal (PGO) inactivation suggesting that it does not hinder Arg141 modification. DDC removes ~76% of the active-site copper from BCuZnSOD as determined spectrophotometrically and by ICP-MS, and 90% SOD activity is lost after incubation of 61  $\mu\text{M}$  BCuZnSOD with 5 mM DDC at 37°C and pH 7.2 for 20 min. Approximately 3% of the active-site copper was converted to  $\text{Cu}^{\text{II}}(\text{cup})_2$  complex over 30 min as determined from its 600-nm absorbance. No loss of SOD activity was detected following BCuZnSOD/cup incubation. The order of inhibition the GSNO-reductase



activity of BCuZnSOD by the colorimetric reagents is: DDC > neo > cup. DDC is a highly efficient inhibitor of the GSNO-reductase activity since it removes copper from BCuZnSOD. Neo partially inhibits the GSNO-reductase activity since it binds to, but does not remove, copper from BCuZnSOD. Cup interacts weakly with the active-site copper consistent with its small effect on the GSNO-reductase activity.

### 3.2 Introduction

In Chapter 2.0, the polyaminocarboxylate metal-ion chelators, EDTA and DTPA, were reported to inhibit the GSNO-reductase activity of BCuZnSOD due to their association with the active-site copper and with Arg141. Since EDTA and DTPA bind to a single active-site copper per homodimer without changing the metal loading or the SOD activity of BCuZnSOD, we proposed that EDTA or DTPA binding prevents access of large (*e.g.*, GSH, GSNO) but not small ( $O_2^{\bullet -}$ ) substrates to the active-site copper and/or that BCuZnSOD exhibits half-site SOD activity. It has been proposed by Fielden *et al.* (147) and demonstrated by Lawrence *et al.* (125) that the two copper centers of CuZnSOD are nonequivalent.

Chelators such as diethyldithiocarbamate (DDC, 1), cuprizone (cup, 5) and neocuproine (neo, 3) are used widely as copper-chelating agents in the colorimetric determination of copper in various samples including biological materials (148-155). They are also used in the identification of mechanisms dependent on free- vs enzyme-bound copper as described below. DDC, a  $Cu^{II}$ -specific reagent (156-158), is frequently used to inhibit CuZnSOD activity *in vitro* and *in vivo* by chelating  $Cu^{II}$  (120, 124, 138, 159-161). For example, the toxicity of superoxide radicals generated from compounds

such as paraquat and 1,4-naphthoquinone 2-sulfonate was demonstrated in DDC-treated erythrocytes to inhibit the SOD activity of CuZnSOD (162, 163). DDC-treated tissues were used to investigate the inhibition of nitrgergic relaxations (NO-dependent) in the presence of CuZnSOD (164, 165).

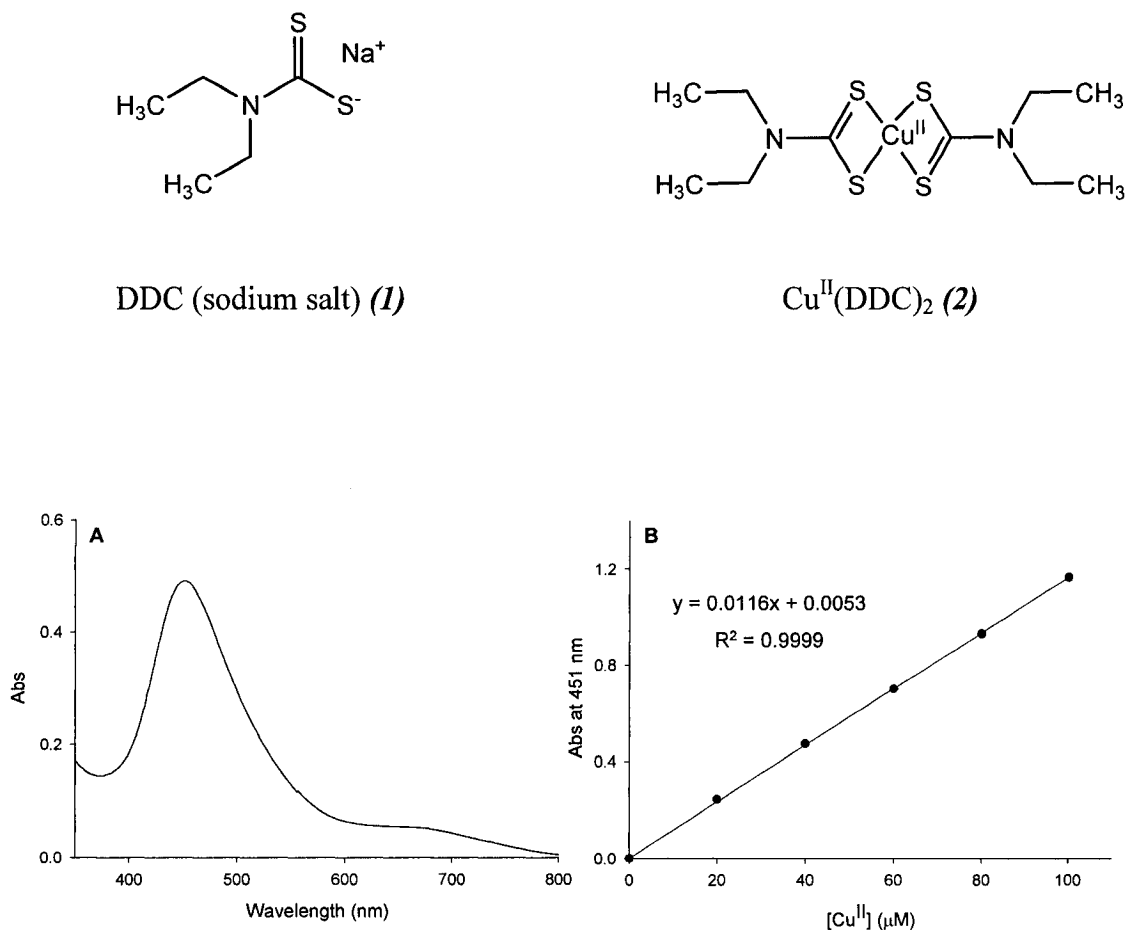
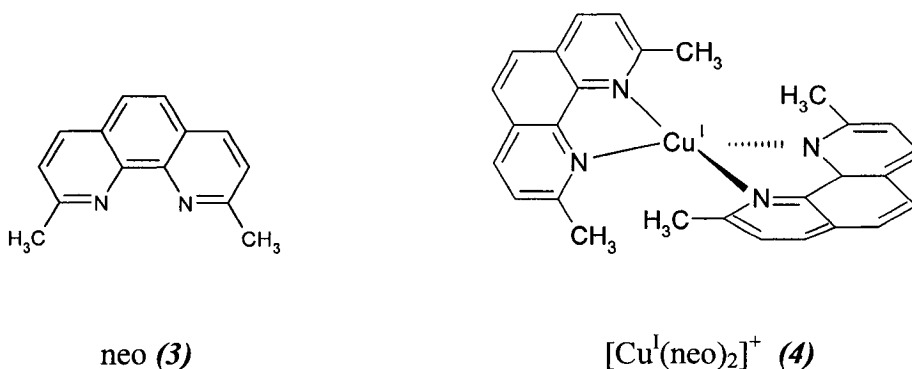


Figure 3.1 **Visible absorption spectrum of Cu<sup>II</sup>(DDC)<sub>2</sub> and calibration curve for the colorimetric determination of copper.** (A) The spectrum of a sample containing 42 μM Cu<sup>II</sup> and 5 mM DDC in H<sub>2</sub>O recorded in a 1-cm quartz cuvette at RT. (B) Calibration curve generated by adding 0–100 μM Cu<sup>II</sup> from a 1000 ppm Cu<sup>II</sup> standard solution in H<sub>2</sub>O to 5 mM DDC in H<sub>2</sub>O and reading the absorbance at 451 nm following mixing in a 1-cm quartz cuvette at RT.

DDC (*1*) chelates cupric ions to form a golden brown complex,  $\text{Cu}^{\text{II}}(\text{DDC})_2$  (*2*) with an absorption maximum at 450 nm (Figure 3.1A). Extinction coefficients reported in the literature include  $12.0 \text{ mM}^{-1}\text{cm}^{-1}$  for the  $\text{Cu}^{\text{II}}$ -DDC species formed in the presence of CuZnSOD (*124*),  $8.0\text{--}12.1 \text{ mM}^{-1}\text{cm}^{-1}$  for *2* in aqueous solutions in the pH range 0.1–9.5 (*124*, *148*, *152*, *166*), and  $12.7 \text{ mM}^{-1}\text{cm}^{-1}$  in amyl alcohol (*152*). DDC is not specific for copper since it forms colored complexes with other metals, including nickelous, ferric, ferrous, bismuth, uranyl, cobaltous, and dichromate ions (*148*).

Neo (2,9-dimethyl-1,10-phenanthroline, *3*) was first employed in the colorimetric determination of copper by Smith and McCurdy (*149*). Neo is specific for the cuprous ion (*167*) since no other cations react with neo to produce the bright orange complex with an absorption maximum at 454 nm (Figure 3.2). The specificity arises because  $\text{Cu}^{\text{I}}$  adopts a tetrahedral geometry with the planes of the two phenanthroline ligands at right angles to each other (*4*) (*149*, *168*). The molar extinction coefficient of  $[\text{Cu}^{\text{I}}(\text{neo})_2]^+$  (*4*) is  $7.95 \text{ mM}^{-1}\text{cm}^{-1}$  in isoamyl alcohol (*149*, *167*), and the colored complex formed over the pH range 3–10 obeys Beer's law between 2.36–166.8  $\mu\text{M}$  Cu with a 0.8 ppm Cu detection limit (*149*).



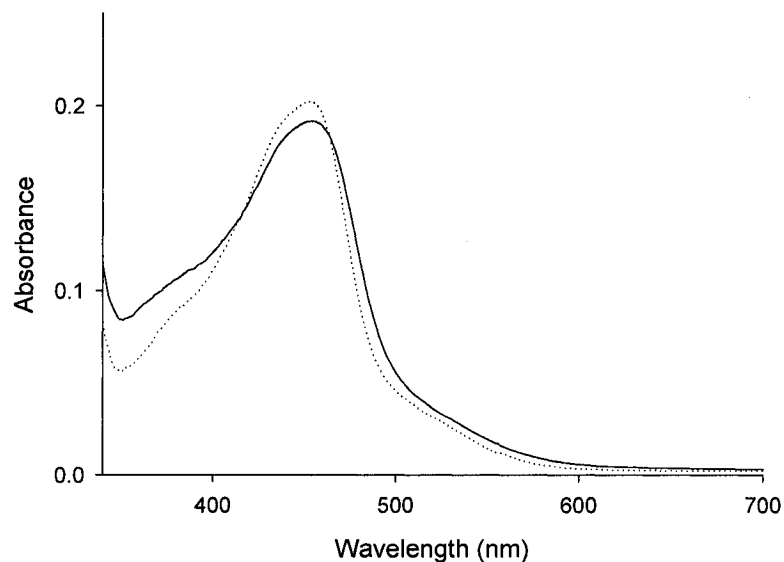
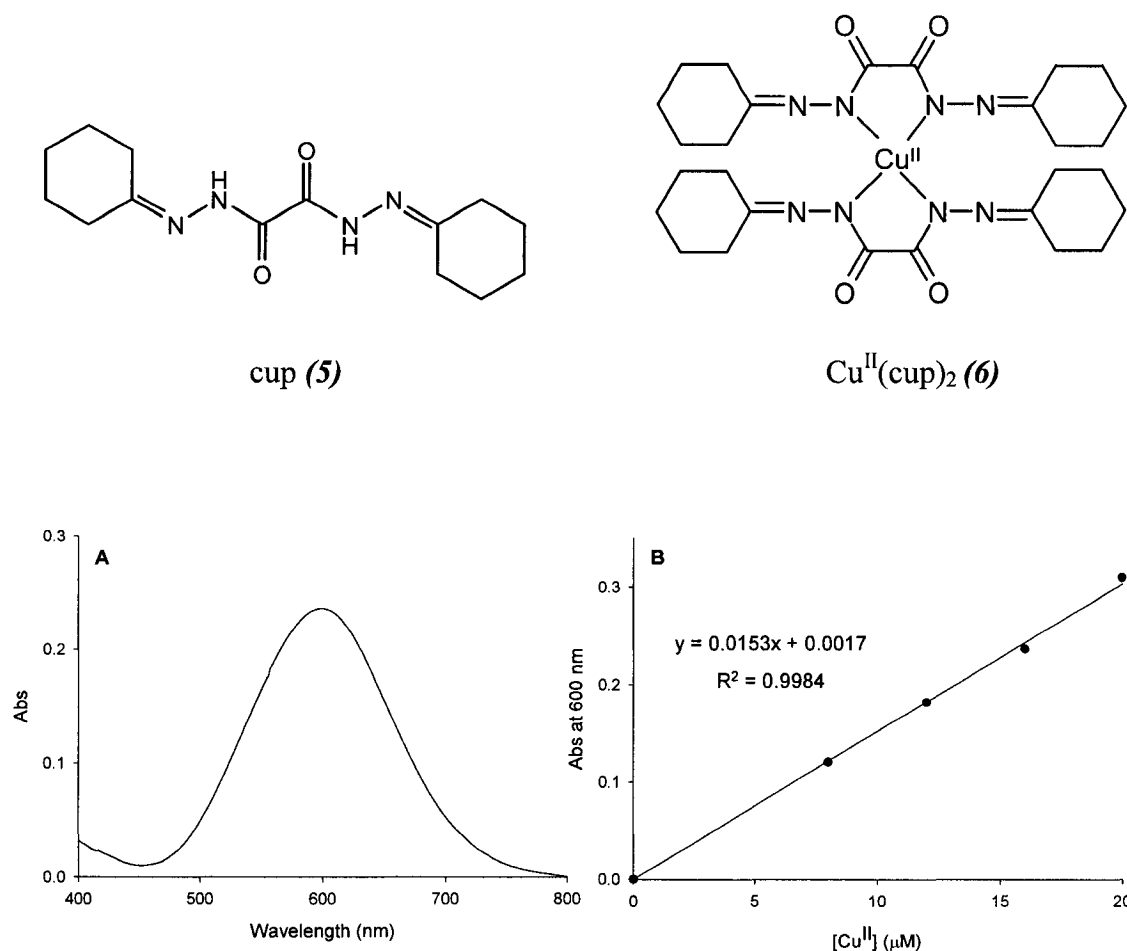


Figure 3.2 **Visible absorption spectrum of  $\text{Cu}^{\text{I}}(\text{neo})_2$  at RT.** Solid line: spectrum in a 1-cm cuvette of 25  $\mu\text{M}$   $\text{CuSO}_4$ , 200  $\mu\text{M}$  GSH, and 80  $\mu\text{M}$  neo in water. Dotted line: The  $\text{Cu}^{\text{I}}(\text{neo})_2$  complex was extracted into isoamyl alcohol by vortexing the sample with an equal volume of isoamyl alcohol and the spectrum of the organic phase was recorded in a 1-cm quartz cuvette.

Because of its specificity for  $\text{Cu}^{\text{I}}$  and the high stability of  $\text{Cu}^{\text{I}}(\text{neo})_2$  ( $K_{\text{stab}} = 1.0 \times 10^{19} \text{ M}^{-2}$ ) (169, 170), neo and its  $\text{Cu}^{\text{I}}$ -neo complex are often used in the study of the  $\text{Cu}^{\text{I}}$ -dependent mechanism of NO release from RSNOs and nitrgic relaxations in response to different stimuli (57, 171, 172).

Like DDC, cup (*bis*-cyclohexanone oxaldihydrazone, **5**) is a  $\text{Cu}^{\text{II}}$ -specific chelator that reacts with the metal in alkaline solution (pH 7.0–9.0) to give a blue complex (**6**) with an extinction coefficient of  $16.0 \text{ mM}^{-1}\text{cm}^{-1}$  at 600 nm (152, 173). Since cup does not form a colored complex with other cations or anions commonly found in biological materials, it was used in the determination of copper in serum (152), whole blood, and in rumen samples (153).



**Figure 3.3 Visible absorption spectrum of  $\text{Cu}^{\text{II}}(\text{cup})_2$  and calibration curve for the colorimetric determination of copper.** (A) The spectrum of a sample containing  $15.4 \mu\text{M}$   $\text{Cu}^{\text{II}}$  and  $0.3 \text{ mM}$  cup in  $\text{H}_2\text{O}$ . (B) Calibration curve generated by adding  $0\text{--}20 \mu\text{M}$   $\text{Cu}^{\text{II}}$  from a  $1000 \text{ ppm}$   $\text{Cu}^{\text{II}}$  standard solution in  $\text{H}_2\text{O}$  to  $0.3 \text{ mM}$  cup in  $\text{H}_2\text{O}$  and reading the absorbance at  $600 \text{ nm}$  following mixing in a  $1\text{-cm}$  quartz cuvette at RT.

As mentioned in Chapter 2, CuZnSOD-catalyzed NO release from GSNO involves GSH reduction of the active-site copper and  $\text{Cu}^{\text{I}}\text{ZnSOD}$  catalyzes the reductive decomposition of GSNO to yield NO (Reactions 2.1–2.3, Section 2.2). According to this mechanism, redox turnover of the active-site copper is a key step as in the SOD activity of the enzyme (Reactions 2.5–2.6, Section 2.2). Jourdeuil *et al.* observed that neo but not cup inhibited the GSNO-reductase activity of CuZnSOD and of  $\text{CuSO}_4$  (Table 3.1)

not cup inhibited the GSNO-reductase activity of CuZnSOD and of CuSO<sub>4</sub> (Table 3.1) (56), while it was demonstrated in Chapter 2 that EDTA and DTPA affect only the GSNO-reductase activity but not the SOD activity of BCuZnSOD. Chelators with different charges (EDTA -4; DTPA -5; DDC -1; neo 0; cup 0), different affinities for Cu<sup>II</sup> or Cu<sup>I</sup>, and different structures likely interact differently with CuZnSOD. Thus, the mechanism by which the colorimetric copper chelators, neo, DDC, and cup, inhibit the GSNO-reductase activity (Reactions 2.1 and 2.2, Section 2.2), the NO-transferase activity (Reactions 2.1', 2.2 and 2.4, Section 2.2), and SOD activity of CuZnSOD (Reactions 2.5, 2.6, Section 2.2) is explored here. The interesting finding is that all three copper reagents

**Table 3.1 Literature data<sup>a</sup> on the CuZnSOD- and CuSO<sub>4</sub>-induced GSNO decomposition of GSNO in the presence of GSH, neo, and cup**

Incubations <sup>b</sup>	% GSNO decomposition	Incubations <sup>c</sup>	% GSNO decomposition
GSNO/CuZnSOD/GSH	90	GSNO/Cu <sup>II</sup> /GSH	>90
GSNO/CuZnSOD/GSH/neo	20	GSNO/Cu <sup>II</sup> /GSH/neo	10
GSNO/CuZnSOD/GSH/cup	>90	GSNO/Cu <sup>II</sup> /GSH/cup	>90

<sup>a</sup>Jourd'heuil *et al.* (56). <sup>b</sup>Samples containing 10  $\mu$ M GSNO, 50  $\mu$ M GSH, 10  $\mu$ M CuZnSOD  $\pm$  1 mM neo or 1 mM cup were incubated at 37°C for 30 min. <sup>c</sup>Same as samples in Footnote *b* except 10  $\mu$ M CuSO<sub>4</sub> replaced 10  $\mu$ M CuZnSOD.

(at  $\leq$  5 mM) examined combine to varying degrees with the active-site copper in CuZnSOD solutions to give visible absorption characteristic of their CuL<sub>2</sub> complexes. Inhibition of the GSNO-reductase activity of CuZnSOD was found to be proportional to the extent of association of the chelators with the active-site copper whereas loss of SOD

complex. The results obtained provide further evidence that the CuZnSOD copper is accessible and reveal how the choice of metal chelator affects the function of the enzyme.

### **3.3 Materials and methods**

#### **3.3.1 Materials**

Bovine erythrocyte CuZnSOD (Roche Molecular Biochemicals) was used without further purification except where indicated. All reagents were of analytical grade or higher. GSNO [Glycine *N*-(*N*-*L*- $\gamma$ -glutamyl-s-nitroso-*L*-cysteinyl)] was obtained from Cayman. DDC (diethyldithiocarbamate, sodium salt), neocuproine (2,9-dimethyl-1,10-phenanthroline hydrochloride), cuprizone (*bis*-cyclohexanone oxaldihydrazone), EDTA (ethylenediamine-*N,N,N',N'*-tetraacetic acid, disodium salt), GSH (glutathione, reduced form), PGO (phenylglyoxal hydrate) were purchased from Sigma, and DTPA (diethylenetriamine-*N,N,N',N'',N''*-pentaacetic acid) and Tris [tris (hydroxymethyl) aminomethane, base] from ICN Biomedicals. Cacodylic acid (dimethylarsenic acid) was obtained from Aldrich and pyrogallol (1, 2, 3-trihydroxybenzene) was from Fisher. Nanopure water (specific resistance 18 M $\Omega$ -cm) obtained from a Millipore Simplicity water purification system was used to prepare all solutions. sodium phosphate buffer was treated with Chelex-100 resin (Bio-Rad) prior to use to remove trace metal ions.

#### **3.3.2 Methods**

##### **3.3.2.1 Visible spectra of CuZnSOD/chelator incubations**

A BCuZnSOD stock solution was prepared in 50 mM sodium phosphate buffer (pH 7.2), and the enzyme concentration was determined spectrophotometrically ( $\epsilon_{258} = 10.3 \text{ mM}^{-1}\text{cm}^{-1}$  per dimer (105, 174)). Absorption characteristic of the CuL<sub>2</sub> complexes

10.3 mM<sup>-1</sup>cm<sup>-1</sup> per dimer (105, 174)). Absorption characteristic of the CuL<sub>2</sub> complexes (2, 4, and 6) and changes in the *d-d* absorption at 680 nm of Cu<sup>II</sup>ZnSOD (50 – 690 μM) were monitored at 37°C in the presence of 380 μM – 5 mM cup, DDC, and neo plus GSH. Copper removal from BCuZnSOD by DDC and cup was monitored spectrophotometrically whereas the extent of copper removal from BCuZnSOD with neo in the presence of GSH was estimated after extracting the [Cu<sup>I</sup>(neo)<sub>2</sub>]<sup>+</sup> complex with isoamyl alcohol ( $\epsilon_{454} = 7.95 \text{ mM}^{-1}\text{cm}^{-1}$  (175)). CuL<sub>2</sub> extinction coefficients were determined by diluting 1000 ppm Cu standard into excess chelator in H<sub>2</sub>O. Absorbance readings were carried out in 1-cm cells on an Agilent 8453 UV-visible diode-array or a Beckman DU 650 spectrophotometer equipped with thermostated cell compartments.

### 3.3.2.2 Pyrogallol autooxidation assay of SOD activity

BCuZnSOD (36 – 92 μM) in 50 mM sodium phosphate buffer (pH 7.2) was incubated with 0.5 – 5 mM chelator ± GSH at 37°C for 30 min. Aliquots were removed from the preincubates every 10 min and the SOD activity of BCuZnSOD determined by following its inhibition of pyrogallol (Py) autooxidation using the literature procedure (105). Briefly, 40 mM Py stock solution was prepared in 10 mM HCl, and 50 mM Tris/1 mM DTPA was adjusted to pH 8.2 with cacodylic acid. BCuZnSOD aliquots from the preincubates were diluted with sodium phosphate buffer (pH 7.2) before addition to the Tris cacodylate assay buffer (pH 8.2) in a 1-cm quartz cuvette at 37°C. Py was added to a final concentration of 200 μM and following rapid mixing, the absorbance at 320 nm was read every 15 s over 3 min to monitor the rate of Py oxidation. The percent inhibition (%*I*, Eq 3.1) of Py oxidation was calculated from the initial slopes of A<sub>320</sub> vs time plots generated in the absence (Slope<sub>Py</sub>) and presence (Slope<sub>s</sub>) of BCuZnSOD. The relative



SOD activities (Eq 3.2) are the ratios of the initial slopes difference for the samples of BCuZnSOD/chelators  $\pm$  GSH measured at  $t < 1$  min ( $\text{Slope}_0$ ) and  $t = t$  min ( $\text{Slope}_t$ ).

$$\%I = \frac{(\text{Slope}_{\text{Py}} - \text{Slope}_s)}{\text{Slope}_{\text{Py}}} \times 100 \quad 3.1$$

$$\% \text{ relative SOD activity} = \left[ \frac{(\text{Slope}_{\text{Py}} - \text{Slope}_t)}{(\text{Slope}_{\text{Py}} - \text{Slope}_0)} \right] \times 100 \quad 3.2$$

### 3.3.2.3 GSNO-reductase activity of CuZnSOD

Experiments were performed as described in Section 2.3.2.4. That is, solutions containing GSNO, BCuZnSOD and GSH in the presence (chel) or absence (con) of chelators were incubated at 37°C for 30 min. The GSNO concentration was followed spectrophotometrically ( $\epsilon_{333} = 0.76 \text{ mM}^{-1} \text{ cm}^{-1}$ ) at the S-NO absorption band (25) to monitor the effects of the chelators on the GSNO-reductase activity of BCuZnSOD with GSH as a donor:

$$\Delta A_{333} = A_{333}(t=30) - A_{333}(t=0) \quad 3.3$$

$$\% \text{ GSNO degradation} = \left( \frac{\Delta A_{333}}{A_{333}(t=0)} \right) \times 100 \quad 3.4$$

$$\% \text{ Rel GSNO degradation} = (\Delta A_{333})_{\text{chel}} / (\Delta A_{333})_{\text{con}} \times 100 \quad 3.5$$

### 3.4 Results

#### 3.4.1 $\text{CuL}_2$ absorption grows in the spectra of the CuZnSOD/chelator incubations

When 5 mM DDC (*1*) was added to 52  $\mu\text{M}$  BCuZnSOD, a new absorption band at 451 nm due to the  $\text{Cu}^{\text{II}}(\text{DDC})_2$  complex (*2*) was observed (Figure 3.4A). After 30 min incubation at 37°C, ~ 76% of the BCuZnSOD copper was detected as  $\text{Cu}^{\text{II}}(\text{DDC})_2$  (Figure 3.4B). The rapid removal of copper from the active site by DDC is consistent with previous reports (*120, 138*) that this chelator is a highly effective reagent in the preparation of the copper-free enzyme, and is additionally supported by our ICP-MS results (Table 2.1, Section 2.4.2). Also, copper removal from BCuZnSOD is biphasic, indicating that the affinity of the protein dimer for one  $\text{Cu}^{\text{II}}$  is less than for the second  $\text{Cu}^{\text{II}}$  (Figure 3.4B). Communication between the monomers concerning the occupancy of metal binding sites has been reported previously (*176*) and will be discussed in detail below.

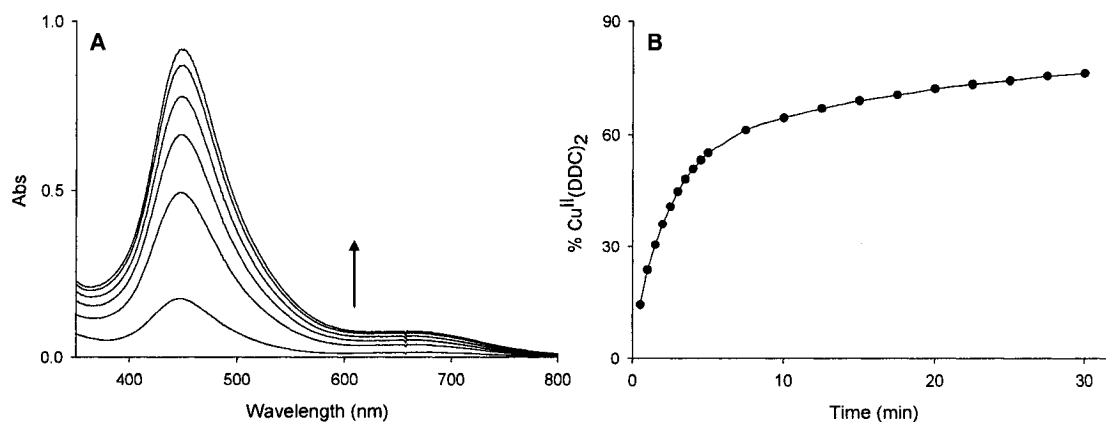


Figure 3.4  $\text{Cu}^{\text{II}}(\text{DDC})_2$  absorption vs time of the CuZnSOD/DDC incubation. (A) Spectrum at  $t = 0, 2.5, 5, 10, 20,$  and  $30$  min of 52  $\mu\text{M}$  BCuZnSOD with 5 mM DDC. (B) Percent BCuZnSOD copper detected as  $\text{Cu}^{\text{II}}(\text{DDC})_2$  calculated from absorbance at 451 nm. Samples were in 50 mM sodium phosphate buffer (pH 7.2) at 37°C, and the absorbance was recorded immediately after DDC addition to BCuZnSOD and at 0.5- or 2.5-min intervals over 30 min.

The absorption band of  $\text{Cu}^{\text{II}}(\text{cup})_2$  (**6**) at 600 nm was observed when 3 mM cup was added to 690  $\mu\text{M}$  BCuZnSOD (Figure 3.5A). However, only ~3% of the BCuZnSOD copper was detected as  $\text{Cu}^{\text{II}}(\text{cup})_2$  and a higher BCuZnSOD concentration was required to observe the  $\text{CuL}_2$  absorption peak compared to that for DDC (690 vs 52  $\mu\text{M}$  protein) (Figure 3.5B). Thus, the binding of cup to BCuZnSOD is weak and unlikely to remove copper from the active site.

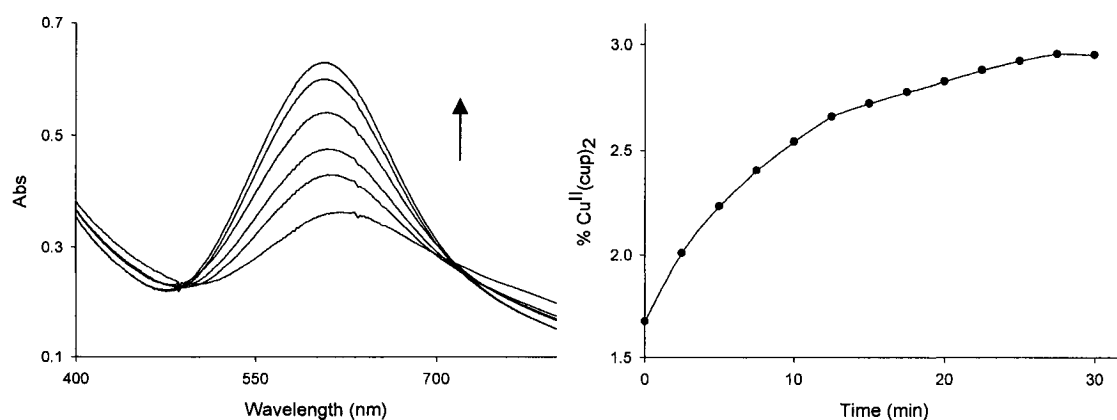


Figure 3.5  $\text{Cu}^{\text{II}}(\text{cup})_2$  absorption vs time of the CuZnSOD/cup incubation. (A) Spectrum at  $t = 0, 2.5, 5, 10, 20,$  and  $30$  min of  $690 \mu\text{M}$  BCuZnSOD with  $3 \text{ mM}$  cup. (B) Percent BCuZnSOD copper detected as  $\text{Cu}^{\text{II}}(\text{cup})_2$  calculated from the absorbance at  $600 \text{ nm}$  in (A). Samples were in  $50 \text{ mM}$  sodium phosphate buffer ( $\text{pH } 7.2$ ) at  $37^\circ\text{C}$ , and absorbance was recorded immediately after cup addition to BCuZnSOD and at  $2.5\text{-min}$  intervals over  $30 \text{ min}$ .

The  $\text{Cu}^{\text{I}}$ -specific chelator, neo (**3**), was added to  $\text{Cu}^{\text{II}}\text{ZnSOD}$  in the presence of GSH. The  $680\text{-nm}$   $d-d$  absorption band of  $\text{Cu}^{\text{II}}\text{ZnSOD}$  decreased indicating reduction of  $\text{Cu}^{\text{II}}$  to  $\text{Cu}^{\text{I}}$  (Figure 3.6A insert) while a new peak appeared at  $454 \text{ nm}$ , which is assigned to  $[\text{Cu}^{\text{I}}(\text{neo})_2]^+$  (Figure 3.6A). The time course of  $[\text{Cu}^{\text{I}}(\text{neo})_2]^+$  formation is given in Figure 3.6B. Approximately  $6\%$  of the active-site copper formed a complex with neo

during 25 min incubation at 37°C, which suggests that neo may compete with the reduced protein (Cu<sup>I</sup>ZnSOD) for Cu<sup>I</sup>.

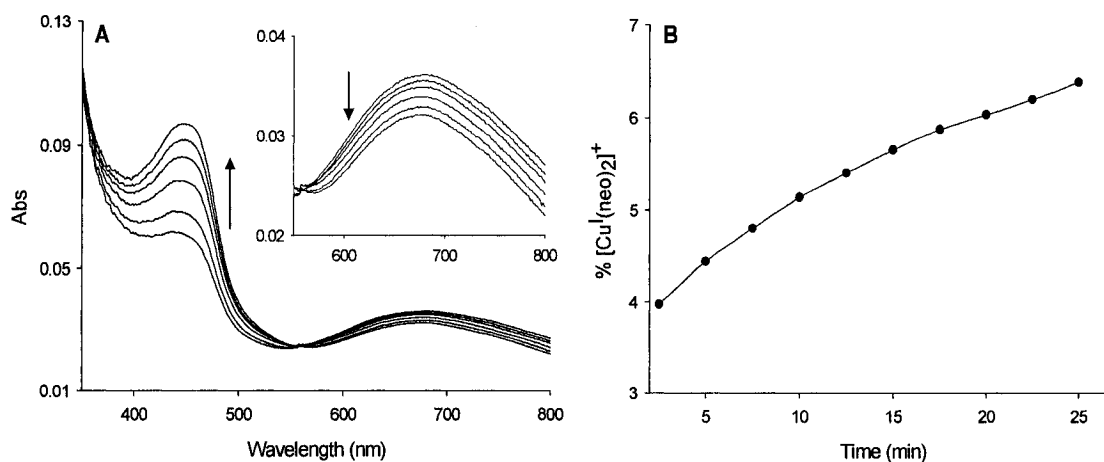
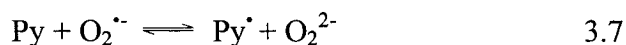
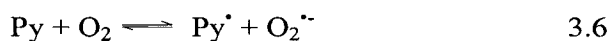


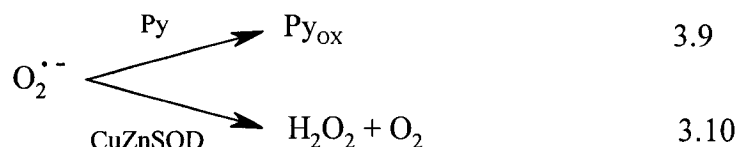
Figure 3.6 [Cu<sup>I</sup>(neo)<sub>2</sub>]<sup>+</sup> absorption vs time of the CuZnSOD/GSH/neo incubation. (A) Spectrum at t = 2.5, 5, 10, 15, 20, and 25 min of 95 μM BCuZnSOD with 190 μM GSH and 380 μM neo. The inset shows the amplified Cu<sup>II</sup> d-d absorption band. (B) Percent BCuZnSOD copper detected as [Cu<sup>I</sup>(neo)<sub>2</sub>]<sup>+</sup> calculated from the absorbance at 454 nm after extraction into isoamyl alcohol. Samples were in 50 mM sodium phosphate buffer (pH 7.2) at 37°C, and the absorbance was recorded immediately after GSH and neo addition to BCuZnSOD and at 2.5-min intervals over 25 min.

### 3.4.2 Effects of preincubation with the chelators and GSH on SOD activity

SOD activity can be measured by monitoring Py autoxidation. The oxidized product (Py<sub>ox</sub>) has an absorption peak at 320 nm and its formation involves O<sub>2</sub><sup>•-</sup> generation, which then acts as a chain propagating species:



In the presence of CuZnSOD, competition between the enzyme and Py for  $O_2^{\bullet -}$  decreases the rate of  $Py_{ox}$  formation (105):



SOD activity was found to be linear in BCuZnSOD concentration up to 6 nM enzyme (Figure 3.7). The non-zero inhibition in the absence of CuZnSOD may be due to the existence of active components in the enzyme solution which are resistant to 1 mM DTPA (105).

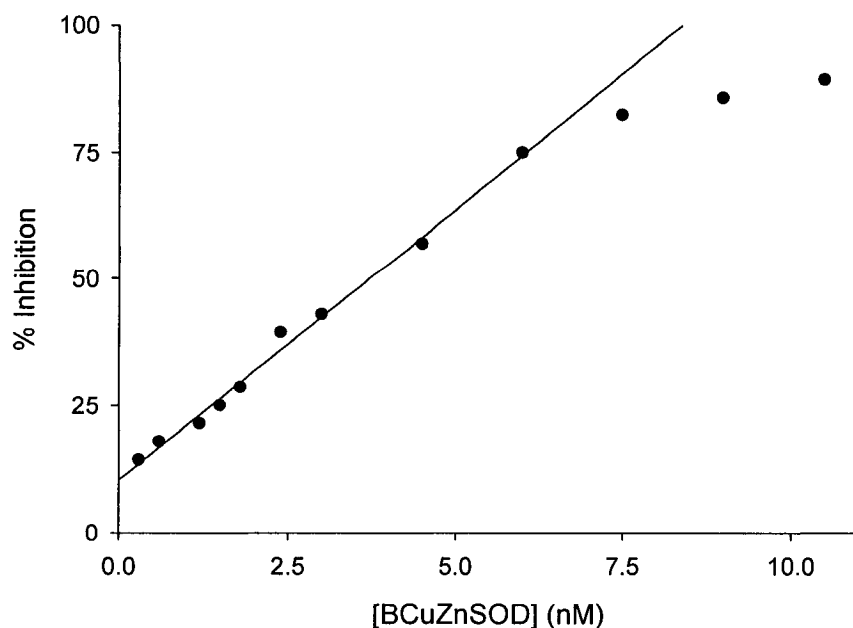


**Figure 3.7 Inhibition calibration curve for the pyrogallol autooxidation assay for SOD activity.** Py oxidation was inhibited by the presence of BCuZnSOD, and the % inhibition calculated by Eq 3.1 is plotted vs the concentration of BCuZnSOD. Procedure: A 10- $\mu$ L aliquot of 40 mM Py stock solution was added to 2 mL of BCuZnSOD in Tris-cacodylate/1 mM DTPA assay buffer (pH 8.2) in a 1-cm quartz cuvette in thermostated cell holder at 37°C and mixed rapidly. The absorbance at 320 nm was read every 15 s over 3 min. The blank was Tris-cacodylate/1 mM DTPA assay buffer (pH 8.2).

Figure 3.8 shows the relative SOD activities of 5 nM BCuZnSOD after preincubation with the Cu<sup>II</sup> chelators at 37°C over 30 min. Preincubation with cup has little effect on the SOD activity of BCuZnSOD. In contrast, over 90% SOD activity was lost within 20 min preincubation of BCuZnSOD with DDC (Figure 3.8), and this can largely be attributed to copper removal from the enzyme (Table 2.1).

As described in Section 2.4, GSH reduced the active-site Cu<sup>II</sup> of BCuZnSOD to Cu<sup>I</sup> during a 30-min preincubation (Figure 2.2A), but resulted in no activity loss (Figure 2.3). Similarly no SOD activity was lost during 30-min preincubation with neo ± GSH (Figure 3.8). This is consistent with the results of Jourdain *et al.* (56), who also found that the SOD activity was not inhibited by preincubation of CuZnSOD with neo.

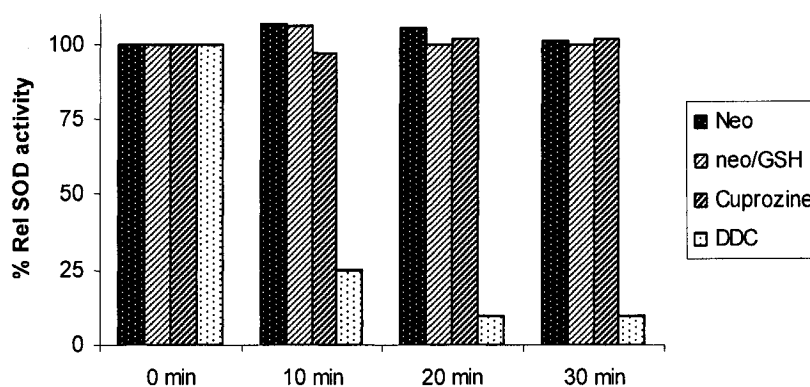


**Figure 3.8 Effects of preincubation with the chelators ± GSH on the SOD activity of BCuZnSOD.** BCuZnSOD (61–92 μM) was preincubated with 5 mM neo, 5 mM neo plus 5 mM GSH, 0.5 mM cup or 5 mM DDC in 50 mM sodium phosphate buffer (pH 7.2) at 37°C for 30 min. Aliquots were removed every 10 min, diluted 100-fold, 10 μL was added to 2 mL of assay buffer [50 mM Tris cacodylate/1 mM DTPA (pH 8.2), 37°C], and assayed for SOD activity as described in the legend of Figure 3.7. The SOD activity of BCuZnSOD from the 0 min incubates was taken as 100%. Each bar represents the mean of two measurements with an average error of ~1%.

### 3.4.3 Effects of the chelators on the GSNO-reductase activity of CuZnSOD

As shown in Table 3.2, in the presence of 30  $\mu$ M BCuZnSOD and 5 mM GSH, 36%  $\pm$  2 GSNO (0.47 mM) was decomposed in 30 min at 37°C, as compared with 5.4%  $\pm$  0.2 GSNO decomposition in the absence of GSH (data not shown). Less than 5% of the GSNO decomposed when 2 mM DDC was also present. Addition of 2 mM neo inhibited GSNO decomposition by > 50%, while 0.33 mM cup inhibited decomposition by ~20% (Table 3.2).

Table 3.2 Effects of cup, neo, and DDC on the GSNO-reductase activity of BCuZnSOD with GSH as a donor substrate<sup>a</sup>

Incubation	GSNO/CuZnSOD/GSH	+ cup	+ neo	+ DDC
% GSNO degradation	35.6	28.5 $\pm$ 0.3	16.2 $\pm$ 0.4	4.9 $\pm$ 0.5
Rel GSNO degradation	100	80.0 $\pm$ 0.9	45.5 $\pm$ 1.1	13.7 $\pm$ 1.3

<sup>a</sup>Solutions containing 470  $\mu$ M GSNO, 5 mM GSH, 30  $\mu$ M BCuZnSOD, 2 mM DDC, 2 mM neo or 0.33 mM cup were incubated in 50 mM sodium phosphate buffer (pH 7.2) at 37°C for 30 min. The GSNO remaining was determined spectrophotometrically ( $\epsilon_{333}$  = 0.76 mM<sup>-1</sup> cm<sup>-1</sup>) and the % GSNO degradation and Rel GSNO degradation were calculated using Eq 3.4 and 3.5, respectively, and the values represent the mean  $\pm$  SD of triplicates.

## 3.5 Discussion

CuZnSOD is a homodimeric enzyme with one tightly bound ( $K_d$  = 6 fM), redox-active copper atom per subunit (47, 100). The enzyme is stable over a wide range of pH

values (5.2–9.5), and up to 75°C at neutral pH (177). The active-site copper, which is coordinated to four imidazole nitrogens and a water molecule with a distorted square-pyramidal geometry in Cu<sup>II</sup>ZnSOD (Figure 3.9), is required for SOD activity (47, 174, 178). In fact, the copper is the site of primary interaction of O<sub>2</sub><sup>•−</sup> with the protein (47), and the x-ray structure shows that the metal lies at the bottom of a narrow channel. An electrostatic loop consisting of the positively charged side chains of Arg141, Lys120, and Lys134, which are located at 5, 12, and 13 Å, respectively, from the copper (58), guides the anionic superoxide substrate to the active site. These residues also play a significant role in promoting access of substrates such as water, small anions, and other ligands to the active-site copper (141).

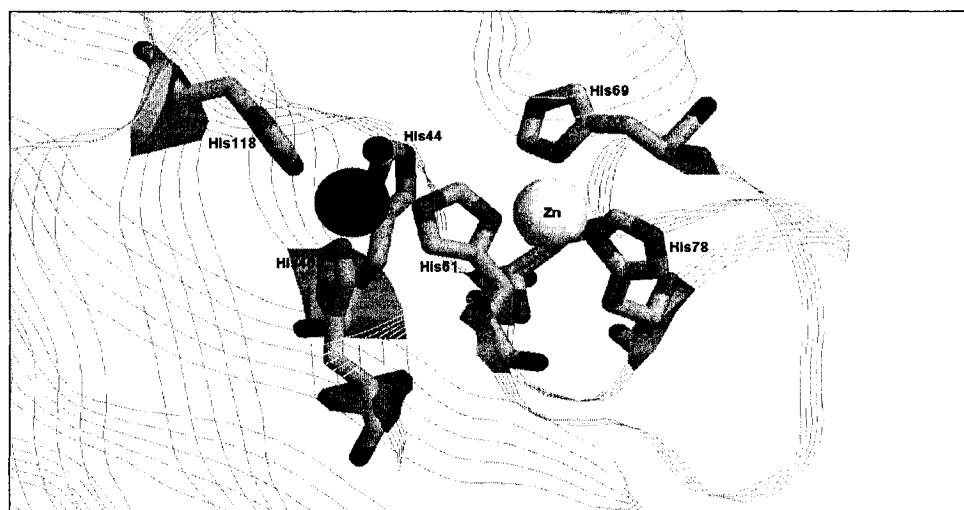


Figure 3.9 **Metal binding site of the CuZnSOD monomer.** The residues numbering is that of bovine CuZnSOD. Figure adopted from Ref (120).

Cu<sup>II</sup>ZnSOD has a weak *d-d* absorption band at 680 nm [ $\epsilon_{680} = 300 \text{ M}^{-1} \text{ cm}^{-1}$  (47)] and incubation with EDTA or DTPA was shown to decrease the 680-nm absorption



band by  $\leq 22\%$  (Figure 2.1, Section 2.4.1). These chelators do not decrease the SOD activity when preincubated with the enzyme at pH 7.2 (Figure 2.3, Section 2.4.4), indicating no removal of the active-site  $\text{Cu}^{\text{II}}$  as confirmed by ICP-MS (Table 2.1, Section 2.4.2).

It was reported that the reaction of DDC with the active-site  $\text{Cu}^{\text{II}}$  of CuZnSOD is concentration-, temperature-, and pH-dependent. At 0.1–1 mM DDC, the  $\text{Cu}^{\text{II}}$ -DDC complex remained bound to the enzyme and the SOD activity did not decrease (*124*). As shown here, 5 mM DDC (~100-fold molar excess) removed 76% of the copper from BCuZnSOD (Figure 3.4B), and 90% SOD activity was lost after preincubation of the enzyme with 5 mM DDC at 37°C for 20 min (Figure 3.8). The ICP-MS results showed 77% Cu and 44% Zn removal from the enzyme in this incubation (Table 2.1, Section 2.4.2).

Evidence for interactions between the two active sites in bovine CuZnSOD dimer has been reported for many years (*125, 147, 179-181*). As mentioned in Chapter 2, coulometric titration curves for BCuZnSOD exhibit a break at one equivalent of titrant per mole of enzyme dimer. Furthermore, addition of  $\text{K}_3\text{Fe}(\text{CN})_6$  or  $\text{K}_2\text{IrCl}_6$  to the enzyme prior to the titration caused one of the  $\text{Cu}^{\text{II}}$  to be nontitratable (*125*). These results suggest that large anions bind to only one of the copper centers, which is in accordance with our finding that the stoichiometry of EDTA and DTPA binding to the BCuZnSOD dimer is ~1 (Figure 2.7, Section 2.4.7) and not 2 as expected for a homodimer. In addition, the reduction potential of the first  $\text{Cu}^{\text{II}}$  in CuZnSOD is different from that of the second  $\text{Cu}^{\text{II}}$ , indicating that the two copper centers in the enzyme are nonequivalent or that cooperative behavior exists between the two centers. Previously, it was reported that

copper binding to bovine EZnSOD is a cooperative process (181): binding of Cu<sup>II</sup> to one subunit lowers the activation energy for Cu<sup>II</sup> binding to the second subunit (181). Thus, it is not surprising that copper removal is biphasic with ~50% loss within 5 min and ~76% loss after 30 min (Figure 3.4 B). Since intersubunit interactions control Fe(CN)<sub>6</sub><sup>3-</sup> or IrCl<sub>6</sub><sup>2-</sup> binding, it is also not surprising that EDTA or DTPA binding to one subunit prevents access of large substrates such as GSNO to the second subunit.

The Cu<sup>II</sup>(cup)<sub>2</sub> absorption detected after 30-min incubation of BCuZnSOD with cup at 37°C (Figure 3.5A) corresponds to only ~3% of the copper in the incubation (Figure 3.5B). Incubation with cup led to no effect on the SOD activity (Figure 3.8) revealing that, like EDTA and DTPA (Chapter 2), cup does not remove copper from the enzyme. Although the Cu<sup>II</sup>(cup)<sub>2</sub> complex exhibits stronger visible absorption than Cu<sup>II</sup>(DDC)<sub>2</sub> or [Cu<sup>I</sup>(neo)<sub>2</sub>]<sup>+</sup> (Table 3.3), negligible binding is detected since cup is a large neutral ligand that likely has poor access to the active-site copper *via* the positively charged channel (49) (Figure 3.9).

**Table 3.3 Millimolar absorptivity ( $\epsilon$ ) of the copper-chelator complexes**

Complex	$\lambda_{\text{max}}$ (nm)	$\epsilon$ (mM <sup>-1</sup> cm <sup>-1</sup> )	Ref.
Cu <sup>II</sup> (DDC) <sub>2</sub>	450	8.0-12.1	(124, 152, 166)
Cu <sup>II</sup> (cup) <sub>2</sub>	600	16.0	(152, 173)
[Cu <sup>I</sup> (neo) <sub>2</sub> ] <sup>+</sup>	454	7.95	(149, 167)

Gradual growth of 454-nm absorbance of the  $[\text{Cu}^{\text{I}}(\text{neo})_2]^+$  complex and decay of the 680-nm band of  $\text{Cu}^{\text{II}}\text{ZnSOD}$  (Figure 3.5A, insert) was detected over 25 min in the BCuZnSOD/GSH/neo incubation (Figure 3.5A). Approximately 14%  $\text{Cu}^{\text{II}}\text{ZnSOD}$  was reduced to  $\text{Cu}^{\text{I}}\text{ZnSOD}$  by 190  $\mu\text{M}$  GSH in 25 min as estimated from the absorbance change of the 680-nm band ( $\epsilon_{680} = 300 \text{ M}^{-1}\text{cm}^{-1}$ , (47)). However, less than 6% of the total active-site copper was extracted into isoamyl alcohol as the  $[\text{Cu}^{\text{I}}(\text{neo})_2]^+$  complex (Figure 3.5B). Again, no loss of SOD activity was detected following preincubation with neo (Figure 3.8), as previously shown by Jourdain and coworkers (56). Thus, unless extracted, the  $\text{Cu}(\text{neo})_2^+$  complex likely remains bound to the enzyme and upon dilution into the SOD assay buffer, BCuZnSOD remains ~100% active.

A common feature among the chelators (except DDC) is that they bind to the enzyme-associated copper without isolating the metal from the enzyme. Neither EDTA nor DTPA changed the metal loading of BCuZnSOD (Table 2.1, Section 2.4.2) and Jourdain *et al.* noted that the copper-neo complex was not separated from the enzyme by passage through a G-25 column or by ultrafiltration (56). Thus, loss of SOD activity occurs only when chelator addition results in copper no longer being associated with the enzyme. We (Figure 3.8) and others (124, 182) observed that preincubation with 5–10 mM DDC inhibits the SOD activity of BCuZnSOD, but Misra reported (124) that at < 1 mM, DDC associated with active-site copper and the  $\text{Cu}^{\text{II}}\text{ZnSOD}$ -DDC complex had SOD activity equivalent to that of the free enzyme. Misra also reported that > 10 mM DDC removed copper from the active site (124) confirming that loss of SOD activity is caused by isolation of copper from the enzyme.

Fielden *et al.* proposed a half-the-active-sites mechanism for SOD catalysis by CuZnSOD (147), and Rigo *et al.* found that the enzyme half-loaded with copper ( $\text{Cu}_1\text{Zn}_2\text{SOD}$ ) is twice as active as the fully copper-loaded enzyme ( $\text{Cu}_2\text{Zn}_2\text{SOD}$ ) (180). Thus, only 50% of the copper is involved in catalysis and the involvement of one site inhibits catalysis at the second site (180). We observed that EDTA and DTPA bind to half of the enzyme-bound  $\text{Cu}^{\text{II}}$  (Figure 2.7) with no effect on SOD activity (Table 2.2). Removal of 61% copper by DDC within 10 min resulted in 75% loss of activity (Figure 3.4B and Figure 3.8) and removal of 76% copper within 30 min resulted in 90% loss of activity. But if  $\text{Cu}_1\text{Zn}_2\text{SOD}$  exhibits twice the activity as the fully copper loaded enzyme (180), 100% loss of copper from one subunit plus 25% from a second subunit should give rise to a dimer with greater activity than the native  $\text{Cu}_2\text{Zn}_2\text{SOD}$  enzyme. Loss of 90% activity suggests that DDC removes copper from both subunits. Alternatively, DDC may reduce the intrasubunit disulfide between Cys55–Cys144 that influences subunit association (183). The effects of DDC on CuZnSOD other than copper removal should be investigated.

The GSNO-reductase activity of CuZnSOD was demonstrated by Jourd'heuil *et al.* (56). This activity requires the redox turnover of the active-site copper (Reactions 2.1 and 2.2, Section 2.2). Faster reduction of the active-site  $\text{Cu}^{\text{II}}$  by cysteine or ascorbate than GSH (56, 82) or P-SH (82) has been demonstrated suggesting that these small substrates have easier access to the active-site copper. As revealed in Figure 2.2B (Section 2.4.3), association of EDTA and DTPA with the enzyme decreased the rate of  $\text{Cu}^{\text{II}}$  reduction by GSH and consequently inhibited the GSNO-reductase activity of the enzyme (Figure 2.5, Section 2.4.6).

Previous studies demonstrated that  $\text{Cu}^{\text{I}}$  in the free state or in protein- or peptide-bound forms is the active species rather than  $\text{Cu}^{\text{II}}$  in the decomposition of RSNOs (56, 96, 98). Thus, to function as a GSNO-reductase, the first key step is the conversion of  $\text{Cu}^{\text{II}}\text{ZnSOD}$  to its reduced form (Reaction 2.1, Section 2.2), which is followed by  $\text{Cu}^{\text{I}}\text{ZnSOD}$ -catalyzed reductive decomposition of GSNO to yield NO (Reaction 2.2, Section 2.2). The narrow cleft leading to the active site of CuZnSOD will control access of large reagents (reductants or chelators) to the copper as demonstrated by the fact that cysteine and ascorbate are more efficient  $\text{Cu}^{\text{II}}\text{ZnSOD}$  reductants than GSH (56, 82). In some cases, the active-site copper may not directly interact with reducing agents, and long-range electron transfer involving Arg141 has been used to explain the effects of different redox reagents on the redox state of the copper centre (184). Our group observed reduction of the active-site  $\text{Cu}^{\text{II}}$  of CuZnSOD by protein thiols in calbindin D<sub>28K</sub> (82) suggesting that certain protein-based thiols can access the active-site copper. This most likely occur within a protein-protein complex, and we observed indirect evidence for this in our studies on CuZnSOD catalyzed NO transfer from GSNO to oxyhemoglobin (57).

Cup is a sensitive colorimetric reagent for  $\text{Cu}^{\text{II}}$  but not a strong ligand for the active-site copper of CuZnSOD (Figure 3.5). Only ~3% of the enzyme-bound copper interacted with cup (Figure 3.5B) and the  $\text{Cu}^{\text{II}}(\text{cup})_2$  complex detected in the BCuZnSOD/cup incubation was likely associated with the enzyme since no significant change in SOD activity was measured following preincubation with cup (Figure 3.8). It was the weakest inhibitor of the GSNO-reductase activity among the copper chelators tested (Table 3.2; Figure 2.5, Section 2.4.4). We observed only 80% GSNO-reductase

activity in the presence of cup whereas Jour'dheuil *et al.* reported 100% activity (Table 3.1). This inconsistency may result from the concentrations of reactants used in the different studies as discussed below.

The GSNO-reductase activity of BCuZnSOD/GSH was only ~ 54% inhibited by 2 mM neo (Table 3.2) in contrast to the report (56) of 100% inhibition by 1 mM neo (Table 3.1). Under what conditions does neo partially or fully (Tables 3.2 vs 3.1) (56) inhibit the GSNO-reductase activity of CuZnSOD? Removal of ~6% copper should not be sufficient to completely inhibit the GSNO-reductase activity of CuZnSOD, and unlike EDTA and DTPA, neo did not protect Arg141 from PGO modification (Figure 2.4, Section 2.4.5). Thus, accessibility to Arg141 in the active-site channel does not change in the presence of neo and no binding interaction is expected between neo and the guanidium side chain of this residue.

Previously, Noble *et al.* demonstrated that at millimolar GSNO, the product GSSG is an efficient Cu<sup>II</sup> trap (Figure 1.3) and terminates metal-catalyzed GSNO decomposition (27, 34). Our lab reported that the rate of Cu<sup>II</sup>ZnSOD reduction by GSH depends on the thiol concentration up to 5 mM but negligible increase in Cu<sup>II</sup> reduction was observed above 5 mM GSH (82). We suggested that GSSG inhibits reduction of Cu<sup>II</sup>ZnSOD by GSH but adding GSSG (5 mM) had no effect on the 680-nm absorption band or on the SOD activity of BCuZnSOD (Figures 2.1 and 2.3, Section 2.4). Thus, GSSG is unlikely to bind or to remove copper from the enzyme. Instead, the disulfide may locate at the surface of the active-site channel and prevent access of GSH but not O<sub>2</sub><sup>•-</sup> to the active-site copper. Consistent with this view, Ciriolo *et al.* reported that copper does not transfer from the Cu<sup>II</sup>-GSSG complex to the copper-free enzyme (EZnSOD).

They suggested that GSSG-bound copper could not pass through the  $< 4 \text{ \AA}$  narrow neck located at the bottom of the active-site channel to allow copper to equilibrate between the peptide and protein (185). In contrast to  $\text{Cu}^{\text{II}}$ -GSSG, Ciriolo *et al.* reported that  $\text{Cu}^{\text{I}}$ -GSH can donate copper to EZnSOD leading to full reconstitution *via* a  $\text{Cu}^{\text{I}}$ -GSH-enzyme intermediate (185). Since higher GSNO and GSH concentrations were used in our experiments *vs* those of Jourdain *et al.* (56), more GSSG was produced in our samples. Thus, GSH and GSSG may associate with the enzyme and inhibit chelators such as neo from ligating to the copper, and thereby partially rescue the GSNO-reductase activity of the enzyme.

### 3.6 Conclusions

The present study provides additional evidence that chelators can access the active-site copper of CuZnSOD. Inhibition of the GSNO-reductase activity depends on the extent of chelator binding to the active-site copper of CuZnSOD. Furthermore, the enzyme exhibits half-sites SOD activity which is not inhibited by preincubation with the chelators as long as copper is not removed from the enzyme. We found that (1) DDC is a highly efficient inhibitor of both the GSNO-reductase and SOD activities since it removes copper from CuZnSOD; (2) neo inhibits the GSNO-reductase but preincubation with neo does not alter the SOD activity of CuZnSOD, and (3) cup interacts weakly with active-site copper and has little effect on the GSNO-reductase and SOD activities of CuZnSOD. In addition, both GSH, abundant in red blood cells, and its oxidation product GSSG control the GSNO-reductase (Reactions 2.1–2.3, Section 2.2) and NO-transferase (Reactions 2.1', 2.2 and 2.4, Section 2.2) activities of CuZnSOD. Further studies to

determine if GSSG decreases the GSNO-reductase activity by blocking access of GSH and/or GSNO to the active-site copper would be interesting as would further evidence that neo inhibition of the GSNO-reductase activity depends on the GSNO/GSH concentrations used.



## **4.0    Reevaluation based on mass spectrometric analysis of phenylglyoxal as an arginine-specific reagent: Characterization of phenylglyoxal-modified peptides and Cu,Zn-superoxide dismutase**

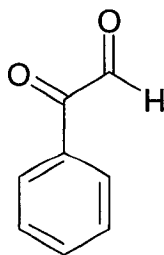
### **4.1    Abstract**

Chemical modification of arginine residues by  $\alpha,\alpha'$ -dicarbonyls is of interest as a tool in enzyme-structure-function studies and in non-enzymatic glycation found with aging and disease. Phenylglyoxal (PGO) has been used as an arginine-specific reagent for close to 40 years but the derivatives formed are not well characterized. In this study, PGO was reacted at pH 8.0 with the arginine-containing peptides, MRF, porcine rennin substrate tetradecapeptide (PRS; DRVYIHPFHLVYS), and adrenocorticotrophic hormone fragment 18–39 (ACTH; RPVKVYPNGAEDESAEAFPLEF), and the products were characterized by ESI and MALDI mass spectrometry (MS). The observed mass increase of the ions ( $2 \times 134$ -18 u) indicated that each of the three peptides formed a condensation product with two PGO molecules, and arginine was found to be the site of PGO modification by tandem MS/MS analysis. The PGO-modified peptides were acetylated by sulfo-NHS acetate indicating that neither the *N*-terminal  $\alpha$ -amino groups nor Lys22 of ACTH reacted with PGO. Exposure of glutathione to PGO resulted in singly to triply PGO-labelled peptide and tandem MS/MS analysis reveals that Cys2 in this tripeptide was the site of PGO labelling. The three exposed arginine residues, but not buried Arg113, in the bovine copper,zinc-superoxide dismutase (BCuZnSOD) monomer were modified in a time-dependent manner on incubation with excess PGO. Mass

increases in intact BCuZnSOD and its tryptic peptides revealed that the protein-based arginines reacted with a single PGO molecule unlike the double PGO-modification observed for the peptide-based arginines. PGO-modified BCuZnSOD formed a NEM-adduct and was fully acetylated indicating that the free Cys6 and 10 lysine residues in each monomer are not reactive with PGO. As previously reported, loss of SOD activity occurred in the BCuZnSOD/PGO incubations.

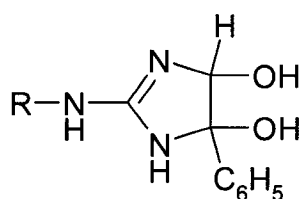
## 4.2 Introduction

Phenylglyoxal (*1*, PGO) reportedly demonstrates its highest reactivity with arginines (*119*) and is considered an arginine-specific reagent (*186*). Although other amino acids such as cysteines, histidine, lysines, glycine, asparagine, and *N*-terminal  $\alpha$ -amino groups of peptides were also found to be PGO modified (*119, 186, 187*), PGO is used extensively to investigate the role of arginine residues in enzyme catalysis (*55, 186, 188-193*). For example, the decreased activity of PGO-modified bovine pancreatic ribonuclease A, bovine copper,zinc-superoxide dismutase (BCuZnSOD), and human *N*-acetyltransferase has been attributed to the derivatization of catalytically important arginine residues (*55, 186, 188*).

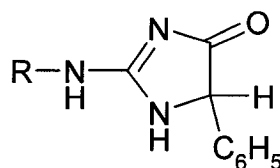


*1*: PGO

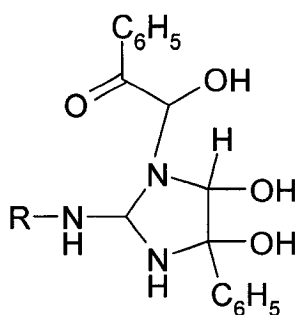
PGO was found to have advantages over other  $\alpha,\alpha'$ -dicarbonyl compounds as an arginine reagent. It reacts under mild conditions ( $\sim$ pH 8) more rapidly and selectively than glyoxal and methylglyoxal (119, 186). 1,2-Cyclohexanedione and malonaldehyde are effective in strong alkaline (194) and strong acid solutions (195), respectively, and although arginine is modified in 2,3-butanedione solutions under mild conditions the reactive species was shown to be a trimer (196, 197). Elemental analyses revealed (119, 186) that two molecules of PGO form a condensation product with one molecule of free or *N*-acetylated arginine [ $\text{HN}=\text{C}(\text{NHR})-\text{NH}_2$ ] and no mono-PGO substituted derivatives are formed. From the known reactions of PGO with amidines ( $\text{HN}=\text{CR}-\text{NH}_2$ ) (198, 199), it was postulated (119, 186) that the first molecule of PGO condenses in the rate-limiting step with the  $\delta$ -guanido group to give **2a**, which undergoes further loss of a water molecule to give **2b**. Addition of a second PGO to a ring nitrogen of **2a** would give **3a** but since periodate ( $\text{IO}_4^-$ ), which oxidatively cleaves 1,2-diols (200), did not alter the  $R_F$  measured by TLC of the arginine-PGO derivative, **3b** resulting from condensation of the second PGO with the glyoxaline OH groups was considered the more likely structure (186). Alternatively, PGO dimers present in the reaction mixture (186, 201) (Figure A2.1, Section A2.1) could condense with the  $\delta$ -guanido group to yield **3b** (186).



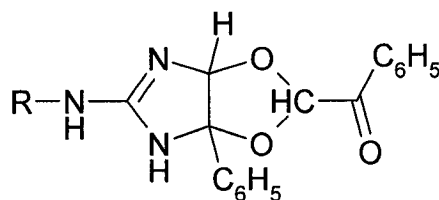
**2a** (M+134 u)



**2b** (M+116 u)

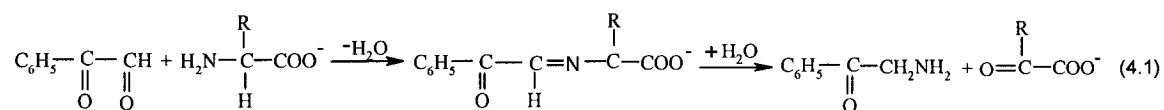


**3a** (M+268 u)



**3b** (M+250 u)

PGO treatment has been proposed as a method to identify free *N*-terminal residues since it induces oxidative deamination of the  $\alpha$ -amino group of peptides and proteins (119, 186):

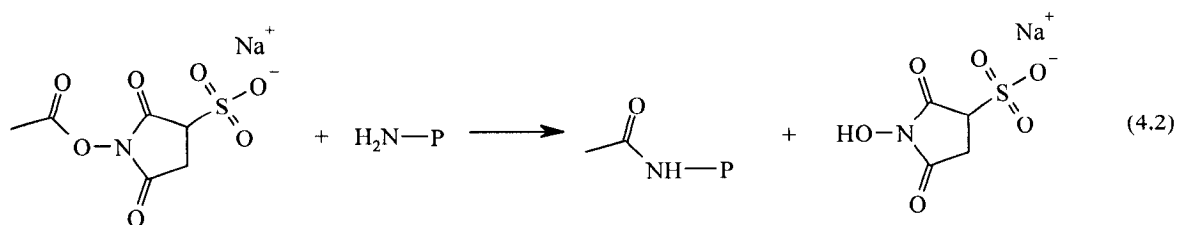


**1**

**4** (M+116 u)

**5** (M-1 u)

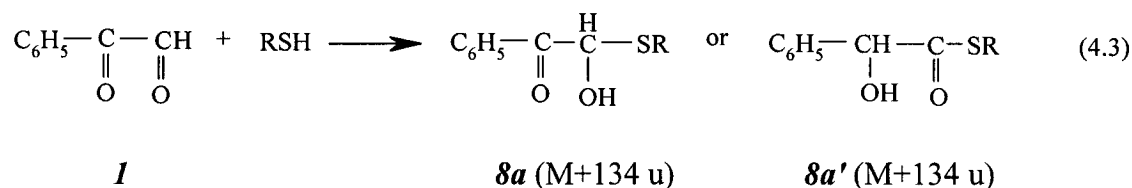
Condensation of PGO with a primary amino group forms the Schiff base **4**, and transamination on hydrolysis of **4** yields the  $\alpha$ -ketoacid **5** (119) as shown in Reaction 4.1. Sulfo-NHS acetate **6**, which stably caps primary amino groups with an acetyl group **7** (202), was used here to probe PGO-induced oxidative deamination.



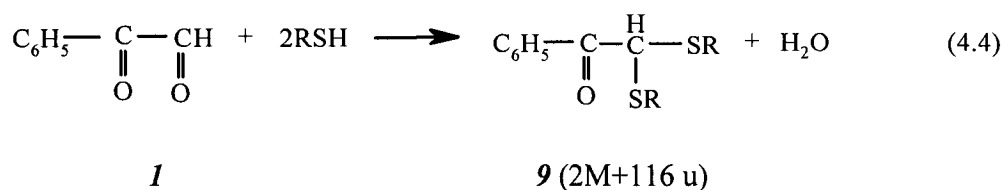
**6**

**7** (M+42 u)

Based on elemental analysis, equimolar PGO was shown to form an addition product with GSH (187). Nucleophilic attack of GSH at the formyl carbonyl carbon produced the hemithioacetal **8a** or hemithioketal **8a'** addition product (203):



In the presence of excess GSH, the dithioacetal **9** was formed (204):



Interestingly, equimolar PGO was reported to form a condensation product with loss of H<sub>2</sub>O with thiols such as free cysteine (but not GSH) that possess an α-amino group in close proximity to the thiol (187).

Typically, millimolar PGO is added to micromolar protein to target arginine residues (50, 55, 186, 205). Despite the difficulty in controlling derivatization in a site-directed manner when excess reagent is employed, a single arginine residue was reported PGO-modified following amino acid analysis of BCuZnSOD exposed to ~4×10<sup>4</sup>-fold molar excess of the dicarbonyl (50, 55). Arg141 was identified as the modified site on two-dimensional peptide mapping of tryptic peptides from the CNBr fragments. Since

PGO-modified BCuZnSOD was found to exhibit only 10–20% residual SOD activity, Arg141 was assumed to be critical for activity (50, 55, 58, 112), and site-directed mutagenesis (109) has corroborated its key role in SOD catalysis. We initially chose PGO as an Arg141 specific reagent to investigate the possible binding of anions close to the active-site copper but accurate mass measurements by ESI-MS of intact PGO-modified BCuZnSOD reveal that the protein is modified at a number of sites. In addition to the four arginine residues, Cys6 and the ten lysine residues in the BCuZnSOD monomer are potential PGO targets (119, 187). Furthermore, lysine as well as arginine modification could contribute to loss of SOD activity since the double K120L,K134T mutant exhibits only 30% SOD activity (206), and acetylation of native BCuZnSOD at 7–8 lysines decreased the activity to 15–20% (50).

If PGO-modification is to be used as a complementary tool to site-directed mutagenesis in structure-function studies on enzymes, it is critical to identify the number and sites of PGO-modification. In the past, the number of chemically modified residues was determined by acid hydrolysis of the peptide bonds in 6 M HCl followed by amino-acid analysis (207, 208). The number of PGO-derivatized arginine residues was assumed equal to the difference in the number of arginines released from the untreated and PGO-treated protein (50, 55, 119, 186). This approach requires that no labels are lost during hydrolysis in 6 M HCl, and that the number of unmodified arginines or other residues are accurately determined (50, 55).

ESI-MS and MALDI-ToF-MS are powerful techniques for identifying peptide and protein modification from observed mass shifts. Mass measurements on the intact protein or peptide reveal the stoichiometry of the modification reaction, and the residues

modified are identified by sequencing the modified peptides by tandem MS (209). PGO modification of low-mass peptides containing arginine, lysine and cysteine residues was examined by MS to re-evaluate the use of PGO as an arginine-specific reagent. The stability of PGO-arginine derivatives at low pH (186) is advantageous for peptide analysis by MS in positive-ion mode. The reactivity of the three residues in low-mass peptides with PGO was established, the modified peptides were characterized, and the stability of the labels to ESI-MS and MALDI-MS analysis was determined. The results demonstrate that: (1) arginine residues are highly reactive with PGO corroborating previous results; (2) doubly PGO-labelled species with a mass consistent with **3a/3b** are formed on incubation of arginine-containing peptides with PGO; (3) the peptides do not undergo PGO-induced deamination of their *N*-terminal  $\alpha$ -amino groups (reaction 4.1); (4) lysine residues are not reactive with PGO; (5) singly PGO-labelled GSH with a mass consistent with **8a/a'** and doubly to triply PGO-labelled GSH are formed in incubations with PGO; and (6) ESI-MS is the method of choice for the analysis of PGO derivatives since they are less stable in the MALDI source. Following MS characterization of the PGO-peptide reactions, PGO-modified BCuZnSOD was analyzed. The results demonstrate that PGO is specific for arginine residues in this protein. Since  $\alpha,\alpha'$ -dicarbonyls are the main participants in the formation of advanced glycation end-products (AGEs) *in vivo* (210-212), proteins containing arginine residues should be particularly susceptible to AGE-induced inactivation.

### **4.3 Materials and methods**

#### **4.3.1 Materials**

Erythrocyte BCuZnSOD and trypsin (modified, sequencing grade) were purchased from Roche Applied Science. Adrenocorticotrophic hormone fragment 18–39 (ACTH), porcine renin substrate tetradecapeptide (PRS), glutathione (GSH; reduced form), type III horse heart cytochrome *c* (cytc), xanthine, xanthine oxidase (33 units/mL), phenylglyoxal (PGO) hydrate ( $C_8H_6O_2 \cdot nH_2O$ ) were obtained from Sigma. Sulfo-NHS acetate was supplied by Pierce and the tripeptide, H-Met-Arg-Phe-OH (MRF), by Bachem AG. Reagents were of analytical grade or higher, and all chemical and biochemicals were used without further purification. Nanopure water (specific resistance 18 M $\Omega$ -cm) from a Millipore Simplicity water purification system was used to prepare all solutions.

#### **4.3.2 Methods**

##### **4.3.2.1 PGO modification reactions**

A 200-mM PGO stock solution in ethanol or methanol was prepared by weight. Stock peptide solutions in water (unless otherwise indicated) were also prepared by weight and BCuZnSOD was determined spectrophotometrically ( $\epsilon_{258} = 10.3 \text{ mM}^{-1} \text{ cm}^{-1}$  per dimer) (47). The PGO modifications were carried out as described previously (55, 119). Briefly, peptide (0.05–1 mM) or BCuZnSOD (30–150  $\mu\text{M}$ ) was incubated with 0.6–45 mM PGO in 250 mM sodium bicarbonate (pH 8.0) at room temperature for the times indicated in the figure legends. TFA (0.1–10%) was added to quench the reactions by lowering the pH below 4, and the small reagents were removed from the peptides and BCuZnSOD using C<sub>18</sub> and C<sub>4</sub> ZipTips (Millipore), respectively. The tips were pre-equilibrated with 5% ACN/0.1% TFA, the tip-absorbed samples were washed three times with the equilibrating solution, and eluted with 60% ACN/0.1% TFA for MS analysis.



Alternatively, the small reagents were removed from BCuZnSOD with water or 0.1% TFA by centrifugal ultrafiltration (3×10 min) at 12,000 rpm and 4°C on an Ultrafree-0.5 filter with a 10,000 MW cut-off (Millipore). Buffer exchange was also carried out by ultrafiltration where desired.

#### **4.3.2.2 NEM and Sulfo-NHS acetate modification reactions**

BCuZnSOD or PGO-modified BCuZnSOD (10  $\mu$ M) in 0.1% TFA was incubated with 1.5 mM NEM at 4°C overnight. NEM was removed from the protein by ultrafiltration prior to tryptic digestion.

Sulfo-NHS acetate modifications were carried out following the supplier's instructions. Briefly, the acetate, either as the solid or as an aqueous solution (prepared just prior to use) was added to untreated or PGO-modified MRF, ACTH, and BCuZnSOD in 250 mM sodium bicarbonate (pH 8.0) to give  $\geq 10$ -fold molar excess of the acetate over free amino groups in the substrates. The mixtures were incubated at room temperature for 1 h, purified using C<sub>18</sub> or C<sub>4</sub> ZipTips and analyzed by MS as described below.

#### **4.3.2.3 Tryptic digestion of BCuZnSOD**

Because of its high stability, BCuZnSOD is frequently denatured by heating to 90°C prior to digestion (213, 214). To avoid loss of the PGO labels, digestion was carried out on the less stable copper-depleted protein at 37°C. A PGO modification reaction containing ~25  $\mu$ M BCuZnSOD was quenched with 1% TFA, 2 mM DDC was added to chelate the copper, and the sample was incubated at room temperature for 2 h. The small reagents were removed and the solvent was changed to 10 mM TrisHCl buffer (pH 7.9)

by ultrafiltration. Trypsin was added (20/1 w/w, protein/trypsin) and copper-depleted BCuZnSOD (20  $\mu$ g) was digested at 37°C for 3 h.

#### **4.3.2.4 ESI-MS and ESI-MS/MS analysis**

The desalted peptides or protein were diluted into 50–60% ACN/0.1% TFA to the final concentrations indicated in the figure legends, and directly infused into the ESI source of a Q-ToF2 (Water Micromass) operating in positive-ion mode. Unless otherwise indicated, the mass spectrometer was operated at a capillary temperature of 80°C and voltages of 3.2 kV (capillary), 45 V (cone), 9.1 kV (ToF), 10 V (collision), 550 V (multiplier), and 2.1 kV (MCP). The instrument was mass calibrated to an accuracy of 5–10 ppm with human [Glu<sup>1</sup>]-fibrinopeptide B ( $M_r$  = 1570.68 u), and the samples were analyzed at an average resolution of 8,000.

Product-ion spectra were recorded on the Q-ToF2 by selecting the  $MH^+$  or  $MH_2^{2+}$  ions of the PGO-modified peptides in the quadrupole, fragmenting these ions in the collision cell, and analyzing the product ions in the ToF analyzer. The transmission window of the quadrupole and the instrumental parameters ( $\underline{L}M$  and  $\underline{H}M$  Res, capillary voltage, cone voltage) were selected to maximize the TIC. The collision cell was pressurized to  $5.5 \times 10^{-5}$  torr with  $N_2$  to affect CID, and the product-ion spectra were recorded at the collision voltages indicated in the figure legends.

#### **4.3.2.5 MALDI-ToF-MS analysis**

Peptides were mixed with an equal volume of matrix [ $\alpha$ -CHCA: 33% ACN/0.1% TFA (2:1 v/v) or saturated 2,5-DHB in ethanol]. Aliquots of 1–2  $\mu$ L were spotted onto a stainless steel MALDI target plate of a Waters Micromass M@LDI<sup>TM</sup> mass spectrometer operating in reflectron, positive-ion mode with accelerating, pulse and

detector voltages of +15 kV, 2.5 kV and 1.8 kV, respectively. External mass calibration was performed with a standard solution containing 10 nmol/mL each of angiotensin I ( $M_r = 1296.6853$  u), PRS ( $M_r = 1758.9331$  u) and ACTH ( $M_r = 2465.1989$  u) in an equal volume of matrix (10 mg/mL of  $\alpha$ -CHCA in 50% ACN/50% ethanol) and the ToF mass analyzer was found to have a mass accuracy of 50 ppm. The samples were analyzed at an average resolution of 10,000.

#### 4.3.2.6 SOD activity assay

SOD activity was monitored by following the inhibition of  $\text{cytc}^{\text{III}}$  reduction as described previously (47). Aliquots of BCuZnSOD from the PGO incubations were diluted 70-fold with 50 mM sodium phosphate buffer (pH 7.8) before addition to the assay solution (10  $\mu\text{M}$   $\text{cytc}^{\text{III}}$  and 50  $\mu\text{M}$  xanthine in the same buffer) in a 1-cm cuvette at 25°C. Xanthine oxidase was added and following rapid mixing,  $\text{cytc}^{\text{III}}$  reduction was monitored at 550 nm every 15 s over 3 min. The xanthine oxidase concentration was adjusted to produce an initial  $\Delta A_{550}$  of  $0.025 \pm 0.003$  absorbance unit/min ( $\sim 5$  munits/mL). Competition with BCuZnSOD for  $\text{O}_2^{\bullet-}$  decreases the rate of  $\text{cytc}^{\text{III}}$  reduction (47).

## 4.4 Results

### 4.4.1 Modification of MRF by PGO and sulfo-NHS acetate

Following a 30-min incubation of 146  $\mu\text{M}$  MRF with equimolar PGO at RT, the MALDI mass spectrum was dominated by the protonated molecular ion,  $(\text{MRF})\text{H}^+$  at  $m/z$  452.7. The relative abundance (RA) of the  $\text{MH}^+$  ion of the **2b** derivative of MRF,  $(\text{MRF}_{2b})\text{H}^+$ , at  $m/z$  568.8 was  $<2.5\%$  (data not shown). In contrast,  $(\text{MRF}_{2b})\text{H}^+$  and

(MRF<sub>3b</sub>)H<sup>+</sup> ions dominated the MALDI (Figure 4.1E, Table 4.1) and ESI (Figure 4.1B, Table 4.1) spectra, respectively, when MRF was incubated with 2.5-fold molar excess of PGO for 1 h. The (MRF<sub>3b</sub>)H<sup>+</sup> ion at m/z 703.6 (Figure 4.1B, Table 4.1) was selected for ESI MS/MS analysis to confirm the site(s) of PGO labelling. The *b*<sub>2</sub> (Met-Arg), *c*<sub>2</sub> (Met-Arg) and *y*<sub>2</sub> (Arg-Phe) fragment ions were shifted by 116 u relative to those in the MS/MS spectrum of untreated MRF, whereas no mass shifts were observed for the *a*<sub>1</sub> (Met) and *y*<sub>1</sub> (Phe) ions (Figure 4.2A vs 4.2B), indicating that Arg2 is modified by PGO. Significantly, the fragment ions of doubly PGO-labelled (MRF<sub>3b</sub>)H<sup>+</sup> have a mass increase of 116 u corresponding to that expected for type **2b** derivatives. Thus, type **3b** ions lose a PGO moiety to yield type **2b** ions during CID and also in the MALDI source (Figure 4.1E, Table 4.1). Also, low-mass fragment ions at m/z 227.120 and 300.139 containing the δ-guanido group were mass shifted by 116 u in contrast to the unmodified Arg fragment ions at m/z 112.093 and 185.108.

No unmodified MRF was detected in the mass spectra following incubation with 50-fold molar excess PGO (Figures 4.1C,F, Table 4.1). In addition to the dominant (MRF<sub>3b</sub>)H<sup>+</sup> ion, a peak with a RA <10% is present in the ESI mass spectrum at m/z 953 (Figure 4.1C, Table 4.1) corresponding to (MRF+4PGO-2H<sub>2</sub>O)H<sup>+</sup>. The detection of quadruply PGO-labeled MRF suggests, as proposed by Takahashi (186), that the PGO dimer also condenses with the δ-guanido group since the MS/MS spectra show no evidence for PGO labelling at additional sites in MRF. Sodiated ions (MNa<sup>+</sup>) of PGO monohydrate (PGO•H<sub>2</sub>O) and dihydrate (PGO•2H<sub>2</sub>O) at m/z 175.06 and 193.05, respectively, and of hydrated PGO dimers, 2PGO•2H<sub>2</sub>O, 2PGO•3H<sub>2</sub>O and 2PGO•4H<sub>2</sub>O, at m/z 327.10, 345.10, and 363.11, respectively, were observed in the ESI mass spectrum

of PGO alone (Figure A2.1, Section A2.1), confirming that PGO dimers were present in the reaction mixture. The 3-h MALDI spectrum (Figure 4.1F, Table 4.1) shows the same peaks as the 1-h ESI spectrum (Figure 4.1C, Table 4.1) but with extra peaks corresponding to the  $MH^+$  ions of  $MRF_{2b}$ ,  $MRF_{2a}$ ,  $MRF_{3b}$  and  $MRF+3PGO-2H_2O$  due to loss of PGO or PGO- $H_2O$  from multiply PGO-labelled MRF.

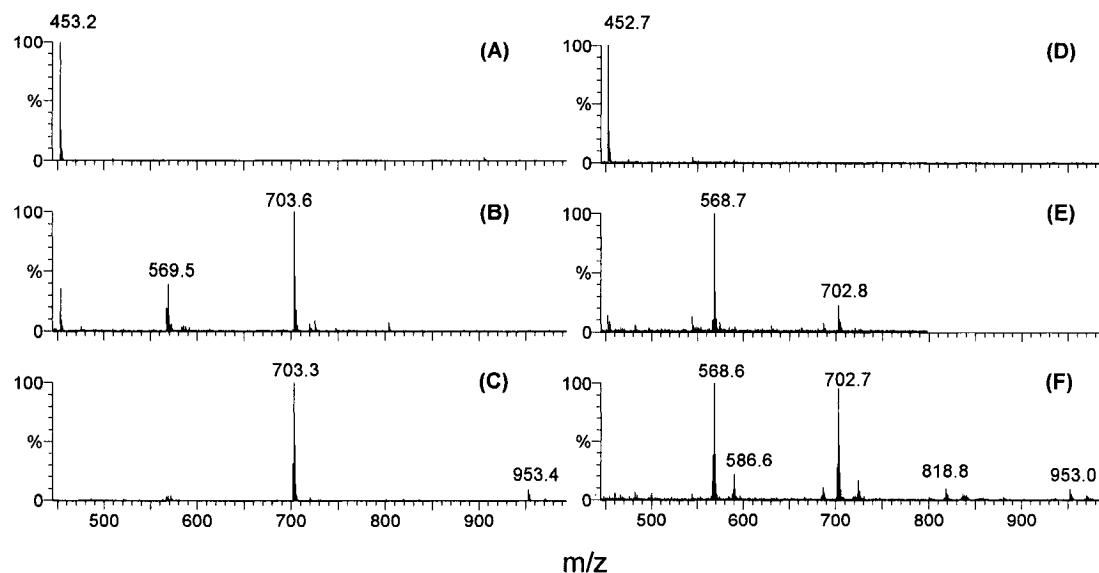


**Figure 4.1 ESI and MALDI mass spectra of PGO-modified MRF peptide.** ESI mass spectrum of: (A) untreated MRF, (B) 0.67 mM MRF and 1.7 mM PGO after 1 h incubation; (C) 0.90 mM MRF and 45 mM PGO after 1 h incubation. MALDI mass spectrum of: (D) untreated MRF; (E) 0.67 mM MRF and 1.7 mM PGO after 1 h incubation; (F) 0.90 mM MRF and 45 PGO mM after 3 h incubation. Experimental conditions: following incubation at RT in 250 mM  $NaHCO_3$  (pH 8.0), 20  $\mu$ L of 1% TFA was added to 110  $\mu$ L of sample to quench the PGO-modification reaction by lowering the pH to 3–4. The peptide was desalted on ZipTip $C_{18}$ , eluted into 60% ACN/0.1% TFA, and directly infused at 1  $\mu$ L/min into the ESI source or 1  $\mu$ L was mixed with 9  $\mu$ L of saturated 2,5-DHB in ethanol, spotted onto a 100-well MALDI plate (1  $\mu$ L per well) and air dried. The instrumental parameters were: ESI-MS: source-block temperature 80°C,  $\underline{LM}$  &  $\underline{HM}$  Res 5.0, capillary voltage 3.2 kV, cone voltage 45 V, collision voltage 10 V, ToF –9.1 kV, and MCP 2.1 kV. MALDI MS: reflectron, positive-ion mode, accelerating voltage +15 kV, pulse voltage ~2.5 kV, and detector voltage 1800 V. Peak assignments are given in Table 4.1.

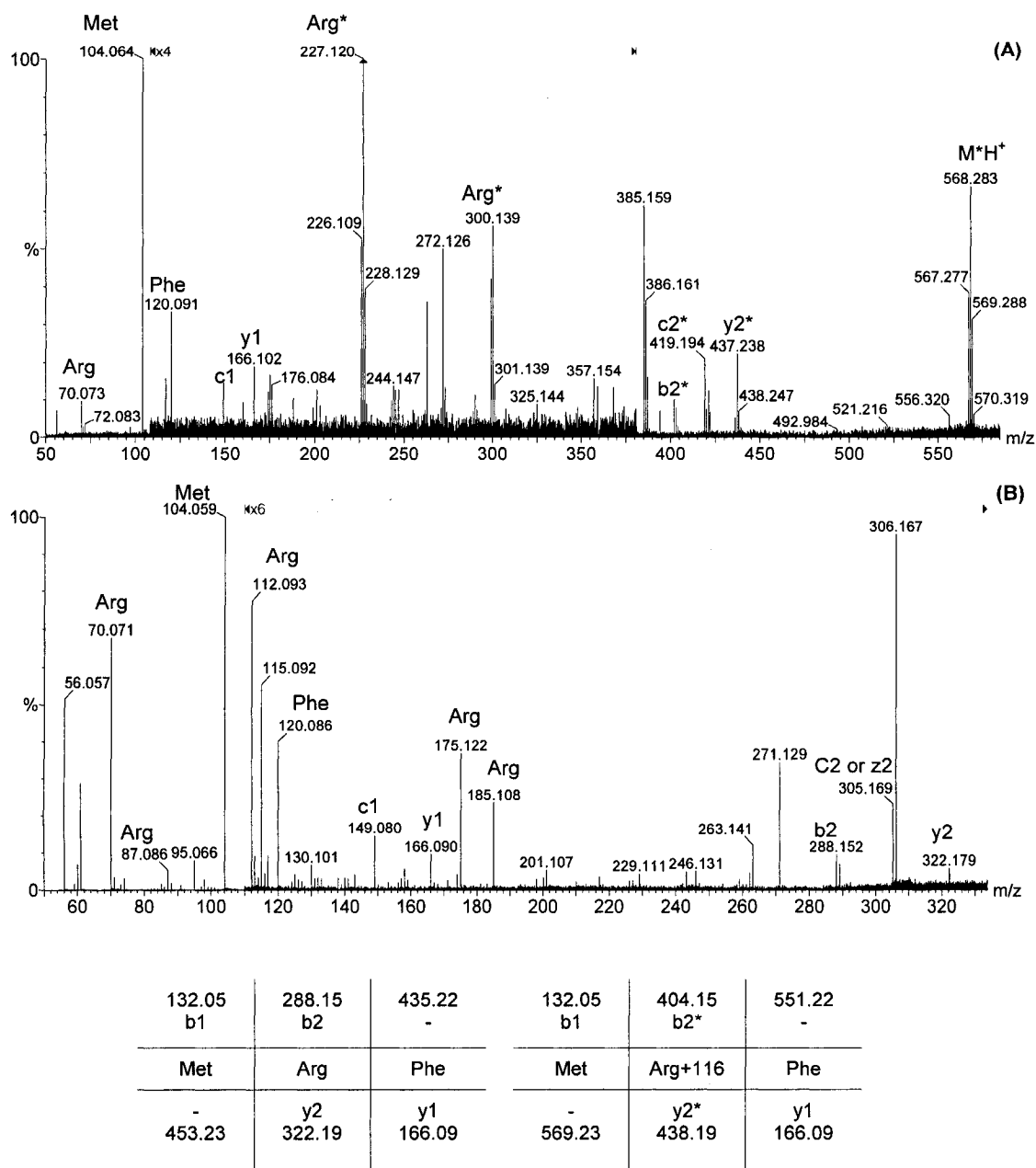


Figure 4.2 ESI MS/MS analysis of doubly PGO-labelled MRF peptide. Product-ion spectrum of the  $MH^+$  ion of (A) unmodified MRF at  $m/z$  453, and (B)  $MRF_{3b}$  at  $m/z$  703. Experimental procedures: the  $MH^+$  ions were selected in Q1 and the fragment ions produced by CID in Q2 were separated in the ToF analyzer. The same samples used in Figures 4.1A and 4.1C were directly infused at 0.5  $\mu$ L/min into the ESI source of the MS operating under the conditions given in the legend of Figure 4.1 with the exceptions: LM Res & HM Res 16.0, collision voltage 45.0 V. Asterisks (\*) denote type **2b** ions. The peak intensities in (A) the  $m/z$  110–380 and (B) the  $m/z$  110–340 ranges were amplified 4- and 6-fold, respectively.

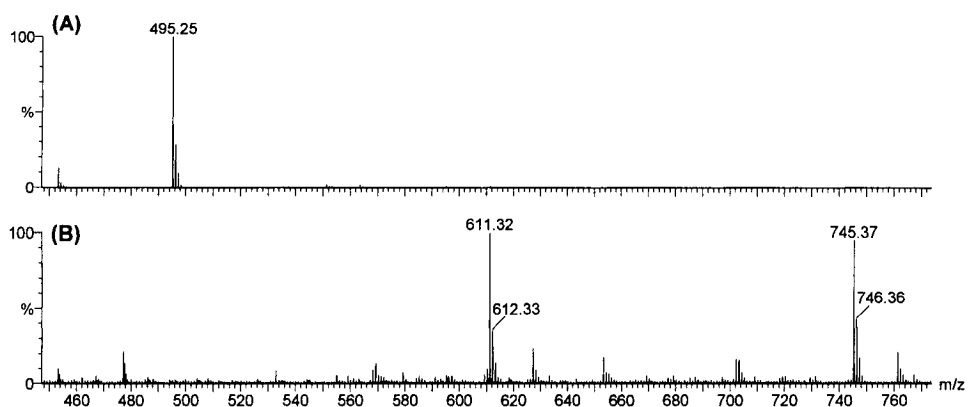


Figure 4.3 **Acetylation of untreated and PGO-labelled MRF.** ESI mass spectrum of: (A) 0.5 mM MRF and 5 mM sulfo-NHS acetate after 1 h incubation; and (B) sample from Figure 1C following dilution to 0.5 mM MRF and 1 h incubation with 5 mM sulfo-NHS acetate. Experimental conditions: Samples were incubated at RT in 250 mM NaHCO<sub>3</sub> (pH 8.0), and the MS procedures are given in the legend of Figure 4.1. Peak assignments are given in Table 4.1.

Takahashi (186) reported that PGO readily deaminated the  $\alpha$ -amino group of peptides and proteins (Reaction 4.1). Thus, to assess deamination, untreated MRF and PGO-modified MRF (the sample from Figure 4.1C) were incubated with 10-fold molar excess of sulfo-NHS acetate. The ESI mass spectra (Figure 4.3, Table 4.1) show that after 1 h incubation, (MRF+CH<sub>2</sub>CO)H<sup>+</sup>, (MRF<sub>2b</sub>+CH<sub>2</sub>CO)H<sup>+</sup>, and (MRF<sub>3b</sub>+CH<sub>2</sub>CO)H<sup>+</sup> ions were observed at m/z 495.3, 569.3, and 703.3, respectively in ESI mass spectra (Figure 4.3, Table 4.1) indicating that the free  $\alpha$ -amino group in MRF did not react with PGO.

#### 4.4.2 Modification of porcine renin substrate (PRS) by PGO

This 14-residue peptide (DRVYIHPFLLVYS) contains Arg2 that reacts with PGO at pH 8.0 (119). The MALDI spectrum of the 1-h incubation of PRS with 50-fold molar excess of PGO was dominated by the MH<sup>+</sup> ion of unmodified PRS (Figure A2.5A, Appendix A2.4), whereas (PRS<sub>2b</sub>)H<sup>+</sup> was dominant after 5 h incubation (Figure 4.4A,

Table 4.1 ), while  $(\text{PRS}_{2a})\text{H}^+$  was more abundant after 4 h incubation (Figure A2.5B, Appendix A2.4). The deconvolved ESI mass spectrum of the 5-h incubation is dominated by  $(\text{PRS}_{3b})\text{H}^+$  but, as seen for MRF,  $(\text{PRS}+4\text{PGO}-2\text{H}_2\text{O})\text{H}^+$  ions are also present (Figure 4.4B, Table 4.1). The doubly charged  $(\text{PRS}_{3b})\text{H}_2^{2+}$  ion at  $m/z$  1005) was selected for ESI MS/MS analysis, and fragment ions containing Arg2 ( $b_2$  to  $b_{13}$  and  $y_{13}$ ) are mass shifted by 116 u whereas the  $y_2$ , and the  $y_5$  to  $y_{12}$  ions that contain His6 and His9 are not mass shifted (Figure 4.4C). Thus, Arg2 must be the site of PGO labelling and, as seen for MRF (Figure 4.2), CID of  $(\text{PRS}_{3b})\text{H}_2^{2+}$  yields type **2b** fragments, providing further evidence that di-PGO substituted derivatives readily fragment in the CID cell.

#### 4.4.3 Modification of ACTH by PGO and sulfo-NHS acetate

This 22-residue peptide (**RPVKVYPNGAEDESAEAFPLEF**) contains Arg1, as well as Lys4, which also may react with PGO (119). Like PRS, the  $(\text{ACTH})\text{H}^+$  ion at  $m/z$  2465.3 dominated the MALDI mass spectrum of the 1-h incubation with 50-fold molar excess of PGO, while after 4 h (Figure A2.6, Appendix A2.4) and 5 h incubation,  $(\text{ACTH}_{2b})\text{H}^+$  ( $m/z$  2581.4) is the base peak with minor  $(\text{ACTH})\text{H}^+$  and  $(\text{ACTH}_{2b}-\text{H}_2\text{O})\text{H}^+$  peaks at  $m/z$  2465.3 and 2563.6 (Figure 4.5A, Table 4.1). The doubly PGO-labelled  $(\text{ACTH}_{3b})\text{H}^+$  ions ( $m/z$  2715.3) dominate the ESI mass spectrum of the 5-h incubation (Figure 4.5B, Table 4.1) as observed for the MRF and PRS peptides (Figures 4.1C and 4.4B). All  $b$  ions detected in the product-ion spectrum of  $(\text{ACTH}_{3b})\text{H}_2^{2+}$  ( $m/z$  1358) are mass shifted by 116 u (Figure 4.5C). However,  $y_{20}$ , the largest  $y$  ion, was not mass shifted, indicating that Arg1 but not Lys4, Asn8 or Gly9 was modified by PGO. Again, CID of doubly-PGO labelled ACTH ions gave rise to only type **2b** fragment ions as noted for MRF and PRS (Figures 4.2A and 4.4C).



Acetylation studies support the MS/MS data. Both native and PGO-modified ACTH are doubly and triply acetylated by sulfo-NHS acetate (Figure 4.6, Table 4.1).  $(\text{ACTH}+2\text{CH}_2\text{CO})\text{H}^+$  and  $(\text{ACTH}+3\text{CH}_2\text{CO})\text{H}^+$  ions dominate the ESI mass spectrum of acetylated ACTH, and the corresponding ions,  $(\text{ACTH}_{2b/3b}+2\text{CH}_2\text{CO})\text{H}^+$  and  $(\text{ACTH}_{2b/3b}+3\text{CH}_2\text{CO})\text{H}^+$ , dominate the spectrum of acetylated PGO-modified-ACTH, consistent with the  $\delta$ -guanido group being the only target of PGO in ACTH. Thus, the free  $\alpha$ -amino terminus and the  $\epsilon$ -amino of Lys4 as well as one unknown group (likely tyrosine (215)) are targets of sulfo-NHS acetate (Reaction 4.4).

#### 4.4.4 Modification of glutathione (GSH) by PGO

The dominant ions observed in the ESI mass spectrum of a 5-h GSH/PGO incubation (2:1 molar ratio) are  $(\text{GSH})\text{H}^+$  at  $m/z$  308.1,  $(\text{GSH}_{8a/a'})\text{H}^+$  at  $m/z$  442.1 and an ion arising from doubly PGO-labelled GSH  $(\text{GSH}+2\text{PGO}-12)\text{H}^+$  at  $m/z$  563.6 (Figure 4.7A, Table 4.2). ESI MS/MS analysis of  $(\text{GSH}_{8a/a'})\text{H}^+$  revealed that fragment ions containing Cys2 ( $b_2$ ,  $b_3$  and  $y_2$ ) are mass shifted by 134 u suggesting that Cys2 is the target of PGO.  $(\text{GSH}_{8a/a'})\text{H}^+$  is unstable under the MS/MS conditions since  $(\text{GSH})\text{H}^+$  ( $m/z$  308.25) and its  $b_2$ ,  $y_2$  and  $z_2$  fragment ions at  $m/z$  233.18, 179.15 and 162.12, respectively, are also seen in the product-ion spectrum in Figure 4.7C. The structure of the  $(\text{GSH}+2\text{PGO}-12)\text{H}^+$  ion at  $m/z$  563.6 was not further elucidated by MS/MS.

Following GSH incubation with 50-fold molar excess of PGO,  $\text{MH}^+$  and  $\text{MNa}^+$  ions derived from addition and condensation products dominated (Figure 4.7B, Table 4.2):  $\text{GSH}+\text{PGO}-33$  ( $m/z$  409.1),  $\text{GSH}+\text{PGO}-\text{H}_2\text{O}$  ( $m/z$  424.1),  $\text{GSH}+\text{PGO}$  ( $m/z$  464.1),  $\text{GSH}+2\text{PGO}-\text{H}_2\text{O}$  ( $m/z$  558.2),  $\text{GSH}+2\text{PGO}-16$  ( $m/z$  560.2/582.1), and  $\text{GSH}+3\text{PGO}-16$  ( $m/z$  694.2). The latter two  $\text{MH}^+$  ions ( $m/z$  560.2, 694.2) exhibit similar product-ion

spectra (Figures 4.7D and 4.7E) indicating that they are modified at the same site, and the 116-u mass shift in the  $b_2$  and  $y_2$  ions suggests that PGO targets Cys2. As seen previously for MRF, PRS, ACTH, and here for GSH (Figures 4.2A, 4.4C, 4.5C, 4.7D), doubly PGO-labelled peptides yield only singly PGO-labelled fragment ions, as do derivatives such as (GSH+3PGO-16) (Figure 4.7E), which is likely formed on reaction with the PGO dimer.

Since both thiol and  $\delta$ -guanido groups were found to be derivatized, attempts were made to compare by mass spectrometry the relative reactivity of PGO with GSH and MRF. However, when equal concentrations of GSH and MRF in 60%ACN/0.1% TFA were directly infused into the Z-spray ion source of the mass spectrometer, the RA of (GSH) $H^+$  was <10% that of (MRF) $H^+$  in the resulting ESI mass spectrum (Figure A2.7A, Appendix A2.4). Ion suppression is the likely reason why (MRF $_{2b}$ ) $H^+$  and (MRF $_{3b}$ ) $H^+$  but no GSH-derived ions were observed in the ESI mass spectrum of an 80-min GSH/MRF/PGO (1:1:50) incubation (Figure A2.7A, Appendix A2.4). A comparison of Figure 4.1C and Figure 4.7B reveals that MRF $_{3b}$  is the main component in the 1-h MRF/PGO (1:50) incubation whereas multiple derivatized ions are present in the 4-h GSH/PGO (1:50) incubation. Thus, the  $\delta$ -guanido group of arginine may be more susceptible to PGO-labelling than cysteine. An early report (200) of complex formation between bicarbonate and the guanidinium group, which lowers its  $pK_a$  and thus promotes nucleophilic attack at the carbonyl carbon of PGO, also suggests that this reagent is more reactive with arginine residues than with cysteine or lysine residues.

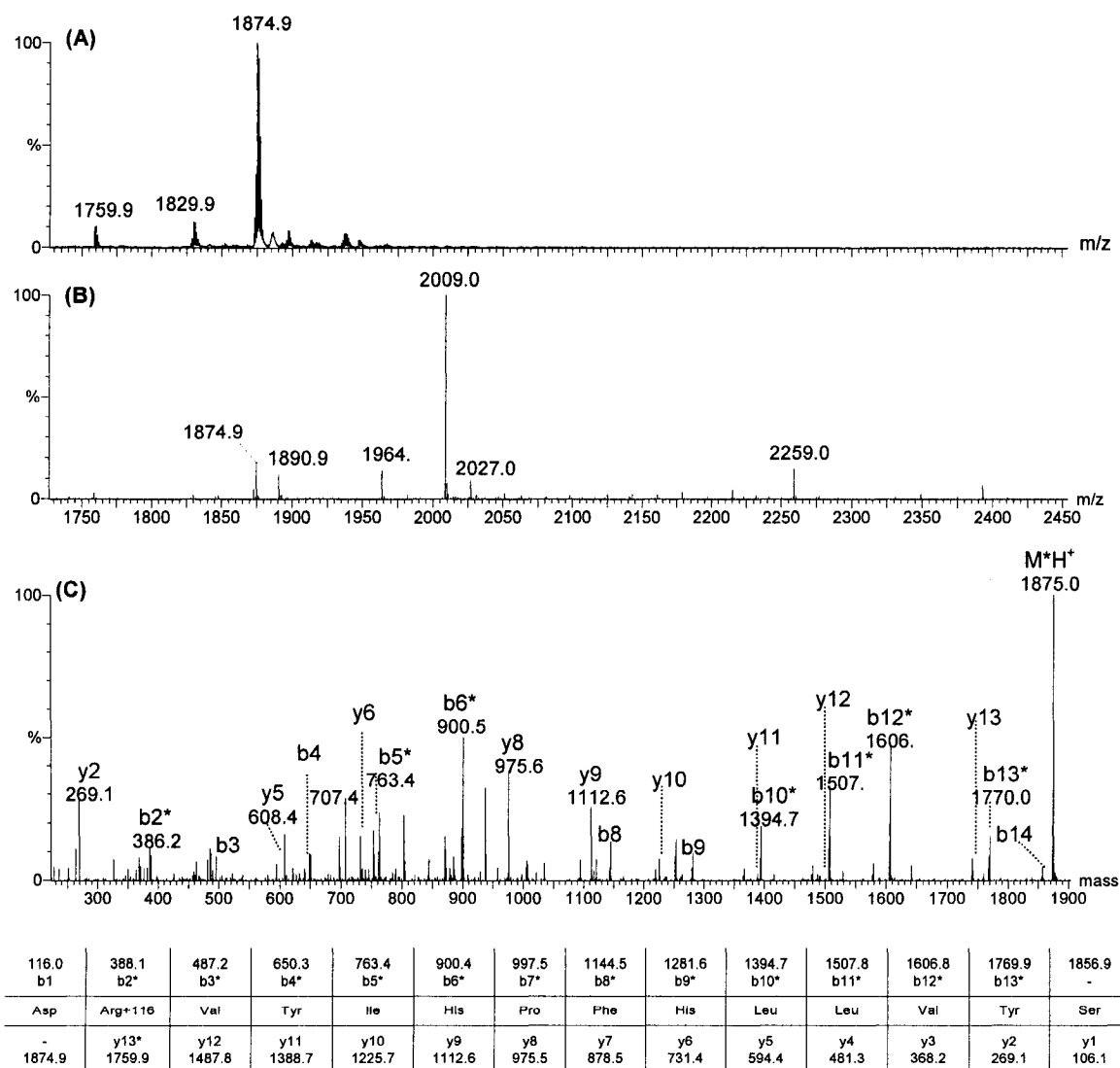
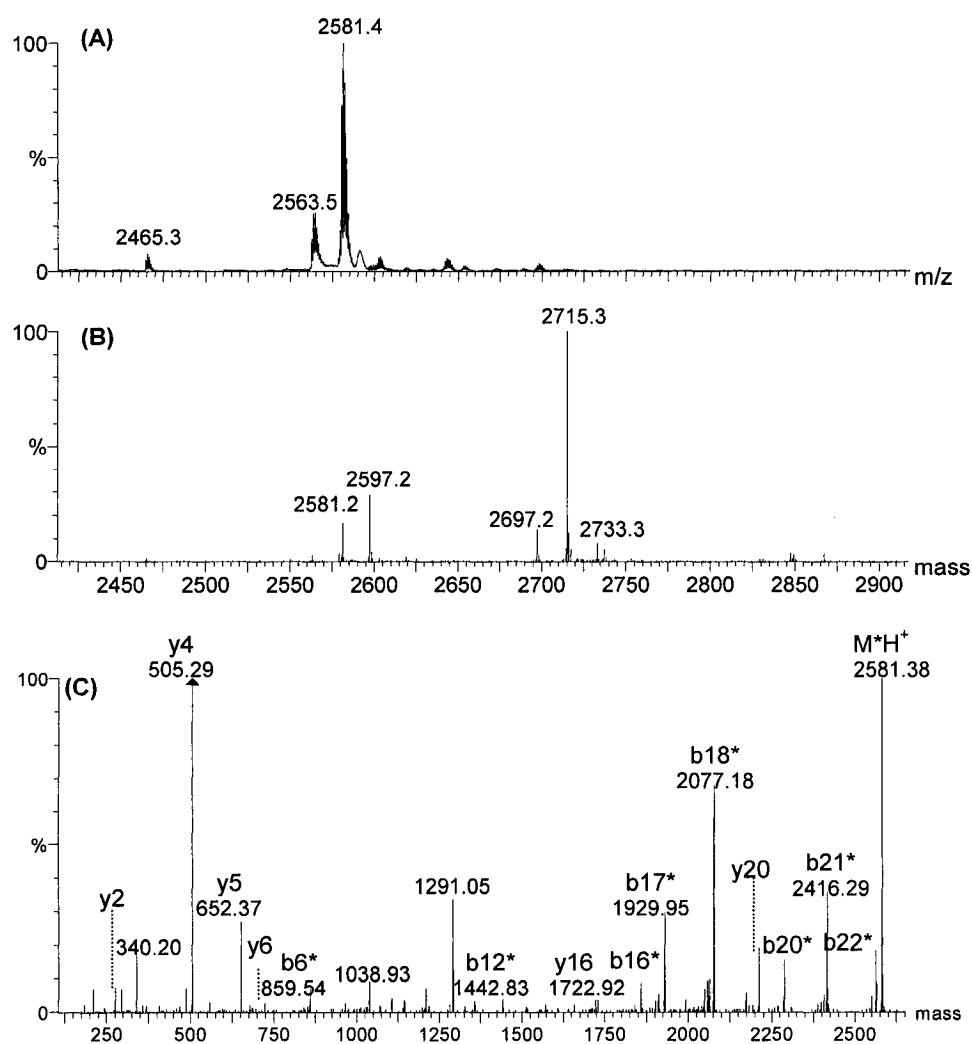


**Figure 4.4 Mass spectrometric analysis of PGO-modified porcine renin substrate (PRS).** (A) MALDI, (B) ESI, and (C) product-ion mass spectrum of 80  $\mu$ M PRS and 4 mM PGO after 5 h incubation. Experimental conditions: the sample was incubated at RT in 250 mM  $\text{NaHCO}_3$  (pH 8.0), and 10  $\mu$ L of 10% TFA was added to 37  $\mu$ L of sample to quench the PGO-modification reaction by lowering the pH to 3–4. The peptide was desalted on a ZipTipC<sub>18</sub>, eluted into 60% ACN/0.1% TFA, and directly infused at 1  $\mu$ L/min (B) or 0.5  $\mu$ L/min (C) into the ESI source or diluted 40-fold, mixed with an equal volume of matrix solution (10 mg/mL  $\alpha$ -CHCA in 1:1 ACN/EtOH), spotted (1  $\mu$ L per well) onto a 100-well MALDI plate and air-dried. The MS parameters are given in the legend of Figure 4.1. To record the product-ion spectrum in (C), the doubly charged  $(\text{PRS}_{36}+2\text{H})^{2+}$  ion at  $m/z$  1005 was selected in Q1 and the fragment ions produced by CID in Q2 at a collision voltage of 32 V were separated in the ToF analyzer. (B) and (C) are the mass spectra processed using MaxEnt 3. Asterisks (\*) in (C) denote type **2b** ions. Peak assignments for (A) and (B) are given in Table 4.1.



273.11 b1*	370.16 b2*	469.23 b3*	597.33 b4*	696.39 b5*	.....	2076.94 b18*	2173.99 b19*	2287.08 b20*	2416.12 b21*	2563.19 -
Arg+116	Pro	Val	Lys	Val	.....	Phe	Pro	Leu	Glu	Phe
- 2581.20	y21 2309.10	y20 2212.04	y19 2112.98	y18 1984.88	.....	y5 652.33	y4 505.27	y3 408.21	y2 259.13	y1 166.09

**Figure 4.5 Mass spectrometric analysis of PGO-modified ACTH.** (A) MALDI, (B) ESI, and (C) product-ion mass spectrum of 80  $\mu$ M ACTH and 4 mM PGO after 5 h incubation. The experimental conditions are given in the legend to Figure 4.4. To record the product-ion spectrum in (C), the doubly charged  $(\text{ACTH}_{36}+2\text{H})^{2+}$  ion at  $m/z$  1358 was selected in Q1 and the fragment ions produced by CID in Q2 at a collision voltage of 65 V were separated in the ToF analyzer. (B) and (C) are the mass spectra processed using MaxEnt 3. The peak intensity in (C) in the  $m/z$  220–2500 range was 2-fold amplified. Asterisks (\*) in (C) denote type *2b* ions. Peak assignments for (A) and (B) are given in Table 4.1.

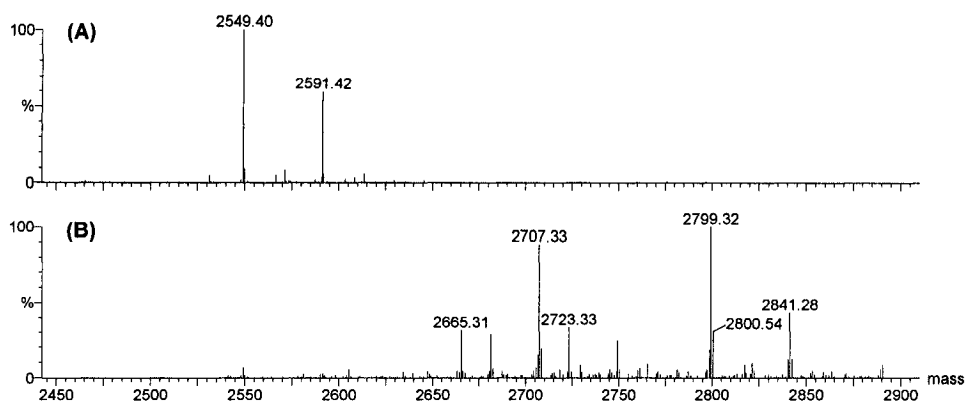


Figure 4.6 **Acetylation of untreated and PGO-labelled ACTH.** ESI mass spectrum of: (A) 56  $\mu$ M ACTH and 1.1 mM sulfo-NHS acetate after 1 h incubation; and (B) the sample from Figure 4.5 following dilution to 60  $\mu$ M ACTH and 1 h incubation with 1.2 mM sulfo-NHS acetate. Experimental conditions: Samples were incubated at RT in 250 mM  $\text{NaHCO}_3$  (pH 8.0), and the MS procedures are given in the legend of Figure 4.1. The mass spectra were processed using MaxEnt 3, and peak assignments are given in Table 4.1.

#### 4.4.5 Modification of BCuZnSOD by PGO and NEM

The deconvolved ESI mass spectrum of native BCuZnSOD exhibited a dominant peak at  $m/z$  with  $M_r = 15,592$  u (Figure 4.8A, Table 4.3). This is in good agreement with the predicted  $M_r$  of 15,551 u of the apoprotein monomer calculated from its amino acid sequence (PDB: 2SODB) with the additional mass of +42 u due to *N*-terminal acetylation (216) and the loss of 2 u due to the single disulfide bond between Cys55 and Cys144 (107). Following incubation of BCuZnSOD with 10-fold molar excess of PGO at room temperature for 1 h, a weak peak appeared at 15,725 u ( $M_r + 133$ ) (Figure 4.8B, Table 4.3) corresponding to the singly PGO-modified monomer. The extent of PGO labelling increased as the PGO concentration or incubation time was increased (Figures 4.8, 4.9) with doubly and triply PGO-labelled derivatives increasing in intensity at the expense of singly labelled protein over 6 h (Figure 4.9, Table 4.3). Quadruply labelled species are also clearly detectable in the 6-h spectrum although they are of low

RA (< 20%). Table 4.3 summarizes all the peaks observed in the ESI mass spectra of PGO-derivatized BCuZnSOD over the range of conditions examined here. Since PGO-H<sub>2</sub>O, 2PGO, 2PGO-H<sub>2</sub>O, 3PGO, 3PGO-H<sub>2</sub>O, 3PGO-2H<sub>2</sub>O, 4PGO-H<sub>2</sub>O, and 4PGO-2H<sub>2</sub>O derivatives are detected, the MS results are in sharp contrast to the data from amino-acid analysis indicating that a single arginine residue was modified by PGO in BCuZnSOD (50, 55).

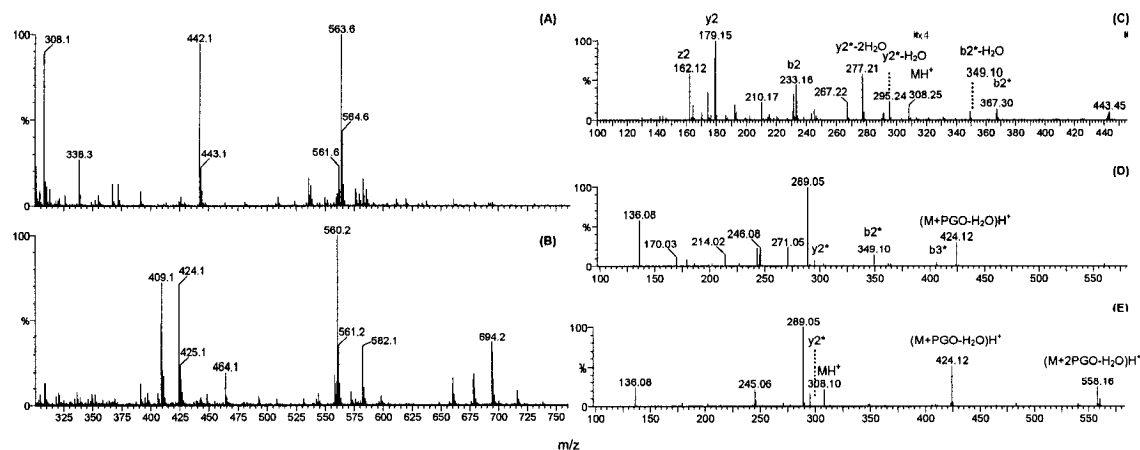
Protein from a ~7-h BCuZnSOD/PGO (1:40) incubation was digested with trypsin to identify the residues modified by PGO. Peptides containing Arg77, Arg126, and Arg141 exhibited a  $\Delta M_r$  of 116 u after PGO modification (Table 4.4), suggesting that these arginines formed type 2*b* PGO derivatives. Previously (55), Arg141 was identified as the modified site by two-dimensional peptide mapping of the tryptic peptides. Evidence for labelling of Arg113, which is buried was not found in accordance with no missed cleavages at this residue (Table 4.4). Also, unlike the PGO reactions with the small peptides (Figures 4.1, 4.4–4.5), no doubly PGO-labelled BCuZnSOD tryptic peptides were detected suggesting that steric hindrance may prevent double PGO-labelling of arginine residues in the folded protein. Since only three singly PGO-labelled arginine-containing peptides were observed (Table 4.4) and quadruply PGO-labelled intact BCuZnSOD was detected (Figure 4.9; 16,091 and 16,108 u), the formation of doubly PGO-labelled arginine derivatives (on reaction with two PGO molecules or with a single PGO dimer) cannot be ruled out. Such doubly labelled derivatives may be unstable under the conditions used for copper depletion and tryptic digestion. The less abundant quadruple derivatives may involve labelling at less reactive sites such as Arg113,

although is unlikely since no missed cleavages at Arg113 were detected as mentioned above.

**Table 4.1 Assignment of peaks in the derivatized MRF, PRS, and ACTH peptides<sup>a</sup>**

Peptide	Mr (u)	Observed ions	m/z	$\Delta m$	Figure
MRF	452.2	(MRF)H <sup>+</sup>	453.2	0	4.1A-C
		(MRF <sub>2b</sub> )H <sup>+</sup>	569.5	116.3	
		(MRF <sub>3b</sub> )H <sup>+</sup>	703.6	250.4	
		(MRF+4PGO-2H <sub>2</sub> O)H <sup>+</sup>	953.4	500.2	
		(MRF)H <sup>+</sup>	452.7	-0.5	4.1D-E
		(MRF <sub>2a</sub> )H <sup>+</sup>	586.6	133.4	
		(MRF <sub>2b</sub> )H <sup>+</sup>	568.7	115.5	
		(MRF <sub>3b</sub> )H <sup>+</sup>	702.7	249.5	
		(MRF+3PGO-2H <sub>2</sub> O)H <sup>+</sup>	818.8	365.6	
		(MRF+4PGO-2H <sub>2</sub> O)H <sup>+</sup>	953.0	499.8	
PRS	1757.9	(MRF+CH <sub>2</sub> CO)H <sup>+</sup>	495.25	42.05	4.3A
		(MRF <sub>2b</sub> +CH <sub>2</sub> CO)H <sup>+</sup>	611.32	158.12	4.3B
		(MRF <sub>3b</sub> +CH <sub>2</sub> CO)H <sup>+</sup>	745.37	292.17	
		(PRS)H <sup>+</sup>	1759.9	1.0	4.4A
		(PRS <sub>2b</sub> )H <sup>+</sup>	1874.9	116.0	
		(PRS <sub>2b</sub> )H <sup>+</sup>	1874.9	116.0	4.4B
		(PRS <sub>3a</sub> )H <sup>+</sup>	2027.0	268.1	
		(PRS <sub>3b</sub> )H <sup>+</sup>	2009.0	250.1	
ACTH	2464.2	(PRS+4PGO-2H <sub>2</sub> O)H <sup>+</sup>	2259.0	500.1	
		(ACTH)H <sup>+</sup>	2465.3	0.1	4.5A
		(ACTH <sub>2b</sub> )H <sup>+</sup>	2581.4	117.2	
		(ACTH <sub>2b</sub> -H <sub>2</sub> O)H <sup>+</sup>	2563.5	98.3	
		(ACTH <sub>2a</sub> )H <sup>+</sup>	2597.2	132.0	4.5B
		(ACTH <sub>2b</sub> )H <sup>+</sup>	2581.2	116.0	
		(ACTH <sub>3a</sub> )H <sup>+</sup>	2733.3	268.1	
		(ACTH <sub>3b</sub> )H <sup>+</sup>	2715.3	250.1	
		(ACTH <sub>3b</sub> -H <sub>2</sub> O)H <sup>+</sup>	2697.2	232.0	
		(ACTH+2CH <sub>2</sub> CO)H <sup>+</sup>	2549.40	84.2	4.6A
		(ACTH+3CH <sub>2</sub> CO)H <sup>+</sup>	2591.42	126.22	
		(ACTH <sub>2b</sub> +2CH <sub>2</sub> CO)H <sup>+</sup>	2665.31	200.11	4.6B
		(ACTH <sub>2b</sub> +3CH <sub>2</sub> CO)H <sup>+</sup>	2707.33	242.13	
		(ACTH <sub>3b</sub> +2CH <sub>2</sub> CO)H <sup>+</sup>	2799.32	334.12	
		(ACTH <sub>3b</sub> +3CH <sub>2</sub> CO)H <sup>+</sup>	2841.28	376.08	

<sup>a</sup>Peaks from the mass spectra shown in Figures 4.1, 4.3–4.5(A, B), and 4.6.



130.05 b1	233.06 b2	290.08 -	130.05 b1	367.06 b2*	424.08 -	130.05 b1	349.06 b2*	406.08 -
Glu	Cys	Gly	Glu	Cys+134	Gly	Glu	Cys+116	Gly
- 308.09	y2 179.05	y1 76.04	- 442.09	y2* 313.05	y1 76.04	- 424.09	y2* 295.05	y1 76.04

**Figure 4.7 Mass spectrometric analysis of PGO-modified GSH.** ESI mass spectrum of (A) 0.9 mM GSH and 0.45 mM PGO after 5 h incubation; and (B) 0.9 mM GSH and 45 mM PGO after 4 h incubation. Product-ion spectrum of (C)  $(\text{GSH}_{8a/a'})\text{H}^+$  at  $m/z$  442.1 in A; (D)  $(\text{GSH}+2\text{PGO}-16)\text{H}^+$  at  $m/z$  560.2 in B; and (E)  $(\text{GSH}+3\text{PGO}-16)\text{H}^+$  at  $m/z$  694.2 in B. Experimental conditions: Samples were incubated in 250 mM  $\text{NaHCO}_3$  (pH 8.0) at RT, and 10  $\mu\text{L}$  of 10% TFA was added to 50  $\mu\text{L}$  of sample to quench the PGO-modification reaction by lowering the pH to 3–4. The peptide was desalted on a ZipTipC<sub>18</sub>, eluted into 30  $\mu\text{L}$  of 60% ACN/0.1% TFA, and directly infused at 1  $\mu\text{L}/\text{min}$  (A, B) or 0.5  $\mu\text{L}/\text{min}$  (C–E) into the ESI source. To record the product-ion spectrum in (C–E), the parent ions were selected in Q1 and the fragment ions produced by CID in Q2 at a collision voltage of 30 V were separated in the ToF analyzer. The instrumental parameters are given in the legend of Figure 1 expect in (C–E) LM Res & HM Res were 16.0, and the collision voltage was 30 V. The peak intensities in C the  $m/z$  310–450 ranges were 4-fold amplified. Asterisks (\*) denote type  $\delta a/a'$  ions in C, and type  $\delta a/a' - \text{H}_2\text{O}$  ions in (D, E). Peak assignments for (A) and (B) are given in Table 4.2.



**Table 4.2 Assignment of peaks in PGO-derivatized GSH<sup>a</sup>**

Peptide	Mr (u)	Observed ions	m/z	$\Delta m$	Figure
GSH	307.1	(GSH)H <sup>+</sup>	308.1	0	4.7A
		(GSH <sub>8α/α'</sub> )H <sup>+</sup>	442.1	134.0	
		(GSH+2PGO-12)H <sup>+</sup>	563.6	255.5	
		(GSH)H <sup>+</sup>	308.1	0	4.7B
		(GSH+PGO-33)H <sup>+</sup>	409.1	101.0	
		(GSH+PGO-H <sub>2</sub> O)H <sup>+</sup>	424.1	116.0	
		(GSH+PGO-H <sub>2</sub> O)Na <sup>+</sup>	464.1	156.0	
		(GSH+2PGO-H <sub>2</sub> O)H <sup>+</sup>	558.2	250.1	
		(GSH+2PGO-16)H <sup>+</sup>	560.2	252.1	
		(GSH+2PGO-16)Na <sup>+</sup>	582.1	274.0	
		(GSH+3PGO-16)H <sup>+</sup>	694.2	386.1	

<sup>a</sup>Peaks from the mass spectra shown in Figures 4.7A, B.

To probe if the protein's single free sulfhydryl group at Cys6 was modified, BCuZnSOD derivatized with 100-fold molar excess of PGO (Figure 4.10B) was further incubated with 150-fold molar excess of NEM in 0.1% TFA at 4°C overnight. No loss of PGO-labels from BCuZnSOD occurred during this incubation period (Figure 4.10B vs C), and the spectra (Figures 4.10A, C) reveal that the native and PGO-modified protein were singly NEM-labelled. Also, the tryptic peptide T2 (A4–K9) containing Cys6 was mass shifted by 125 u (Figures 4.10E, F) as expected on NEM labelling of its free sulfhydryl. Additionally, the peak of tryptic peptide T10 (T114–R126; m/z 748.9) is not seen in the peptide map of the PGO-modified protein (Figure 4.10F) corroborating PGO-modification of Arg126.

Table 4.3 Assignment of peaks in PGO- and/or NEM-derivatized BCuZnSOD<sup>a</sup>

Peak	Calc Mass (Da)	Observed mass (Da)	$\Delta m$	Figure
E	15591	15592	1	4.8A
E E+PGO	15591 15725	15592 15725	1 0	4.8B
E E+PGO E+PGO-H <sub>2</sub> O E+2PGO E+2PGO-H <sub>2</sub> O	15591 15725 15707 15859 15841	15592 15724 15707 15858 15841	1 -1 0 -1 0	4.8C
E E+PGO E+PGO-H <sub>2</sub> O E+2PGO E+2PGO-H <sub>2</sub> O E+3PGO E+3PGO-H <sub>2</sub> O	15591 15725 15707 15859 15841 15993 15975	15592 15725 15708 15859 15842 15995 15975	1 0 1 0 1 2 0	4.8D
E E+PGO E+PGO-H <sub>2</sub> O E+2PGO-H <sub>2</sub> O	15591 15725 15707 15841	15592 15724 15708 15842	1 -1 1 1	4.9-1 h
E E+PGO E+PGO-H <sub>2</sub> O E+2PGO-H <sub>2</sub> O E+3PGO-H <sub>2</sub> O	15591 15725 15707 15841 15975	15592 15724 15708 15842 15975	1 -1 1 1 0	4.9-2 h
E+PGO E+PGO-H <sub>2</sub> O E+2PGO-H <sub>2</sub> O E+3PGO-H <sub>2</sub> O	15725 15707 15841 15975	15723 15707 15841 15974	-2 0 0 -1	4.9-3 h
E+PGO E+2PGO-H <sub>2</sub> O E+3PGO-H <sub>2</sub> O	15725 15841 15975	15724 15840 15974	-2 1 -1	4.9-4 h
E+PGO E+2PGO-H <sub>2</sub> O E+3PGO-H <sub>2</sub> O	15725 15841 15975	15724 15841 15974	-2 0 -1	4.9-5 h
E+2PGO-H <sub>2</sub> O E+3PGO-H <sub>2</sub> O E+4PGO-2H <sub>2</sub> O E+4PGO-H <sub>2</sub> O	15841 15975 16091 16109	15841 15974 16091 16108	0 -1 0 -1	4.9-6 h
E+NEM E+3PGO-H <sub>2</sub> O (E+3PGO-H <sub>2</sub> O)+NEM	15716 15975 16100	15716 15973 16099	0 -2 -1	4.10

<sup>a</sup>Peaks from the mass spectra shown in Figures 4.8–4.10. “E” presents the BCuZnSOD

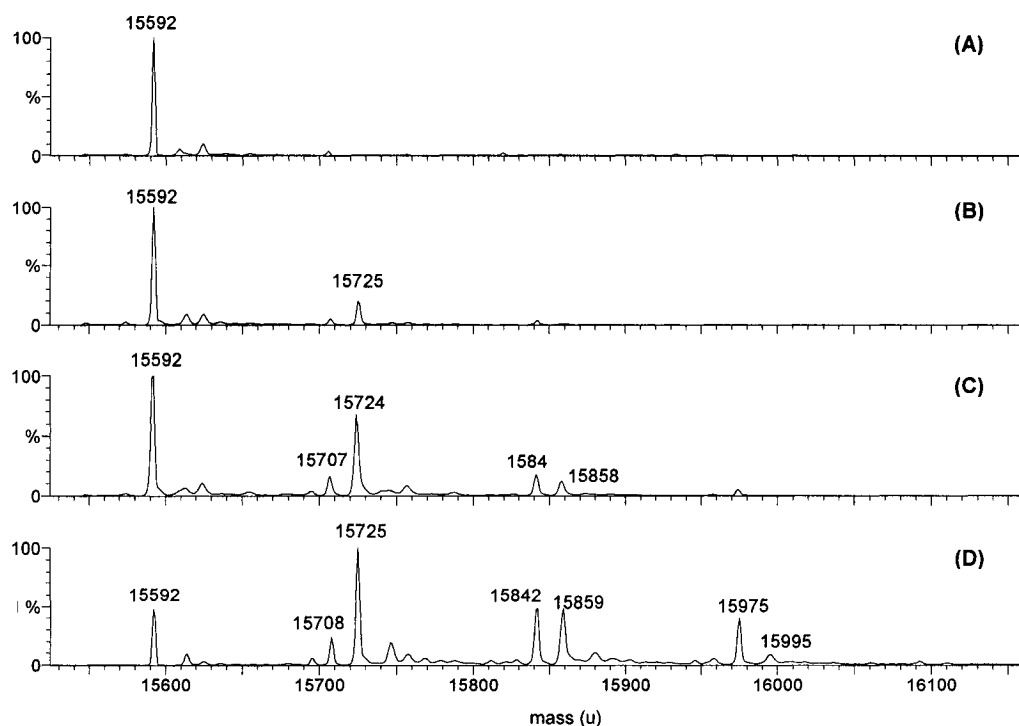


**Figure 4.8 PGO-concentration-dependence of BCuZnSOD modification.** Deconvolved ESI mass spectrum of: **(A)** native BCuZnSOD; **(B)** 150  $\mu$ M BCuZnSOD and 1.5 mM PGO; **(C)** 94  $\mu$ M BCuZnSOD and 4.7 mM PGO; and **(D)** 62  $\mu$ M BCuZnSOD and 6.2 mM PGO. Experimental conditions: Samples were incubated in 250 mM  $\text{NaHCO}_3$  (pH 8.0) at RT for 1 h, the protein was desalted 2–3 $\times$  by ultrafiltration with 0.1% TFA, diluted 10-fold into 50% ACN/0.1% TFA, and analyzed as described in the legend to Figure 4.1. Peak assignments are given in Table 4.3.

#### 4.4.6 Modification of BCuZnSOD by sulfo-NHS acetate

The 1–2-u lower than expected mass shifts observed for some PGO derivatives of intact BCuZnSOD (Figures 4.8, 4.9, Table 4.3) and for some of its tryptic peptides (Table 4.4) would suggest that PGO-induced oxidative deamination of amino groups (Reaction 4.1) in the protein. Thus, PGO-modification of free amino groups was probed by incubating native and PGO-modified BCuZnSOD with 200-fold molar excess of sulfo-NHS acetate for 1 h at room temperature. MS analysis revealed that acetylation of native BCuZnSOD gave rise to predominantly 9–10 labels with the expected mass shifts

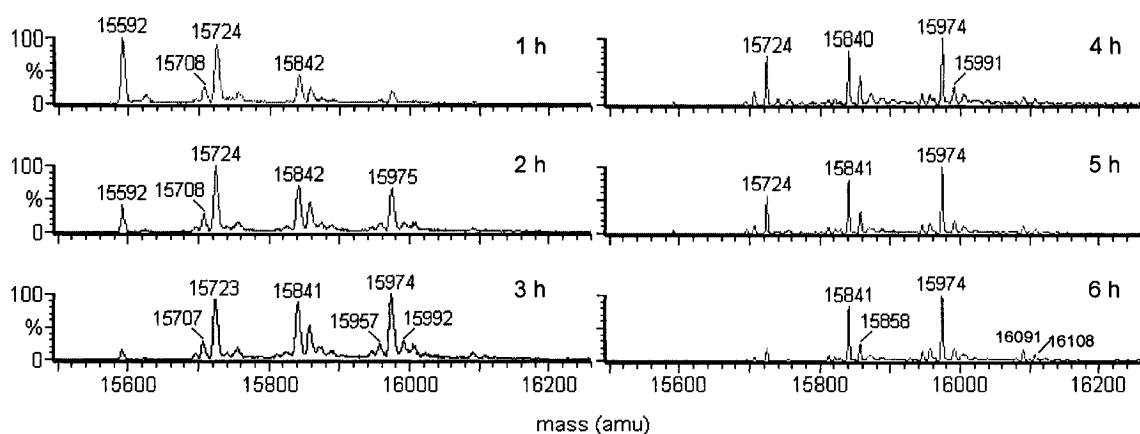
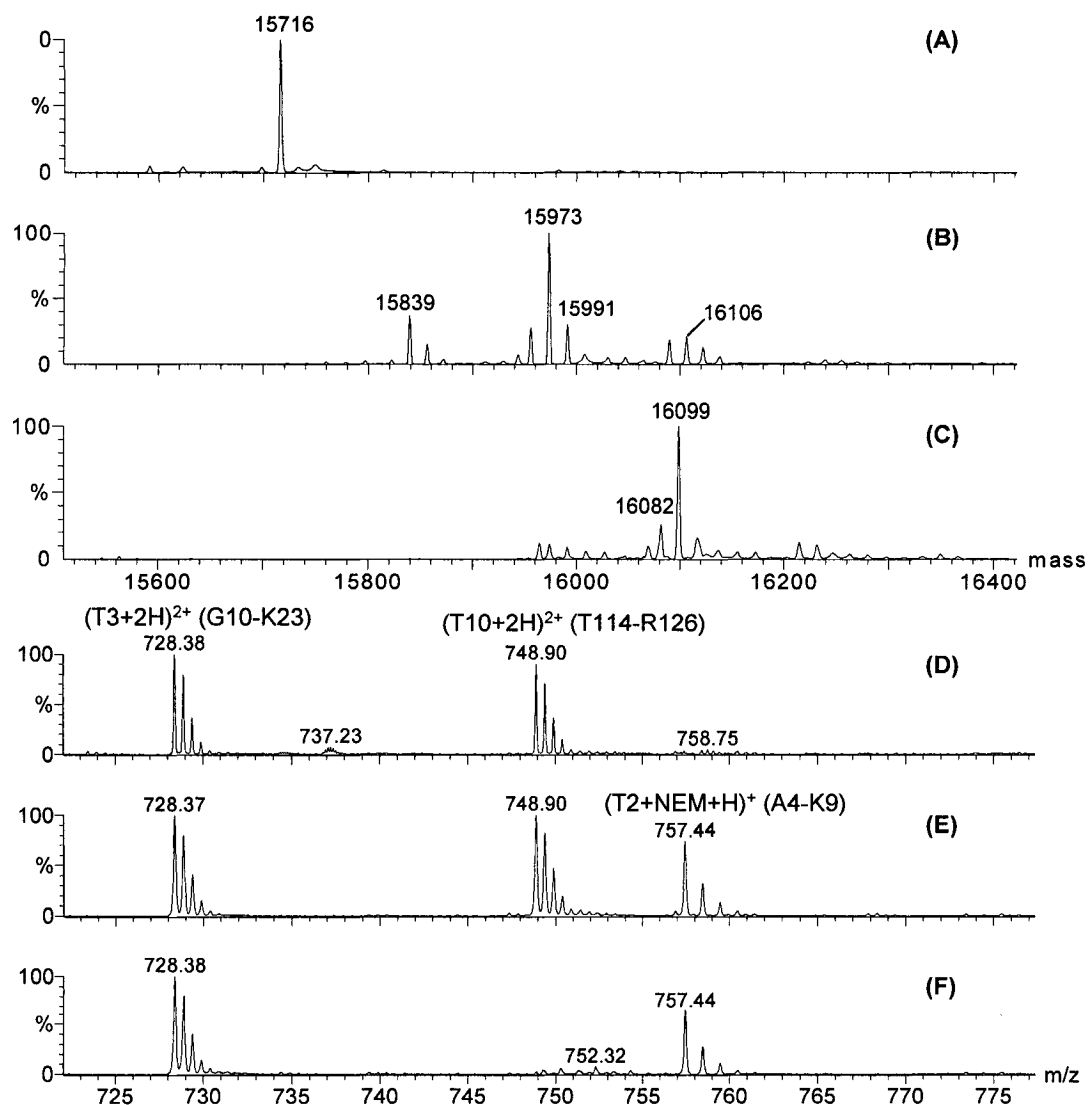


Figure 4.9 **Time-dependence of BCuZnSOD modification by 40-fold excess PGO.** Deconvoluted ESI mass spectrum of 100  $\mu$ M BCuZnSOD and 4.0 mM PGO in 250 mM NaHCO<sub>3</sub> (pH 8.0) after incubation at RT for the times indicated in the figures. A 1.4- $\mu$ L aliquot was removed, desalted on a ZipTipC<sub>4</sub>, eluted into 60% ACN/0.1% TFA, and analyzed as described in the legend to Figure 4.1. Peak assignments are given in Table 4.3.

Table 4.4 **Arg-containing tryptic peptides from PGO-modified BCuZnSOD<sup>a</sup>**

Sequence	Calc Mass (Da)	Observed ions		$\Delta m$	Assigned modification
		m/z	mass (Da)		
HGGPKDDE <u>R</u> HVGDLG	2216.1	(778.446+3H) <sup>3+</sup>	2332.3	116	PGO-H <sub>2</sub> O
NVTADK (69-89)		(784.117+3H) <sup>3+</sup>	2349.4	133	PGO
		(1175.674+2H) <sup>2+</sup>	2349.3	133	PGO
HVGDLGNVTADKNGV	3706.0	(927.529+4H) <sup>4+</sup>	3706.1	0	none
AIVDIVDPLISLSGEYSII		(1236.380+3H) <sup>3+</sup>	3706.1		
<u>G</u> R (78-113)		(1854.120+2H) <sup>2+</sup>	3706.2		
NGVAIVDIVDPLISLSG	2499.4	(834.161+3H) <sup>3+</sup>	2499.5	0	none
EYSII <u>G</u> R (90-113)		(1250.733+2H) <sup>2+</sup>	2499.5		
TMVVHEKPDDL <u>G</u> RGG	2298.1	(805.746+3H) <sup>3+</sup>	2414.2	116	PGO-H <sub>2</sub> O
NEESTK (114-134)		(1208.110+2H) <sup>2+</sup>	2414.2	116	PGO-H <sub>2</sub> O
TGNAGS <u>R</u> LACGVIGIA K (135-151)	1586.8	(851.973+2H) <sup>2+</sup>	1702.0	116	PGO-H <sub>2</sub> O

<sup>a</sup>10  $\mu$ g sample containing triply PGO-labelled BCuZnSOD was digested with trypsin (20:1, w/w) in 10 mM TrisHCl buffer (pH 7.9) at 37°C for 3 h. The experimental procedures are given in the legend of Figure 4.10.



**Figure 4.10 Thiol alkylation of native and PGO-modified BCuZnSOD.** Deconvolved ESI mass spectrum of: **(A)** 10  $\mu\text{M}$  native BCuZnSOD and 1.5 mM NEM after overnight incubation; **(B)** 37  $\mu\text{M}$  BCuZnSOD and 3.7 mM PGO after 5 h incubation; **(C)** 12  $\mu\text{M}$  PGO-modified BCuZnSOD from B after desalting and incubation with 1.8 mM NEM for overnight. The  $m/z$  725–775 range of the ESI mass spectra of tryptic peptides containing Cys6 and Arg126 from digests of: **(D)** native BCuZnSOD, **(E)** Sample A, and **(F)** Sample C. Experimental procedures: NEM and PGO incubations were carried out in 0.1% TFA at 4°C and in 250 mM  $\text{NaHCO}_3$  (pH 8.0) at RT, respectively. For digestion, 20  $\mu\text{g}$  of copper-depleted protein was incubated with trypsin (20:1, w/w) in 10 mM TrisHCl buffer (pH 7.9) at 37°C for 3 h, diluted into 20  $\mu\text{L}$  of 60% ACN/0.1%TFA and directly infused at 1  $\mu\text{L}/\text{min}$  into the Z-spray ion source of the mass spectrometer. Samples were analyzed as described in the legend to Figure 4.1. Peak assignments for (A)–(C) are given in Table 4.3.

**Table 4.5 Assignment of peaks in PGO- and/or sulfo-NHS acetate-derivatived BCuZnSOD<sup>a</sup>**

Peak	Calc Mass (Da)	Observed mass (Da)	$\Delta m$	Figure
E+8CH <sub>2</sub> CO	15927	15926	-1	4.12A
E+9CH <sub>2</sub> CO	15969	15968	-1	
E+10CH <sub>2</sub> CO	16011	16010	-1	
E	15591	15590	1	4.12B
E+PGO	15725	15723	2	
E+PGO-H <sub>2</sub> O	15707	15705	2	
E+2PGO-H <sub>2</sub> O	15841	15839	2	
E+2PGO-2H <sub>2</sub> O	15823	15820	3	
E+3PGO-H <sub>2</sub> O	15975	15973	2	
E+3PGO-2H <sub>2</sub> O	15957	15955	2	
E+4PGO-2H <sub>2</sub> O	16091	16089	2	
E+9CH <sub>2</sub> CO	15969	15968	-1	4.12C
E+10CH <sub>2</sub> CO	16011	16010	-1	
(E+PGO)+10CH <sub>2</sub> CO	16145	16143	2	
(E+PGO-H <sub>2</sub> O)+9CH <sub>2</sub> CO	16085	16084	-1	
(E+PGO-H <sub>2</sub> O)+10CH <sub>2</sub> CO	16127	16126	-1	
(E+2PGO-H <sub>2</sub> O)+10CH <sub>2</sub> CO	15261	16260	-1	
(E+3PGO-H <sub>2</sub> O)+10CH <sub>2</sub> CO	16395	16393	-2	
(E+3PGO-2H <sub>2</sub> O)+10CH <sub>2</sub> CO	16377	16376	-1	
(E+4PGO-2H <sub>2</sub> O)+10CH <sub>2</sub> CO	16511	16511	0	

<sup>a</sup>Peaks from the mass spectrum shown in Figures 4.11. “E” presents the BCuZnSOD

of + 42 u per acetyl label (Figure 4.11A, Table 4.5). Protein modified with only 8 labels was in low abundance (Figure 4.11A, Table 4.5), consistent with the presence of 10 lysine residues in each subunit and with a previous study where acylation at 7–8 lysines was reported (50). All peaks, with or without mass deficits, of PGO-modified BCuZnSOD (Figure 4.11B, Table 4.5) were acetylated to the same extent (Figure 4.11C,

Table 4.5) as the native protein, indicating that PGO-induced oxidative deamination of the protein's  $\epsilon$ -amino groups (Reaction 4.1) is unlikely, and the  $\alpha$ -amino group is *N*-acetylated (216).

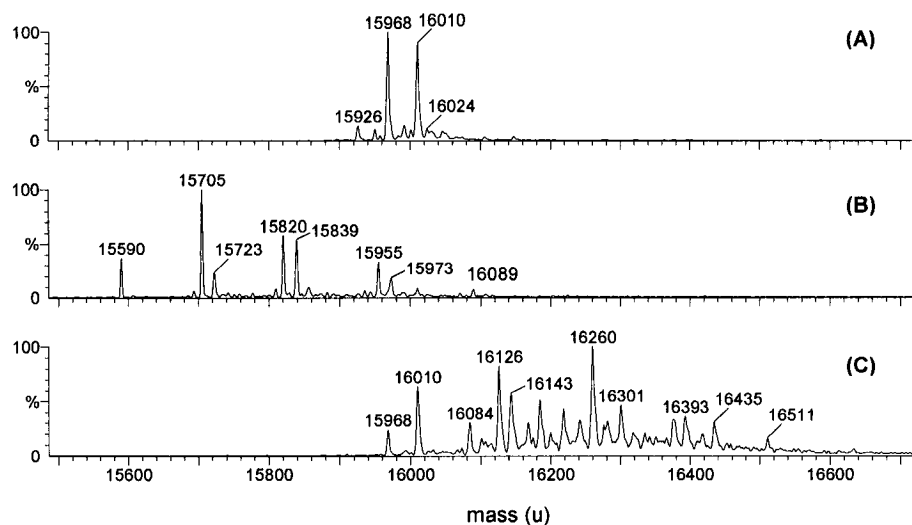
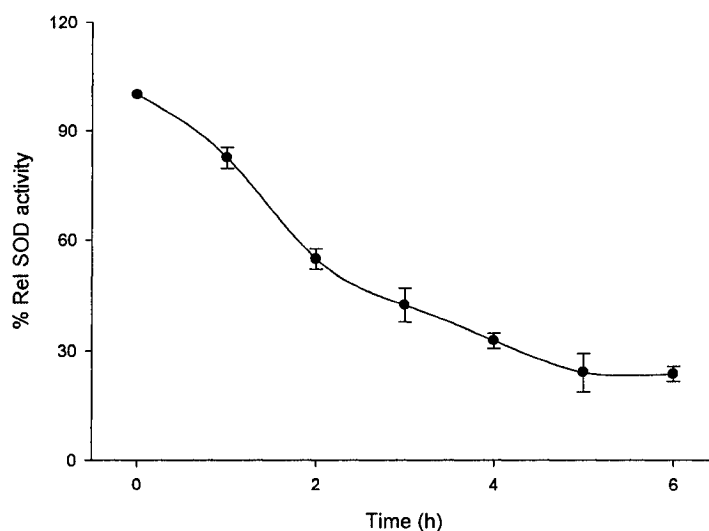


Figure 4.11 **Acetylation of native and PGO-modified BCuZnSOD.** Deconvolved ESI mass spectrum of: (A) 30  $\mu$ M BCuZnSOD and 6.0 mM sulfo-NHS acetate after 1 h incubation; (B) 30  $\mu$ M BCuZnSOD and 3 mM PGO after 2-h incubation; and (C) sample B after 6.0 mM sulfo-NHS acetate was added and the sample was further incubated for 1 h. Experimental conditions: Incubations were carried out in 250 mM NaHCO<sub>3</sub> (pH 8.0) at RT, and analyzed as described in the legend to Figure 4.1. Peak assignments are given in Table 4.5.

#### 4.4.7 SOD activity of PGO-modified BCuZnSOD

BCuZnSOD incubated with a 40-fold molar excess of PGO for 1 h exhibited 83% residual SOD activity (Figure 4.12) whereas 50% of the protein is singly or doubly PGO labelled under these conditions (1-h spectrum, Figure 4.9). The residual SOD activity dropped from  $\sim$ 40% to  $\sim$ 25% during 3–6 h incubation, although essentially no unmodified protein remained after 3 h (Figure 4.9). Previously (50, 55, 58), it was reported that PGO-modification at Arg141 resulted in loss of 80–90% of SOD activity

and this residue was assumed critical for SOD activity (55, 58, 112). Site-directed mutagenesis (109) corroborated the key role of this residue in SOD catalysis since the R143D and R143E mutants exhibit 100-fold less activity compared to the wild-type enzyme. Accurate mass measurements by ESI-MS of intact PGO-modified BCuZnSOD reveal that the protein is derivatized at three of its four arginine residues, and modification of Arg141 must occur slowly under our conditions since ~5 h are required to reach a plateau in the PGO-induced inhibition of SOD activity (Figure 4.12). Lysine residues also play a role in catalysis since the double K120L,K134T mutant exhibits only 30% SOD activity (206), and acylation at 7–8 lysines decreased the activity to 15–20% (50). However, PGO-induced oxidative deamination unlikely contributed to the loss of activity seen in Figure 4.12 since it does not alter the reactivity of the protein towards sulfo-NHS acetate (Figure 4.11B vs 4.11C).



**Figure 4.12 Effect of preincubation with PGO on the SOD activity of BCuZnSOD.** Aliquots were removed at the times indicated from the incubation of 100  $\mu$ M BCuZnSOD with 4.0 mM PGO in Figure 4.9. After 70-fold dilution, 10  $\mu$ L was added to 3 mL of assay buffer (50 mM sodium phosphate buffer, pH 7.8), and assayed for SOD activity at RT as described in Section 4.3.2.6. The SOD activity of BCuZnSOD was taken as 100% at  $t=0$  min.



## 4.5 Discussion

### 4.5.1 PGO modification of small peptides

The mass spectra reported here confirm that PGO is reactive under mild conditions (pH 8) with arginine residues in peptides and that the derivatives can be detected by ESI-MS. An examination of Figures 4.1, 4.4, and 4.5 reveals that the PGO-derivatives of MRF, PRS, and ACTH are less stable in the MALDI source. The derivatives might be photosensitive to the N<sub>2</sub> laser (337 nm) since they absorb at 340 nm (186, 217), or more energy may be transferred to the ions in the MALDI source leading to their dissociation. This would be consistent with the unstable behavior of the multiply PGO-labelled peptides in CID (Figured 4.2, 4.4C, 4.5C, 4.7D, and 4.7E). Their low stability in the MALDI source clearly makes ESI the ionization method of choice in analyzing PGO-modified peptides and proteins by MS.

The extent and nature of the PGO-derived labels were dependent on the PGO concentration, the peptide/PGO ratio, and the incubation time. Within 1 h at a peptide/PGO ratio of 1:50, essentially all free  $\delta$ -guanido groups in the peptides examined were detected as type **2b** derivatives, and these react at longer incubation times with a second PGO molecule to give type **3b** derivatives. Type **2a** and **3a** ions arising from simple 1:1 and 1:2 PGO addition products also were detected (Figures 4.1F, 4.4B and 4.5B; Table 4.1) but with RAs  $\leq$  30% of those ions arising from the condensation products. Previously, elemental analysis had revealed that following 20 h reaction at pH 8 and 25°C, PGO present at a 2.2-fold molar excess condensed with 2.4 mmoles free arginine to give exclusively the **3b** derivative (186). This is consistent with the present results since type **3b** ions dominate the ESI mass spectra of incubations of the arginine-

containing peptides, MRF, PRS, and ACTH, with 50-fold excess of PGO (Figures 4.1C, 4.4B, and 4.5B; Table 4.1). Loss of water from the **2a** and **3a** derivatives is likely due to condensation in solution since we (Table 4.1) and others (212) observed addition (**2a/3a**) as well as condensation products (**2b/3b**) in the ESI mass spectra. Elemental analysis (119, 186) also indicated that condensation occurred in solution since type **3b** (di-PGO arginine) ions were reported. Also, since monosubstituted PGO derivatives are detected in the mass spectra at shorter times (e.g., Figure 4.1B), reaction of the first molecule of PGO with the  $\delta$ -guanido group cannot be the rate-limiting step in the formation of the disubstituted products as was previously proposed (119, 186). The results recently reported by Saraiva *et al.* (212) support our observations. They found that the monosubstituted condensation derivative (type **2b**) dominates the mass spectrum of a 1-h, 70°C acetyl-arginine/PGO (1:1) incubation with minor di-condensation and addition products (212).

PGO is known to dimerize in solution (186, 201) and the free PGO dimer was observed in the ESI mass spectrum (Figure A2.1, Appendix A2.1). The condensation products of triply and quadruply labelled MRF, PRS, and GSH presumably with 3 and 4 PGO moieties bound to a single  $\delta$ -guanido or thiol, were also detected in the ESI mass spectra (Figures 4.1C, 4.1F, 4.4B and 4.7B). This suggests that the PGO dimer may also react with the  $\delta$ -guanido or thiol groups but these derivatives were not characterized by MS/MS since they are unstable under the conditions used for CID (Figure 4.7E).

PGO reportedly possesses low reactivity with the  $\epsilon$ -amino side chain of free lysine (186) but no evidence for PGO-modification of Lys4 in ACTH was detected here. Reaction of ACTH with PGO clearly gave rise to type **2a**, **2b**, **3a**, **3b**, and ACTH+PGO-2H<sub>2</sub>O derivatives (Figure 4.5B, Table 4.1) due to reaction with the  $\delta$ -guanido group of

Arg1 since the  $y_{20}$  ion remained unmodified (Figure 4.5C). Reactivity with sulfo-NHS acetate, which blocks primary amines, confirmed that Lys4 and the *N*-terminus of PGO-labelled ACTH were unmodified. The third acetylated site is unknown but it may be due to non-covalent interaction of the  $-\text{CH}_2\text{CO}$  group with the peptide in the gas phase (communication with Pierce technical support) or due to nucleophilic attack by the  $-\text{OH}$  group of Tyr6 on the carbonyl carbon of  $\text{CH}_3\text{CO}-$  in sulfo-NHS acetate (215). A sample containing mainly  $\text{ACTH}_{2b}$  and  $\text{ACTH}_{3b}$  derivatives was *bis*- and *tris*-acetylated to the same extent as unmodified ACTH (Figure 4.6B vs 4.6A; Table 4.1), confirming that PGO exhibits low reactivity with lysine residues (186). However, PGO has been proposed as a tool to determine free *N*-terminals in peptides and proteins since it reportedly readily deaminated  $\alpha$ -amino groups (Reaction 4.1) (186). This is clearly not the case here for MRF or ACTH since the peptides are acetylated to the same extent before and after PGO-modification (Figures 4.3 and 4.6; Table 4.1).

Based on elemental analysis, Schubert reported that PGO reacted with GSH and cysteine to yield a 1:1 addition product ( $\delta a/a'$ ), and cysteine also formed a condensation product (187). We confirmed the formation of  $\text{GSH}_{\delta a/a'}$  derivatives ( $\text{MH}^+$  ions at  $m/z$  442.1) on incubation with a 0.5 molar equivalent of PGO but also  $(\text{GSH}+2\text{PGO}-12)\text{H}^+$  ( $m/z$  563.6) derived from doubly PGO-labelled GSH exhibited high RA (Figure 4.7A). In the presence of 50-fold molar excess PGO,  $\text{MH}^+$  and  $\text{MNa}^+$  ions derived from condensation products dominated:  $\text{GSH}+\text{PGO}-33$  ( $m/z$  409.1),  $\text{GSH}+\text{PGO}-\text{H}_2\text{O}$  ( $m/z$  424.1/462.1),  $\text{GSH}+2\text{PGO}-\text{H}_2\text{O}$  ( $m/z$  558.1),  $\text{GSH}+2\text{PGO}-16$  ( $m/z$  560.2/582.1), and  $\text{GSH}+3\text{PGO}-16$  ( $m/z$  694.2) (Figure 4.7B). Thus, contrary to Schubert's proposal (187), formation of condensation products may not require the presence of a nearby  $\alpha$ -amino

group as in free cysteine. MS/MS analysis confirmed that Cys2 was the target in all the PGO-modified GSH derivatives (Figures 4.7C-E). However, no evidence in the ESI mass spectrum at  $m/z$  731 (Figure 4.7A) was obtained for the thioketal (type **9**) derivative (Reaction 4.3) in the presence of excess GSH. In fact, the  $MH^+$  ion of doubly PGO-labelled GSH is slightly more abundant than that of  $GSH_{8a/a'}$  (Figure 4.7A), suggesting that the latter is more reactive with PGO than free GSH. Alternatively, the PGO dimer may be more reactive than the monomer with GSH but then little  $GSH_{8a/a'}$  should be formed with 50-fold excess PGO, which is not the case (Figure 4.7B). However, multiply PGO-labelled GSH may be less stable than  $GSH_{8a/a'}$  in the ESI source. Loss of 16 u from doubly ( $m/z$  560.2) and triply ( $m/z$  694.2) PGO-labelled GSH (Figure 4.7B) suggests fragmentation of one of the PGO labels since  $(GSH+2PGO-H_2O)H^+$  ( $m/z$  558.16, Figure 4.7E) and  $(GSH+PGO-H_2O)H^+$  ( $m/z$  424.12, Figures 4.7D,E) ions are observed in the product-ion spectra of  $(GSH+3PGO-16)H^+$  and  $(GSH+2PGO-12)H^+$ , respectively. The mechanism of loss of 12 and 33 u, respectively, from doubly ( $m/z$  563.6 in Figure 4.7A) and singly ( $m/z$  409.1 in Figure 4.7B) PGO-labelled GSH (Figures 4.7A,B) is unknown but is under investigation

#### 4.5.2 PGO modification of BCuZnSOD

Examination of the crystal structure reveals that Arg126 is the most exposed and Arg113 the most buried of the four arginine residues in the BCuZnSOD monomer. Consistent with their accessibility, tryptic peptides containing Arg77, Arg126, and Arg141 were found to be PGO-modified on ESI-MS analysis of a digest of predominantly triply PGO-labelled BCuZnSOD (Table 4.4). As can be seen from Figures 4.8 and 4.9, the extent of PGO-labelling of BCuZnSOD depends on the PGO

concentration and incubation time. However, PGO was reported to selectively modify bovine BCuZnSOD at Arg141 (50, 55) under conditions (*e.g.*, incubation of 4  $\mu$ M of BCuZnSOD with 15 mM PGO in 0.125 M sodium bicarbonate at pH 8.5 and room temperature for 2 h (50)), that are expected to modify all accessible arginines. Thus, as the present data show, ESI-MS analysis redefines the reactivity of PGO with arginine residues in BCuZnSOD, and the results are consistent with those reported for other proteins. For example, two to three of the four arginines in bovine pancreatic ribonuclease A were modified within 30 min on incubation of a 0.36 mM (0.5%) solution of the enzyme with 112 mM (1.5%) PGO at pH 8.0 and 25°C (186). This is consistent with the high solvent accessibility of Arg39 and Arg85 *vs* the low solvent accessibilities of Arg10 and Arg33 in bovine ribonuclease A (218).

Does PGO induce modification of BCuZnSOD residues other than arginine? The side chains of cysteine (187) and lysine residues (119, 186), and *N*-terminal  $\alpha$ -amino groups (119, 186) reportedly react with PGO in addition to the  $\delta$ -guanido group of arginine (119, 186). Since Cys55 and Cys144 form an intrasubunit disulfide bond (107, 183), the side chain of Cys6 possesses the only free –SH group in the BCuZnSOD monomer. However, Cys6 is somewhat buried and it plays an important role in the thermostability of BCuZnSOD (140, 219). As judged from the ESI-MS of the intact protein, both native and triply PGO-labelled BCuZnSOD were fully derivatized with a single NEM group (Figures 4.10A, C; Table 4.3), indicating that PGO does not react with the free thiol in the protein. To confirm the NEM-modification site, tryptic digests of the two samples were analyzed by ESI-MS, and the peptide containing Cys6 (T2; A4–K9) was found to be singly NEM-labelled in both cases (Figure 4.10E, F). Thus, although

Cys6 exhibits reactivity with 150-fold excess NEM, it is unreactive with 100-fold excess PGO. This is somewhat surprising given the high reactivity of GSH with PGO (Figure 4.7A,B).

*N*-terminal acetylation is one of the most common protein modifications in eukaryotes (220, 221). Acetylation of proteins is catalyzed by a variety of acetyltransferases that transfer acetyl groups from acetyl-coenzyme A to the  $\alpha$ -amino group of the *N*-terminal residue or to the  $\epsilon$ -amino group of lysine residues at various positions (220-223). The *N*-terminal residue of BCuZnSOD is alanine and the observed mass of 15,592 u (Table 4.3) vs the theoretical mass of 15,551 u based on the sequence is consistent with the  $\alpha$ -amino group of Ala1 being acetylated ( $\Delta m = 42$  u) *in vivo*. The remaining primary amino groups in BCuZnSOD are contributed by 10 lysine residues per subunit. The results of ACTH modification (Figures 4.5C and 4.6B) indicated that PGO is more reactive with arginine than lysine residues, and it also appears that PGO induced negligible oxidative deamination of the 10 lysine residues in the BCuZnSOD monomer. Following incubation with sulfo-NHS acetate, an acetylating reagent specific for primary amino groups (Reaction 4.2) (202), the peaks of singly, doubly and triply PGO-labelled BCuZnSOD were further mass shifted by +420 u (Figure 4.11C, Table 4.5) consistent with the acetylation of 10 amino groups per subunit. Trypsin no longer cleaved the PGO-modified protein at the *C*-terminal of Arg126 (Figure 4.10F), Arg77, or Arg141 (Table 4.4) providing further evidence that these residues are PGO modification sites.

PGO-modified MRF was singly acetylated (Figure 4.3, Table 4.1), and PGO-modified ACTH *bis*- and *tris*-acetylated (Figure 4.6, Table 4.1) consistent with the presence of a single primary amino in MRF (the *N*-terminus), and two such groups in

ACTH (Lys4 and the *N*-terminus). Thus, contrary to Takahashi's report (186) that PGO readily deaminated the  $\alpha$ -amino group of peptides and proteins (Reaction 4.1), this cannot have occurred in detectable yields under our PGO-modifying conditions.

As an electrophile, the reactivity of PGO toward primary ammonium, guanidinium, or sulfhydryl groups depends on the  $pK_a$  of these groups in peptides and proteins. The free guanidinium group has a  $pK_a$  of  $\sim 12.5$  vs values between 8.8 and 11.1 for sulfhydryl,  $\epsilon$ - and  $\alpha$ -ammonium groups. Thus, on increasing the reaction pH, the N atoms of the guanidinium group should be more susceptible to electrophilic attack by PGO. Although Cys residues are more powerful nucleophiles than Lys or Arg residues at pH 8.0, PGO-labelled Cys6 in BCuZnSOD was not detected probably due to its low accessibility. The lack of PGO-labelling of  $\epsilon$ - and  $\alpha$ -amino groups in the peptides and BCuZnSOD may arise from the instability of their adducts at pH 8.0. However, it has been observed that PGO-induced transamination (Reaction 4.1) is specific for  $\alpha$ -amino groups at low pH but only a single report of this was found in the literature (224).

#### 4.6 Conclusions

The present study confirms that PGO readily modifies arginine residues in peptides and proteins. No evidence was obtained for PGO-induced oxidative deamination of lysine or of the free *N*-terminus in the MRF and ACTH peptides. The dominant arginine derivatives in the peptides were the doubly PGO-labelled, type **3b** species, but minor triple and quadruple labelling was also detected, suggesting that the PGO dimer may react directly with the peptides. In contrast, no doubly PGO-labelled tryptic peptides were detected in the peptide maps of BCuZnSOD revealing that multiple PGO-labelling

of arginines may be unfavorable in proteins, possibly for steric reasons. Thus, if this proves to be the case for proteins in general, the number of PGO labels detected by ESI-MS in the intact protein could be used to indicate the number of reactive and accessible arginines under various conditions.

PGO readily reacts with the thiol in GSH to produce not only the 1:1 addition adduct ( $\text{GSH}_{8a/a'}$ ) as reported previously (187), but also multiply PGO-labelled condensation adducts. In contrast, the partially buried free Cys6 in BCuZnSOD was not found to react with PGO in accordance with the low yield of NEM-induced alkylation under mild conditions (Figure A2.4A, Section A2.3).

Clearly, PGO is not a site-specific modifying reagent for Arg141 in BCuZnSOD as previously reported (55). Furthermore, since activity loss becomes significant only when most of the enzyme is multiply PGO-labelled, the catalytically important Arg141 clearly does not demonstrate the highest reactivity with PGO of the three accessible arginines (Arg126, Arg77, and Arg141).

We (57, 82) and others (56) have reported that BCuZnSOD moonlights as a GSNO reductase and that the anionic metal chelators, EDTA and DTPA, inhibit this activity. We demonstrated in Chapter 2 that both EDTA and DTPA bind to BCuZnSOD (225), and since Arg141 has been implicated in anion binding to CuZnSOD (58), we attempted to selectively modify this residue following the literature procedure (55). Unfortunately, because of its reactivity with all three exposed arginines in BCuZnSOD, PGO-modification does not provide a homogeneous sample of protein singly PGO-modified at Arg141. Such a derivative is required to further probe the role of Arg141 in anion binding in the active-site channel of BCuZnSOD using techniques such as



isothermal titration calorimetry (Chapter 2). Attempts to overexpress the human protein in yeast and *E. coli* hosts are discussed in the next chapter.

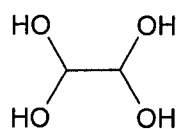
#### **4.7 Acknowledgements**

This research was supported by grants from the Natural Sciences and Engineering Research Council of Canada (NSERC), and the Canadian Institutes for Health Research (CIHR) to A. M. English. We would like to thank Alain Tessier in Centre for Biological Applications of Mass Spectrometry for help with the MS measurements.

## Appendix 2.0 Supplementary Experimental Data for Chapter 4.0

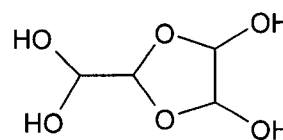
### A2.1 Characterization of PGO dimer in solution by ESI-MS

Oligomeric glyoxal in aqueous solution was reported in the literature (226-228). The equilibrium constant between dimeric ( $G_2$ ) and monomeric ( $G$ ) glyoxal ( $[G_2]/[G]^2$ ) is  $0.56 \text{ M}^{-1}$  at  $25^\circ\text{C}$  and is little affected by changes in ionic strength and pH but increases rapidly with increasing temperature (226). The equilibrium between the monomer, dimer, and trimer also depends strongly on the glyoxal concentration in aqueous solution (Table A2.1) and the hydrated monomeric, dimeric, and trimeric forms of glyoxal have the structures below (227, 228):



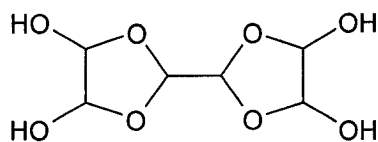
(1)

ethane *bis*-gemdiol



(2)

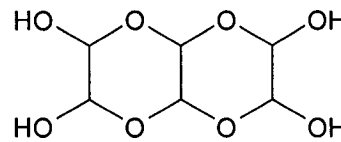
dioxolane dimer



(3)

bis(dioxolane) trimer

or



(4)

triethanedial dihydrate

It is possible that the PGO dimer present in solution may react with guanido groups (186) since condensation products containing three and four PGO moieties were

detected in the ESI mass spectra (Figures 4.1C, 4.1F, 4.4B and 4.7B). To probe for dimers, a PGO solution at the same concentration (200 mM) used in the modification reactions was prepared and analyzed by ESI-ToF-MS. The results in Figure A2.1 indicate that peaks corresponding to both the PGO monomer and dimer but not trimer were present in the solution (Table A2.2). The ions detected were the mono- and dihydrated PGO monomer and di-, tri- and tetrahydrated dimer which presumably arises by combining the monomeric forms:

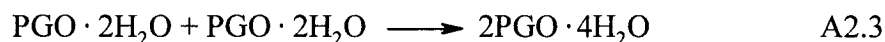
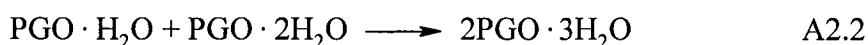
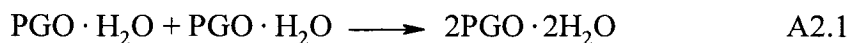


**Table A2.1 Concentration of glyoxal monomer vs total glyoxal concentration in aqueous solution<sup>a</sup>**

% total glyoxal <sup>b</sup> (w/w)	% glyoxal monomer
5	39
40	11

<sup>a</sup>From <http://www.inchem.org/documents/sids/sids/107222.pdf>

<sup>b</sup>Commercial glyoxal is 40% (w/w) in H<sub>2</sub>O.

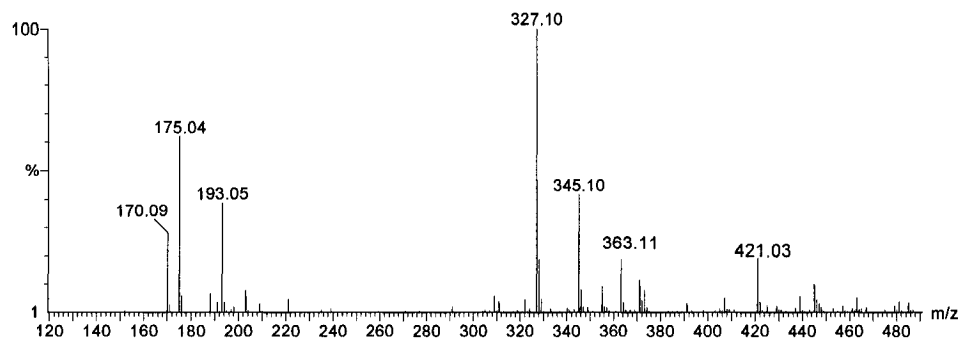


**Figure A2.1 Mass spectrometric analysis of PGO.** A 200 mM PGO stock solution was prepared by dissolving the reagent in ethanol. To record the ESI mass spectrum, PGO was diluted to 500  $\mu$ M with H<sub>2</sub>O and directly infused at 1  $\mu$ L/min into the Z-spray ion source of the mass spectrometer. The instrumental parameters are given in the legend of Figure 4.1. Peak assignments are given in Table A2.2.

**Table A2.2 Assignment of PGO peaks in water<sup>a</sup>**

Chemical	Mr (u)	Observed ions	m/z of MNa <sup>+</sup>		$\Delta m$
			calculated	observed	
PGO	134.13	(PGO•H <sub>2</sub> O)Na <sup>+</sup>	175.15	175.04	-0.11
		(PGO•2H <sub>2</sub> O)Na <sup>+</sup>	193.17	193.05	-0.12
		(2PGO•2H <sub>2</sub> O)Na <sup>+</sup>	327.30	327.10	-0.2
		(2PGO•3H <sub>2</sub> O)Na <sup>+</sup>	345.32	345.10	-0.22
		(2PGO•4H <sub>2</sub> O)Na <sup>+</sup>	363.34	363.11	-0.23

<sup>a</sup>Peaks from the mass spectrum shown in Figure A2.1.

## **A2.2 Characterization of the thermal- and pH-stabilities of the PGO derivatives in BCuZnSOD by ESI-MS**

BCuZnSOD is a highly stable enzyme with essentially a pH-independent rate constant ( $2 \times 10^9 \text{ M}^{-1} \text{ s}^{-1}$ ) for the catalysis of superoxide disproportionation (53, 54) and invariant spectroscopic properties between pH 5–9.5 (229, 230). However, PGO

derivatives of arginine are reversible at neutral or higher pH but stable at pH < 4 (55, 119, 186). To assess the stability of PGO-modified BCuZnSOD under neutral and acidic conditions, aliquots from the same incubation were desalted by 3× ultrafiltration with H<sub>2</sub>O or 50 mM AcONH<sub>4</sub> (pH 4.0) and the mass spectra were measured immediately (Figures A2.2A,B) or after standing at RT for 24 h (Figures A2.2C,D).

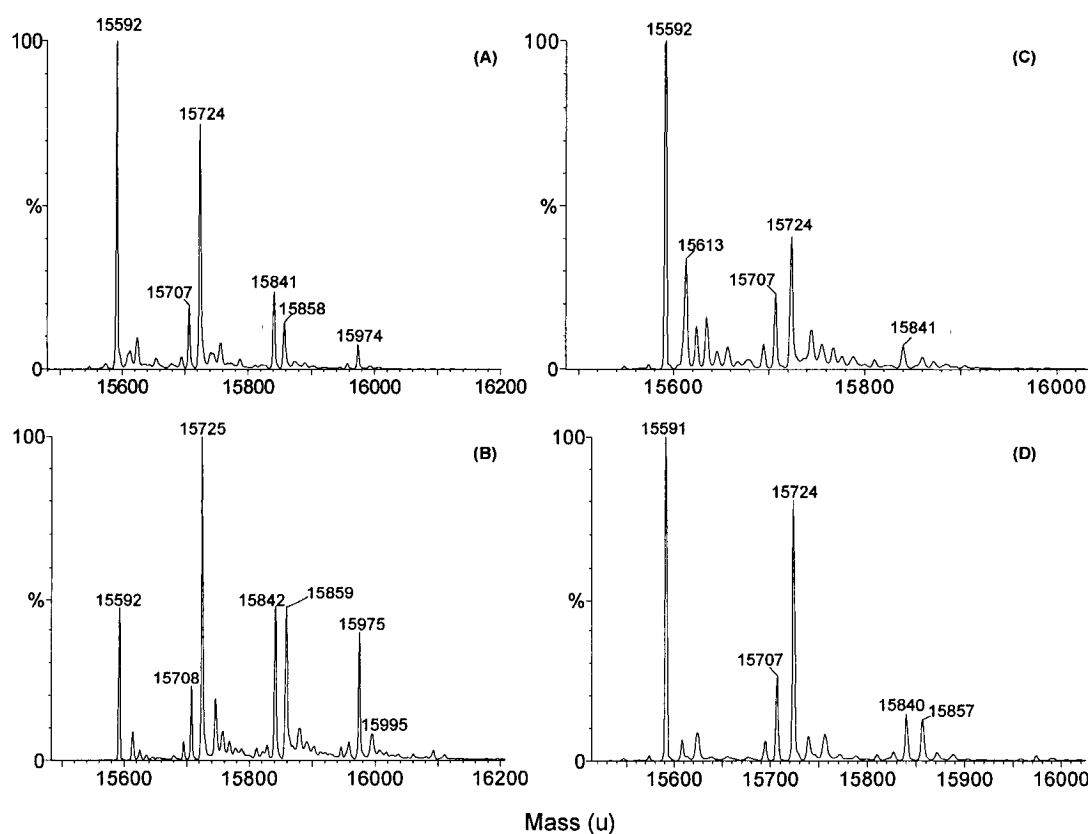


**Figure A2.2 Mass spectrometric analysis of the stability of PGO-modified BCuZnSOD at low pH.** Deconvolved ESI mass spectra of BCuZnSOD/PGO incubation recorded immediately after desalting by (A) a H<sub>2</sub>O wash, or (B) a AcONH<sub>4</sub> (pH 4.0) wash; (C) sample washed with H<sub>2</sub>O and (D) sample washed with AcONH<sub>4</sub> after standing at RT for 24 h. Experimental conditions: 94  $\mu$ M BCuZnSOD was incubated with 9.4 mM PGO in 250 mM NaHCO<sub>3</sub> (pH 8.0) with gentle shaking at RT for 1 h, aliquots were desalted by ultrafiltration (12,000 rpm, 10 min, Ultrafree-0.5, Millipore) with 3× H<sub>2</sub>O or 3× AcONH<sub>4</sub> (pH 4.0), and analyzed immediately or after 24 h storage at RT. The sample was diluted 20-fold into 50% ACN/0.1% TFA and directly infused at 1  $\mu$ L/min into the Z-spray ion source of the mass spectrometer. The mass spectrometric procedures are given in the legend of Figure 4.1. Peak assignments are given in Table A2.3.

**Table A2.3 Assignment of peaks in PGO- or NEM-derivatized BCuZnSOD**

Peak <sup>a</sup>	Calc Mass (Da)	Observed mass (Da)	$\Delta m$	Figure
E	15591	15592	1	A2.2A
E+PGO	15725	15724	-1	
E+PGO-H <sub>2</sub> O	15707	15707	0	
E+2PGO-H <sub>2</sub> O	15841	15841	0	
E+2PGO	15859	15858	-1	
E+3PGO-H <sub>2</sub> O	15975	15974	-1	
E	15591	15592	1	A2.2B
E+PGO	15725	15725	0	
E+PGO-H <sub>2</sub> O	15707	15708	1	
E+2PGO-H <sub>2</sub> O	15841	15842	1	
E+2PGO	15859	15859	0	
E+3PGO-H <sub>2</sub> O	15975	15975	0	
E+3PGO	15993	15995	2	
E	15591	15592	1	A2.2C
E+PGO	15725	15724	-1	
E+PGO-H <sub>2</sub> O	15707	15707	0	
E+2PGO-H <sub>2</sub> O	15841	15840	-1	
E	15591	15591	1	A2.2D
E+PGO	15725	15724	-1	
E+PGO-H <sub>2</sub> O	15707	15707	0	
E+2PGO-H <sub>2</sub> O	15841	15840	-1	
E+2PGO	15859	15857	-2	
E	15591	15592	1	A2.3A
E+PGO	15725	15724	0	
E+PGO-H <sub>2</sub> O	15707	15707	1	
E+2PGO-H <sub>2</sub> O	15841	15841	1	
E+2PGO	15859	15858	0	
E+3PGO-H <sub>2</sub> O	15975	15974	0	
E	15591	15591	0	A2.3B
E+PGO	15725	15723	-2	
E	15591	15591	0	A2.4
E+NEM	15716	15716/7	0/1	

<sup>a</sup>Peaks from the mass spectra shown in Figures A2.2–A2.4; E represents unmodified BCuZnSOD.

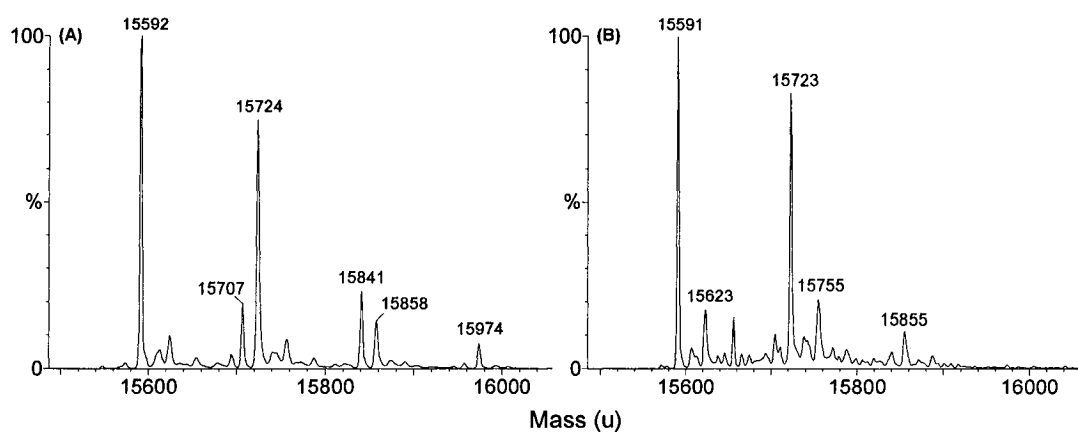


**Figure A2.3 Mass spectrometric analysis of the thermostability of PGO-modified BCUZnSOD.** Deconvolved ESI mass spectra of a BCUZnSOD/PGO incubation **(A)** before, **(B)** after heating to 90°C for 5 min. Experimental conditions: 94  $\mu$ M BCUZnSOD was incubated with 9.4 mM PGO in 250 mM NaHCO<sub>3</sub> (pH 8.0) at RT for 1 h. Samples were desalted by ultrafiltration (12,000 rpm, 10 min, Ultrafree-0.5) with 3 $\times$  H<sub>2</sub>O, diluted 10-fold into 50% ACN/0.1% TFA immediately or following heating, and directly infused at 1  $\mu$ L/min into the Z-spray ion source of the mass spectrometer. The mass spectrometric procedures are given in the legend of Figure 4.1. Peak assignments are given in Table A2.3.

The mass spectrum of PGO-modified BCUZnSOD desalted at pH 4.0 exhibits a base peak corresponding to the singly-PGO-derivatized protein and a high abundance of doubly- and triply-PGO-labelled protein as well as a peak from the unmodified protein (Figure A2.2B). Desalting with H<sub>2</sub>O resulted in more extensive loss of PGO from the protein before (Figure A2.2A vs B) or after standing at RT over 24 h (Figure A2.2C vs D) than desalting at pH 4.0. These results are consistent with literature reports (55, 119, 186) and indicate that PGO derivatization should be measured immediately following desalting at low pH. Thus, the PGO-modified samples in Chapter 4 were treated at pHs < 4 and put on ice until use to avoid loss of the labels.

Peptide mass fingerprinting using enzymatic digestion is an essential step in locating the sites of PGO modification. BCuZnSOD is generally denatured by heating to 90°C prior to digestion (213, 214) since it has an unfolding temperature > 80°C (231, 232). To test the thermal stability of PGO-modified BCuZnSOD, samples were desalted with H<sub>2</sub>O and analyzed by MS before and after heating to 90°C for 5 min. Figure A2.3A shows the mass spectrum of the unheated sample with peaks corresponding to doubly and triply PGO-labelled BCuZnSOD clearly visible. However, following heating, these peaks were diminished or lost (Figure A2.3B) indicating that high temperature results in the loss of PGO from derivatized BCuZnSOD. Thus, trypsinolysis of demetallated BCuZnSOD was carried out in Section 4.3.2.3 to obtain peptides that retained their PGO labels.

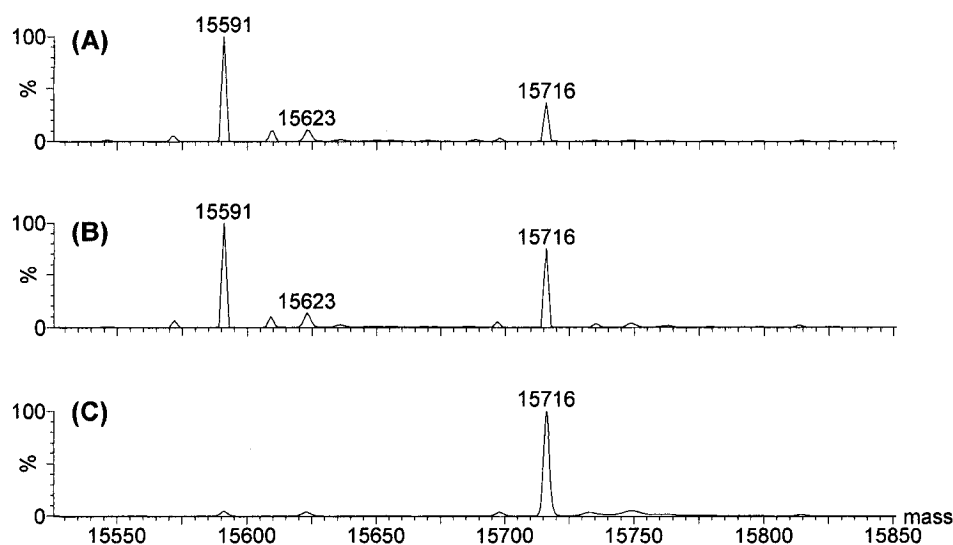


Figure A2.4 **Reactivity of Cys6 in BCuZnSOD with NEM.** Deconvolved ESI mass spectrum of (A) 40-min BCuZnSOD/NEM incubation in H<sub>2</sub>O at RT, (B) 40-min BCuZnSOD/NEM incubation in 0.1% TFA at RT, and (C) overnight BCuZnSOD/NEM incubation in 0.1% TFA at 4°C. Experimental conditions: 10 µM BCuZnSOD was incubated with 1.5 mM NEM and analyzed as described in the legend of Figure 4.1. Peak assignments are given in Table A2.3.



### **A2.3 Mass spectrometric analysis of the NEM labelling of the buried free cysteine residue in BCuZnSOD**

There are three cysteine residues (Cys6, Cys55, and Cys144) in each subunit of BCuZnSOD. Cys55 and Cys144 form an intrasubunit disulfide bond and Cys6 is free but buried (107, 183). Alkylation of the free sulfhydryl groups in proteins using NEM allows reactive free cysteine residues to be identified by mass spectrometry since the resulting NEM-adducts are mass shifted by 125 u. Steric hindrance prevents the reaction of buried sulfhydryl groups with NEM so Cys6 was only partially alkylated in a 40-min BCuZnSOD/NEM (1:150) incubation in H<sub>2</sub>O at RT (Figure A2.4A). Full alkylation of buried cysteines has to be performed under more severe conditions. For example, Cys6 in 2.8  $\mu$ moles of BCuZnSOD in an incubation with 120  $\mu$ moles of NEM was alkylated in 6 M guanidine-hydrochloride/0.01 M EDTA (pH 6.85) at 24°C over 2 h (233).

Since PGO derivatives are more stable at pH < 4.0 (Figures A2.2B and D), the reaction of BCuZnSOD with NEM was carried out in 0.1% TFA at different NEM/BCuZnSOD ratios and incubation times. Complete alkylation of Cys6 was achieved in a 1:150 BCuZnSOD/NEM incubation at 4°C overnight (Figure A2.4C vs B). PGO-modified BCuZnSOD is stable in 0.1% TFA and Cys6 is accessible to NEM at low pH (Figure 4.10F).

### **A2.4 Supplementary mass spectra of the PGO-modified peptides**

The MALDI spectrum of the 1-h incubation of PRS with 50-fold molar excess of PGO was dominated by the MH<sup>+</sup> ion of the unmodified peptide at m/z 1759.9, with a

low abundant (< 10%) (PRS<sub>2b</sub>)H<sup>+</sup> peak at m/z 1875.2 (Figure A2.5A). The latter (PRS<sub>2b</sub>)H<sup>+</sup> ion was dominant after 4-h incubation.

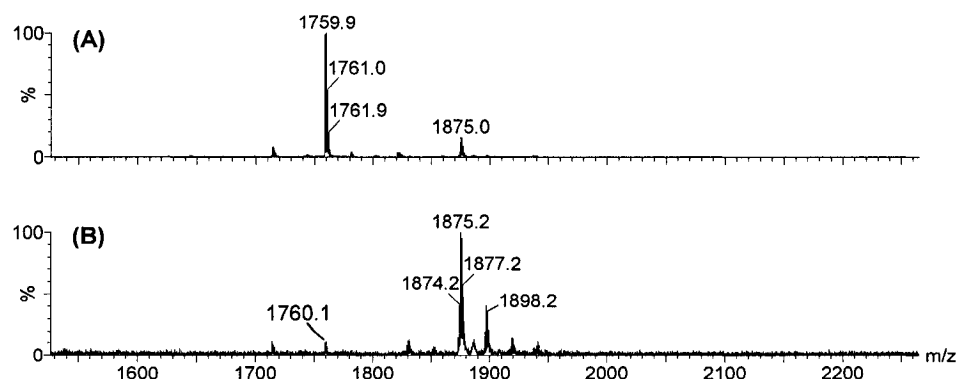


Figure A2.5 **MALDI mass spectrometric analysis of PGO-modified PRS.** Spectrum recorded after (A) 1 h and (B) 4 h incubation of 80  $\mu$ M PRS with 4 mM PGO. Experimental conditions and the MS parameters are given in the legend of Figure 4.4. Peak assignments are given in Table A2.4.

Table A2.4 **Assignment of peaks in the MALDI mass spectra of PGO-derivatized PRS, ACTH, and the ESI mass spectra of the MRF/GSH mixture<sup>a</sup>**

Peptide	Mr (u)	Observed ions	m/z	$\Delta m$	Figure
PRS	1757.9	(PRS)H <sup>+</sup>	1759.9	1.0	A2.5A
		(PRS <sub>2b</sub> )H <sup>+</sup>	1875.0	116.1	
		(PRS)H <sup>+</sup>	1760.1	1.2	A2.5B
		(PRS <sub>2b</sub> )H <sup>+</sup>	1875.2	116.3	
		(PRS <sub>2a</sub> )H <sup>+</sup>	1898.2	250.1	
ACTH	2464.2	(ACTH)H <sup>+</sup>	2466.3	1.1	A2.6
		(ACTH <sub>2b</sub> )H <sup>+</sup>	2582.2	117.0	
MRF	452.2	(MRF)H <sup>+</sup>	453.2	0	A2.7A
GSH	307.1	(GSH)H <sup>+</sup>	308.1	0	
		(MRF <sub>2b</sub> )H <sup>+</sup>	569.5	116.3	A2.7B
		(MRF <sub>3b</sub> )H <sup>+</sup>	703.3	250.1	
		(GSH-H)Na <sub>2</sub> <sup>+</sup>	352.2	0	

<sup>a</sup>Peaks from the mass spectra shown in Figures A2.5–2.7.

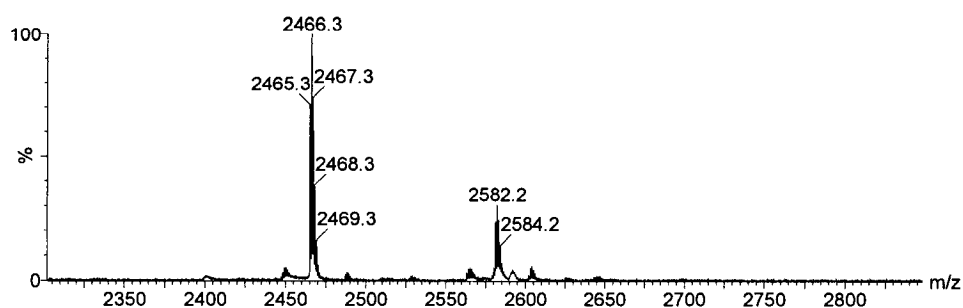


Figure A2.6 **MALDI mass spectrometric analysis of PGO-modified ACTH.** Spectrum recorded after 1 h incubation of 80  $\mu$ M ACTH with 4 mM PGO. The experimental conditions and the MS parameters are given in the legend of Figure 4.5. Peak assignments are given in Table A2.4.

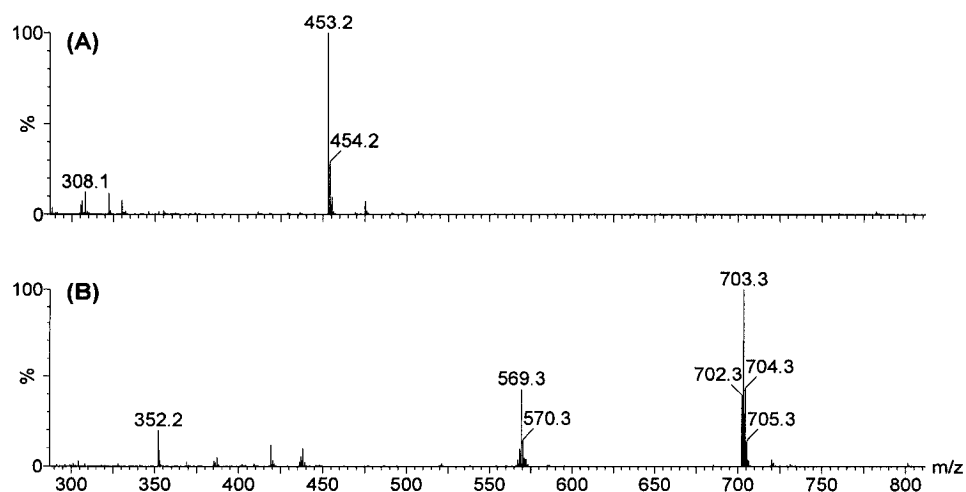


Figure A2.7 **ESI mass spectrometric analysis of the PGO derivatives in an equimolar GSH and MRF incubation.** Spectrum of (A) GSH/MRF incubation, and (B) GSH/MRF/PGO incubation. Experimental conditions: 0.9 mM GSH and 0.9 mM MRF were incubated with 45 mM PGO (where indicated) in 250 mM  $\text{NaHCO}_3$  (pH 8.0) at RT for 80 min, and 50  $\mu$ L of 1% TFA was added to 42  $\mu$ L of sample to quench the PGO-modification reaction by lowering the pH to 3–4. The peptides were desalted on a ZipTipC<sub>18</sub>, eluted into 60  $\mu$ L of 60% ACN/0.1% TFA, and directly infused at 1  $\mu$ L/min into the ESI source. The MS parameters are given in the legend of Figure 4.1, and peak assignments are given in Table A2.4.

Like PRS, the MALDI spectrum of the 1-h incubation of ACTH with 50-fold molar excess of PGO was dominated by the  $MH^+$  ion of unmodified ACTH at  $m/z$  2466.3. In addition, the  $(ACTH_{2b})H^+$  ion was observed with ~30% RA at  $m/z$  2582.2 (Figure A2.6).

When an equimolar GSH and MRF mixture was infused into the ESI mass spectrometer, the RA of the  $(GSH)H^+$  ion at  $m/z$  308.1 was 10% that of the  $(MRF)H^+$  ion at  $m/z$  453.2 was (Figure A2.7A).  $(MRF_{2b})H^+$  ( $m/z$  569.3) and  $(MRF_{3b})H^+$  ( $m/z$  703.3) ions are clearly observed in the ESI mass spectrum of the 80-min GSH/MRF/PGO incubation whereas PGO-labelled GSH derivatives were undetectable (Figure A2.7B). The peak at  $m/z$  352.2 is assigned to the doubly sodiated ion of GSH (Table A2.4). To detect GSH-derived ions in the GSH/MRF mixtures, it would be necessary to separate the peptides first by HPLC.

## **5.0 Construction, expression and purification of human Cu,Zn-superoxide dismutase (hSOD1) in yeast and *E. Coli* hosts**

### **5.1 Introduction**

CuZnSOD, a homodimer with one copper and one zinc per subunit, plays a defensive role by catalyzing the dismutation of the toxic superoxide radicals to hydrogen peroxide and dioxygen (234). In the crystal structure the zinc ion is not accessible to solvent, whereas the copper ion is essential for catalysis (102, 107). The positive guanidinium group of the active-site Arg143 of human CuZnSOD (Arg141 in bovine CuZnSOD), which is only 5 Å away from the copper ion in the active-site cavity (107), plays a crucial role in the catalytic activity and in anion binding as demonstrated by covalent modification with  $\alpha,\alpha'$ -diketones (55, 112, 235, 236) and by site-directed mutagenesis (108, 109, 237, 238). The proposed mechanism for the involvement of this conserved active-site arginine in catalysis includes electrostatic steering of  $O_2^{\bullet -}$  (49, 50, 55, 58, 107, 111, 112) and providing a docking site for the anion close to the catalytic  $Cu^{II}$  (108, 239-241).

We have studied the effects of copper chelators on the GSNO-reductase and SOD activities of bovine CuZnSOD in Chapters 2.0 and 3.0. Inhibition of the GSNO-reductase activity of this enzyme by EDTA and DTPA is due to their association with the active-site copper as demonstrated by ITC (Chapter 2). Since neither EDTA nor DTPA binding alters the SOD activity but decreases PGO accessibility to Arg141 of bovine CuZnSOD, the extent of interaction between the negatively charged chelators and the active-site arginine remains unclear. In addition, the role of the active-site arginine in the

GSNO-reductase activity of CuZnSOD has not been elucidated. Although the arginine-specific reagent, PGO, was reported to specifically neutralize the positive charge of the active-site arginine, it was demonstrated in Chapter 4.0, that three of four arginine residues, including the active-site Arg141 in bovine CuZnSOD, were singly PGO-labelled. Moreover, steric effects caused by the PGO labels as well as their limited stability at neutral pH render PGO-modification less useful in identifying critical arginines.

Thus, to further investigate the role of the active-site Arg143 of human CuZnSOD (hSOD1) in its GSNO-reductase activity and in chelator binding, site-directed mutagenesis was considered a better approach than chemical modification. Expression of recombinant hSOD1 and its single-site mutants (R143A, R143I, R143K and R143E) was the initial goal. Due to time constraints only expression and purification of wild-type hSOD1 was undertaken and preliminary results are presented in this chapter.

## **5.2 Experimental procedures**

### **5.2.1 Materials**

Restriction enzymes (10 units/ $\mu$ L): *Hind*III, *Nco*I and *Eco*RI, T4 DNA ligase (1 unit/ $\mu$ L), calf intestine alkaline phosphatase (1 unit/ $\mu$ L) and DNA ladders were from Fermentas Life Sciences. QIAprep Spin Miniprep Kit, QIAquick PCR Purification Kit and QIAquick Gel Extraction Kit were from QIAGEN Inc. Complete EDTA-free protease inhibitor cocktail tablets were from Roche Applied Science. Agar, isopropyl- $\beta$ -D-thiogalactopyranoside (IPTG) and ampicillin (sodium salt) were purchased from BioShop Canada Inc.  $\beta$ -Mercaptoethanol was from ICN. Dialysis membranes (MWCO:

12–14 kDa) was from Spectrapor (Spectrum Laboratories Inc.). Sephadex G-75 and DEAE-Sepharose CL-6B were obtained from Amersham Biosciences and DEAE-Sephacel was from Sigma.

### 5.2.2 Plasmids and strains

YEp351-hSOD1 (5µg/µL, 30 µL) plasmids containing wild-type, R143A, R143E, R143I and R143K mutants of the hSOD1 gene were generous gifts from Dr. P. John Hart, Health Science Center at San Antonio, the University of Texas. YEp351 is a high copy yeast/*E. coli* shuttle vector carrying the LEU2 selectable marker (Figure 5.1) and can replicate autonomously in *Saccharomyces cerevisiae* and in *E. coli*. It contains the entire sequence of the multiple cloning region of pUC18 with single *SacI*, *SmaI*, *BamHI*, *XbaI*, *SalI*, *PstI*, *SphI*, and *HindIII* restriction sites, and double *EcoRI* and *KpnI* sites (242). As described in the literature (243), YEp351 encoding human wild-type CuZnSOD expressed under the control of the yeast CuZnSOD promoter was constructed by inserting between the *EcoRI* and *BamHI* restriction sites, a 1.1-kb DNA fragment containing the yeast SOD1 gene and promoter with an *NcoI* site at the translation start site. The yeast SOD1 coding region was removed by digestion with *NcoI* and *XbaI*, leaving the yeast SOD1 promoter and the rest of the vector intact. cDNA clones of human wild-type SOD1 and its mutants with an *NcoI* site introduced at the start codon and an *XbaI* site 715 bases downstream were ligated into the vector to direct the expression of the protein under the control of its own promoter.

*Saccharomyces cerevisiae* strain BY4742 lacking the endogenous yeast *sod1* gene (*MATα his3Δ1 leu2Δ0 lys2Δ0 ura3Δ0 SOD1Δ::Kan MX*) was generously provided by Dr. V. Titorenko, Biology Department, Concordia University. The pET-22b(+) vector,

carrying an *N*-terminal *pelB* signal sequence that efficiently directs proteins to the periplasm of bacteria, and *E. coli* strain BL21(DE3) were purchased from Novagen. XL1-Blue *E. coli* cells were obtained from Dr. M. J. Kornblatt, Department of Chemistry and Biochemistry, Concordia University.

### **5.2.3 Transformation of YEp351 and pET-22b(+) plasmid DNA into the non-expression host**

Competent XL1-Blue cells were prepared using CaCl<sub>2</sub> and transformed with plasmid DNA following the protocols given in *Molecular Cloning: A Laboratory Manual* (2<sup>nd</sup> Edition, Sambrook et al.). Briefly, ~50 ng plasmid DNA with and without insert was added to 100 µL XL1-Blue competent cells. After incubation on ice for 10 min, the tubes were placed in a 42°C bath for 90 s, and immediately put on ice for 2 min. Cells transformed with plasmid DNA were added to 500 µL of LB medium and incubated at 37°C with shaking (250 rpm) for 1 h. A 100-µL aliquot of the transformation was spread on LBA agar plates (1% tryptone, 0.5% yeast extract, 1% NaCl, and 0.1% ampicillin containing 1.2% agar) for plasmid DNA with insert or LB agar plates (without ampicillin) for plasmid DNA without insert, and incubated at 37°C overnight.

### **5.2.4 Sub-cloning the hSOD1 gene into the pET-22b(+) vector**

Procedures to transfer the hSOD1 insert from the YEp351-hSOD1 (wild type) plasmid to pET-22b(+) were performed according to the pET System Manual downloaded from the Novagen website, [www.novagen.com](http://www.novagen.com). The steps described below were followed.

***DNA digestion and purification:*** XL1-Blue cells transformed with the YEp351-hSOD1 and pET-22b(+) plasmids were grown overnight in LBA and LB media,



respectively, in a shaker incubator (37°C, 250 rpm). The plasmids were extracted from 3 mL of cell culture using the QIAprep Spin Miniprep Kit (QIAGEN), and doubly digested with *Nco*I and *Hind*III. The YEp351-hSOD1 digestion reaction mixture contained 5 µL of plasmid DNA (0.59 µg/µL), 2 µL of *Nco*I, 1 µL of *Hind*III, 1 µL of H<sub>2</sub>O, and 1 µL of 10× buffer R; the pET-22b(+) digestion reaction mixture contained 30 µL of plasmid DNA (0.13 µg/µL), 2 µL of *Nco*I, 1 µL of *Hind*III, 1 µL of H<sub>2</sub>O, and 3.7 µL of 10× buffer R. Samples were incubated at 37°C for 2 h and analyzed on a 0.7% agarose gel. The restriction-digested pET-22b(+) vector was purified using the QIAquick PCR Purification Kit (QIAGEN), eluted with 28 µL MilliQ H<sub>2</sub>O, and dephosphorylated by incubation of the eluate with 1 µL calf alkaline phosphatase plus 3.2 µL of 10× reaction buffer (supplied with the enzyme) at 37°C for 30 min. The dephosphorylated pET vector was purified on a 0.7% agarose gel and the desired vector band was excised and extracted from the gel using the QIAquick Gel Extraction Kit (QIAGEN). Alternatively, a 10-µL aliquot of the dephosphorylated pET-22b(+) vector was purified using the QIAquick PCR Purification Kit, and eluted with 28 µL of MilliQ H<sub>2</sub>O. The hSOD1 insert from the *Nco*I/*Hind*III digest of YEp351-hSOD1 was gel-purified in the same manner as the pET vector.

***Ligation of gel- and QIAquick-purified plasmids:*** Parallel experiments were carried out to test the ligation efficiency of the gel- vs QIAquick-purified vectors. Tube 1 contained 3 µL of hSOD1 insert (240 ng), 10 µL of the dephosphorylated pET-22b(+) vector that was QIAquick purified (430 ng), 1.5 µL of 10× sample buffer, and 0.5 µL of T4 DNA ligase; tube 2 contained 7 µL of hSOD1 insert (560 ng), 5 µL of the gel-purified dephosphorylated pET-22b(+) vector (165 ng), 2 µL of 10× sample buffer, 5.5 µL of

sterile H<sub>2</sub>O, and 0.5 µL of T4 DNA ligase. A negative control (Tube 3) contained the same contents as Tube 2 except that 7 µL of sterile H<sub>2</sub>O was added instead of the hSOD1 insert. The tubes were incubated at room temperature for 1 h and transformation of XL1-Blue cells was carried out using 5 µL (tube 1) or 10 µL (tube 2 or 3) of the ligation mixtures following the procedures given in Section 5.2.3.

**Restriction-enzyme analysis:** Twelve colonies were picked randomly from plates containing the transformed XL1-Blue cells, and streaked on LBA plates and inoculated in 5 mL of LB medium with ampicillin (100 mg/mL) in 50-mL centrifugation tubes. The 12 plates and 12 tubes were incubated separately overnight at 37°C in an incubator without and with 250 rpm shaking. Plasmid DNAs were extracted from 2 mL of each of the 12 cultures using the QIAprep Spin Miniprep Kit (QIAGEN), eluted in 50 µL of buffer EB (10 mM TrisHCl, pH 8.5), and doubly digested with both *Nco*I and *Hind*III. The digestion reaction was carried out by incubating a mixture of 6 µL of plasmid DNA (95 – 346 ng), 2 µL of *Nco*I, 1 µL of *Hind*III, and 1 µL of 10× buffer R at 37°C for 1 h 20 min, and the digest was analyzed on a 0.7% agarose gel. Cells from a 2-mL culture of the desired transformant as evidenced by DNA gel analysis were sent to Bio S&T (Montreal) for sequencing (Appendix 3.0).

## **5.2.5 Transformation of plasmids containing the hSOD1 gene into the expression hosts**

### **5.2.5.1 Transformation of YEp351-hSOD1 wild type and R143E plasmids into *S. cerevisiae* strain BY4742**

Prior to yeast transformation, the five plasmids containing hSOD1 wild-type and mutant genes were transformed into XL1-Blue cells, harvested from 4-mL cultures,

and sent to Bio S&T for sequencing. Plasmids in EB buffer extracted from 3-mL cultures using the QIAprep Spin Miniprep Kit (QIAGEN) were prepared for storage, and restriction-enzyme analysis was performed on YEp351-hSOD1 (wild type). The digestion solutions containing 1  $\mu$ L of plasmid DNA (0.76  $\mu$ g/ $\mu$ L), 1  $\mu$ L of Y<sup>+</sup>/TANGO<sup>TM</sup> digestion buffer, 7  $\mu$ L of H<sub>2</sub>O, and 1  $\mu$ L each of *Eco*RI, *Nco*I and *Hind*III (where indicated) were incubated at 37°C for 3 h, and analyzed on a 0.7% agarose gel.

Transformation of YEp351-hSOD1 (wild type) and YEp351-hSOD1 (R143E) into *sodI*<sup>-</sup> yeast in the BY4742 genetic background followed the commonly used high efficiency transformation protocol (244). Briefly, *sodI*<sup>-</sup> cells were grown in 50 mL of YPD medium (1% yeast extract, 2% peptone and 2% glucose) at 30°C, 200 rpm to OD<sub>600</sub> ~0.5. The cells were harvested by centrifugation at 3,000 rpm for 5 min, washed in 25 mL of sterile water and resuspend in 500  $\mu$ L of sterile water. Aliquots (250  $\mu$ L) of cell suspension were added to two 1.5-mL sterile microcentrifuge tubes, centrifuged for 30 s and the supernatants were discarded. The cells were resuspended in 360  $\mu$ L of Transformation Mix (240  $\mu$ L of PEG 3500 50% w/v, 36  $\mu$ L of 1.0 M LiAc, 50  $\mu$ L of boiled SS-carrier DNA, and 14  $\mu$ L of sterile H<sub>2</sub>O) with 20  $\mu$ L of 0.76  $\mu$ g/ $\mu$ L YEp351-hSOD1 plasmid. To prepare control cells, 20  $\mu$ L of sterile H<sub>2</sub>O were substituted for the plasmid solution. The cell suspensions were incubated at 42°C for 40 min, centrifuged at 15,000 rpm for 30 s in a MicroMax Microcentrifuge (Thermo Electron Corporation), and the pellets were gently suspended in 1 mL of sterile H<sub>2</sub>O using micropipette tips. Aliquots (100  $\mu$ L) were spread on plates with SC selection medium [6.7 g/L Y-0626 (yeast nitrogen base), 1.6 g/L Y-1376 (without Leu), 20g/L D-glucose (Mallinckrodt Canada Inc.), and 12g/L agar] and incubated at 30°C for 2–3 days.

#### **5.2.5.2 Transformation of the pET-hSOD1(wild type) plasmid into *E. coli* strain BL21(DE3)**

**Preparation of competent BL21(DE3) cells:** A colony of BL21(DE3) cells was selected from an LB plate and inoculated in 10 mL of LB medium. The cells were grown overnight in a shaker incubator at 37°C, 225 rpm, a 0.1 mL-aliquot of the overnight culture was transferred to a sterile flask containing 10 mL of fresh LB medium, the cells were grown under the same condition, and harvested at OD<sub>600</sub> ~0.4. The culture was chilled on ice for 40 min, pelleted at 5,000 rpm for 5 min at 4°C, resuspended in 2.5 mL of sterile ice-cold 50 mM CaCl<sub>2</sub> and incubated on ice for 15 min. The cells were repelleted (5,000 rpm, 5 min, 4°C), the supernatant was carefully discarded, the pellet was resuspended in 400 µL of sterile ice-cold 50 mM CaCl<sub>2</sub>, and put on ice for use or mixed with 15% glycerol (1:1, v/v) and transferred in 0.5-mL aliquots to pre-chilled, sterile Eppendorf tubes for storage at -80°C.

**Transformation:** Following identification by restriction-enzyme analysis and sequencing, the pET-hSOD1 plasmid (~50 ng), extracted from XL1-Blue cells using the QIAprep Spin Miniprep Kit (QIAGEN), was transformed into the expression host, BL21(DE3). The procedure in Section 5.2.3 was followed except that heat shock was performed 60 s at 42°C.

#### **5.2.6 Expression of recombinant hSOD1**

##### **5.2.6.1 Expression of recombinant hSOD1 (wild type) in yeast**

The *sod1*<sup>-</sup> strain carrying the YEp351-hSOD1 wild type plasmid was inoculated in 50 mL of YPD medium and grown at 30°C, 220 rpm for ~48 h. Aliquots (10 mL) were transferred to 500 mL of YPD medium (OD<sub>600</sub> = 0.2) and grown under the same

conditions for the times indicated in the Figure legends, and cells were harvested by centrifugation at 7,000 rpm and 4°C for 10 min. The *sodI*<sup>-</sup> strain without the YEp351-hSOD1 plasmid was grown as a control under the same conditions to identify non-SOD1 expression in the BY4742 strain.

Yeast soluble cell extracts were prepared by glass-bead lysis as described by Nishida *et al.* (253) with minor modifications. Cells harvested from 10-mL cell cultures were suspended in 200–300 µL of lysis buffer (200 mM TrisHCl, 0.1 mM EDTA, 50 mM NaCl, pH 8.0) containing proteinase inhibitor (1 tablet per 100 mL of lysis buffer, Roche) with an equal volume of acid-washed 0.5-mm glass beads, and vortexed vigorously for 4×30 s followed by 30 s cooling on ice. The mixture was centrifuged at 8,000g for 20–60 min at 4°C to remove the cellular debris and glass beads. The supernatant was collected and the pellet was re-extracted by washing with an additional 100–200 µL of buffer. Following centrifugation, the supernatants were combined, analyzed by SDS-PAGE, and stored at -20°C for protein purification. Larger volumes of cells (500 mL) were processed by increasing the volumes proportionately.

#### **5.2.6.2 Expression of recombinant hSOD1 (wild type) in *E. coli***

The BL21(DE3) strain transformed with pET-hSOD1(wild type) was inoculated in 5 mL of LBA medium with or without 200–500 µM Cu<sup>2+</sup> and 5–50 µM Zn<sup>2+</sup>, and grown in an incubation shaker at 37°C, 250 rpm overnight. Aliquots (0.6 mL) were transferred to 60 mL of the same medium and grown under the same conditions for times necessary to reach the OD<sub>600</sub> values indicated in the Figure legends. To induce protein expression, 1 mM IPTG or 1 mM IPTG with 200–500 µM Cu<sup>2+</sup> and 5–50 µM Zn<sup>2+</sup> was added to the LBA medium. After 3–4 h induction, cells were harvested by centrifugation

at 6,000 rpm and 4°C for 15 min, and cells from a non-induced culture (-IPTG) were harvested as a control.

Protein extraction was performed using the BugBuster Protein Extraction Reagent Kit (Novagen) according to the protocol supplied with the kit. Briefly, cells were resuspended by pipetting in the BugBuster reagent solution (5 mL of reagent per gram of wet cell paste), Benzonase nuclease (25 units per mL of BugBuster reagent), and proteinase inhibitor (1 tablet per 100 mL of lysis buffer, Roche) and incubated on a shaking platform for 20 min at room temperature. The insoluble cell debris was removed by centrifugation at 16,000g for 20 min at 4°C, and the supernatant was kept on ice or stored at -20°C until use. Localization of the target protein was performed following the procedures described in pET System Manual ([www.novagen.com](http://www.novagen.com)) with minor modifications. Samples extracted from different fractions discussed below were analyzed by SDS-PAGE.

***Total cell protein (TCP) fraction:*** A 1-mL aliquot of culture was removed and centrifuged in a 1.5-mL microcentrifuge tube at 10,000g for 1 min. The cell supernatant was discarded and removed thoroughly by inversion of the tube and tapping the excess medium onto a Kimwipe. Proteins in the drained pellet were extracted using the BugBuster Protein Extraction Reagent Kit as described above. The extraction solution contained 200 µL of BugBuster, 0.5 µL of Benzonase nuclease and protease inhibitor. A 10-µL aliquot of the cell-lysate supernatant was mixed with an equal volume of 4× SDS sample buffer (62.5 mM TrisHCl, pH 6.8, 25% glycerol, 2% SDS, 5% β-mercaptoethanol, and 0.01% Bromophenol Blue), the mixture was immediately heated for 5 min at 95°C to denature the proteins, and stored at -20°C for SDS-PAGE analysis.

***LBA medium fraction:*** A 40-mL aliquot of cell culture was harvested by centrifugation at 10,000g for 10 min at 4°C, and the cell pellet (0.16 g) was placed on ice for analysis of the periplasmic fraction (next section). A 1-mL aliquot of the supernatant was transferred to a 1.5-mL microcentrifuge tube for SDS-PAGE analysis. Approximately 20 µL of sample solution was concentrated from 500 µL of the supernatant by centrifugal ultrafiltration at 12,000 rpm in a filter tube (cut-off 10 kDa, Millipore), a 5-µL aliquot of the concentrated sample solution was diluted with an equal volume of H<sub>2</sub>O, mixed with 10 µL of 4× SDS sample buffer, immediately heated for 5 min at 95°C to denature the proteins, and stored at -20°C for SDS-PAGE analysis.

***Periplasmic fraction:*** The cell pellet (0.16 g from 40 mL of cell culture) generated in the previous step was resuspended thoroughly in 30 mL of 10 mM TrisHCl (pH 8) containing 20% sucrose, 60 µL of 0.5 M EDTA (pH 8) was added, and the mixture was stirred slowly at room temperature for 10 min. The cells were collected by centrifugation at 10,000g for 10 min at 4°C, the supernatant was discarded, the pellet was resuspended thoroughly in 30 mL of ice-cold 5 mM MgSO<sub>4</sub>, and the cell suspension was stirred slowly on ice for 10 min to release the periplasmic proteins into the buffer. The shocked cells were repelleted by centrifugation and the pellet weight was recorded prior to processing of the soluble cytoplasmic fraction as described in the following section. A 125-µL aliquot of the osmotic-shock supernatant was concentrated to 5 µL as described in the previous step, diluted with an equal volume of H<sub>2</sub>O, mixed with 10 µL of 4× SDS sample buffer, immediately heated for 5 min at 95°C to denature the proteins, and stored at -20°C for SDS-PAGE analysis.

***Soluble cytoplasmic fraction:*** Extraction of proteins from the osmotic-shocked cell pellet (0.099 g) was performed using the BugBuster Protein Extraction Reagent Kit as described above. The extraction mixture contained 0.099 g of cell pellet, 500  $\mu$ L of BugBuster, 0.5  $\mu$ L of Benzonase nuclease, and protease inhibitor. A 10- $\mu$ L aliquot of the supernatant was mixed with 10  $\mu$ L of 4 $\times$  SDS sample buffer, immediately heated for 5 min at 95°C to denature the proteins, and stored at -20°C for SDS-PAGE analysis.

## **5.2.7 Purification of recombinant hSOD1 from yeast and *E. coli* hosts**

### **5.2.7.1 Ammonium sulfate protein precipitation from yeast**

Recombinant hSOD1 was purified from yeast as previously reported (245) with minor modifications. The proteins were salted-out from the lysate supernatant. Solid ammonium sulfate was added with gentle stirring using a magnetic stir bar to the supernatant in an ice bath. The solution was slowly brought to 60% ammonium sulfate saturation and incubated on ice for an additional 30 min. The precipitated proteins were removed by centrifugation at 16,000g for 30 min at 4°C and redissolved in lysis buffer for SDS-PAGE analysis. The supernatant was slowly adjusted to 90% ammonium sulfate saturation and the precipitated proteins again collected by centrifugation at 16,000g for 30 min at 4°C. To further purify the precipitated hSOD1, the precipitate was dissolved in 50 mM sodium phosphate buffer/0.01 mM EDTA (pH 7.2) and dialyzed vs 2 L of the same buffer for ~20 h with 2 changes.

### **5.2.7.2 Gel-filtration chromatography**

A 4- $\times$ 30-cm column packed with Sephadex G-75 resin (~23-mL bed volume) was washed and equilibrated with 50 mM sodium phosphate buffer/0.01 mM EDTA (pH 7.2). The sample solution (1.3 mL) was loaded onto the gel surface and eluted at 0.14



mL/min. Fractions were collected and monitored at 280 nm, the total protein concentration in fractions with an OD<sub>280</sub> value  $\geq 1.1$  was measured by the Bio-Rad assay, and the fractions were analyzed by SDS-PAGE.

#### **5.2.7.3 Anion-exchange chromatography**

DEAE-Sephacel (4- $\times$ 10-cm, ~6-mL bed volume) or DEAE-Sepharose CL-6B (1.5- $\times$ 20-cm, ~20-mL bed volume) columns were packed and equilibrated with 50 mM sodium phosphate buffer/0.01 mM EDTA (pH 7.2). Fractions from the gel-filtration column found to contain hSOD1 were loaded onto the anion-exchange column, washed with 7–10 mL of equilibration buffer, and eluted with a 0–1 M NaCl gradient at the flow rates indicated in the figure legends. Fractions were collected and analyzed by SDS-PAGE as described in the previous section.

#### **5.2.7.4 Heat precipitation of yeast proteins**

Extraction of expressed hSOD1 by heat precipitation of cell proteins was performed according to the method described by Thulin *et al.* for calbindin (246) with minor modifications. Two 1.03-g fractions of yeast cells were resuspended in 4 mL of lysis buffer and cooled on ice. Cells in one suspension were lysed using glass beads, and both suspensions were poured into 8 mL of boiling buffer with vigorous stirring until the temperature of the mixture reached 75°C. The mixtures were immediately cooled on ice with stirring to increase the speed of cooling. Cell debris and heat-precipitated proteins were removed by centrifugation at 15,000g for 25 min at 4°C. The remaining total protein in the supernatants was measured by the Bio-Rad assay and the supernatants were analyzed by SDS-PAGE.

#### **5.2.8 Gel electrophoresis**

### **5.2.8.1 Agarose gel electrophoresis**

The plasmids and restriction-enzyme DNA digests were analyzed using agarose gel electrophoresis. The 0.7% agarose gels were performed by dissolving 0.35 g of agarose in 50 mL of 0.5× TBE containing 10 mg/mL ethidium bromide. The running buffer was 0.5× TBE diluted from 5× TBE [54 g Tris base, 27.5 g boric acid and 20 mL of 0.5 M EDTA (pH 8.0) dissolved in deionized water and brought to 1 L]. Samples were diluted with running buffer when needed, mixed with 6× loading dye (30% glycerol, 0.2% bromophenol blue and 0.2% xylene cyanol), and subjected to electrophoresis at 70 V on 8-×10-cm gels. Fermentas Gene Ruler™ 1 kb and 100 bp DNA ladders (MBI Fermentas) were used as size markers. The bands on the gels were visualized on a UV light-box and photos were taken as required using Polaroid film.

### **5.2.8.2 SDS-polyacrylamide gel electrophoresis (SDS-PAGE)**

Proteins from cell cultures were analyzed by performing electrophoresis under denaturing conditions. The 8-×10-×1.5-mm slab gels consisted of resolving (10%, 12% and 15%) and stacking (4%) gels prepared following the instructions provided with the acrylamide/bis-acrylamide (30%/0.8% w/v, Bio-Rad). Protein samples were diluted 1:4 with SDS-sample buffer [4.0 mL of distilled water, 1.0 mL of 0.5 M TrisHCl (pH 6.8), 0.8 mL of glycerol, 1.6 mL of 10% SDS, 0.4 mL of β-mercaptoethanol, and 0.2 mL of 0.05% (w/v) bromophenol blue], and heated at 95°C for 5 min prior to loading. The gel was run at constant current (25–50 mA) in running buffer in a Bio-Rad Mini-PROTEIN® II Cell. A solution of 5× SDS-PAGE running buffer (pH 8.3) was prepared by dissolving 15 g of Tris base, 5 g of SDS, and 72 g of glycine in 1 L of deionized H<sub>2</sub>O and diluted to 1× before use. Protein molecular weight markers (MBI Fermentas) were used to estimate

the molecular weights of unknown proteins in the samples. Proteins were visualized by staining the gels with GelCode<sup>®</sup> Blue stain reagent (Pierce).

#### **5.2.8.3 Western blot analysis of hSOD1**

The expressed hSOD1 was probed by western blotting following the procedures as given here. Samples were electrophoresed on 10 or 12% SDS-polyacrylamide gels, and transferred to polyvinylidene difluoride (PVDF, Bio-Rad) membranes in transfer buffer [25 mM Tris, 192 mM glycine (pH 8.3)] at 60 V for 4 h at 4°C. After transfer, blots were blocked at 4°C with agitation overnight. The blocking solution was 5% fat-free milk (Instant skim milk, Nestlé Carnation) in PBS (diluted from 10× PBS prepared by dissolving 40 g of NaCl, 1 g of KCl, 7.2 g of Na<sub>2</sub>HPO<sub>4</sub>, 1.2 g of KH<sub>2</sub>PO<sub>4</sub> in 500 mL of H<sub>2</sub>O and adjusting the pH to 7.4). The membrane was rinsed 5× for 5 min with wash buffer (10 mM TrisHCl, 100 mM NaCl, and 0.1% Tween-20, pH 7.4), and incubated for 1 h at room temperature in the primary antibody [0.4 µg/mL rabbit anti-human CuZnSOD (Stressgen) in blocking solution]. After removal of the primary antibody, the membrane was rinsed as before, and incubated with the secondary antibody [1:3000 goat anti-rabbit/horseradish peroxidase (Bio-Rad) in blocking solution], for 1 h with agitation at room temperature. Blots were rinsed 4× for 5 min in wash buffer with agitation at room temperature, and proteins were detected by incubating the membrane with TMB (3,3',5,5'-tetramethyl benzidine) for 10 min to visualize the CuZnSOD bands. The membrane was washed in deionized water, air dried and scanned using a scanner (Umax PowerLook III).

#### **5.2.9 Determination of SOD activity**

The SOD activity of the cell extracts, the purified fractions, and the reconstituted enzyme (Section 5.2.10) was assayed by monitoring inhibition of xanthine/xanthine oxidase-mediated reduction of cytochrome *c*, as described in Section 2.3.2.3.

#### **5.2.10 Spectrophotometric analysis**

UV-Vis spectra of purified and reconstituted hSOD1 samples were measured in Beckman DU800 spectrophotometer using a 1-cm quartz cuvette. The reconstituted enzyme was prepared by incubating 26  $\mu\text{M}$  purified hSOD1 with 500  $\mu\text{M}$   $\text{Cu}^{2+}$  and 500  $\mu\text{M}$   $\text{Zn}^{2+}$  at 4°C for 20 h. The sample was desalted on a NAP-5 column (Amersham Biosciences), concentrated by centrifugal ultrafiltration at 12,000 rpm for 10 min at 4°C in a 10 kDa cut-off filter tube (Millipore). The total protein was measured by the Bio-Rad assay using bovine serum albumin (Bio-Rad) as a standard.

#### **5.2.11 Mass spectrometry**

The mass spectrum of purified hSOD1 was measured to determine its molecular weight. The desalted sample was diluted into 50% ACN/0.1% TFA to a final concentration of 5~10  $\mu\text{M}$  and directly infused into the Z-spray source of a Q-ToF 2 mass spectrometer (Water Micromass) at a flow rate of 1  $\mu\text{L}/\text{min}$ . The experimental details are the same as those given in Section 4.3.2.4.

### **5.3 Results**

#### **5.3.1 Overexpression and purification of hSOD1 (wild type) in yeast**

##### **5.3.1.1 Analysis of the YEp351-hSOD1 vector**

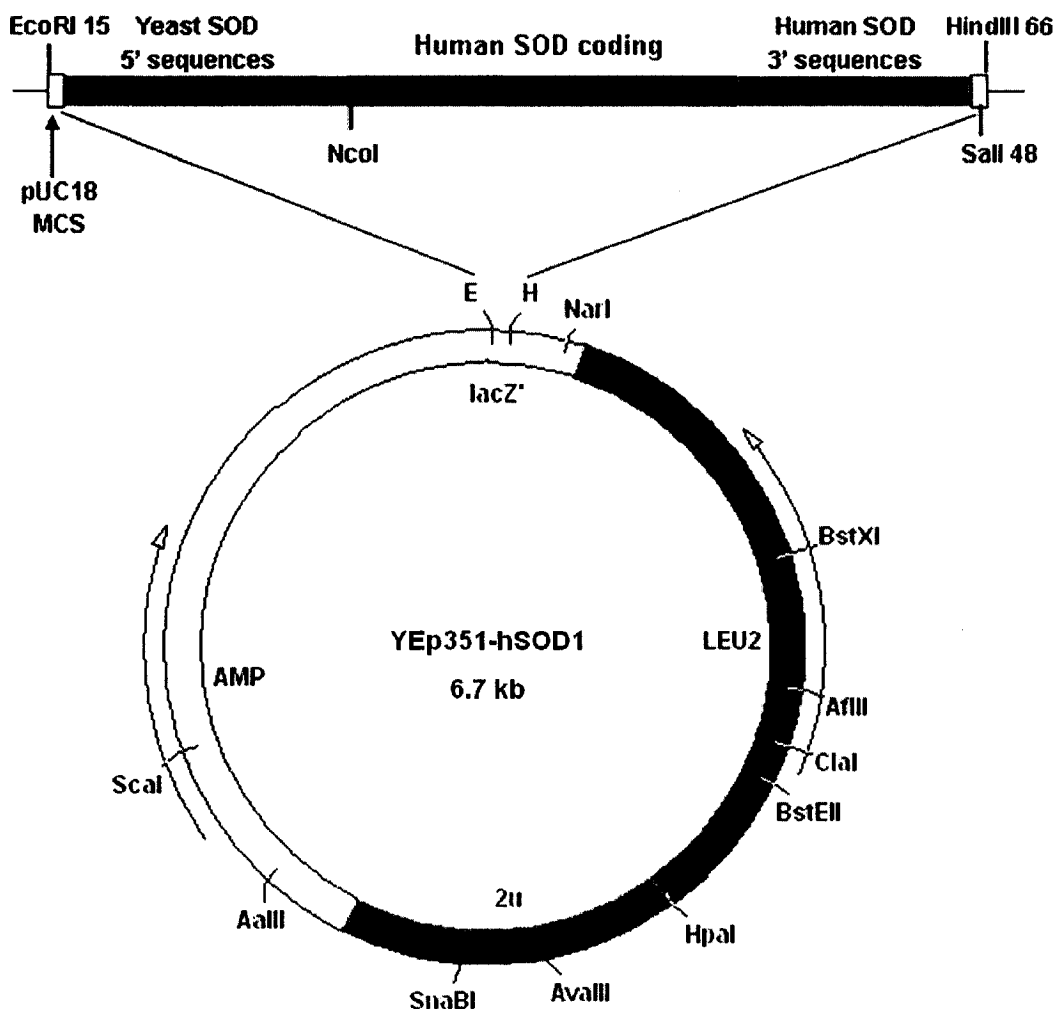


Figure 5.1 Schematic description of plasmid YEp351-hSOD1. The plasmid contains the pUC18 multiple cloning site (MCS) and the hSOD1 gene inserted between *NcoI* and *SalI*. Engineering of this plasmid is described in Ref (243). (E = *EcoRI*, H = *HindIII*).

The hSOD1 gene with upstream yeast SOD 5' sequences and downstream human SOD 3' sequences was cloned into YEp351 between *EcoRI* and *HindIII* sites (Figure 5.1) (243). The SOD1 coding region is flanked by *NcoI* and *SalI* sites. This construct was confirmed by restriction enzyme analysis with *EcoRI*, *NcoI* and *HindIII*. Since *HindIII* and *NcoI* are unique, linearized plasmid was seen on gel analysis of the *HindIII* and *NcoI* digests (Lanes 4 and 5, Figure 5.2). Bands at 4.4 kbp and 2.3 kbp were

observed for the *EcoRI* digest (Lane 3) as expected since *EcoRI* cuts the plasmid twice. The double *EcoRI/HindIII* digest released the 1.1 kbp insert together with the 4.4 kbp fragment and an additional 1.2 kbp fragment (Lane 6). The hSOD1 coding region plus the downstream human SOD sequences has a size of 750 bp consistent with the *NcoI/HindIII* fragment (Lane 7). The YEp351-hSOD1 insert was sequenced and the sequence is listed in Appendix 3.0.

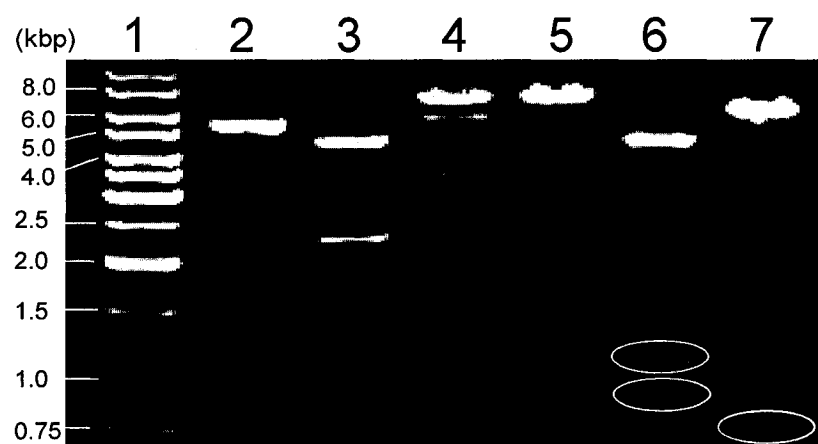


Figure 5.2 **Restriction enzyme analysis of plasmid YEp351-hSOD1.** Lane 1, 1 kb Ladder; lane 2, uncut plasmid; lane 3, plasmid cut with *EcoRI*; lane 4, plasmid cut with *HindIII*; lane 5, plasmid cut with *NcoI*; lane 6, plasmid cut with *HindIII* and *EcoRI*; and lane 7, plasmid cut with *HindIII* and *NcoI*. Analysis was carried out on a 0.7% agarose gel.

### 5.3.1.2 Expression of hSOD1 in yeast

Cell-lysate supernatants from *sod1<sup>-</sup>* BY4742 yeast and the strain transformed with YEp351-hSOD1 (wild type) grown for 25 h ( $OD_{600} = 9$ ) and 46 h ( $OD_{600} = 11$ ) in YPD were analyzed by SDS-PAGE. hSOD1 was overexpressed to a comparable extent in the 25-h and 46-h cultures (lanes 3, 4, Figure 5.3A). No hSOD1 band was observed in the 25-h control culture (lane 8). Proteins in the 46-h cell-lysate supernatant were salted-out and no hSOD1 band was visualized in the 60% ammonium sulfate precipitate (lane 7) but

it was enriched in the 90% ammonium sulfate precipitate (lane 6). The bands seen for BCuZnSOD (lane 2) are due to the monomer at 16 kDa and two closely spaced bands at ~32 kDa due to dimeric forms (183). Western blotting (Figure 5.3B) confirmed the SDS-

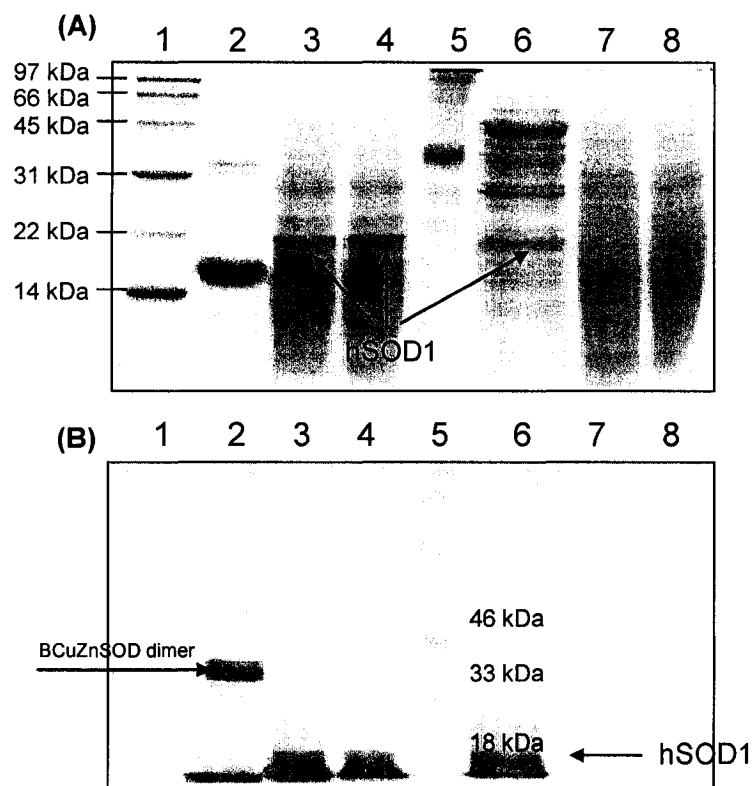
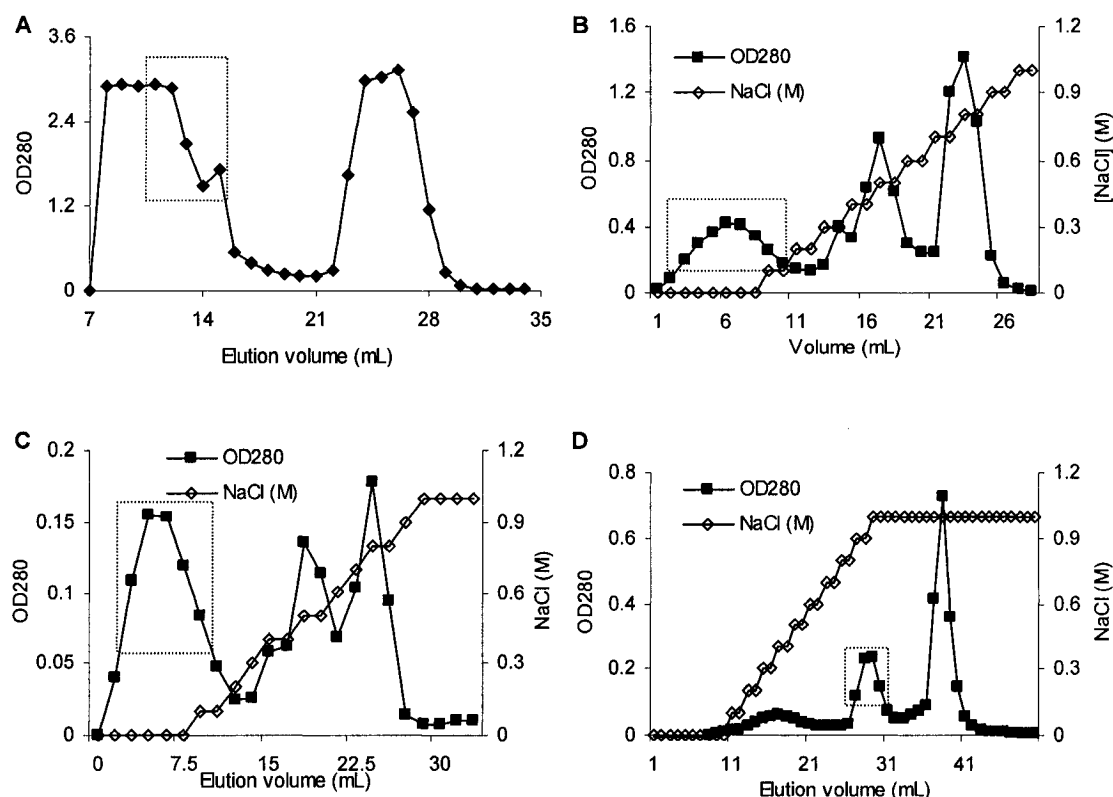


Figure 5.3 (A) SDS-PAGE (15%) and (B) Western blot (10%) analysis of hSOD1 expression in *sod1<sup>-</sup>* BY4742 Cells. (A) and (B): lane 2, bovine CuZnSOD (14.7  $\mu$ g); lanes 3 and 4, cell-lysate supernatants from yeast transformed with YEp351-hSOD1 (wild type) after 46-h and 25-h growth, respectively; lanes 6 and 7, proteins precipitated from 46-h cell-lysate supernatant at 90% and 60%  $(\text{NH}_4)_2\text{SO}_4$  saturation, respectively; lane 8, cell-lysate supernatant from 25-h culture without plasmid. A total of 55  $\mu$ g of protein was loaded per lane unless indicated. Markers as shown in lanes 1 and 5 of (A) and lane 5 of (B).

PAGE results since hSOD1 is observed only in lanes 3, 4, and 6 of both gels. Since a 10% gel was employed for Western blotting, the hSOD1 band was at the dye front and the 16 kDa monomer band of BCuZnSOD ran off the gel. Although hSOD1 and BCuZnSOD have similar masses (15,846 vs 15,590 u; Figure 6.2B vs C), the human enzyme appears at 18–22 kDa on SDS gels for unknown reasons (247-249).

### 5.3.1.3 Purification of hSOD1 from yeast

After 46 h growth, 7.6 g of cells were harvested from 500 mL of cell culture. The cell-lysate supernatant contained 309 mg/18 mL total protein and 120 mg/1.5 mL total protein was present in the 60–90% ammonium sulfate fraction, which was applied to



**Figure 5.4 hSOD1 purification by gel filtration and anion-exchange chromatography.** (A) A total of 106 mg protein in 1.5 mL of lysis buffer was applied to a 4×30-cm Sephadex G-75 column; (B) Fractions 4, 6 and 7 (3 mL) from A containing 13.6 mg protein was combined and applied to a 4×10-cm DEAE-Sephacel column; (C) 4 mL of dialyzed sample containing 3.6 mg protein was applied to a 4×10-cm DEAE-Sephacel column; and (D) 5 mL of dialyzed sample containing 4.5 mg protein was applied to a 1.5×20-cm DEAE-Sepharose CL-6B column. The dialyzed sample was prepared by 20-h dialysis of fraction 5 from A combined with fractions 3–10 from B against 2 changes of 50 mM sodium phosphate buffer/0.01 mM EDTA (pH 7.2) at 4°C. Proteins were eluted from the Sephadex G-75 and DEAE-Sephacel columns under gravity flow, and from the DEAE-Sepharose CL-6B column at 0.5 mL/min with the equilibration buffer (50 mM sodium phosphate buffer/0.01 mM EDTA, pH 7.2) ± a salt gradient (0–1 M NaCl) as indicated in Figures. The fractions inside the rectangles contained hSOD1 as revealed by SDS-PAGE analysis (See Figure 5.5).



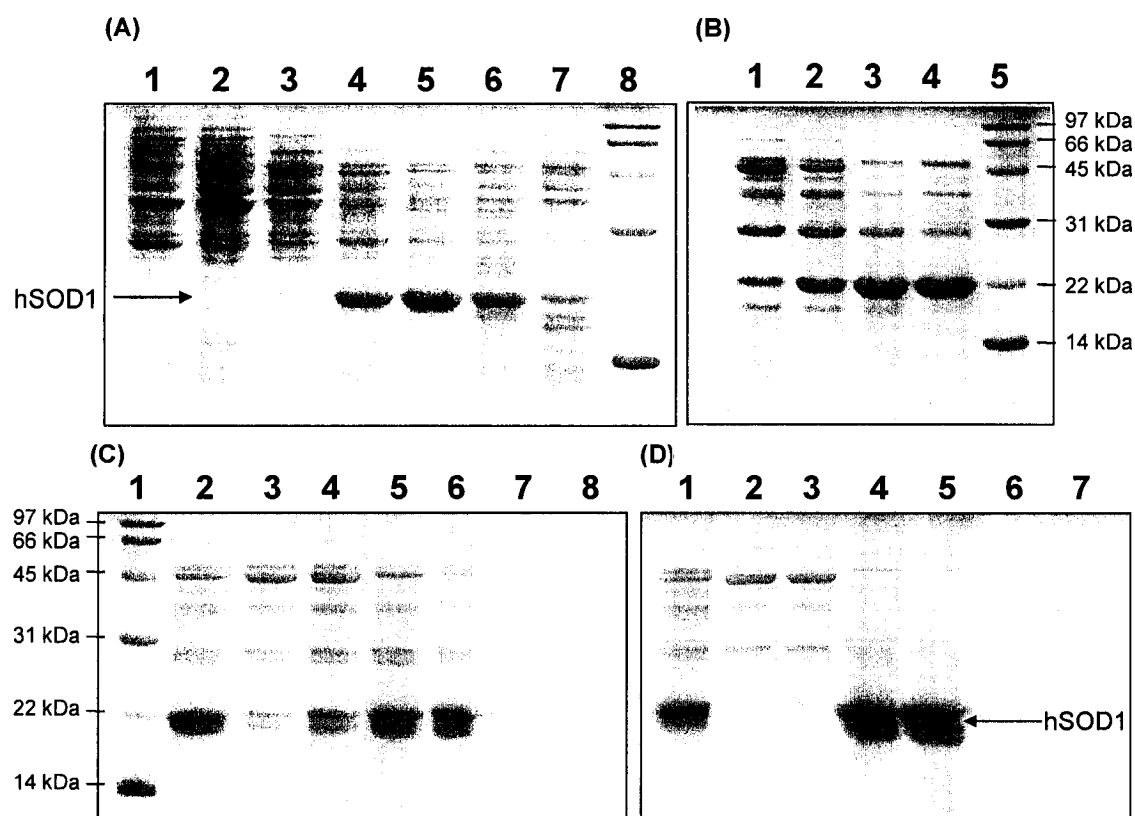


**Figure 5.5 SDS-PAGE (15%) analysis of hSOD1 purification from yeast cells.** Fractions from **(A)** the Sephadex G-75 (Figure 5.4A): lanes 1–7, fractions eluted at 8–14 mL, 20  $\mu$ g protein/lane; lane 8, protein-size markers, **(B)** the DEAE-Sephacel (Figure 5.4B): lanes 1–4, fractions eluted at 5–8 mL, 15  $\mu$ g protein/lane; Lane 5, protein-size markers, **(C)** the DEAE-Sephacel (Figure 5.4C): lane 1, protein-size markers; lane 2, dialyzed sample, 15  $\mu$ g/lane; lanes 3–6 and 7–8, fractions eluted at 3–7.5 mL and at 19.5–21 mL, 30  $\mu$ L of eluate/lane, **(D)** the DEAE-Sephacel CL-6B (Figure 5.4D): lane 1, same as lane 2 in C; lanes 2–7, fractions eluted at 17–18 mL, 28–29 mL, and 37–38 mL, 30  $\mu$ L of eluate/lane; lane 8, protein-size markers. The dialyzed sample was prepared as described in the legend of Figure 5.4.

a Sephadex G-75 column. The eluate was monitored at 280 nm and the fractions with  $OD_{280} > 1.1$  (Figure 5.4A) were analyzed by 15% SDS-PAGE, and those eluting at 11–15 mL were found to contain ~21 mg total protein (Bio-Rad assay) and to be enriched in hSOD1 (Figure 5.5A). No protein was detected in the fractions at 23–28 mL (data not shown).

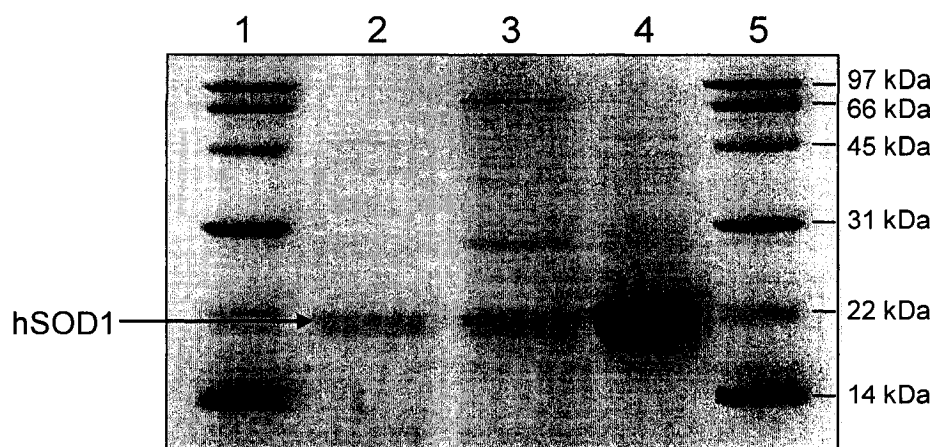


Figure 5.6 SDS-PAGE (15%) analysis of hSOD1 present in yeast cells after heat shock. Supernatants containing 13  $\mu$ g of protein without (lane 2) and with (lane 3) prior cell lysis; lane 4, 15  $\mu$ g of reconstituted hSOD1; lanes 1 and 5, protein-size markers. Experimental: Supernatants from 1 g of heat-shocked yeast cells in 4 mL of lysis buffer were prepared as described in Section 5.2.7.4. Reconstituted hSOD1 was prepared by incubation of purified protein with  $\text{Cu}^{2+}$  and  $\text{Zn}^{2+}$  as described in Section 5.2.10.

To further purify hSOD1, ~14 mg protein was applied to a DEAE-Sephacel column (Figure 5.4B). The hSOD1 fractions (~6 mg total protein) that eluted between 3–10 mL (no NaCl) (Rectangle in Figure 5.4B) were shown by SDS-PAGE analysis (Figure 5.5B) to be impure. The low affinity of hSOD1 ( $\text{pI} = 4.5$ ) (250) for the DEAE-Sephacel column at pH 7.2 was initially attributed to the presence of high salt since the sample was not dialyzed prior to loading on the Sephadex G-75 column. However, when a dialyzed sample containing 3.6 mg protein was loaded on the column, hSOD1 again eluted (~2.5 mg total protein) before starting the salt gradient (Figure 5.4C vs 5.5C) indicating that DEAE-Sephacel does not bind hSOD1 expressed from YEp351-hSOD1 (wild type). hSOD1 was also eluted from a DEAE-Sepharose CL-6B column at  $> 0.7$  M NaCl (Figure 5.4D) and the total protein in the fractions containing hSOD1 (Rectangle in Figure 5.4D)

was 1.64 mg, which is only 36% of the 4.5 mg protein loaded compared with 69% elution from the DEAE-Sepharose column. Thus, less protein impurity was present in samples from the DEAE-Sepharose vs the DEAE-Sepharose column (Figure 5.5D vs 5.5C).

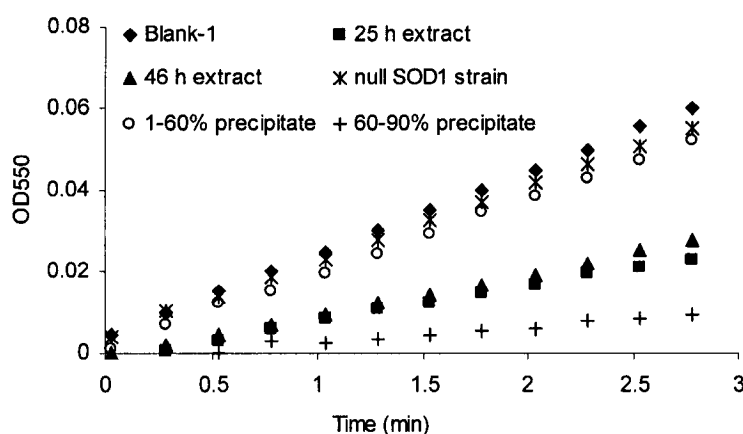


Figure 5.7 **SOD activity in the yeast-cell extracts.** Activities of the samples (4.6–10  $\mu$ L) from Figure 5.3A were determined in a 3-mL assay volume containing 110  $\mu$ g of total protein. Assay details are given in Section 2.3.2.3.

#### 5.3.1.4 Purification of hSOD1 from yeast after heat shock treatment

Heat precipitation of bacterial proteins was described in the purification of human calbindin D<sub>28K</sub> (246). Because of the high thermostability of CuZnSOD, heat shock of yeast cells was investigated in hSOD1 purification. After heat shock, supernatants from 1 g of cells contained 17 mg and 22 mg of total protein without and with prior glass-bead lysis. SDS-PAGE analysis (Figure 5.6) showed that less contaminating proteins were present in the supernatants. Thus, purification and concentration steps should benefit from heat shock and this should be further investigated.

**Table 5.1 Purification of recombinant hSOD1 from yeast cells**

Fraction		Total protein <sup>a</sup> (mg)	Specific activity <sup>b</sup> (units/mg)
cell-lysate supernatant <sup>c</sup>	25 h (-plasmid)	ND	2.6
	25 h (+plasmid)	ND	10
	46 h (+plasmid)	309.1	9.1
(NH <sub>4</sub> ) <sub>2</sub> SO <sub>4</sub> precipitate <sup>d</sup>	60% saturation	101.7	2.6
	90% saturation	122.2	14.8
Dialyzed sample <sup>e</sup>		13.3	150.2
After DEAE-Sepharose CL-6B <sup>f</sup>		4.84	304.8
			286.7
Reconstituted hSOD1 <sup>g</sup>		ND	1038.1

<sup>a</sup>Protein content obtained after each purification step was determined using the Bio-Rad assay. <sup>b</sup>The specific SOD activity was determined using the xanthine oxidase-cyt *c* reduction assay (Section 2.3.2.3). Assays were carried out by diluting 4.6–10  $\mu$ L of sample into the assay solution to a final volume of 3 mL. <sup>c</sup>Lysates from cells  $\pm$  YEp351-hSOD1 plasmid after 25 h or 46 h growth. <sup>d</sup>Precipitates obtained on saturating the cell-lysate supernatant after 46 h growth with 60% and 90% ammonium sulfate. <sup>e</sup>The dialyzed sample prepared as described in the legend of Figure 5.4. <sup>f</sup>Fractions at 28 and 29 mL (Figure 5.4D). <sup>g</sup>Fractions at 28–29 mL Figure 5.4D) after incubation with 500  $\mu$ M Cu<sup>2+</sup> and 500  $\mu$ M Zn<sup>2+</sup> at 4°C for 20 h followed by NAP-5 gel-filtration and ultrafiltration (Section 5.2.10).

### 5.3.1.5 Yield of hSOD1 from yeast and specific activity of fractions

After 46-h growth, 7.65 g cells were harvested from 500 mL of culture, and 309 mg of total protein was measured in the cell-lysate supernatant. After purification, 4.84 mg of protein was obtained indicating that the yield of hSOD1 was ~10 mg/L, which is < 2% of the soluble cellular protein based on the total protein in the cell lysate..

The SOD activity of the cell-lysate supernatant and of the fractions obtained after each purification step was measured to check the activity of the expressed enzyme

(Figure 5.7 and Table 5.1). Consistent with the SDS-PAGE and Western blot results, low SOD activity was detected in the cell-lysate supernatant from 25-h *sod1<sup>-</sup>* yeast cells without YEp351-hSOD1. Fractions from the transformed cells exhibited increasing SOD activity with purification but the precipitate at 60% ammonium sulfate saturation had negligible SOD activity as expected (Figure 5.7). The specific activity of the cell-lysate supernatant was ~10 units/mg and that of the DEAE eluate ~300 units/mg, which is increased to 1,038 units/mg after 20 h incubation with  $\text{Cu}^{2+}$  and  $\text{Zn}^{2+}$  (Table 5.1).

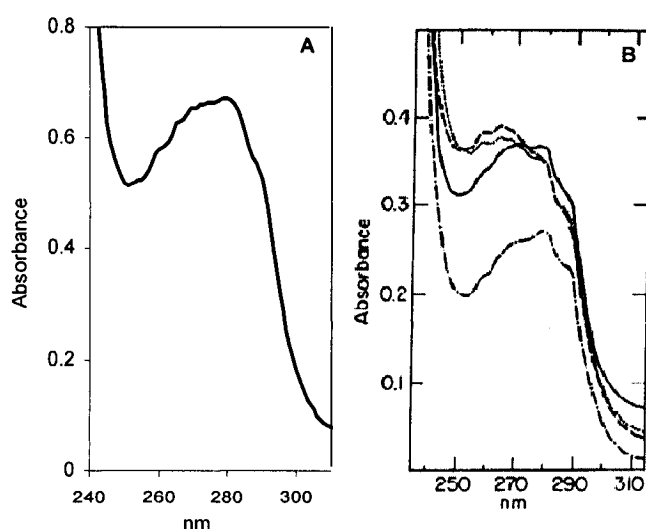


Figure 5.8 Comparison of the UV absorbance spectra of reconstituted hSOD1 produced in yeast with apo- and reconstituted hSOD1 produced in *E. coli* (249). (A) A 2-mg/mL sample of reconstituted hSOD1 was prepared as described Section 5.2.10. (B) Samples (1 mg/mL) in  $\text{H}_2\text{O}$  of hSOD1 purified from *E. coli*. Cells were grown on standard medium (solid line) or on medium supplemented with 2 ppm of  $\text{Zn}^{2+}$  and 200 ppm of  $\text{Cu}^{2+}$  (dashed line); reconstituted hSOD1 (dotted line), and apohSOD1 (symbol and line). hSOD1 was expressed in *E. coli* strain A1645 transformed with pSOD $\beta$ 1T11, and details of the media and the cell growth conditions are given in (249).

### 5.3.1.6 UV absorption spectrum of reconstituted hSOD1

The UV spectra of recombinant hSOD1 isolated from *E. coli* grown with and without added  $\text{Cu}^{2+}$  and  $\text{Zn}^{2+}$ , and of the apo- and reconstituted recombinant enzyme as

reported by Hartman *et al.* (249) are shown in Figure 5.8B. The reconstituted hSOD1 prepared here exhibits a spectrum (Figure 5.8A) similar to that reported for the enzyme isolated from non-metal-supplemented media (Figure 5.8B). This suggests that reconstitution (Section 5.2.10) did not lead to full metal loading of the protein. Hence, the copper content of reconstituted hSOD1 was determined colorimetrically with DDC [ $\epsilon_{450} = 12.0 \text{ mM}^{-1}\text{cm}^{-1}$  (124)]. From the reading at 450 nm after 30 min incubation (Figure 5.9), 19.6  $\mu\text{M}$  copper was determined in 51.5  $\mu\text{M}$  hSOD1, revealing that only ~20% of the copper sites in the enzyme were loaded with metal following the attempted reconstitution.

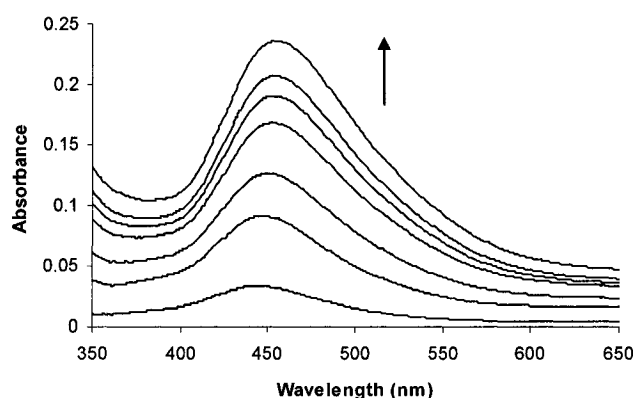


Figure 5.9 **Absorbance spectra vs time of reconstituted hSOD1 following DDC addition.** DDC (750  $\mu\text{M}$ ) was added to 51.5  $\mu\text{M}$  reconstituted hSOD1 in 10 mM sodium phosphate buffer (pH 7.2), and spectra were recorded at  $t = 0, 2.5, 5, 10, 15, 20,$  and 30 min at RT in a 1-cm quartz cuvette. Reconstituted hSOD1 was prepared as described in Section 5.2.10.

### 5.3.1.7 ESI-mass spectrum of recombinant hSOD1 from yeast

The mass of purified protein was determined by ESI mass spectrometry (Figure 5.10). The main component had a mass of 15,846 u, matching the expected mass of 15,845 u of hSOD1 with a *N*-acetylated *N*-terminus (247). A low abundant peak with a

mass of 31,692 u is assigned to the hSOD1 dimer, while the peak with a mass of 24,168 u arises from an unidentified protein.

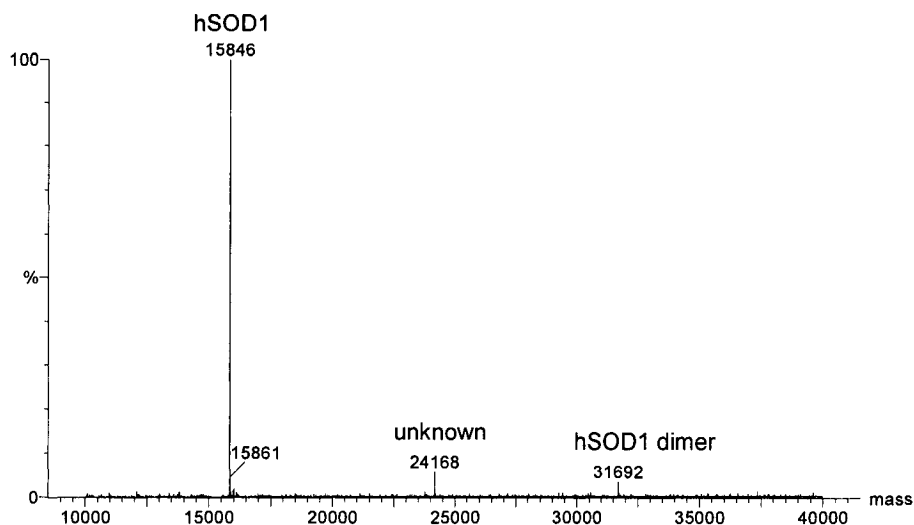


Figure 5.10 ESI mass spectrum of recombinant hSOD1 from yeast. Purified hSOD1 (lane 4 in Figure 5.5D) was desalted on a ZipTipC<sub>18</sub> and was eluted with 60% ACN/0.1 TFA. The eluate (5  $\mu$ M hSOD1) was directly infused at 1  $\mu$ L/min into the ESI source. The MS parameters are given in the legend of Figure 4.1.

### 5.3.2 Overexpression of hSOD1 in *E. coli*

#### 5.3.2.1 Transfer of hSOD1 from YEp351-hSOD1 to pET-22b(+)

To construct the pET-hSOD1(wild type) plasmid (Figure 5.11), the hSOD1 insert was cut from YEp351-hSOD1 by *Hind*III/*Nco*I digestion (Figure 5.12), and ligated into the *Hind*III/*Nco*I digested (Figure 5.12) and dephosphorylated pET-22b(+) vector. XL1-Blue transformants were observed on LBA agar plates for ligation mixtures containing gel-purified or QIAquick-purified pET-22b(+). Plasmids extracted from twelve colonies following overnight growth were analyzed by *Hind*III and *Nco*I digestion. As shown in Figure 5.13, the uncut plasmids had the expected size (> 6 kbp) (Lanes 2, 4, 6 in Figures

5.13A B) and the doubly digested plasmids yielded the expected hSOD1 insert at 750 bp (Lanes 3, 5 and 7 in Figures 5.13A,B), indicating that the XL1-Blue cells were transformed with the desired pET-hSOD1 construct.

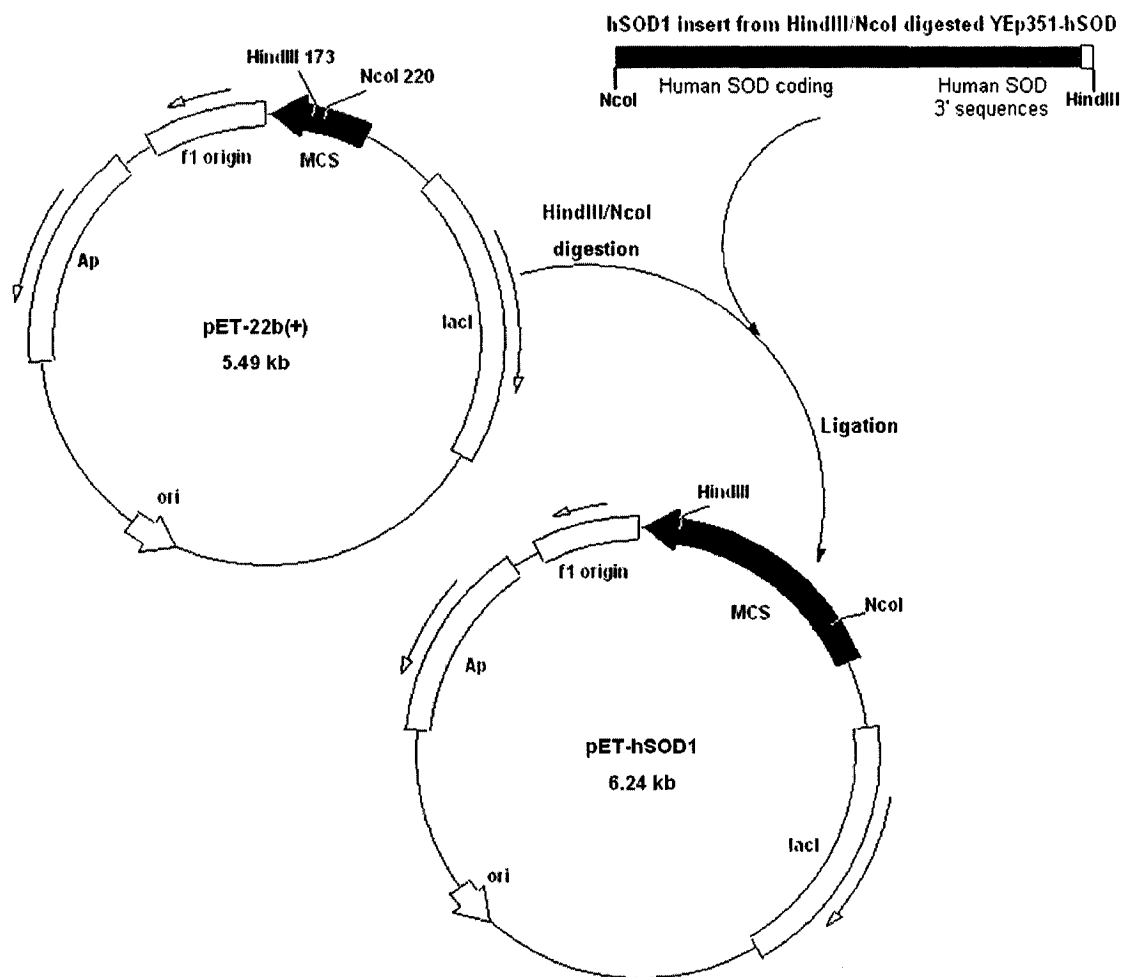


Figure 5.11 **Construction of pET-hSOD1 plasmid.** The hSOD1 insert was transferred from YEp351-hSOD1 to pET-22b(+) as described in Section 5.2.4.



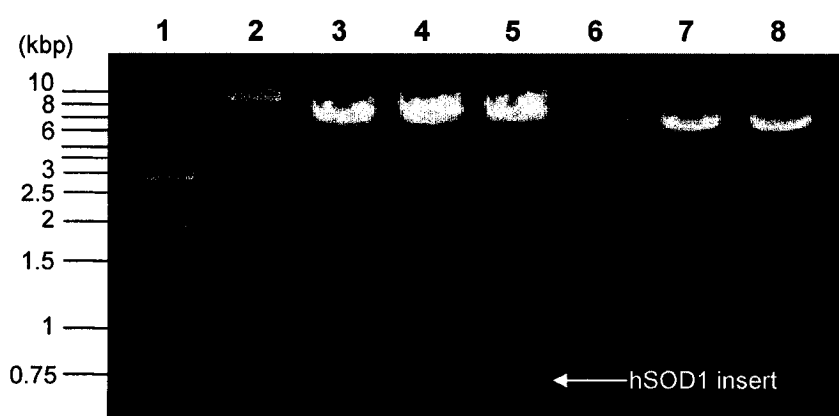


Fig 5.12 Restriction digestion analysis of the YEp351-hSOD1 and pET-22b(+) plasmids. Lane 1, 1 kb DNA Ladder; lane 2, uncut YEp351-hSOD1 (600 ng); lanes 3–5, YEp351-hSOD1 cut with *Hind*III and *Nco*I (600, 900, and 900 ng/lane); lane 6, uncut pET-22b(+) (650 ng) and lanes 7–8, pET-22b(+) cut with *Hind*III and *Nco*I (1000 ng/lane).

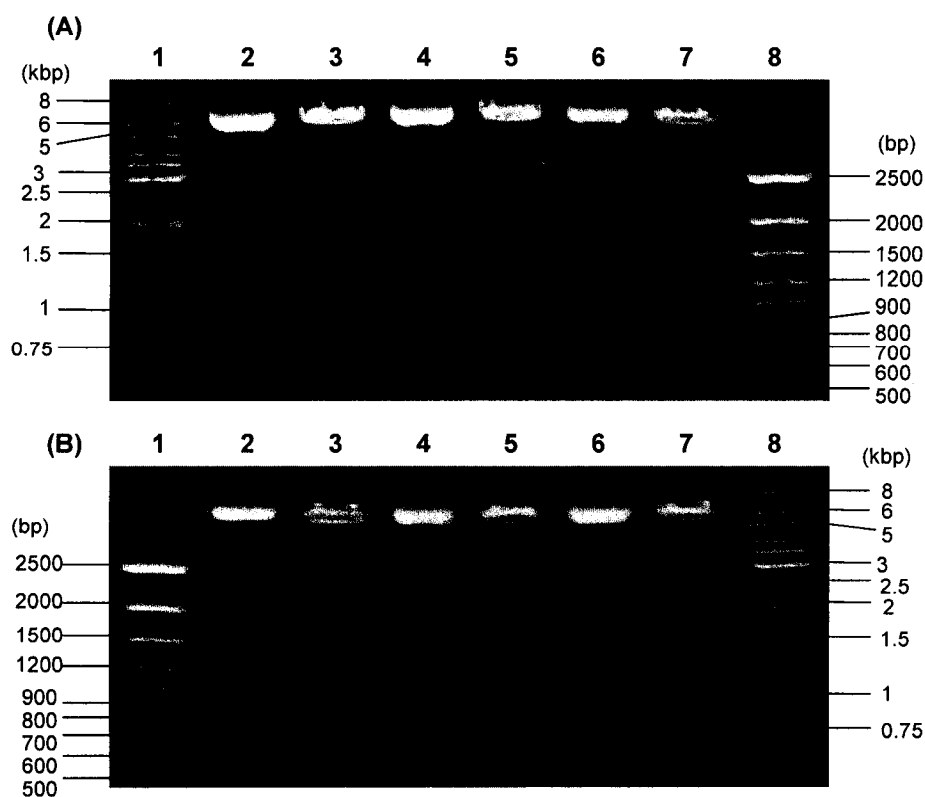


Fig 5.13 Restriction digestion analysis of the pET-hSOD1(wild type) vector. Lanes 2, 4 and 6 in (A) and (B), uncut pET-hSOD1; lanes 3, 5 and 7 in (A) and (B), pET-hSOD1 cut with *Hind*III and *Nco*I; lanes 1(A) and 8(B) 1 kb Ladders (Fermentas); lanes 1(B) and 8(A), 100 bp Ladders (Fermentas).

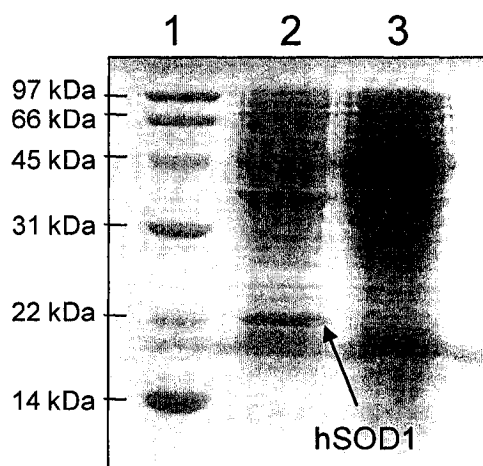


Fig 5.14 **SDS-PAGE (15%) analysis of hSOD1 expression in BL21(DE3) cells.** Lane 1, protein size markers; lane 2, cell-lysate supernatant following IPTG induction; lane 3, cell-lysate supernatant from uninduced cells. The cell-lysate supernatants were prepared as described in Section 5.2.6.2.

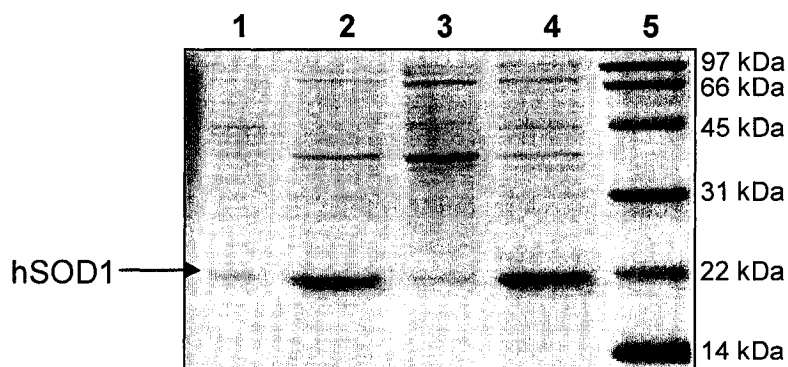


Fig 5.15 **SDS-PAGE (15%) analysis of hSOD1 localization in BL21(DE3) cells.** Lane 1, total cell protein extracted from 0.1 mg cells; lane 2, proteins in 62.5 µL of the culture growth medium; lane 3, proteins in the periplasmic fraction extracted from 0.33 mg cells; lane 4, proteins in cytoplasmic fraction extracted from 1.6 mg cells; lane 5, protein size markers. Cells were grown in 40 mL of LBA at 37°C, 250 rpm until  $OD_{600} = 0.84$ , 1 mM IPTG together with 200 µM  $Cu^{2+}$  and 50 µM  $Zn^{2+}$  were added into the culture followed by 4 h induction ( $OD_{600} = 2.23$ ), and 0.16 g cells were harvested from the 40-mL culture.

### 5.3.2.2 Expression of hSOD1 in BL21(DE3)

BL21(DE3) cells transformed with pET-hSOD1 were grown in 60 mL of LBA medium to  $OD_{600} = 1$ . A 30-mL aliquot of the culture was induced with IPTG and grown for additional 4 h ( $OD_{600} = 2.69$ ; 0.30 g cell harvest) while another 30-mL aliquot was grown under the same conditions without IPTG induction ( $OD_{600} = 3.67$ ; 0.23 g cell harvest). The hSOD1 band was observed by SDS-PAGE in the cell-lysate supernatant from the induced culture but not from the uninduced culture (Figure 5.14).

Since the pET-22b(+) vector targets proteins to the periplasmic space, the localization of hSOD1 in the host was examined. SDS-PAGE analysis revealed that hSOD1 was present in the growth medium (lane 2) and the cytoplasmic fraction (lane 4) but not in the periplasmic fraction (lane 3; Figure 5.15). The periplasm fraction was prepared from less cells than the cytoplasmic fraction (0.33 mg vs 1.6 mg), but the results, nonetheless, suggest that the target protein leaked from the periplasm into the medium. Furthermore, as the hSOD1 band obtained from 62.5  $\mu$ L of the culture growth medium (from a 40-mL culture) and from the cytoplasmic fraction of 1.6 mg cells (from 160 mg cells per 40-mL culture) were comparable (lane 2 vs 4, Figure 5.15), more hSOD1 must have been targeted to the periplasm than to the cytoplasm. Unfortunately, the sample used to visualize total cell proteins (lane 1, Figure 5.15) contained less protein than the other samples since only 0.1 mg of cells were analyzed.

### 5.3.2.3 Optimization hSOD1 expression in *E. coli*

IPTG was added at different  $OD_{600}$  values to establish the effect on hSOD1 leakage to the medium. Cultures were grown as indicated in Figure 5.16C, and the hSOD1 present in the cell-lysate supernatant from 0.4 mg cells and in 50  $\mu$ L of culture

medium was compared by SDS-PAGE. Induction with IPTG at  $OD_{600} \leq 1.4$  resulted in leakage of hSOD1 from the cells into the medium (lanes 2–4, Figure 5.16B) but negligible leakage was detected at  $OD_{600} \geq 2.3$  (lanes 5,6, Figure 5.16B). Hence, more hSOD1 was present in the cell-lysate supernatant of cultures induced at higher vs lower  $OD_{600}$  (Figure 5.16A).

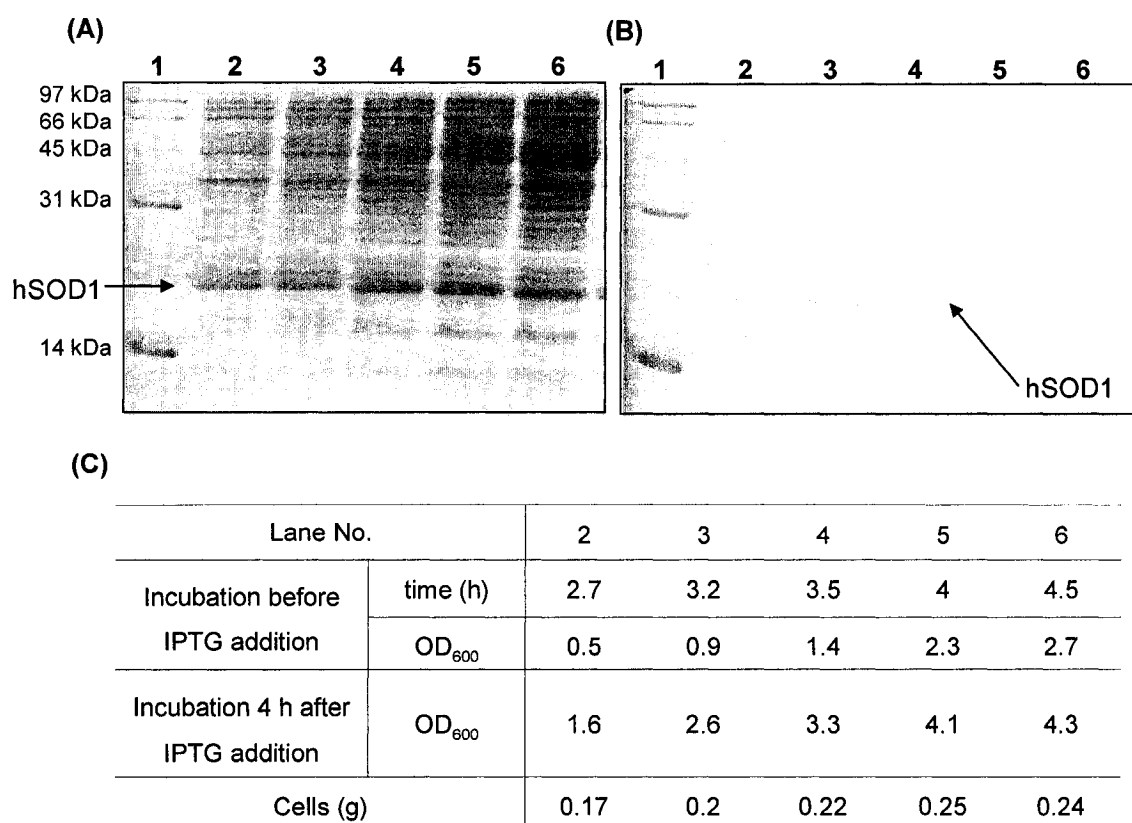


**Fig 5.16 SDS-PAGE (15%) analysis of hSOD1 in the (A) cell-lysate supernatants and (B) growth medium under (C) different BL21(DE3) growth conditions.** Lane 1, protein-size markers; lanes 2–6, samples from the cell cultures described in (C). (A) 0.4 mg cells/lane; (B) 50  $\mu$ L growth medium/lane. The cell cultures were grown in 25 mL LBA containing 500  $\mu$ M  $Cu^{2+}$  and 5  $\mu$ M  $Zn^{2+}$  at 37°C, 250 rpm for the times and  $OD_{600}$  values indicated in C; 1 mM IPTG was added followed by 4-h induction, and the cells harvested at the final  $OD_{600}$  values listed in C. The cell-lysate supernatants were prepared as described in Section 5.2.6.2.

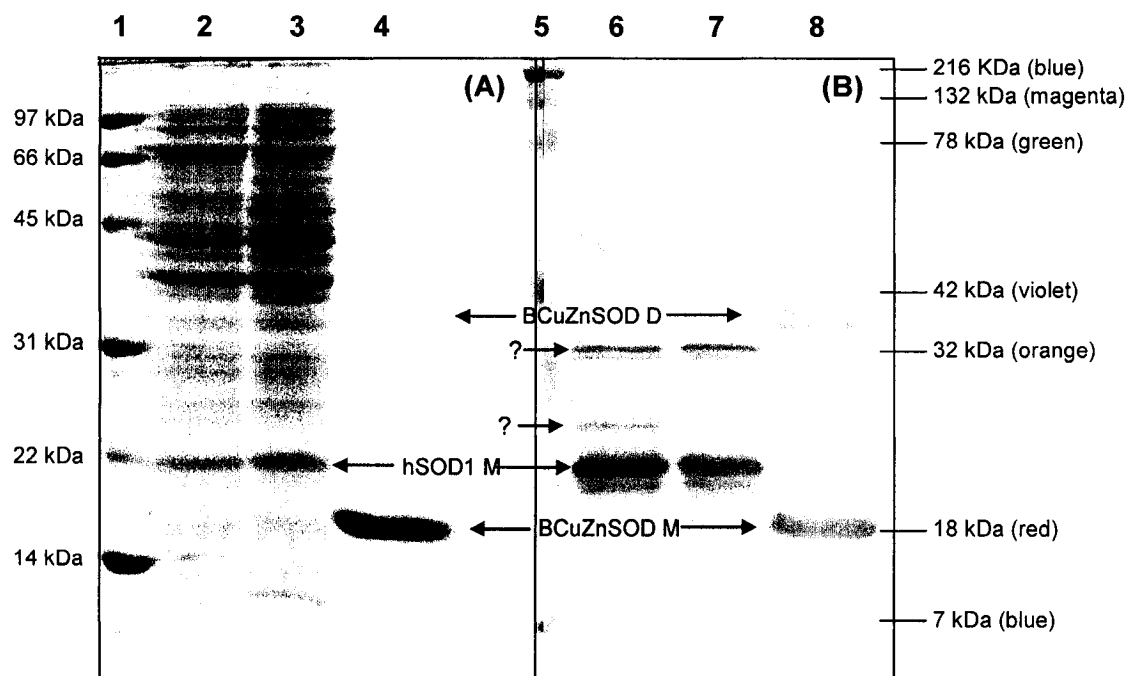


Figure 5.17 (A) SDS-PAGE (12%) and (B) Western blot (12%) analysis of hSOD1 expression in BL21(DE3) cells. Lane 1, protein-size markers; lanes 4 and 8, BCuZnSOD; lane 5, colored protein-size markers; lanes 2 and 6: sample from lane 3 of Figure 5.16A; lanes 3 and 7: sample from lane 5 of Figure 5.16A.

Expression of hSOD1 in the cell-lysate supernatants from lanes 3 and 5 (Figure 5.16A) was also compared using Western blotting. The hSOD1 monomer band at 22 kDa on the SDS gel (lanes 2,3; Figure 5.17A) is also seen on the PVDF membrane (lanes 6,7; Figure 5.17B) confirming that hSOD1 was expressed in BL21(DE3). Bands present at > 22 and ~32 kDa (lanes 6,7; Figure 5.17B) are not likely the hSOD1 dimer since this is generally visualized close to the 45-kDa protein-size marker (251). Both the BCuZnSOD monomer band (M) at ~15 kDa and two faint dimer bands (D) above 31 kDa on the SDS gel (lane 4; Figure 5.17A) are clearly seen on the PVDF membrane (lane 8; Figure 5.17B). Unfortunately, the yield of hSOD1 expressed in BL21(DE3) cannot be

estimated from Figure 5.17B since the amount of BCuZnSOD added to the gel was not determined.

#### 5.4 Discussion

A *Saccharomyces cerevisiae* *sod1<sup>-</sup>* strain in the EGY118 genetic background (*MAT $\alpha$* , *leu2-3, 11* *his3 $\Delta$ trp1-239* *ura3-52* *sod1 $\Delta$ A::LEU2*) was used previously as an expression host for hSOD1 and its mutants (243, 245). The reported SOD activity (assayed by inhibition of 6-hydroxydopamine autoxidation at pH 7.4) (252) in the soluble protein extract prepared from EGY118 cells grown to late logarithmic phase in liquid YPD medium was  $1390 \pm 0.13$  units/mg protein (243). This value is 100 times higher than the SOD activity found in our crude extracts (Table 5.1) indicating that hSOD1 is not highly overexpressed in the BY4742 strain in YPD medium (without selection) as revealed by SDS-PAGE analysis of the cell lysates (Figure 5.3A). Also, copper is not effectively taken up by hSOD1 in the BY4742 strain (Figures 5.8A and 5.9). Thus, to achieve higher overexpression of active hSOD1 and its mutants, the *sod1<sup>-</sup>* EGY118 strain (243, 245) may be a better host.

Protein precipitation by ammonia sulfate, anion-exchange (DEAE-cellulose, DEAE Sephadex A-50, Sepharose CL-6B, and DE-52), gel filtration (Sephadex G-75, Fractogel 55), hydrophobic interaction (fast-flow phenyl-Sepharose) and immobilized metal-ion affinity ( $\text{Cu}^{\text{II}}$ -IDA-Agarose) chromatography have been used in the purification of recombinant hSOD1 from yeast and *E. coli* (245, 249, 253-255). A combination of ammonium sulfate precipitation (Figure 5.3), Sephadex G-75 gel-filtration (Figure 5.5A) and DEAE-Sepharcel (Figures 5.5B and C) or DEAE-Sepharose CL-6B (Figure 5.5D)

anion-exchange chromatography were used here to purify hSOD1 from yeast. Better separation was obtained on DEAE-Sepharose CL-6B (Figure 5.5D) so this resin is recommended for hSOD1 purification. DEAE-Sephacel did not adsorb hSOD1 effectively (Figures 5.4B and C).

The SOD specific activity increased following each purification step (Table 5.1). However, minor contaminant protein bands are still visible on the gels after the anion-exchange purification step (Figures 5.5B–D). In an early report (249), highly purified hSOD1 was obtained from *E. coli* strain A1645 by running the sample twice on a DE-52 column. In another report, a fast-flow phenyl-Sepharose hydrophobic interaction column was used to purify hSOD1 from yeast (245). Since highly pure hSOD1 was not obtained from the DEAE-Sepharose CL-6B column (Figure 5.5D), these alternative methods should be considered in further work.

**Table 5.2 Literature values for enzyme activity and metal content of hSOD1 preparations<sup>a</sup>**

Medium	Activity units/mg	mol/subunit <sup>e</sup>		Ref
		Cu	Zn	
Standard <sup>b</sup>	167	0.07	1.62	(249)
+metals <sup>c</sup>	2730	0.88	0.90	
Reconstituted hSOD1 <sup>d</sup>	2931	0.81	0.88	

<sup>a</sup>Values determined for highly purified hSOD1 preparations. <sup>b</sup>hSOD1 prepared from *E. coli* grown on standard medium. <sup>c</sup>hSOD1 prepared from *E. coli* grown on medium supplemented with 2 ppm of Zn<sup>2+</sup> and 200 ppm of Cu<sup>2+</sup>. <sup>d</sup>Reconstituted hSOD1 prepared by simultaneous addition of Cu<sup>2+</sup> and Zn<sup>2+</sup> to the highly purified apoenzyme. <sup>e</sup>Metal content determined by atomic absorption.

Why is the SOD activity much lower in the yeast host used here than that reported (243). Hartman *et al.* found a significant difference between the SOD activity and metal content of hSOD1 purified from *E. coli* grown on standard medium vs medium supplemented with 2 ppm of  $\text{Zn}^{2+}$  and 200 ppm of  $\text{Cu}^{2+}$  (Table 5.2) (249). Our results, including the UV absorption spectrum of purified hSOD1 after reconstitution (Figure 5.8A), the colorimetric determination of copper in the purified enzyme (19.6  $\mu\text{M}$  copper per 51.5  $\mu\text{M}$  hSOD1 dimer, Figure 5.9), and the enzyme activity measured throughout the purification (Table 5.1) indicate that the enzyme was not fully loaded with copper. In contrast, high SOD activity was detected in the cell-lysate supernatants from EGY118 yeast cells (243) and grown on YEPD or SD medium without additional copper (243, 245, 253, 256). Hence, the reasons for the poor copper binding properties of hSOD1 in the BY4742 host need to be further investigated. Also, the poor expression of hSOD1 in yeast (Figure 5.3A, lanes 3, 4, and 6) may be due to the use of YPD medium without selection in Section 5.3.1.2. Vectors like YEpl351 containing the 2 $\mu$  origin of replication are often expelled by yeast during growth without selection pressure. This oversight should be corrected in future attempts to express hSOD1 in yeast.

Since the yield of hSOD1 expressed in yeast was < 10 mg/L, overexpression of the enzyme in *E. coli* was investigated. Successful expression of human and yeast CuZnSOD and their mutants in *E. coli* has been reported previously (249, 253-256). For example, Nishida *et al.* reported that the G85R and G93A mutants of yeast CuZnSOD cytoplasmically expressed from the pET-3d plasmid in *E. coli* strain BL21(DE3) yielded 5.0 mg of pure protein per liter of culture (253). Hartman *et al.* constructed the vector



pSOD $\beta$ 1T11, and transformation of *E. coli* strain A1645 with this vector resulted in 10 mg CuZnSOD per litre (249).

Shi *et al.* expressed hSOD1 from the pET-22b(+) vector in BL21(DE3) cells and hSOD1 corresponded to 30% of the total soluble bacterial protein (255). Based on this report, the hSOD1 insert in YEp351-hSOD1 located between *Nco*I and *Hind*III restriction sites was inserted into pET-22b(+) to yield pET-hSOD1(wild type) (Figures 5.12 and 5.13), and the enzyme was expressed under the induction of IPTG in *E. coli* strain BL21(DE3), (Figure 5.14). pET-22b(+) carries an *N*-terminal *pelB* signal sequence for periplasmic localization to facilitate protein purification (257, 258). However, hSOD1 was detected in the growth medium and in the cytoplasmic fractions, but it did not concentrate in the periplasmic space as expected (Figure 5.15). Leakage from the periplasm into the culture medium suggests damage of the cell envelope (257), and this appeared to be greater in samples with  $OD_{600} \leq 1.4$  and less in samples with  $OD_{600} \geq 2.3$  (Figures 5.16B,C).

hSOD1 was well expressed from pET-hSOD1 in *E. coli* strain BL21(DE3) (Figure 5.17). Thus, optimization of hSOD1 targetting to the periplasmic space should be investigated. Also, the SOD activity in the cell-lysate supernatant as well as copper and zinc uptake by hSOD1 in BL21(DE3) should be further studied. The purification procedure could be simplified by heat precipitation of bacterial proteins (246) combined with immobilized metal-ion affinity chromatography (255). Interaction of chelators with the active-site copper of BCuZnSOD was confirmed in Chapters 2 and 3, but it is unclear whether Arg141 (Arg143 in hSOD1) is involved in chelator binding. Production of

highly purified recombinant hSOD1 and mutants such as R143E will help answer this unresolved question.

#### **5.4 Acknowledgements**

We thank Dr. P. John Hart (University of Texas Health Science Center) for plasmids YEp351-hSOD1 (wild type, R143A, R143E, R143I, and R143K); and Dr. Vladimir Titorenko (Concordia University) for the wild-type and *sod1<sup>-</sup>* BY4742 yeast strains.

### **Appendix 3.0 DNA sequences of human CuZnSOD (wild type, R143A, R143E, R143I and R143K) inserts in the YEp351 and pET-22b(+) plasmids**

*E. coli* strain XL1-Blue transformed with YEp351-hSOD1 (wild type and its four Arg143 mutants) and with pET-hSOD1(wild type) were sent to Bio S&T (Montreal) to confirm the sequence of each insert. The sequencing data given below indicate that all the hSOD1 inserts, which are in bold font, possess the expected amino acid sequence. The DNA codons and the corresponding single-letter amino acid code for residue 143 are in bold underlined font.

#### **A3.1 YEp351-hSOD1(wild type)**

##### DNA Sequence: Forward

```
TTCACACAGGAAACAGCTATGACATGATTACGAATTCGAGCTCGGTACCCGGGGATCCCCATTGGCATGAT
GCGAAATTGGACGTAAGCATCTCTGAAGTGCAGCCGATTGGACGTGCGACTCACCCACTCAGGACATGATC
TCAGTAGCGGGTTCGATAAGGCGATGACAGCGCAAATGCCGCTTACTGGAAGTACAGAACCCGCTCCCTTA
GGGGCACCCACCCAGCACGCCGGGGGGTTAAACCGGTGTGTGCGAATTAGTAAGCGGACATCCCTTCCGC
TGGGCTCGCCATCGCAGATATATATATAAGAAGATGGTTTTGGGCAAATGTTTAGCTGTAACTATGTTGCG
GAAAAACAGGCAAGAAAGCAATCGCGCAAACAAATAAAACATAATTAATTTACCATGGCGACGAAGGCCGT
GTGCGTGCTGAAGGGCGACGGCCAGTGCAGGGCATCATCAATTCGAGCAGAAGGAAAGTAATGGACCAG
TGAAGGTGTGGGGAAGCATTAAAGGACTGACTGAAGGCCTGCATGGATTCCATGTTTCATGAGTTTGGAGAT
AATACAGCAGGCTGTACCAGTGCAGGTCCTCACTTTAATCCTCTATCCAGAAAACACGGTGGGCCAAAGGA
TGAAGAGAGGCATGTTGGAGACTTGGGCAATGTGACTGCTGACAAAGATGGTGTGGCCGATGTGTCTATTG
AAGATTCTGTGATCTCACTCTCAGGAGACCATTGCATCATTGGCCGCACACTGGTGGTCCATGAAAAA
```

### DNA Sequence: Reverse

AAACGACGGCCAGTGCCAAGCTTGCATGCCTGCAGGTCGACTCTAGATGGCAAATACAGGTCATTGAAAC  
AGACATTTTAACTGAGTTTTATAAACTATACAAATCTTCCAAGTGATCATAAATCAGTTTCTCACTACAG  
GTACTTTAAAGCAACTCTGAAAAAGTCACACAATTACACTTTTAAGATTACAGTGTTTAATGTTTATCAGG  
ATACATTTCTACAGCTAGCAGGATAACAGATGAGTTAAGGGGCCTCAGACTACATCCAAGGGAATGTTTAT  
TGGGCGATCCCAATTACACCACAAGCCAAACGACTTCCAGCGTTTCCTGTCTTTGTACTTTCTTCATTTCC  
ACCTTTGCCCCAAGTCATCTGCTTTTTTCATGGACCACAGTGTGCGGCCAATGATGCAATGGTCTCCTGAGA  
GTGAGATCACAGAATCTTCAATAGACACATCGGCCACACCATCTTTGTCAGCAGTCACATTGCCCAAGTCT  
CCAACATGCCTCTCTTCATCCTTTGGCCCACCGTGTTTTCTGGATAGAGGATTAAAGTGAGGACCTGCACT  
GGTACAGCCTGCTGTATTATCTCCAACTCATGAACATGGAATCCATGCAGGCCTTCAGTCAGTCCTTTAA  
TGCTTCCCCACACCTTCACTGGTCCATTACTTTCTTCTGCTCGAAATTGATGATGCCCTGCACTGGGCCG  
TCGCCCTTCAGCACGCACACGGCCTTCGTGCGCATGGTAAATTAATTATGTTTTATTTGTTT

### YEp351-hSOD1(WT): Total DNA sequence

TTACACAGGAAACAGCTATGACATGATTACGAATTCGAGCTCGGTACCCGGGGATCCCCATTGGCATGAT  
GCGAAATTGGACGTAAGCATCTCTGAAGTGCAGCCGATTGGACGTGCGACTCACCCACTCAGGACATGATC  
TCAGTAGCGGGTTCGATAAGGCGATGACAGCGCAAATGCCGCTTACTGGAAGTACAGAACCCGCTCCCTTA  
GGGGCACCCACCCCAGCACGCCGGGGGGTTAAACCGGTGTGTGCGAATTAGTAAGCGGACATCCCTTCCGC  
TGGGCTCGCCATCGCAGATATATATATAAGAAGATGGTTTTGGGCAAATGTTTAGCTGTAACATGTTGCG  
GAAAAACAGGCAAGAAAGCAATCGCGCAAACAAATAAAACATAATTAATTTACC**ATGGCGACGAAGGCCGT**  
**GTGCGTGCTGAAGGGCGACGGCCAGTGCAGGGCATCATCAATTT**CGAGCAGAAGGAAAGTAATGGACCAG  
**TGAAGGTGTGGGGAAGCATTAAAGGACTGACTGAAGGCCTGCATGGATTCCATGTT**CATGAGTTTGGAGAT  
**AATACAGCAGGCTGTACCAGTGCAGGTCCTCACTTTAATCCTCTATCCAGAAAACACGGTGGGCCAAAGGA**  
**TGAAGAGAGGCATGTTGGAGACTTGGGCAATGTGACTGCTGACAAAGATGGTGTGGCCGATGTGTCTATTG**  
**AAGATTCTGTGATCTCACTCTCAGGAGACCATTGCATCATTGGCCGCACACTGGTGGTCCATGAAAAAGCA**  
**GATGACTTGGGCAAAGGTGGAATGAAGAAAGTACAAAGACAGGAAACGCTGGAAGT**CGTTTGGCTTGTGG  
**TGTAATTGGGATCGCCCAATAAACATTCCCTTGGATGTAGTCTGAGGCCCTTAACTCATCTGTTATCCTG**  
CTAGCTGTAGAAATGTATCCTGATAAACATTAAACACTGTAATCTTAAAGTGTAATTGTGTGACTTTTTTC  
AGAGTTGCTTTAAAGTACCTGTAGTGAGAACTGATTTATGATCACTTGGAAGATTTGTATAGTTTTATAA

AACTCAGTTAAAAATGTCTGTTTCAATGACCTGTATTTTGCCATCTAGAGTCGACCTGCAGGCATGCAAGCT  
TGGCACTGGCCGTCGTTT

### **Amino acid sequence of wild-type hSOD1: 153 aa**

1 ATKAVCVLKG DGPVQGIINF EQKESNGPVK VWGSIKGLTE GLHGFHVHEF GDNTAGCTSA  
61 GPHFNPLSRK HGGPKDEERH VGD LGNVTAD KDG VADVSIE DSVISLSGDH CIIGRTLTVH  
121 EKADDLGKGG NEESTKTGNA GSRLACGVIG IAQ

### **A3.2 YEp351-hSOD1(R143E)**

#### **DNA Sequence: Forward**

GATTACGAATTCGAGCTCGGTACCCGGGGATCCCCATTGGCATGATGCGAAATTGGACGTAAGCATCTCTG  
AAGTGCAGCCGATTGGACGTGCGACTCACCACCTCAGGACATGATCTCAGTAGCGGGTTCGATAAGGCGAT  
GACAGCGCAAATGCCGCTTACTGGAAGTACAGAACCCGCTCCCTTAGGGGCACCCACCCAGCACGCCGGG  
GGGTAAACCGGTGTGTCGGAATTAGTAAGCGGACATCCCTTCCGCTGGGCTCGCCATCGCAGATATATAT  
ATAAGAAGATGGTTTTGGGCAAATGTTTAGCTGTAACATATGTTGCGGAAAAACAGGCAAGAAAGCAATCGC  
GCAAACAAATAAAACATAATTAATTTACCATGGCGACGAAGGCCGTGTGCGTGCTGAAGGGCGACGGCCCA  
GTGCAGGGCATCATCAATTTTCGAGCAGAAGGAAAGTAATGGACCAGTGAAGGTGTGGGGAAGCATTAAAGG  
ACTGACTGAAGGCCTGCATGGATTCCATGTTTCATGAGTTTGGAGATAATACAGCAGGCTGTACCAGTGCAG  
GTCCTCACTTTAATCCTCTATCCAGAAAACACGGTGGGCCAAAGGATGAAGAGAGG

#### **DNA Sequence: Reverse**

GTAAACAGCGGCCAGTGCAAGCTTGCATGCCTGCAGGTCGACTCTAGATGGCAAATACAGGTCATTGAAA  
CAGACATTTTAACTGAGTTTTATAAACTATACAAATCTTCCAAGTGATCATAAATCAGTTTCTCACTACA  
GGTACTTTAAAGCAACTCTGAAAAAGTCACACAATTACACTTTTAAGATTACAGTGTTAATGTTTATCAG  
GATACATTTCTACAGCTAGCAGGATAACAGATGAGTTAAGGGGCCTCAGACTACATCCAAGGGAATGTTTA  
TTGGGCGATCCCAATTACACCACAAGCCAACCTCACTTCCAGCGTTTCCTGTCTTTGTACTTTCTTCATTTT  
CACCTTTGCCCAAGTCATCTGCTTTTTTCATGGACCACAGTGTGCGGCAATGATGCAATGGTCTCCTGAG  
AGTGAGATCACAGAATCTTCAATAGACACATCGGCCACACCATCTTTGTCAGCAGTCACATTGCCCAAGTC

TCCAACATGCCTCTCTTCATCCTTTGGCCACCGTGTTTTCTGGATAGAGGATTAAAGTGAGGACCTGCAC  
TGGTACAGCCTGCTGTATTATCTCCAAACTCATGAACATGGAATCCATGCAGGCCTTCAG

### YEp351-hSOD1(R143E): Total DNA sequence

GATTACGAATTCGAGCTCGGTACCCGGGGATCCCCATTGGCATGATGCGAAATTGGACGTAAGCATCTCTG  
AAGTGCAGCCGATTGGACGTGCGACTCACCCACTCAGGACATGATCTCAGTAGCGGGTTCGATAAGGCGAT  
GACAGCGCAAATGCCGCTTACTGGAAGTACAGAACCCGCTCCCTTAGGGGCACCCACCCCAGCACGCCGGG  
GGGTAAACCGGTGTGTGCGGAATTAGTAAGCGGACATCCCTTCCGCTGGGCTCGCCATCGCAGATATATAT  
ATAAGAAGATGGTTTTGGGCAAATGTTTAGCTGTAAGTATGTTGCGGAAAAACAGGCAAGAAAGCAATCGC  
GCAAACAAATAAAACATAATTAATTTACCATGGCGACGAAGGCCGTGTGCGTGCTGAAGGGCGACGGCCCA  
**GTGCAGGGCATCATCAATTTGAGCAGAAGGAAAGTAATGGACCAGTGAAGGTGTGGGGAAGCATTAAGG**  
**ACTGACTGAAGGCCTGCATGGATTCCATGTTTCATGAGTTTGGAGATAATACAGCAGGCTGTACCAGTGCAG**  
**GTCCTCACTTTAATCCTCTATCCAGAAAACACGGTGGGCCAAAGGATGAAGAGAGGCATGTTGGAGACTTG**  
**GGCAATGTGACTGCTGACAAAGATGGTGTGGCCGATGTGTCTATTGAAGATTCTGTGATCTCACTCTCAGG**  
**AGACCATTGCATCATTGGCCGCACACTGGTGGTCCATGAAAAAGCAGATGACTTGGGCAAAGGTGGAAATG**  
**AAGAAAGTACAAAGACAGGAAACGCTGGAAGT****GAGTTGGCTTGTGGTGTAATTGGGATCGCCCAATAAACA**  
TTCCCTTGGATGTAGTCTGAGGCCCTTAAGTCACTCTGTTATCCTGCTAGCTGTAGAAATGTATCCTGATA  
AACATTAAACACTGTAATCTTAAAAGTGTAATTGTGTGACTTTTTTCAGAGTTGCTTTAAAGTACCTGTAGT  
GAGAACTGATTTATGATCACTTGAAGATTTGTATAGTTTTATAAACTCAGTTAAAATGTCTGTTTCAA  
TGACCTGTATTTTGCCATCTAGAGTCGACCTGCAGGCATGCAAGCTTGCACTGGCCGCTGTTTAC

### Amino acid sequence of hSOD1(R143E): 153 aa

1 ATKAVCVLKG DGPVQGIINF EQKESNGPVK VWGSIKGLTE GLHGFHVHEF GDNTAGCTSA  
61 GPHFNPLSRK HGGPKDEERH VGD LGNVTAD KGVADVSI E DSVISLSGDH CIIGRTL VVH  
121 EKADDLGKGG NEESTKTGNA GSELACGVIG IAQ

### **A3.3 YEp351-hSOD1(R143K)**

#### DNA Sequence: Forward

CAGGAAACAGCTATGACATGATTACGAATTCGAGCTCGGTACCCGGGGATCCCCATTGGCATGATGCGAAA

TTGGACGTAAGCATCTCTGAAGTGCAGCCGATTGGACGTGCGACTCACCCACTCAGGACATGATCTCAGTA  
GCGGGTTCGATAAGGCGATGACAGCGCAAATGCCGCTTACTGGAAGTACAGAACCCGCTCCCTTAGGGGCA  
CCCACCCCAGCACGCCGGGGGGTTAAACCGGTGTGTGCGAATTAGTAAGCGGACATCCCTTCCGCTGGGCT  
CGCCATCGCAGATATATATATAAGAAGATGGTTTTGGGCAAATGTTTAGCTGTAAGTATGTTGCGGAAAAA  
CAGGCAAGAAAGCAATCGCGCAAACAAATAAAACATAATTAATTTACCATGGCGACGAAGGCCGTGTGCGT  
GCTGAAGGGCGACGGCCAGTGCAGGGCATCATCAATTTGAGCAGAAGGAAAGTAATGGACCAGTGAAGG  
TGTGGGGAAGCATTAAAGGACTGACTGAAGGCCTGCATGGATTCCATGTTTCATGAGTTTGGAGATAATACA  
GCAGGCTGTACCAGTGCAGGTCCTCACTTTAATCCTCTATCCAGAAAACACGGTGGGCCAAAGG

**DNA Sequence: Reverse**

TGTAAACAGCGGCCAGTGCAGCTTGCATGCCTGCAGGTCGACTCTAGATGGCAAATACAGGTCATTGAA  
ACAGACATTTTAACTGAGTTTATAAACTATACAAATCTTCCAAGTGATCATAAATCAGTTTCTCACTAC  
AGGTACTTTAAAGCAACTCTGAAAAAGTCACACAATTACACTTTTAAGATTACAGTGTTTAATGTTTATCA  
GGATACATTTCTACAGCTAGCAGGATAACAGATGAGTTAAGGGGCCTCAGACTACATCCAAGGGAATGTTT  
ATTGGGCGATCCCAATTACACCACAAGCCAACTTACTTCCAGCGTTTCCTGTCTTTGTACTTTCTTCATTT  
CCACCTTTGCCCAAGTCATCTGCTTTTTTCATGGACCACCAGTGTGCGGCCAATGATGCAATGGTCTCCTGA  
GAGTGAGATCACAGAATCTTCAATAGACACATCGGCCACACCATCTTTGTCAGCAGTCACATTGCCCAAGT  
CTCCAACATGCCTCTCTTCATCCTTTGGCCACCGTGTTTTCTGGATAGAGGATTAAAGTGAGGACCTGCA  
CTGGTACAGCCTGCTGTATTATCTCCAACTCATGAACATGGAATCCATGCAGG

**YEp351-hSOD1(R143K): Total DNA sequence**

CAGGAAACAGCTATGACATGATTACGAATTCGAGCTCGGTACCCGGGGATCCCCATTGGCATGATG  
CGAAATTGGACGTAAGCATCTCTGAAGTGCAGCCGATTGGACGTGCGACTCACCCACTCAGGACAT  
GATCTCAGTAGCGGGTTCGATAAGGCGATGACAGCGCAAATGCCGCTTACTGGAAGTACAGAACCC  
GCTCCCTTAGGGGCACCCACCCCAGCACGCCGGGGGGTTAAACCGGTGTGTGCGAATTAGTAAGCG  
GACATCCCTTCCGCTGGGCTCGCCATCGCAGATATATATATAAGAAGATGGTTTTGGGCAAATGTT  
TAGCTGTAAGTATGTTGCGGAAAAACAGGCAAGAAAGCAATCGCGCAAACAAATAAAACATAATTA  
ATTTACCATGGCGACGAAGGCCGTGTGCGTGCTGAAGGGCGACGGCCAGTGCAGGGCATCATCAA  
TTTCGAGCAGAAGGAAAGTAATGGACCAGTGAAGGTGTGGGGAAGCATTAAAGGACTGACTGAAGG

CCTGCATGGATTCCATGTTTCATGAGTTTGGAGATAATACAGCAGGCTGTACCAGTGCAGGTCCTCA  
 CTTTAATCCTCTATCCAGAAAACACGGTGGGCCAAAGGATGAAGAGAGGCATGTTGGAGACTTGGG  
 CAATGTGACTGCTGACAAAGATGGTGTGGCCGATGTGTCTATTGAAGATTCTGTGATCTCACTCTC  
 AGGAGACCATTGCATCATTGGCCGCACACTGGTGGTCCATGAAAAAGCAGATGACTTGGGCAAAGG  
 TGGAAATGAAGAAAAGTACAAAGACAGGAAACGCTGGAAGTAAGTTGGCTTGTGGTGTAAATTGGGAT  
 CGCCCAATAAACATTCCCTTGGATGTAGTCTGAGGCCCTTAACTCATCTGTTATCCTGCTAGCTG  
 TAGAAATGTATCCTGATAAACATTAAACACTGTAATCTTAAAAGTGAATTGTGTGACTTTTTCAG  
 AGTTGCTTTAAAGTACCTGTAGTGAGAACTGATTTATGATCACTTGAAGATTTGTATAGTTTTA  
 TAAAACTCAGTTAAATGTCTGTTTCAATGACCTGTATTTTGCCATCTAGAGTCGACCTGCAGGCA  
 TGCAAGCTTGCACTGGCCGCTGTTTACA

#### Amino acid sequence of hSOD1 (R143K): 153 aa

1 ATKAVCVLKG DGPVQGIINF EQKESNGPVK VWGSIKGLTE GLHGFHVHEF GDNTAGCTSA  
 61 GPHFNPLSRK HGGPKDEERH VGD LGNV TAD KDG VADV SIE DSVISLSGDH CIIGRTL VVH  
 121 EKADDLGKGG NEESTKTGNA GSKLACGVIG IAQ

### **A3.4 YEp351-hSOD1(R143A)**

#### DNA Sequence: Forward

CAGGAAACAGCTATGACATGATTACGAATTCGAGCTCGGTACCCGGGGATCCCCATTGGCATGATGCGAAA  
 TTGGACGTAAGCATCTCTGAAGTGCAGCCGATTGGACGTGCGACTCACCCACTCAGGACATGATCTCAGTA  
 GCGGGTTTCGATAAGGCGATGACAGCGCAAATGCCGCTTACTGGAAGTACAGAACCCGCTCCCTTAGGGGCA  
 CCcACCCACGACGCCGGGGGGTTAAACCGGTGTGTGCGGAATTAGTAAGCGGACATCCCTTCCGCTGGGCT  
 CGCCATCGCAGATATATATATAAGAAGATGGTTTTGGGCAAATGTTTAGCTGTAACATATGTTGCGGAAAAA  
 CAGGCAAGAAAGCAATCGCGCAAACAAATAAAACATAATTAATTTACCATGGCGACGAAGGCCGTGTGCGT  
 GCTGAAGGGCGACGGCCAGTGCAGGGCATCATCAATTTGAGCAGAAGGAAAAGTAATGGACCAGTGAAGG  
 TGTGGGGAAGCATTAAAGGACTGACTGAAGGCCTGCATGGATTCCATGTTTCATGAGTTTGGAGATAATACA  
 GCAGGCTGTACCAGTGCAGGTCCTCACTTTAATCCTCTATCCAGAAAACACGGTGGG

#### DNA Sequence: Reverse



GTGTAAACAGCGGCCAGTGCAAGCTTGCATGCCTGCAGGTCGACTCTAGATGGCAAAATACAGGTCATTGA  
AACAGACATTTTAACTGAGTTTATAAACTATACAAATCTTCCAAGTGATCATAAATCAGTTTCTCACTA  
CAGGTACTTTAAAGCAACTCTGAAAAAGTCACACAATTACACTTTTAAGATTACAGTGTTAATGTTTATC  
AGGATACATTTCTACAGCTAGCAGGATAACAGATGAGTTAAGGGGCCTCAGACTACATCCAAGGGAATGTT  
TATTGGGCGATCCCAATTACACCACAAGCCAAAGCACTTCCAGCGTTTCCTGTCTTTGTACTTTCTTCATT  
TCCACCTTTGCCCCAAGTCATCTGCTTTTTCATGGACCACCAGTGTCGGCCAATGATGCAATGGTCTCCTG  
AGAGTGAGATCACAGAATCTTCAATAGACACATCGGCCACACCATCTTGTGTCAGCAGTCACATTGCCCAAG  
TCTCCAACATGCCTCTCTTCATCCTTTGGCCCACCGTGTTTCTGGATAGAGGATTAAAGTGAGGACCTGC  
ACTGGTACAGCCTGCTGTATTATCTCCAAACTCATGAACATGGAATCCATGCAGGCCTTCAGTCAGTCCTT  
TAA

#### YEp351-hSOD1(R143A): Total DNA sequence

CAGGAAACAGCTATGACATGATTACGAATTCGAGCTCGGTACCCGGGGATCCCCATTGGCATGATGCGAAA  
TTGGACGTAAGCATCTCTGAAGTGCAGCCGATTGGACGTGCGACTCACCCTCAGGACATGATCTCAGTA  
GCGGGTTCGATAAGGCGATGACAGCGCAAATGCCGCTTACTGGAAGTACAGAACCCGCTCCCTTAGGGGCA  
CCCACCCAGCACGCCGGGGGGTTAAACCGGTGTGTGCGAATTAGTAAGCGGACATCCCTTCCGCTGGGCT  
CGCCATCGCAGATATATATATAAGAAGATGGTTTTGGGCAAATGTTTAGCTGTAACATATGTTGCGGAAAA  
CAGGCAAGAAAGCAATCGCGCAAACAAATAAAACATAATTAATTTACCATGGCGACGAAGGCCGTGTGCGT  
GCTGAAGGGCGACGGCCCAGTGCAGGGCATCATCAATTTGAGCAGAAGGAAAGTAATGGACCAGTGAAGG  
TGTGGGAAGCATTAAAGGACTGACTGAAGGCCTGCATGGATTCCATGTTTCATGAGTTTGGAGATAATACA  
GCAGGCTGTACCAGTGCAGGTCTCACTTTAATCCTCTATCCAGAAAACACGGTGGGCCAAAGGATGAAGA  
GAGGCATGTTGGAGACTTGGGCAATGTGACTGCTGACAAAGATGGTGTGGCCGATGTGTCTATTGAAGATT  
CTGTGATCTCACTCTCAGGAGACCATTGCATCATTTGGCCGCACACTGGTGGTCCATGAAAAGCAGATGAC  
TTGGGCAAAGGTGGAATGAAGAAAGTACAAAGACAGGAAACGCTGGAAGTGC<sup>1</sup>TTGGCTTGTGGTGTAAAT  
TGGGATCGCCCAATAAACATTCCCTTGGATGTAGTCTGAGGCCCCCTTAACATCATCTGTTATCCTGCTAGCT  
GTAGAAATGTATCCTGATAAACATTAAACACTGTAATCTTAAAAGTGAATTGTGTGACTTTTTTCAGAGTT  
GCTTTAAAGTACCTGTAGTGAGAACTGATTTATGATCACTTGAAGATTGTATAGTTTTATAAACTCA  
GTTAAATGTCTGTTTCAATGACCTGTATTTTGCCATCTAGAGTCGACCTGCAGGCATGCAAGCTTGCACT  
GGCCGCTGTTTACAC

**Amino acid sequence of hSOD1 (R143A): 153 aa**

1 ATKAVCVLKG DGPVQGIINF EQKESNGPVK VWGSIKGLTE GLHGFHVHEF GDNTAGCTSA  
61 GPHFNPLSRK HGGPKDEERH VGD LGNVTAD KDG VADVSIE DSVISLSGDH CIIGRTLNVH  
121 EKADDLGKGG NEESTKTGNA GSALACGVIG IAQ

**A3.5 YEp351-hSOD1(R143I)**

**DNA Sequence: Forward**

GATTACGAATTCGAGCTCGGTACCCGGGGATCCCCATTGGCATGATGCGAAATTGGACGTAAGCATCTCTG  
AAGTGCAGCCGATTGGACGTGCGACTCACCCACTCAGGACATGATCTCAGTAGCGGGTTCGATAAGGCGAT  
GACAGCGCAAATGCCGCTTACTGGAAGTACAGAACCCGCTCCCTTAGGGGCACCCACCCAGCACGCCGGG  
GGGTAAACCGGTGTGTGCGAATTAGTAAGCGGACATCCCTTCCGCTGGGCTCGCCATCGCAGATATATAT  
ATAAGAAGATGGTTTTGGGCAAATGTTTAGCTGTAAGTATGTTGCGGAAAAACAGGCAAGAAAGCAATCGC  
GCAAACAAATAAAACATAATTAATTTACCATGGCGACGAAGGCCGTGTGCGTGCTGAAGGGCGACGCCCCA  
GTGCAGGGCATCATCAATTTGAGCAGAAGGAAAGTAATGGACCAGTGAAGGTGTGGGGAAGCATTAAGG  
ACTGACTGAAGGCCTGCATGGATTCCATGTTTCATGAGTTTGGAGATAATACAGCAGGCTGTACCAGTGCAG  
GTCCTCACTTTAATCCTCTATCCAGAAAACACGGTGGGCCAAAGGATGAAGAGAGG

**DNA Sequence: Reverse**

GTGTAAACAGCGCCAGTGCAAGCTTGCATGCCTGCAGGTCGACTCTAGATGGCAAAATACAGGTCATTGA  
AACAGACATTTTAACTGAGTTTTATAAACTATACAAATCTTCCAAGTGATCATAAATCAGTTTCTCACTA  
CAGGTACTTTAAAGCAACTCTGAAAAAGTCACACAATTACACTTTTAAAGATTACAGTGTTTAATGTTTATC  
AGGATACATTTCTACAGCTAGCAGGATAACAGATGAGTTAAGGGGCCTCAGACTACATCCAAGGGAATGTT  
TATTGGGCGATCCCAATTACACCACAAGCCAAAATACTTCCAGCGTTTCTGTCTTTGTACTTTCTTCATT  
TCCACCTTTGCCCAAGTCATCTGCTTTTTTCATGGACCACCAGTGTGCGGCCAATGATGCAATGGTCTCCTG  
AGAGTGAGATCACAGAATCTTCAATAGACACATCGGCCACACCATCTTTGTCAGCAGTCACATTGCCCCAAG  
TCTCCAACATGCCTCTCTTCATCCTTTGGCCCACCGTGTTTTCTGGATAGAGGATTAAAGTGAGGACCTGC  
ACTGGTACAGCCTGCTGTATTATCTCCAAACTCATGAACATGGAATCCATGCAGGCC

### YEp351-hSOD1(R143I): Total DNA sequence

GATTACGAATTCGAGCTCGGTACCCGGGGATCCCCATTGGCATGATGCGAAATTGGACGTAAGCATCTCTG  
AAGTGCAGCCGATTGGACGTGCGACTCACCCACTCAGGACATGATCTCAGTAGCGGGTTCGATAAGGCGAT  
GACAGCGCAAATGCCGCTTACTGGAAGTACAGAACCCGCTCCCTTAGGGGCACCCACCCCAGCACGCCGGG  
GGGTAAACCGGTGTGTCTCGGAATTAGTAAGCGGACATCCCTTCCGCTGGGCTCGCCATCGCAGATATATAT  
ATAAGAAGATGGTTTTGGGCAAATGTTTAGCTGTAACTATGTTGCGGAAAAACAGGCAAGAAAGCAATCGC  
GCAAAACAAATAAAACATAATTAATTTACCATGGCGACGAAGGCCGTGTGCGTGCTGAAGGGCGACGGCCCA  
GTGCAGGGCATCATCAATTTTCGAGCAGAAGGAAAGTAATGGACCAGTGAAGGTGTGGGGAAGCATTAAAGG  
ACTGACTGAAGGCCTGCATGGATTCCATGTTTCATGAGTTTGGAGATAATACAGCAGGCTGTACCAGTGCAG  
GTCCTCACTTTAATCCTCTATCCAGAAAAACACGGTGGGCCAAAGGATGAAGAGAGGCATGTTGGAGACTTG  
GGCAATGTGACTGCTGACAAAGATGGTGTGGCCGATGTGTCTATTGAAGATTCTGTGATCTCACTCTCAGG  
AGACCATTGCATCATTGGCCGCACACTGGTGGTCCATGAAAAAGCAGATGACTTGGGCAAAGGTGGAAATG  
AAGAAAGTACAAAGACAGGAAACGCTGGAAGTATTTTGGCTTGTGGTGTAAATTGGGATCGCCCAATAAACA  
TTCCCTTGGATGTAGTCTGAGGCCCTTAACTCATCTGTTATCCTGCTAGCTGTAGAAATGTATCCTGATA  
AACATTAAACACTGTAATCTTAAAAGTGTAAATTGTGTGACTTTTTTCAGAGTTGCTTTAAAGTACCTGTAGT  
GAGAACTGATTTATGATCACTTGAAGATTTGTATAGTTTTATAAACTCAGTTAAAATGTCTGTTTCAA  
TGACCTGTATTTTGCCATCTAGAGTCGACCTGCAGGCATGCAAGCTTGCACTGGCCGCTGTTTACAC

### Amino acid sequence of hSOD1(R143I): 153 aa

1 ATKAVCVLKG DGPVQGIINF EQKESNGPVK VWGSIKGLTE GLHGFHVHEF GDNTAGCTSA  
61 GPHFNPLSRK HGGPKDEERH VGD LGNVTAD KDG VADVSIE DSVISLSGDH CIIGRTLTVH  
121 EKADDLGKGG NEESTKTGNA GSILACGVIG IAQ

### **A3.6 pET-hSOD1(wild type)**

#### DNA Sequence: Forward

CTAGAAATAATTTTGTTTAACTTTAAGAAGGAGATATACATATGAAATACCTGCTGCCGACCGCTGCTGCT  
GGTCTGCTGCTCCTCGCTGCCACCGGCGATGGCCATGGCGACGAAGGCCGTGTGCGTGCTGAAGGGCGA  
CGGCCCAGTGCAGGGCATCATCAATTTTCGAGCAGAAGGAAAGTAATGGACCAGTGAAGGTGTGGGGAAGCA



CGACTCACTATAGGGGAATTGTGAGCGGATAACAATTCCCCTCTAGAAATAATTTTGTTTAACTTTAAGAA  
GGAGATATACATATGAAATACCTGCTGCCGACCGCTGCTGCTGGTCTGCTGCTCCTCGCTGCCCAGCCGGC  
GATGGCC**ATGGCGACGAAGCCG**TGTGCGTGCTGAAGGGCGACGGCCCAGTGCAGGGCATCATCAATTT**CG**  
**AGCAGAAGGAAAGTAATGGACCAGTGAAGGTGTGGGGAAGCATTAAAGGACTGACTGAAGGCCTGCATGGA**  
**TTCCATGTT**CATGAGTTTGGAGATAATACAGCAGGCTGTACCAGTGCAGGTCCTCACTTTAATCCTCTATC  
CAGAAAACACGGTGGGCCAAAGGATGAAGAGAGGCATGTTGGAGACTTGGGCAATGTGACTGCTGACAAAG  
ATGGTGTGGCCGATGTGTCTATTGAAGATTCTGTGATCTCACTCTCAGGAGACCATTGCATCATTGGCCGC  
ACACTGGTGGTCCATGAAAAAGCAGATGACTTGGGCAAAGGTGGAAATGAAGAAAGTACAAAGACAGGAAA  
CGCTGGAAGT**CGTTTGGCTTGTGGT**GTAATTGGGATCGCCCAATAAACATTCCCTTGGATGTAGTCTGAGG  
CCCCTTAACTCATCTGTTATCCTGCTAGCTGTAGAAATGTATCCTGATAAACATTAAACACTGTAATCTTA  
AAAGTGTAATTGTGTGACTTTTTTCAGAGTTGCTTTAAAGTACCTGTAGTGAGAACTGATTTATGATCACT  
TGGAAGATTTGTATAGTTTTATAAACTCAGTTAAATGTCTGTTTCAATGACCTGTATTTTGCCATCTAG  
AGTCGACCTGCAGGCATGCAAGCTTGCGGCCGCACTCGAGCACCACCACCACCACCCTGAGATCCGGCTG  
CTAACAAAGCCCGAAAGGAAGCTGAGTTGGCTGCTGCCACCGCTGAGCAATAA

**Amino acid sequence of wild-type hSOD1: 154 aa**

1 ATKAVCVLKG DGPVQGIINF EQKESNGPVK VWGSIKGLTE GLHGFHVHEF GDNTAGCTSA  
61 GPHFNPLSRK HGGPKDEERH VGD LGNVTAD KDG VADVSIE DSVISLSGDH CIIGRTLTVH  
121 EKADDLGKGG NEESTKTGNA GS**R**LACGVIG IAQ

## **6.0 The role of CuZnSOD in *S*-nitrosation and denitrosation of cysteine residues in rat Hb**

### **6.1 Abstract**

Mass spectrometric analysis revealed that two  $\beta$ -Cys and one  $\alpha$ -Cys in Hb from rat RBCs are alkylated by NEM as compared to one  $\beta$ -Cys and one  $\alpha$ -Cys in Sigma rat Hb. DTNB titration revealed  $3.97 \pm 0.30$  and  $2.28 \pm 0.13$  free cysteine residues/tetramer in rat Hb from the two sources, and  $0.72 \pm 0.04$  cysteine residues/tetramer for human Hb. *Trans-S*-nitrosation occurred on incubating the oxygenated protein (oxyHb) with the low-molecular-weight *S*-nitrosothiols, GSNO and CysNO. Up to 4 cysteines in rat oxyHb were *S*-nitrosated by CysNO as determined by the Saville assay, and the extent of Hb-SNO formation was proportional to the CysNO/oxyHb ratio. Using GSNO as a NO donor, the SNO content measured by the Saville assay suggested that rat Hb is more readily *S*-nitrosated than human Hb consistent with the different DTNB reactivity of their cysteine residues. Both Cys $\beta$ 125 and Cys $\beta$ 93 in rat RBC oxyHb can be *S*-nitrosated and *S*-glutathiolated in GSNO/oxyHb (10:1) incubations, and peptide mass fingerprinting of Glu-C and tryptic digests reveals that Cys $\beta$ 125 is more reactive, consistent with the reported DTNB data. *S*-nitrosation of rat oxyHb is not catalyzed by added bovine Cu,Zn-superoxide dismutase (BCuZnSOD) in oxyHb/GSNO (1:10) incubations although  $5.2 \pm 0.53$   $\mu$ M CuZnSOD (dimer) was found in rat RBCs. CuZnSOD may play a role in NO release from rat Hb-SNO in the presence of GSH, and metal chelators inhibit the enzyme as described with GSNO as a substrate in Chapter 2. The rate of Hb-SNO degradation catalyzed by the active-site copper in CuZnSOD is slower than by free copper ions which

can be attributed to steric hindrance. Our observations indicate that caution is required in proposing mechanisms responsible for RBC-derived vasoactivity in human blood based on the rat model.

## 6.2 Introduction

Carrying O<sub>2</sub> from the lung to tissues is the main physiological function of hemoglobin (Hb) in red blood cells (RBCs). Recent evidence has revealed that Hb also serves to regulate the chemistry of nitric oxide (NO) and conserve, rather than consume, its bioactivity by the formation of *S*-nitrosohemoglobin (Hb-SNO) (19, 57, 61-65, 72, 87, 93). Hb-SNO has been suggested to act as a physiological regulator of blood flow and oxygen delivery (19, 61, 62, 64, 65, 72, 92, 93), a hypoxia-activated NO donor (259, 260), and an inhibitor of platelet aggregation (16).

The mechanism of Hb-SNO formation *in vivo* is incompletely understood. Until the report by Jia *et al.* (19), it was generally accepted that NO was consumed or depleted by its rapid reaction with oxyhemoglobin (oxyHb or HbO<sub>2</sub>) ( $k = 3.4 \times 10^7 \text{ M}^{-1}\text{s}^{-1}$ ) to produce methemoglobin (metHb or HbFe<sup>III</sup>) and nitrate (Reaction 1.14, Section 1.5.1), or with the heme in deoxyhemoglobin (deoxyHb or HbFe<sup>II</sup>) ( $k = 2.6 \times 10^7 \text{ M}^{-1}\text{s}^{-1}$ ) to form iron-nitrosyl-hemoglobin (HbFe<sup>II</sup>NO) (Reaction 1.13, Section 1.5.1). Neither product exhibits the bioactivity characteristic of NO (68, 261, 262), but Jia *et al.* (19) reported that a small but significant amount of circulating oxyHb is *S*-nitrosated at Cys $\beta$ 93, and proposed that Hb-SNO may have a significant role in the transduction of NO-related activities that control blood pressure and facilitate efficient delivery of oxygen to tissues. Continuous cycling of Hb *in vivo* between oxygenated and deoxygenated states that

influence the propensity for binding vs release of NO has been investigated in the Stamler group (19, 62-65, 72, 87, 90, 93). Cys $\beta$ 93 as a site of NO binding to Hb has been characterized by mass spectrometry (263), FTIR (264), and X-ray crystallography (89, 265). The levels of Hb-SNO (micromolar) (92) were reported to be higher in oxygenated vs deoxygenated blood of adults (61, 266, 267) and newborns (268), although this has been disputed. Some observations indicated no arterial-to-venous Hb-SNO gradients (84) and very low (nanomolar) or undetectable Hb-SNO in human arterial blood (79, 84, 269). These observations do not support the proposition that Hb-SNO is a vasodilator with activity allosterically modulated by oxygen (19, 65, 259, 270).

Mechanisms of Hb-SNO formation upon exposure of Hb to RSNOs (19, 62), NO (63, 64), and nitrite (61, 78) have been proposed. Gow *et al.* observed that superoxide dismutase (CuZnSOD) increases the yield of nitrosyl Hb (HbFe<sup>II</sup>NO and Hb-SNO) in reactions of human oxyHb with NO (64). *Trans-S*-nitrosation (Reaction 1.15, Section 1.5.3) is commonly used to synthesize *S*-nitrosated proteins from small RSNOs such as GSNO or CysNO (19, 62). A copper-ion requirement for this reaction was proposed by our group (264). Later, we proposed that CuZnSOD acts as a GSNO-transferase, and that NO is channelled from GSNO to Cys $\beta$ 93 in human oxyHb within a CuZnSOD/Hb complex. This gives rise to Hb-SNO under physiological conditions with conservation of NO-bioactivity rather than quenching through NO<sub>3</sub><sup>-</sup> formation (Reaction 1.14, Section 1.5.1). The proposed mechanism of CuZnSOD-catalyzed Hb-SNO formation is given by Reactions 2.1–2.4 (57).

Hb-SNO is detectable (~266 nM) in rat but not in human RBCs (< 1 nM) using the chemiluminescence technique reported by Bryan *et al.* (79). The finding



reported in this article (79) and observations from other studies (83, 271-273) have demonstrated that differences in Hb thiol reactivity exists among species leading to significant differences in nitroso/nitrosyl content when rat and human Hb are mixed with NO (79), CysNO (273), or GSNO (29).

In the present study, the reactivity of thiol groups in rat Hb isolated from RBCs and commercial rat Hb (Sigma) toward DTNB and NEM was compared spectrophotometrically and using mass spectrometry. The abundance of CuZnSOD in rat RBCs was determined, and the GSNO-transferase activity of bovine CuZnSOD using human and rat oxyHb as substrates was compared. The thiols in rat oxyHb that were *S*-nitrosated and *S*-glutathiolated were identified and their reactivity evaluated. Since metal chelators inhibit its GSNO-reductase activity (Chapter 2) (56, 225), the effects of metal chelators on CuZnSOD-catalyzed NO release from rat were also investigated. MetHb-SNO was synthesized from oxyHb by *trans*-*S*-nitrosation with excess CysNO.

The present results provide an explanation for the observation that basal levels of NO-adducts are considerably higher in rat vs human RBCs (79). Also, CuZnSOD-catalyzed dissociation of NO from Hb-SNO could promote transfer of NO bioactivity to targets such as thiols in the RBC membrane prior to Hb deoxygenation. Highly conserved Cys $\beta$ 93 has been associated with NO transport by human Hb, but its role may be more limited in rat Hb due to the existence of highly reactive Cys $\beta$ 125. Thus, caution must be exercised in the selection of animal models for the study of *S*-nitrosation chemistry and its importance in the vascular system.

### **6.3 Materials and methods**

### 6.3.1 Materials

Rat hemoglobin (Sigma) and bovine erythrocyte CuZnSOD (BCuZnSOD) (Roche Molecular Biochemicals) were used without further purification unless otherwise indicated. Rat (Sprague-Dawley strain) red blood cells (RBCs) were generously supplied by Dr. Chi Chung Chan of Merck Frosst (Montreal) and Carmen Gagnon of Hospital Ste-Justine (Montreal). The total protein assay kit was obtained from Bio-Rad, and Drabkin's reagent, *L*-cysteine, 5,5'-dithio-bis(2-nitrobenzoic acid) (DTNB), *N*-(1-naphthyl) ethylenediamine dihydrochloride (NEDA), mercuric chloride, ammonium sulfamate, sulfanilamide, DEAE-Sephacel anion-exchanger, sodium nitrite, and *N*-ethylmaleimide (NEM) were purchased from Sigma. *S*-nitroso-*L*-glutathione (GSNO) was from Cayman, acetonitrile (HPLC grade) was from Fisher, trifluoroacetic acid (TFA, HPLC grade) was from Aldrich, ZipTips were from Milipore, and NAP-5 and NAP-10 Sephadex G-25 gel-filtration columns were from Amersham Bioscience. Nanopure water from a Millipore system was used to prepare all solutions.

### 6.3.2 Methods

#### 6.3.2.1 oxyHb preparation from Sigma rat Hb

Lyophilized rat metHb (HbFe<sup>III</sup>) from the bottle was dissolved in 20 mM sodium phosphate buffer/1 mM EDTA (pH 7.2) to give ~5 mM Hb. The solution was centrifuged at 12,000 rpm for 2 min, and the supernatant was stored at 4°C prior to use. The metHb concentration was determined spectrophotometrically ( $\epsilon_{500\text{ nm}} = 10$  and  $\epsilon_{630\text{ nm}} = 4.4\text{ mM}^{-1}\text{cm}^{-1}$  per heme) (274). Na<sub>2</sub>S<sub>2</sub>O<sub>4</sub> in 5-fold molar excess was added to reduce metHb to deoxyHb (HbFe<sup>II</sup>), and the protein was separated from low-molecular-weight species on a 1.5-×20-cm Sephadex G-25 column. OxyHb was formed on aeration and

identified and quantitated spectrophotometrically [ $\epsilon_{541} = 13.8 \text{ mM}^{-1}\text{cm}^{-1}$  (72) or  $\epsilon_{415} = 125 \text{ mM}^{-1}\text{cm}^{-1}$  (275) per heme]. The iron oxidation state was monitored using the absorbance ratio at 576/541 nm, taking 1.14 as normal value for oxyHb (83).

#### **6.3.2.2 oxyHb preparation from rat RBCs**

Rat blood was collected in heparinized tubes and centrifuged at 2,200g at 4°C for 10 min to pellet the RBCs. The plasma was removed, the RBCs were washed twice with 5 volumes of 0.9% NaCl, and centrifuged at 2,200g at 4°C for 10 min. Hb was obtained from the lysate by freezing the RBCs to -80°C followed by thawing and centrifugation at 12,000 rpm at 4°C for 10 min to remove the residual membranes. The supernatant was dialyzed (MWCO 6,000–8,000) for 24 h against 2 changes of 50 mM sodium phosphate buffer (pH 7.2) at 4°C to remove GSH. The concentration of oxyHb was determined spectrophotometrically as described above or measured using Drabkin's reagent (57).

#### **6.3.2.3 CuZnSOD-free Hb preparation**

CuZnSOD is present in RBCs and can be removed from Hb by anion-exchange chromatography (57). A 1.5- $\times$ 7-cm DEAE-Sepacel (Sigma) anion-exchange column preequilibrated with 50 mM sodium phosphate buffer (pH 7.5) was employed to remove CuZnSOD. Following the procedure described in (138), briefly, 2 mM Hb in 0.5 mL of 50 mM sodium phosphate buffer (pH 7.5) was loaded onto the column. The eluent was 100 mM NaCl in the equilibration buffer, and the eluted Hb fraction was twice reapplied to the anion-exchange column to remove CuZnSOD thoroughly. The CuZnSOD-free Hb was desalted on a NAP-5 G-25 gel-filtration column and concentrated by ultrafiltration.

#### **6.3.2.4 Hb-SNO Preparation**

CysNO was prepared immediately before use by combining equal volumes of 100 mM of *L*-cysteine in 250 mM HCl with 100 mM sodium nitrite in water. The reaction solution turned orange red-colored instantly indicating CysNO formation. The pH was adjusted to pH 7.2 by adding 1 M NaOH dropwise. Hb-SNO was prepared by incubating oxyHb with GSNO or CysNO at the molar ratios indicated in the figure legends in the presence or absence of 10–30  $\mu$ M BCuZnSOD at RT for 30 min in the dark in 10 mM PBS or 50 mM sodium phosphate buffer (pH 7.2). The reagent concentrations used in the different experiments are indicated in the figure legends. Excess CysNO or GSNO and other low-molecular-weight reagents were removed on NAP-5 or NAP-10 G-25 gel-filtration columns or on ZipTipC<sub>4</sub> tips. The Hb concentration was determined using Drabkin's reagent or the Bio-rad protein assay.

#### **6.3.2.5 Hb-NEM preparation**

Rat oxyHb in its native form was incubated with excess NEM at room temperature for 30 min at the concentrations indicated in the figure legends. The denatured Hb was prepared by incubating 4.5  $\mu$ M protein in 100 mM sodium phosphate buffer (pH 7.4) containing 1% SDS for 90 min at RT. The NEM-modified Cys residues were identified by ESI-MS and MALDI-MS. To establish the number of free thiols following *S*-nitrosation, 76  $\mu$ M oxyHb from rat RBCs was incubated at RT with 10-fold molar excess of GSNO for 30 min and then with 50-fold molar excess of NEM for 30 min in 10 mM sodium phosphate buffer (pH 7.2). The NO- and NEM-adducts on the  $\alpha$ - and  $\beta$ -chains were identified by ESI-MS and MALDI-MS.

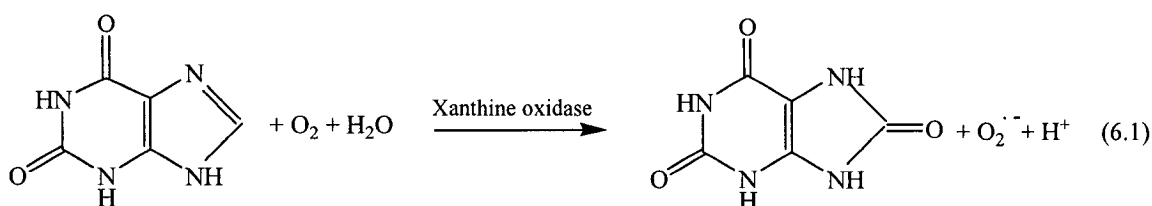
#### **6.3.2.6 Preparation of copper-free CuZnSOD (EZnSOD)**

EZnSOD was prepared as described by Cocco *et al.* (126) with minor modifications. Briefly, ~0.1 mM bovine CuZnSOD in 10 mM PBS (pH 7.4) was incubated with 3.0 mM DDC at 37°C for 3 h, and the sample was loaded on a NAP-5 column equilibrated with 10 mM PBS (pH 7.4) to remove excess DDC. The yellow protein eluate was centrifuged at 39,000g for 30 min to remove the neutral  $\text{Cu}^{\text{II}}(\text{DDC})_2$  complex from the enzyme by precipitating the former. EZnSOD in the colourless supernatant was further purified by centrifugal ultrafiltration on an Ultrafree-0.5 filter (cut-off 10K, Millipore). The concentration of EZnSOD was determined using the Bio-Rad protein assay.

#### **6.3.2.7 Extraction of CuZnSOD from rat RBCs**

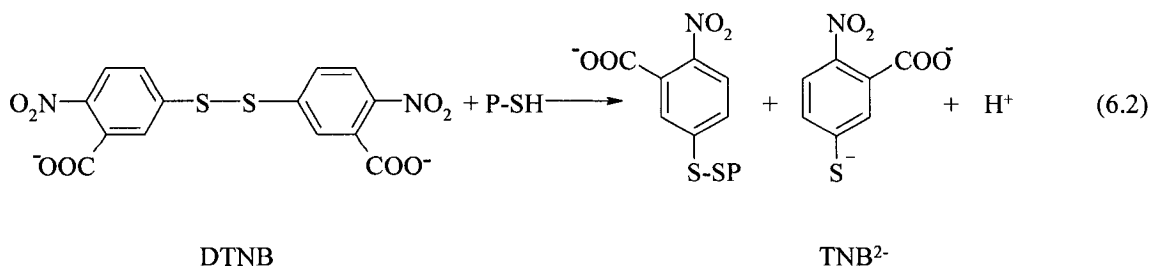
CuZnSOD was extracted following the published procedure (47) with minor modifications. Rat RBCs (0.5 mL) from Hospital Sainte-Justine were added to 0.5–1.0 mL of deionized water, centrifuged at 12,000 rpm for 15 min, and the hemolysate was collected. The precipitate was washed with 0.2–1.0 mL of deionized water, centrifuged at 12,000 rpm for 15 min, the supernatant was combined with the hemolysate, and 250  $\mu\text{L}$  was added to 400  $\mu\text{L}$  of chloroform/ethanol (37.5/62.5, v/v) to precipitate Hb. After centrifugation at 2,500g for 10 min, the supernatant enriched in CuZnSOD was separated from Hb precipitate, added to an Ultrafree-0.5 filter (cut-off 10K, Millipore), and centrifuged at 12,000 rpm for 5×15 min at 4°C to remove low-molecular-weight species such as GSH. The concentrated ultrafiltrate (40–75  $\mu\text{L}$ ) was transferred to a 1-mL vial and stored at -20°C prior to analysis by 10% SDS-PAGE (Section 5.2.8.2), and activity analysis.

The SOD activity was determined by xanthine oxidase-cytochrome<sup>III</sup> assay as described in Section 2.3.2.3. The  $O_2^{\cdot-}$  radical is generated enzymically by oxidation of xanthine in the presence of xanthine oxidase (Reaction 6.1) (47, 127). The rate of cytochrome<sup>III</sup> reduction by the superoxide radicals is monitored at 550 nm (Reaction 2.7, Section 2.3.2.3), and CuZnSOD competes for superoxide (Reaction 2.8, Section 2.3.2.3). Hence, the CuZnSOD concentration in the sample is determined from the decreased rate of cytochrome<sup>III</sup> reduction (276, 277) by 1  $\mu$ L of rat RBC extract (or 1  $\mu$ L of 10 $\times$  diluted extract).



#### 6.3.2.8 Spectrophotometric determination of free Cys residues using DTNB

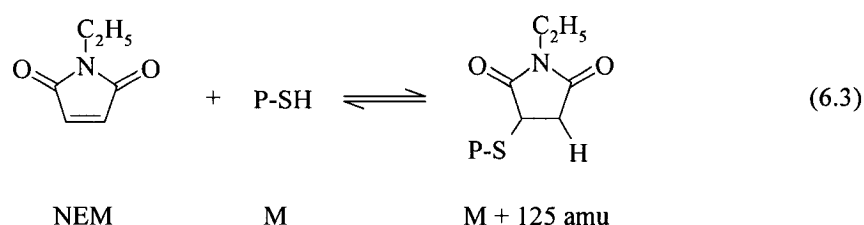
DTNB, also called Ellman's Reagent, is frequently used to determine free sulfhydryl groups (276). This aromatic disulfide reacts with accessible protein-SH groups (P-SH) to form a protein mixed disulfide and  $\text{TNB}^{2-}$ , which has an intense yellow color due to its absorbance at 412 nm ( $\epsilon = 13.6 \text{ mM}^{-1}\text{cm}^{-1}$ ) (29):



A 34-mM stock DTNB solution was prepared prior to use by dissolving DTNB in aqueous 95% ethanol. The  $\text{TNB}^{2-}$  product from Hb/DTNB incubations was monitored at 450 nm ( $\epsilon = 7.0 \text{ mM}^{-1}\text{cm}^{-1}$ ) since the Soret band interferes at 412 nm (278). The absorbance at 450 nm vs time at RT of 2–7  $\mu\text{M}$  native and denatured (Section 6.3.2.5) rat Hb in 0.1 M sodium phosphate buffer/1 mM EDTA (pH 7.27) with 340  $\mu\text{M}$  DTNB was recorded over 30 min at 30-s intervals in a 1-cm cuvette on an Agilent 8453 diode-array or a Beckman DU 650 spectrophotometer. Additionally, the reaction of free cysteine with DTNB was examined under the same experimental conditions. Beer's law plots were prepared from the absorbance readings at 412 nm and 450 nm of standards containing known concentrations (20–80  $\mu\text{M}$ ) of *L*-cysteine with 340  $\mu\text{M}$  DTNB.

### 6.3.2.9 Mass spectrometric determination of free Cys residues using NEM

NEM is a highly reactive reagent with protein-based Cys residues (Reaction 6.3). Each NEM label mass shifts a protein by 125 u which is conveniently measured by mass spectrometry.



OxyHb prepared from rat RBCs or rat metHb (Sigma) were incubated at the concentration indicated in the figure legends with 50–100-fold molar excess of NEM at RT for 30 min. Excess NEM was removed on a NAP-5 gel-filtration column or on a ZipTipC<sub>4</sub>, and the number of NEM-labels per  $\alpha$ - and  $\beta$ -chain were measured by ESI-MS

on a Q-ToF 2 (Waters Micromass) or SSQ 7000 (ThermoFinnigan) instrument. The sites of NEM-labelling were identified by MALDI-MS on a Waters Micromass M@LDI analyzer.

#### **6.3.2.10 Tryptic and Glu-C digestion of protein samples**

Tryptic digestion at a Hb/trypsin ratio of 40/1 (w/w) was carried out in 10 mM TrisHCl buffer (pH 7.9) or 100 mM  $\text{NH}_4\text{HCO}_3$  (pH ~8.5) at 37°C for the times indicated in the figure legends. Alternatively, endoproteinase Glu-C digestion was performed in 50 mM  $\text{AcONH}_4$  (pH 4.0) at 35°C for 2–4 h at a Hb/Glu-C ratio of 20/1 (w/w). The digests were analyzed using MALDI-ToF-MS or ESI-ToF-MS.

#### **6.3.2.11 ESI-ToF-MS analysis**

The desalted tryptic digests or protein samples were diluted into 50–60% ACN/0.1% TFA to the final concentrations indicated in the figure legends and directly infused at a flow rate of 1–2  $\mu\text{L}/\text{min}$  into the ESI source of the Q-ToF 2 or at 5  $\mu\text{L}/\text{min}$  into the ESI source of the SSQ 7000. The instruments were operated in positive-ion mode, and the Q-ToF 2 instrumental parameters were set as follows (unless otherwise indicated): capillary 80°C, capillary 3.2 kV, cone 45 V, collision cell 10 V, multiplier 550 V, MCP 2.1 kV, ToF 9.1 kV. The instrument was calibrated using human [Glu<sup>1</sup>]-fibrinopeptide B as a standard, and the average resolution and mass accuracy were 8000 and 5–10 ppm, respectively. The SSQ 7000 instrumental parameters and instrument calibration are indicated in the figure legends. Since the  $\beta$ -chain signals were lower than the  $\alpha$ -chain signals, the Hb samples were occasionally injected *via* a CapLC system (Waters) attached to the ESI source of the Q-ToF 2. The protein samples were desalted and separated on a Symmetry300<sup>TM</sup>  $\text{C}_{18}$  trap column (0.18- $\times$ 23.5-mm, 5- $\mu\text{m}$ , Waters) to



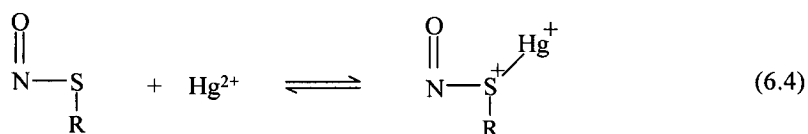
achieve higher signals for the  $\beta$ -chain. The column was equilibrated with solvent A (10% ACN/0.1% TFA) and gradient elution (5:5:50:95:95:5% B in 3/22/5/10/5 min; solvent B: 90% ACN/0.1% TFA) was performed at a flow rate of 1  $\mu$ L/min following injection of 3–5  $\mu$ L of sample.

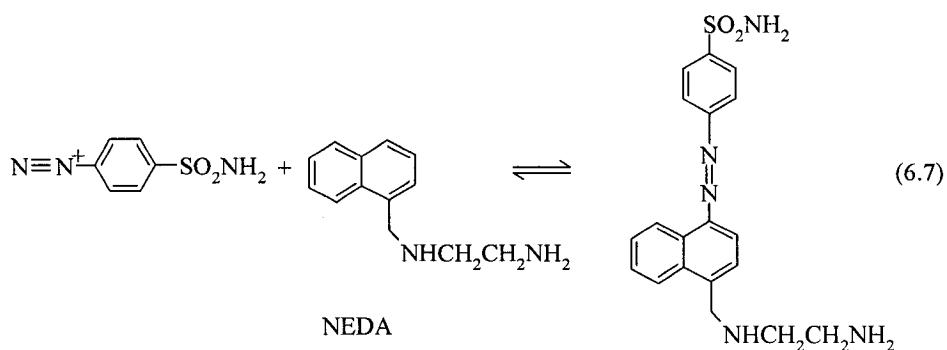
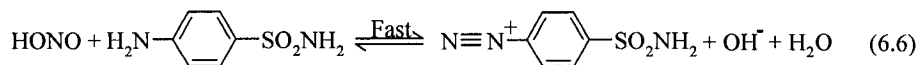
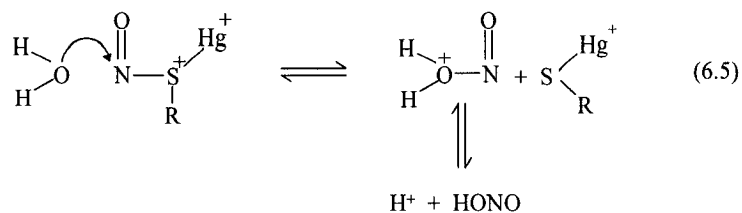
#### 6.3.2.12 MALDI-ToF-MS analysis

Peptides were mixed with an equal volume of matrix [10 mg/mL  $\alpha$ -CHCA in 50% ethanol/50% ACN or in 33% ACN/0.1% TFA (2:1, v/v)]. Aliquots of 1–2  $\mu$ L were spotted onto a stainless steel MALDI target plate of a Waters Micromass M@LDI™ mass spectrometer operated in reflectron, positive-ion mode with accelerating, pulse and detector voltages of +15 kV, ~2.5 kV and 1800 V, respectively. The mass was calibrated externally using 10 pmol/ $\mu$ L each of angiotensin I, PRS, and ACTH in an equal volume of matrix (10 mg/mL  $\alpha$ -CHCA in 50% ACN/50% ethanol).

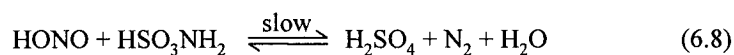
#### 6.3.2.13 Determination of the *S*-nitrosothiol content of rat Hb (Sigma) by the Saville assay

This assay (279) is based on the colorimetric determination of HONO after decomposition of the S-NO bond with  $\text{Hg}^{2+}$  under acidic conditions (Reactions 6.4 and 6.5). The released HONO reacts with sulfanilamide to form a diazonium cation (Reaction 6.6), which couples with *N*-(1-naphthyl)ethylenediamine dihydrochloride (NEDA) to form a reddish-purple azo dye (Reaction 6.7) that absorbs at 540 nm.





Sulfamate in 0.4 M HCl was first used to remove interfering HONO (Reaction 6.8) present in the reactants (25):



Hb-SNO was prepared by incubation of rat oxyHb (Sigma) in 10 mM sodium phosphate buffer (pH 7.2) with 2–100-fold molar excess of CysNO at RT for 30 min in the dark and purified on a NAP-5 column to remove low-molecular-weight reagents. The *S*-nitrosothiol content of purified Hb-SNO was determined from the difference in absorbance at 540 nm in samples that were incubated with the Griess reagents with and without  $\text{Hg}^{2+}$  (279). Briefly, samples from the NAP-5 column were diluted into 0.4 M HCl to a final Hb concentration of 10–50  $\mu\text{M}$ . Aliquots (420  $\mu\text{L}$ ) were added to 2-mL

reaction vials, and mixed with 80  $\mu\text{L}$  of 0.5 % w/v ammonium sulfamate in  $\text{H}_2\text{O}$  for 1–2 min to remove HONO (Reaction 6.8). A solution (800  $\mu\text{L}$ ) containing sulfanilamide and  $\text{HgCl}_2$  (1 volume of 1% w/v  $\text{HgCl}_2$  in  $\text{H}_2\text{O}$  and 4 volumes of 3.4% w/v sulfanilamide in 0.4 M HCl) or just sulfanilamide (1 volume of  $\text{H}_2\text{O}$  and 4 volumes of 3.4% w/v sulfanilamide in 0.4 M HCl) was added to the vials, followed by 700  $\mu\text{L}$  of 0.1% w/v of NEDA in 0.4 M HCl to give a final volume of 2.0 mL. The samples were incubated at RT for 10 min prior to reading the absorbance at 540 nm. Blanks (no Hb-SNO) with and without  $\text{Hg}^{2+}$  were prepared by the same procedure. The RSNO content of the Hb samples was calculated using a standard curve prepared with 0–25  $\mu\text{M}$   $\text{NaNO}_2$  (the ammonium sulfamate step was omitted for the  $\text{NaNO}_2$  standards) or with 0–25  $\mu\text{M}$  GSNO. The GSNO concentration was determined spectrophotometrically assuming  $\epsilon_{333} = 767 \text{ mM}^{-1}\text{cm}^{-1}$  (84).

Decomposition of Hb-SNO in incubates (10–70  $\mu\text{M}$ ) in the presence and absence of  $\text{CuSO}_4$  (5  $\mu\text{M}$ ),  $\text{CuZnSOD}$  (10  $\mu\text{M}$ ), GSH (125  $\mu\text{M}$ ) and copper chelators (200–500  $\mu\text{M}$  DTPA, EDTA, and/or neocuproine) was determined from the difference in the RSNO concentration measured by Saville assay before and after 30-min incubation at 37°C. All reagents were prepared in Chelex-100 treated 10 mM PBS (pH 7.2) and absorbance at 540 nm was read in a 1-cm cuvette at RT.

## 6.4 Results

### 6.4.1 CuZnSOD in rat RBCs

***SDS-PAGE analysis of CuZnSOD extracted from rat RBCs.*** CuZnSOD was extracted in triplicate (Table 6.1) from rat RBCs obtained from Hospital Sainte-Justine

(Section 6.3.2.7). SDS-PAGE analysis clearly shows that CuZnSOD was enriched in the three extracts (Figure 6.1). Minor bands on the gel indicate that contaminating proteins were also present.

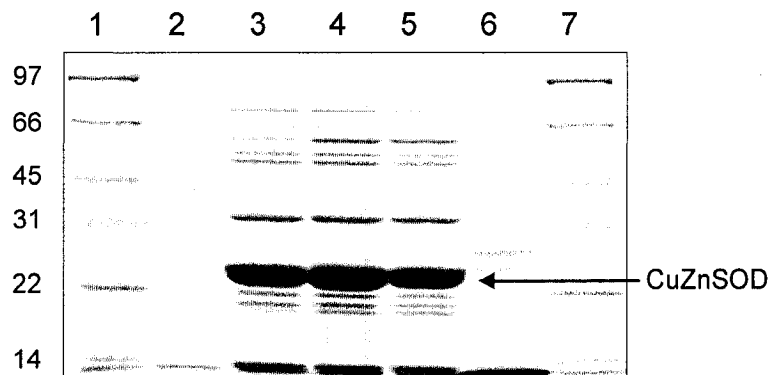


Figure 6.1 10% SDS-PAGE analysis of CuZnSOD extracted from rat RBCs. Lanes 1 and 7: protein-size markers (in kDa); lanes 2 and 6: 2.4 and 19  $\mu$ g of BCuZnSOD; lane 3: 2.5  $\mu$ L of extract 3; lane 4: 5  $\mu$ L of extract 1; lane 5: 10  $\mu$ L of extract 2. The volumes used in the preparation of extracts 1–3 and their SOD activity are given in Table 6.1.

**ESI-MS analysis of the CuZnSOD extracts from rat RBCs.** The proteins in extract 3 were characterized using ESI-mass spectrometry. Three main components with masses of 15,819 u, 14,111 u (dimer: 28,222 u), and 14,664 u (dimer: 29,328 u) were detected (Figure 6.2) consistent with the protein bands on SDS-PAGE (Figure 6.1). The peak with a mass of 15,819 u corresponds to rat CuZnSOD (Figure 6.2A), which has a theoretical mass of 15820 u calculated from its amino acid sequence mass (15,780.5 u) with *N*-terminal acetylation (+42 u) and a single disulfide bond (-2 u) (PDB: NP\_058746; Table 1.1, Section 1.4.4). The two other peaks do not correspond to Hb and need to be identified. Figures 6.2B and C show the deconvolved ESI mass spectra of hSOD1 expressed in yeast (Chapter 5) and BCuZnSOD, respectively, with masses in good agreement with the calculated mass (15,845 and 15,591 u) [Section 4.4.5 and Ref (247)].

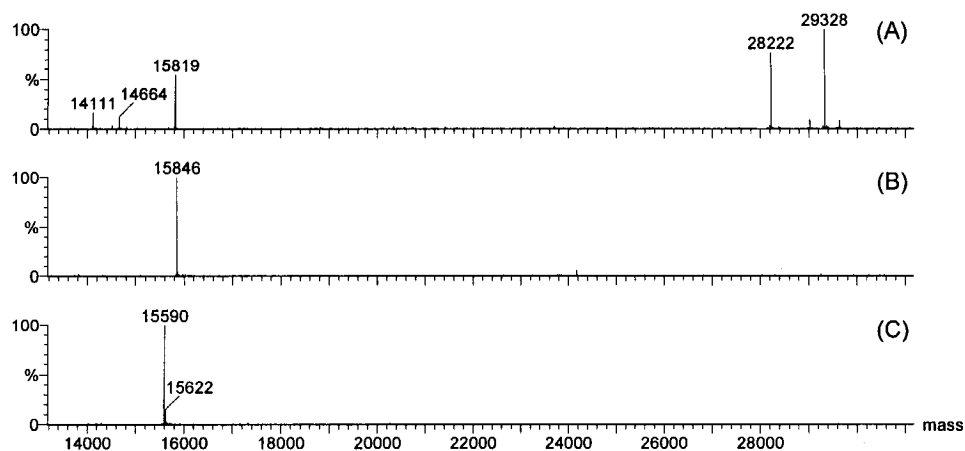


Figure 6.2 **Deconvolved ESI mass spectra of rat, human, and bovine CuZnSOD.** (A) Rat CuZnSOD in 10  $\mu\text{L}$  of extract 3 (Table 6.1). The sample was desalted on a ZipTipC<sub>4</sub> and eluted from the tip into 30  $\mu\text{L}$  of 60% ACN/0.1% TFA for MS analysis. (B) Bovine and (C) human CuZnSOD (5–10  $\mu\text{M}$ ) samples in 50% ACN/0.1% TFA were prepared from the commercial protein (Roche) and that expressed in yeast (Chapter 5), respectively. To record the ESI mass spectrum, proteins were directly infused at a flow rate of 1  $\mu\text{L}/\text{min}$  into the Z-spray ion source of the Q-ToF 2 mass spectrometer. The instrumental parameters were: source block temperature 80°C,  $\text{LM}$  &  $\text{HM}$  Res 5.0, capillary 3.2 kV, cone 45 V, collision 10 V, ToF –9.1 kV and MCP 2.1 kV. The average resolution and accuracy were 8000 and 5–10 ppm, respectively, and instrument calibration was achieved using human [Glu1]-fibrinopeptide B.

***Estimation of CuZnSOD concentration in rat RBCs*** To determine the amount of CuZnSOD in rat RBCs, the SOD activity in the extracts was measured and [CuZnSOD] was calculated using a standard curve prepared with BCuZnSOD [ $\epsilon_{258} = 10.3 \text{ mM}^{-1}\text{cm}^{-1}$ , (29, 276)] (Figure 6.3). The calibration equation of %I vs [BCuZnSOD] in nM was  $y = 13.968x + 6.692$  ( $R^2 = 0.979$ ), and the average CuZnSOD concentration in rat RBCs calculated from the %I was  $5.20 \pm 0.53 \mu\text{M}$  (Table 6.1).

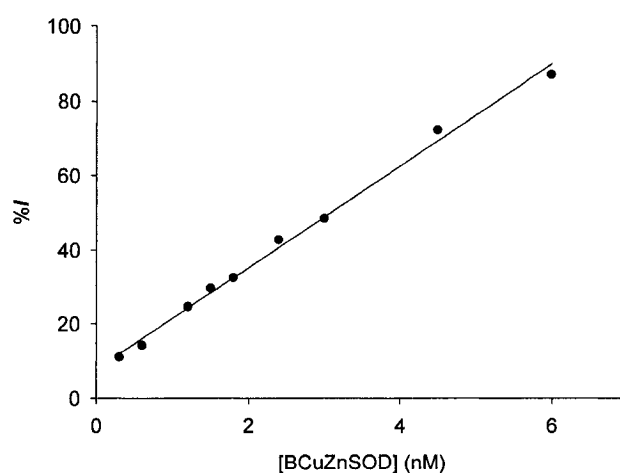


Figure 6.3 **Inhibition calibration curve for the determination of CuZnSOD concentration.** Curve generated by adding standards of known concentration of 0–6 nM BCuZnSOD in 50 mM sodium phosphate buffer/0.1 mM EDTA (pH 7.8) to 3 mL of SOD assay solution. The absorbance was read at 550 nm in a 1-cm quartz cuvette at RT, and the %I determined as described in Sections 6.3.2.7 and 2.3.2.3.

**Table 6.1 Estimation of CuZnSOD concentration in rat RBCs<sup>a</sup>**

Extract #	1	2	3
RBCs (mL) <sup>b</sup>	0.5	0.5	0.5
Total hemolysate (mL) <sup>c</sup>	2.05	2.07	0.8
Extract volume (μL) <sup>d</sup>	44	72	50
%I <sup>e</sup>	37.25	27.34	55.01
	39.39	29.47	55.04
	41.36	31.09	57.29
Average %I	39.33 ± 2.06	29.30 ± 1.88	55.78 ± 1.31
[CuZnSOD] in extract (μM)	7.01	4.86	14.89
[CuZnSOD] in RBCs (μM)	5.06	5.79	4.76

<sup>a</sup>The CuZnSOD concentration (μM) in rat RBCs was calculated from the change in cytc<sup>III</sup> reduction rate (Sections 6.3.2.7 and 2.3.2.3). <sup>b</sup>Volume of packed RBCs. <sup>c</sup>Total volume of hemolysate following addition of deionized water (Section 6.3.2.7). <sup>d</sup>Extracted from 250 μL of hemolysate. <sup>e</sup>Percent inhibition of cytc<sup>III</sup> reduction measured in the presence of 1 μL of extract in 3 mL of assay solution (Sections 6.3.2.7 and 2.3.2.3).

#### 6.4.2 Reactive Cys residues in rat Hb

**Spectrophotometric determinations.** The reactivity of free sulfhydryl with DTNB was characterized using *L*-cysteine. Plots of the absorbance at 412 nm and 450 nm vs [*L*-cysteine] in the presence of 340  $\mu\text{M}$  DTNB yielded two straight lines with good linearity correlation coefficients (Figure 6.4). The slopes,  $12.9 \text{ mM}^{-1}\text{cm}^{-1}$  at 412 nm and  $7.2 \text{ mM}^{-1}\text{cm}^{-1}$  at 450 nm, are in good agreement with the literature values (60).

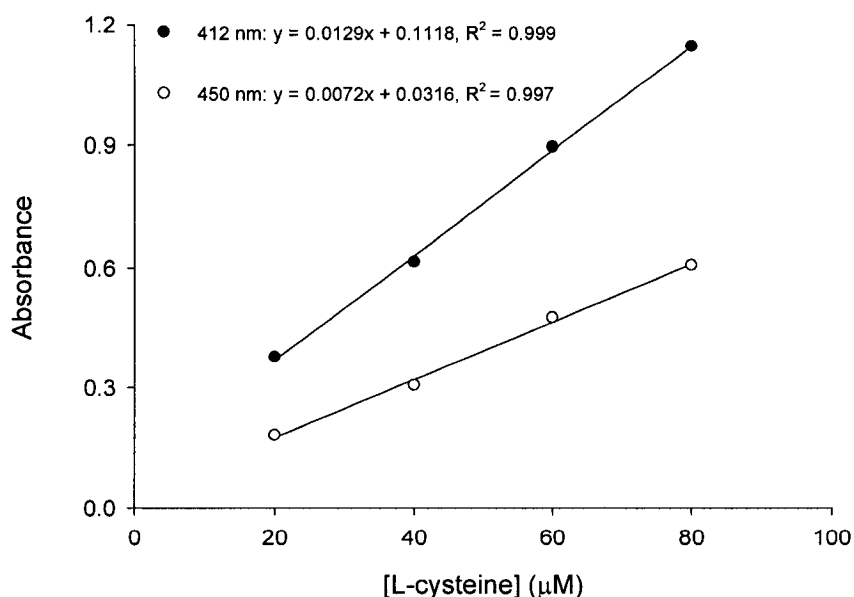
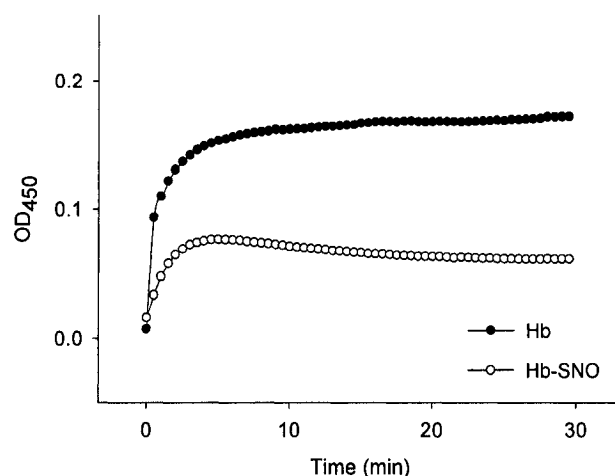


Figure 6.4 **Plots of 412-nm and 450-nm absorbance vs *L*-cysteine concentration in the presence of DTNB.** 20–80  $\mu\text{M}$  *L*-cysteine in 100 mM sodium phosphate buffer/1 mM EDTA was mixed with 340  $\mu\text{M}$  DTNB, and absorbances at 412 nm and 450 nm were read in a 1-cm cuvette at RT. The blank was 100 mM sodium phosphate buffer/1 mM EDTA; thus, the non-zero intercepts are due to DTNB absorption at the measured wavelengths.

Reactive Cys residues in rat Hb (Table 1.3) was probed by monitoring the 450-nm absorbance vs time in the presence of 340  $\mu\text{M}$  of DTNB. A total of  $3.97 \pm 0.30$  Cys residues per oxyHb tetramer from rat RBCs were titrated over 30 min (solid circles,

Figure 6.5) indicating that  $\sim 6$  Cys residues were inaccessible to DTNB. Only  $1.68 \pm 0.13$  Cys residues per Hb tetramer were titrated in a sample that was preincubated with 10-fold molar excess of GSNO (opened circles, Figure 6.5) suggesting that  $\sim 2$  Cys residues were modified by GSNO. The observed decrease in absorbance at 450 nm after 5 min is likely caused by reaction between Hb-SNO and  $\text{TNB}^{2-}$ .



**Figure 6.5 Plots of 450-nm absorption vs time in the DTNB titration of Cys residues in oxyHb from rat RBCs and its Hb-SNO derivative.** The 450-nm absorbance was recorded at 30-s intervals after 340  $\mu\text{M}$  DTNB was added to 6.8  $\mu\text{M}$  oxyHb or 6.8  $\mu\text{M}$  Hb-SNO. OxyHb prepared from rat RBCs (Section 6.3.2.2) was diluted with 100 mM sodium phosphate buffer/1 mM EDTA (pH 7.27). Hb-SNO was prepared by incubating 75  $\mu\text{M}$  oxyHb with 750  $\mu\text{M}$  GSNO for 30 min at RT in 100 mM sodium phosphate buffer (pH 7.4) in the dark. The sample was desalted and the buffer changed to 100 mM sodium phosphate buffer/1 mM EDTA (pH 7.27) using a NAP-5 column. Protein concentrations were determined using Drabkin's reagent.

Under the same conditions,  $2.28 \pm 0.13$  Cys residues per Hb tetramer (solid circles, Figure 6.6) were titrated with DTNB in Sigma rat Hb. After 90 min incubation with 1% SDS,  $6.39 \pm 0.21$  Cys residues (open circles, Figure 6.6) were titrated. Only 0.72



$\pm 0.04$  Cys residue per human Hb tetramer was titrated with DTNB (data not shown). Thus, Sigma human Hb straight from the bottle, which is mainly in the met form, appears not to possess two reactive Cys $\beta$ 93 residues as expected (280).

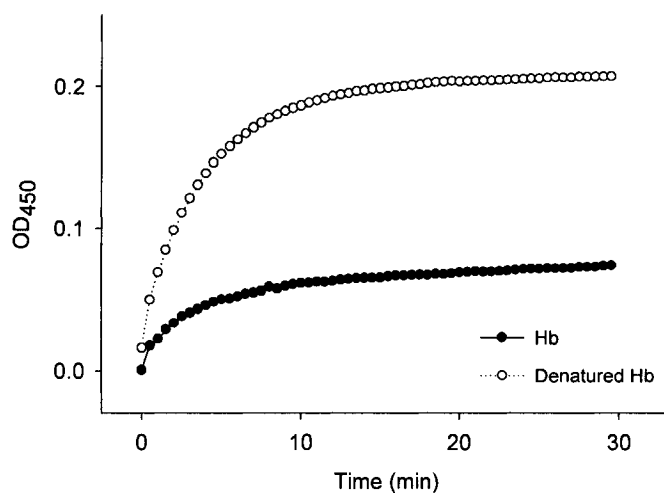
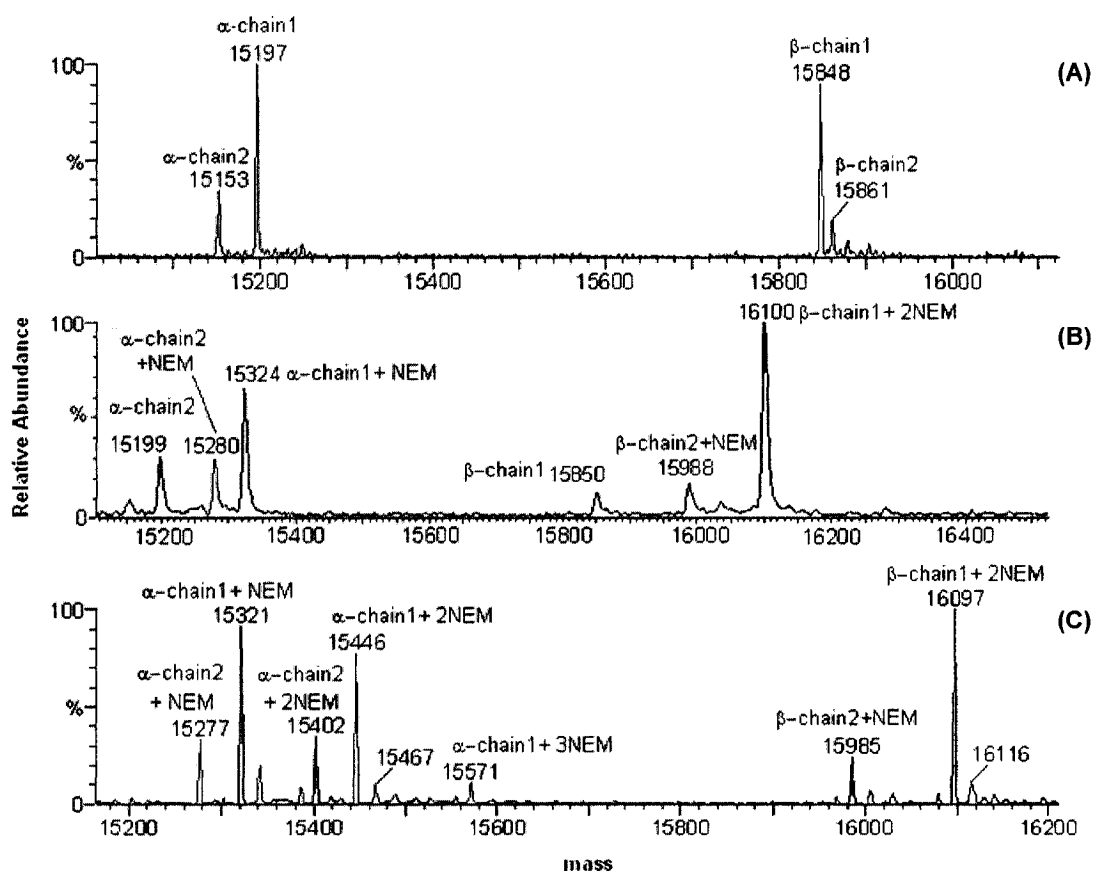


Figure 6.6 Plot of 450-nm absorption vs time in the DTNB titration of Cys residues in native and denatured Sigma rat Hb. The 450-nm absorbance was recorded at 30-s intervals after 340  $\mu$ M DTNB was added to 4.5  $\mu$ M Sigma Hb from the bottle (closed circles) and 4.5  $\mu$ M denatured Hb (open circles). Denatured Hb was prepared as described in Section 6.3.2.5, and Hb concentrations were determined using Drabkin's reagent.

**Mass spectrometric determinations.** The deconvolved ESI mass spectrum (Figure 6.7A) reveals the presence of two isoforms of both the  $\alpha$ - and  $\beta$ -chains of Hb from rat RBCs and the corresponding amino acid sequences are listed in Table 6.2. On incubation with 100-fold molar excess of NEM, 1–3 NEM adducts ( $\Delta m = 125$  per NEM) were detected on the  $\alpha$ -chain1 and 1–2 NEM adducts on the  $\alpha$ -chain2 (Figure 6.7C) whereas both  $\alpha$ -chains were singly NEM labelled when incubated with 50-fold molar excess of NEM (Figure 6.7B). Thus, two of the three Cys residues on the  $\alpha$ -chains are

partially buried, presumably Cys $\alpha$ 104 and Cys $\alpha$ 111 (Section 1.5.4). The two Cys residues on  $\beta$ -chain1 (Table 1.3) are highly reactive with NEM (Figures 6.7B,C), but the  $\beta$ -chain2 was only singly NEM labelled by 50- or 100-fold molar excess NEM (Figures 6.7B,C). This is consistent with the presence of only one Cys residue in the  $\beta$ -chain of the minor form of rat Hb (Tables 1.3 and 6.2).



**Figure 6.7 ESI-MS analysis of reactive Cys residues in RBC rat oxyHb.** Deconvolved mass spectrum of (A) 5  $\mu$ M rat oxyHb; (B)  $\sim$ 2  $\mu$ M NEM-labelled rat oxyHb (NEM/Hb = 50); (C) 10  $\mu$ M NEM-labelled rat oxyHb (NEM/Hb = 100). Experimental procedures: (B) 76  $\mu$ M and (C) 350  $\mu$ M oxyHb prepared from rat RBCs was incubated with the indicated molar excess of NEM at RT for 30 min. Excess NEM was removed on a NAP-5 gel-filtration column or on a ZipTipC<sub>4</sub>, the samples were diluted 35-fold into 50% ACN/0.1% TFA, and directly infused at a flow rate of 1  $\mu$ L/min into the ESI source of the Q-TOF 2 mass spectrometer. The instrument parameters are given in the legend of Figure 6.2.

**Table 6.2 Amino acid sequences of the major and minor isoforms of rat Hb<sup>a</sup>**

Major isoform	$\alpha$ -chain1 (PDB:AAA41308)	1 VLSADDKTNIKN <b>C</b> WGKIGGGHGGEYGEELQ 30 31 RMFAAFPTTKTYFSHIDVSPGSAQVKAHGK 60 61 KVADALAKAADHVEDLPGALSTLSDLHAHK 90 91 LRVDPVNFKFLSH <b>C</b> LLVTLA <b>C</b> HHPGDFTPA 120 121 MHASLDKFLASVSTVLTSKYR
	$\beta$ -chain1 (PDB:P02091)	1 VHLTDAEKAAVNLWGKVPDDVGGEALGR 30 31 LLVVYPWTQRYFDSFGDLSSASAIMGNPKV 60 61 KAHGKKVINAFNDGLKHLNLTGTFEHLSE 90 91 LH <b>C</b> DKLHVDPENFRLLGNMIVIVLGHHLGK 120 121 EFTP <b>C</b> AQAQAFQKVVGAVASALAHKYH
Minor isoform	$\alpha$ -chain2 (PDB: xp_34078)	1 VLSAADKTNIKN <b>C</b> WGKIGGGHGGEYGEELQ 30 31 RMFAAFPTTKTYFSHIDVSPGSAQVKAHGK 60 61 KVADALAKAADHVEDLPGALSTLSDLHAHK 90 91 LRVDPVNFKFLSH <b>C</b> LLVTLA <b>C</b> HHPGDFTPA 120 121 MHASLDKFLASVSTVLTSKYR
	$\beta$ -chain2 (PDB: AAB30299)	1 VHLTDAEKATVSGLWGKVPDNLVGAELGR 30 31 LLVVYPWTQRYFSKFGDLSSASAIMGNPQV 60 61 KAHGKKVINAFNDGLKHLNLTGTFEHLSE 90 91 LH <b>C</b> DKLHVDPENFRLLGNMIVIVLGHHLGK 120 121 EFTPSAQAAQFQKVVGAVASALAHKYH

<sup>a</sup>Sequences from the NCBI protein database (<http://www.ncbi.nlm.nih.gov>). Cys residues are underlined in bold font.

The reactive Cys residues in Sigma rat Hb were also investigated. As shown in Figure 6.8, singly NEM-labelled  $\alpha$ - and  $\beta$ -chains were detected in a 60-min NEM/Hb

(80:1) incubation, consistent with the titration of ~2 Cys residues per Sigma Hb tetramer by DTNB (Figure 6.6).

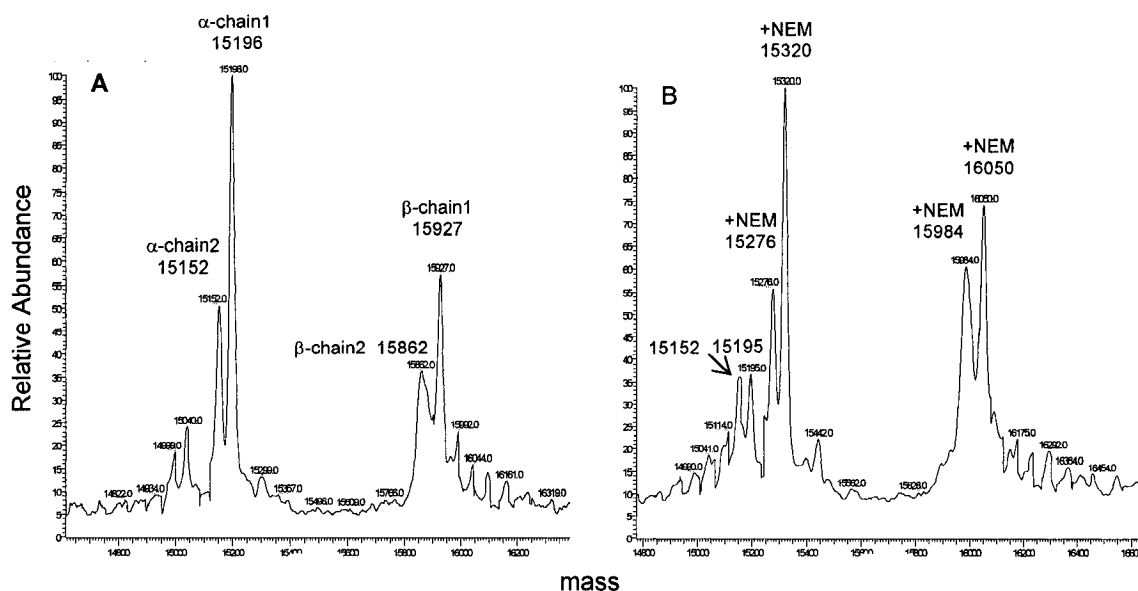


**Figure 6.8 ESI-MS analysis of reactive Cys residues in Sigma rat oxyHb.** Deconvolved mass spectrum of (A) ~20  $\mu$ M rat oxyHb; (B) ~10  $\mu$ M NEM-labelled rat oxyHb (NEM/Hb = 80). Experimental procedures: The samples were diluted 50-fold into 50% ACN/0.1% TFA, and directly infused at a flow rate of 3  $\mu$ L/min into the ESI source of the SSQ 7000 mass spectrometer. Instrument parameters: source temperature 70°C, capillary temperature 185°C, spray 4.0 kV, cone 40 V, sheath-gas 35 psi. The mass-scale calibration was carried out using myoglobin and *L*-methionyl-arginyl-phenylalanyl-alanine acetate (MRFA) as reference compounds. Protein mass spectra were deconvoluted using BioWorks software (ThermoFinnigan).

#### 6.4.3 *S*-Nitrosation and *S*-thiolation of Hb from rat RBCs

*S*-Nitrosation of rat Hb and identification of the reactive sites were carried out using oxyHb prepared from rat RBCs. The iron oxidation state of the Hb sample was checked spectrophotometrically, and the absorbance ratio at 576/541 nm was 1.06 (Figure 6.9) which is close to the value of 1.14 in the oxy-state (83). The deconvolved

mass spectra after oxyHb incubation with 10-fold molar excess GSNO  $\pm$  20  $\mu$ M BCuZnSOD are shown in Figure 6.10. An NO adduct (15,227 u) with 13% abundance relative to the unlabelled  $\alpha$ -chain1 (100%) was observed suggesting that one of the three Cys residues was *S*-nitrosated. Peaks corresponding to the  $\beta$ -chain1 plus one NO (15,878 u), plus two NO (15,907 u), plus one GS (16,153 u), plus one NO and one GS (16,183 u), and plus two GS (16,458 u) adducts were detected (Figure 6.10) indicating that the Cys residues were either *S*-nitrosated or *S*-thiolated in the GSNO incubation. The single Cys residue in the  $\beta$ -chain2 was *S*-nitrosated (15,891 u). A comparison of Figures 6.10A and B reveals that when BCuZnSOD was presented in the oxyHb/GSNO incubation the extent of nitrosation did not increase significantly.

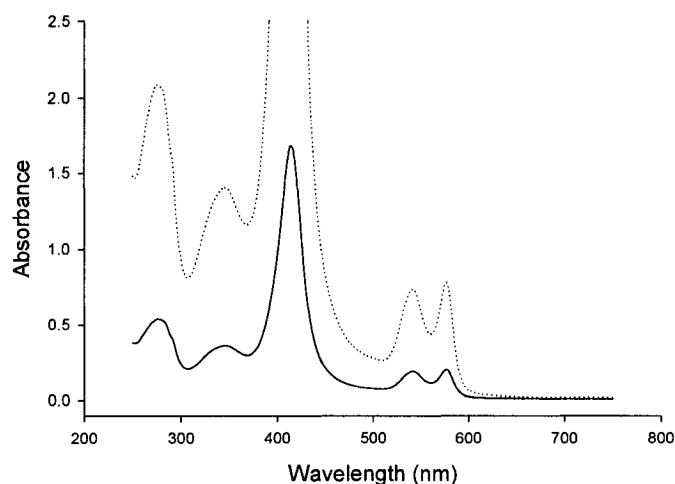
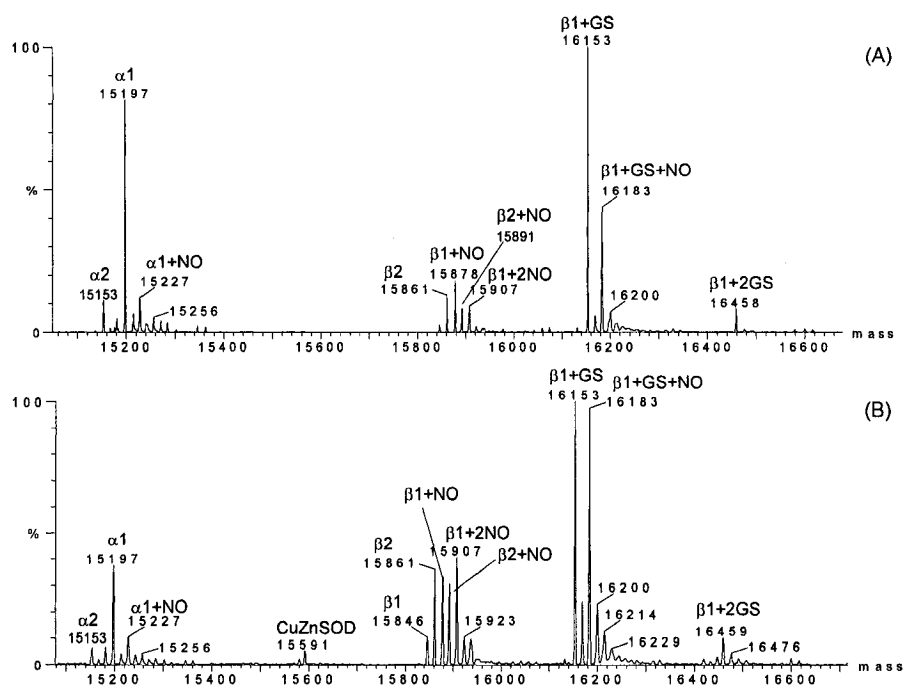


Figure 6.9 **UV-Vis spectra of rat oxyHb.** Absorbance of 4.6  $\mu$ M (solid line) and 18.4  $\mu$ M (dotted line) oxyHb in 50 mM sodium phosphate buffer (pH 7.4) was recorded in a 1-cm cuvette at RT. OxyHb was prepared from rat RBCs and CuZnSOD was removed as described in Section 6.3.2.3



**Figure 6.10 LC-ESI-MS analysis of the RBC rat oxyHb/GSNO incubation in (A) the absence and (B) the presence of BCuZnSOD.** Rat oxyHb (670  $\mu$ M) was incubated with 6.7 mM GSNO  $\pm$  20  $\mu$ M BCuZnSOD at RT for 10 min in 50 mM sodium phosphate buffer (pH 7.2). Samples for MS analysis were diluted 100-fold into 50 mM AcONH<sub>4</sub> (pH 4.0), and 3  $\mu$ L was injected into the trap *via* the autosampler. The CapLC system was equipped with a Symmetry300<sup>TM</sup> C<sub>18</sub> trap column (Waters) and the sample was eluted from the trap under a gradient of 5:5:50:95:95:5% B in 3/22/5/10/5 min at a flow rate of 1  $\mu$ L/min, where B is 90% ACN/0.1% TFA. The eluent was directly introduced into the Z-spray ESI source of the Q-TOF 2 mass spectrometer which was operated under the conditions given in the legend of Figure 6.2.

***S-Nitrosation of Sigma rat Hb.*** Samples were prepared by incubating 0.5 mM rat oxyHb with CysNO at molar ratios of 0, 2, 10, 40, or 100 in 10 mM PBS (pH 7.2) at room temperature for 30 min in the dark. Hb was purified on a Sephadex G-25 column, and its concentration was determined using the Bio-Rad protein assay. UV-Vis spectra measured before and after incubation with CysNO indicated that Hb had changed from oxy to the met state (Figure 6.11).

**Table 6.3 S-Nitrosation of Sigma rat oxyHb as determined by Saville assay**

CysNO/Hb molar ratio <sup>a</sup>	Nitrite/oxyHb (mol/mol)		SNO/HbO <sub>2</sub> <sup>b</sup> (mol/mol)
	Without Hg <sup>2+</sup>	With Hg <sup>2+</sup>	
2	0.00	0.05	0.05
10	0.33	1.21	0.88
40	0.27	3.01	2.74
100	0.35	4.40	4.05

<sup>a</sup>Hb-SNO was prepared by incubation of 0.5 mM Sigma rat oxyHb with 1.0–50 mM CysNO at RT for 30 min. Samples were desalted on a NAP-5 column and treated with ammonium sulfamate prior to analysis by the Saville assay. OxyHb exposed to the same reagents except CysNO was used as the blank. <sup>b</sup>Calculated from the difference in the nitrite measured in the presence and absence of added Hg<sup>2+</sup> (Section 6.3.2.13).

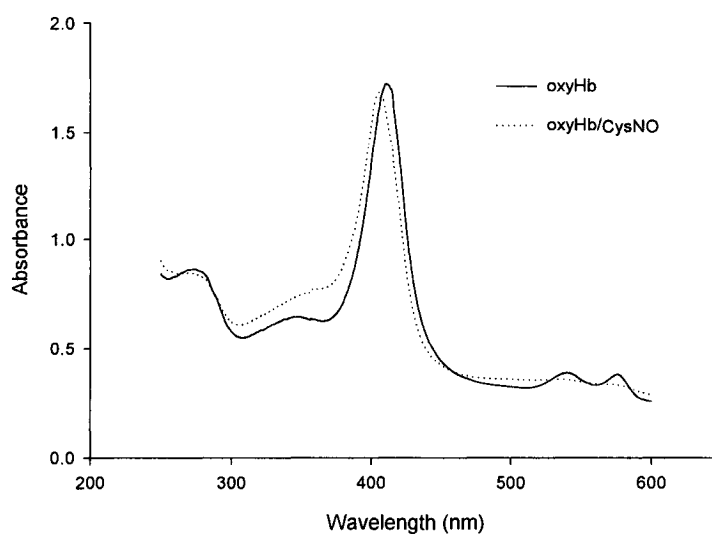


**Figure 6.11 UV-Vis spectra of Sigma rat oxyHb and Hb-SNO derivative.** Absorbance between 250 and 600 nm of 1.9  $\mu$ M of oxyHb and 2.5  $\mu$ M of oxyHb/CysNO incubate were recorded in a 1-cm cuvette. OxyHb in 10 mM phosphate buffer (pH 7.2) was prepared from rat metHb (Sigma) as described in Section 6.3.2.2, and Hb-SNO in 10 mM PBS (pH 7.2) was prepared by incubation oxyHb (Sigma) with CysNO (CysNO/Hb = 10) at RT for 30 min in the dark and purified on a NAP-10 column.

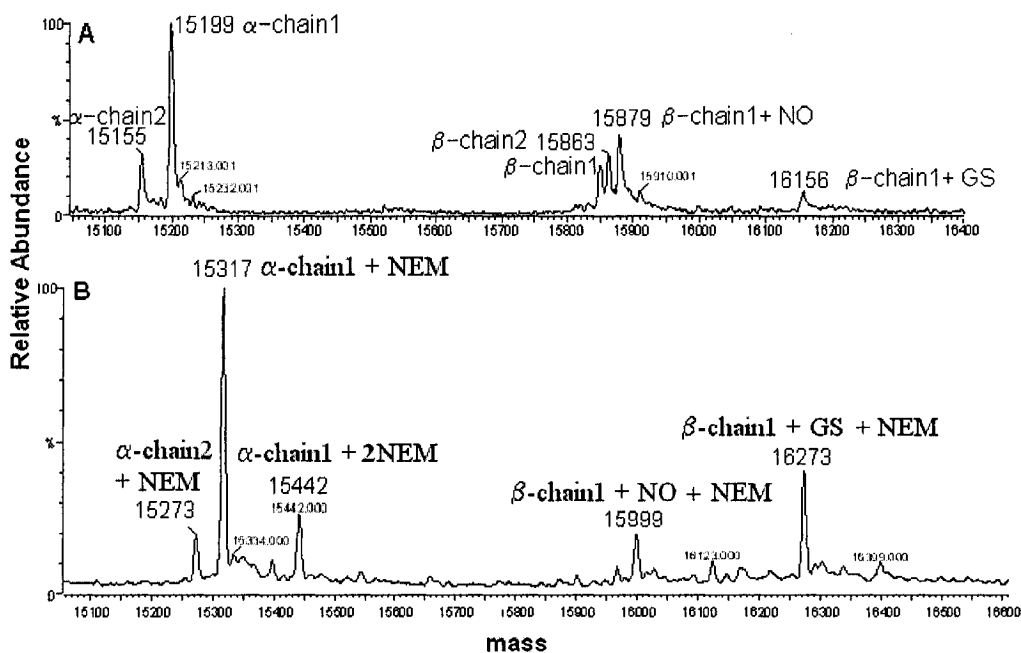


Figure 6.12 **ESI-MS analysis of GSNO and NEM-modified RBC rat oxyHb.** Mass spectrum of  $\sim 2 \mu\text{M}$  (A) Hb-SNO and (B) (Hb-SNO)-NEM. Rat oxyHb ( $76 \mu\text{M}$ ) was incubated with  $760 \mu\text{M}$  GSNO at RT for 30 min and then with  $3.8 \text{ mM}$  NEM at RT for 30 min in  $10 \text{ mM}$  sodium phosphate buffer (pH 7.2). Samples were desalted on a NAP-5 gel filtration column, diluted 38-fold into  $50\% \text{ ACN}/0.1\% \text{ TFA}$ , and directly infused at a flow rate of  $1 \mu\text{L}/\text{min}$  into the ESI source of the Q-TOF 2 mass spectrometer. The mass spectrometric conditions are given in the legend of Figure 6.2.

The amounts of Hb-SNO produced in the different incubations were determined by the Saville assay (Table 6.3). Up to 4 Cys residues in rat oxyHb were *S*-nitrosated and the extent of *S*-nitrosation was proportional to the CysNO/oxyHb ratio.

Additionally, *S*-nitrosation by a 10-fold molar excess of GSNO of  $0.2\text{--}0.7 \text{ mM}$  oxyHb from different species was compared using the Saville assay. After 30 min incubation at room temperature, the SNO/Hb ratios (mol/mol) in Sigma rat ( $0.5 \text{ mM}$ ), human adult ( $0.2 \text{ mM}$ ) and fetal ( $0.7 \text{ mM}$ ) Hb incubations were  $1.48 \pm 0.39$ ,  $0.44 \pm 0.02$ , and  $0.60 \pm 0.10$ , respectively (data not shown). The result suggests that the reactivity of the Cys residues towards *S*-nitrosation is comparable among different Hbs and consistent



**Table 6.4 Tryptic peptides of the two isoforms of rat Hb<sup>a</sup>**

$\alpha$ -chain1 mass = 15197.3 u		$\alpha$ -chain2 mass = 15153.3 u	
Sequence [residue number]	M <sub>r</sub> (u)	Sequence [residue number]	M <sub>r</sub> (u)
VLSADDK [1-7]	746.381	VLSAADK [1-7]	702.391
<u>NCWGK</u> [12-16]	606.258	<u>NCWGK</u> [12-16]	606.258
IGGHGGEYGEEALQR [17-31]	1571.733	IGGHGGEYGEEALQR [17-31]	1571.733
MFAAFPTTK [32-40]	1012.505	MFAAFPTTK [32-40]	1012.505
TYFSHIDVSPGSAQVK [41-56]	1734.858	TYFSHIDVSPGSAQVK [41-56]	1734.858
VADALAK [62-68]	686.396	VADALAK[62-68]	686.396
AADHVEDLPGALSTLSDLHAHK [69-90]	2296.145	AADHVEDLPGALSTLSDLHAHK [69-90]	2296.145
VDPVNFK [93-99]	817.433	VDPVNFK [93-99]	817.433
<u>FLSHCLLVTLACHHPGDFTPAMHASLDK</u> [100-127]	3060.477	<u>FLSHCLLVTLACHHPGDFTPAMHASLDK</u> [100-127]	3060.477
FLASVSTVLTSK [128-139]	1251.707	FLASVSTVLTSK [128-139]	1251.707
$\beta$ -chain1 mass = 15848.2 u		$\beta$ -chain1 mass = 15861.2 u	
Sequence [residue number]	M <sub>r</sub> (u)	Sequence [residue number]	M <sub>r</sub> (u)
VHLTDAEK [1-8]	911.471	VHLTDAEK [1-8]	911.471
AAVNLWGK [9-17]	914.497	ATVSGLWGK [9-17]	917.497
VNPDDVGGEALGR [18-30]	1297.626	VNPDNVGAEALGR [18-30]	1310.658
LLVVYPWTQR [31-40]	1273.718	LLVVYPWTQR [31-40]	1273.718
YFDSFGDLSSASAIMGNPK [41-59]	2005.909	FGDLSSASAIMGNPQVK [45-61]	1720.845
VINAFNDGLK [67-76]	1089.582	VINAFNDGLK [67-76]	1089.582
HLDNLK [77-82]	738.402	HLDNLK [77-82]	738.402
<u>GTF AHLSELHCDK</u> [83-95]	1456.677	<u>GTF AHLSELHCDK</u> [83-95]	1456.677
LHVDPENFR [96-104]	1125.557	LHVDPENFR [96-104]	1125.557
LLGNMIVIVLGHHLGK [105-120]	1713.012	LLGNMIVIVLGHHLGK [105-120]	1713.012
<u>EFTPSAQAAFQK</u> [121-132]	1339.623	<u>EFTPSAQAAFQK</u> [121-132]	1323.646
VVAGVASALAHK [133-144]	1121.656	VVAGVASALAHK [133-144]	1121.656

<sup>a</sup>Peptides with masses > 600 u are listed, and those containing Cys residues (bold font) are underlined. The data source is given in the footnote to Table 6.2.

with the greater number of free Cys residues in rat Hb (Table 3.1). The higher level of S-nitrosation in the rat Hb/GSNO incubation compared to the incubation with 10-fold molar excess CysNO (0.88 mol/mol, Table 6.3) may be due to incomplete removal of GSNO which is more stable than CysNO.

Table 6.5 **Glu-C peptides of the two isoforms of rat Hb<sup>a</sup>**

$\alpha$ -chain1 mass = 15197.3 u		$\alpha$ -chain2 mass = 15153.3 u	
Sequence [residue number]	M <sub>r</sub> (u)	Sequence [residue number]	M <sub>r</sub> (u)
<u>VLSADDKTNIKNCWGKIGGHGGE</u> [1-23]	2398.170	<u>VLSAADKTNIKNCWGKIGGHGGE</u> [1-23]	2354.18
ALQRMFAAFPTTKTYFSHIDVSPGSAQVKAHGKKVA DALAKAADHVE [28-74]	5009.5973	ALQRMFAAFPTTKTYFSHIDVSPGSAQVKAHGKKVA DALAKAADHVE [28-74]	5009.597
<u>DLPGALSTLSDLHAHKLRVDPVNFKFLSHCLLVTLAC</u> <u>HHPGDFTPAMHASLDKFLASVSTVLTSKYR</u> [75-141]	7337.809	<u>DLPGALSTLSDLHAHKLRVDPVNFKFLSHCLLVTLAC</u> <u>HHPGDFTPA MHASLDKFLASVSTVLTSKYR</u> [75-41]	7337.809
$\beta$ -chain1 mass = 15848.2 u		$\beta$ -chain1 mass = 15861.2 u	
Sequence [residue number]	M <sub>r</sub> (u)	Sequence [residue number]	M <sub>r</sub> (u)
VHLTDAE [1-7]	783.376	VHLTDAE [1-7]	783.376
KAAVNGLWGKVNPDVVGGE [8-26]	1924.964	KATVSGLWGKVNPDNVGAE [8-26]	1940.995
ALGRLLVVYPWTQRYFDSFGDLSSASAIMGNPKVKA HGKKVINAFNDGLKHLNKGTF AHLSE [27-90]	7041.687	ALGRLLVVYPWTQRYFSKFGDLSSASAIMGNPKVKA HGKKVINAFNDGLKHLNKGTF AHLSE [27-90]	7054.718
LHCDKLHVDPE [91-101]	1304.618	<u>LHCDKLHVDPE</u> [91-101]	1304.618
NFRLLGNMIVIVLGHHLGKE [102-121]	2259.267	NFRLLGNMIVIVLGHHLGKE [102-121]	2259.267
FTPCAQAFAFQKV VAGVASALAHKYH [122-146]	2614.348	FTPSQAFAFQKV VAGVASALAHKYH [122-146]	2598.371

<sup>a</sup>Peptides with masses > 600 u are listed, and those containing Cys residues (bold font) are underlined. The data source is given in the footnote to Table 6.2.

#### 6.4.4 Identification of the sites of rat Hb *S*-nitrosation and *S*-thiolation by MALDI-ToF-MS

The sites of rat Hb *S*-nitrosation was first investigated in the singly *S*-nitrosated and *S*-thiolated protein (Figure 6.12A) prepared by incubation of RBC oxyHb with 10-fold molar excess of GSNO. Since the S-NO bond in *S*-nitrosated Hb is light, heat, and pH-sensitive, the *S*-nitrosation site cannot be directly determined by MALDI-MS. To overcome this problem, an indirect method was used here. Following *S*-nitrosation, the remaining unreacted thiols in singly labelled Hb-SNO were blocked by incubation with a 50-fold molar excess of NEM in 10 mM PBS (pH 7.2) at room temperature for 30 min. ESI-MS analysis of the product (Hb-SNO)-NEM (Figure 6.12B) reveals that only Cys

residues in the  $\beta$ -chain were NO- or GS-labelled and the unreacted Cys residues in  $\alpha$ - and  $\beta$ -chains were NEM-labelled. Untreated Hb, fully NEM-labelled Hb-NEM, Hb-SNO, and (Hb-SNO)-NEM were digested with trypsin or Glu-C. The mass shifts of the Cys-containing peptides were compared, and those with a 125-u mass shift in the Hb-NEM but not the (Hb-SNO)-NEM mass fingerprint are assumed to contain a *S*-nitrosation site.

The  $\alpha$ - and  $\beta$ -chains of the two isoforms of rat Hb from RBCs identified by ESI-MS (Figure 6.7A) yielded the Glu-C and tryptic peptides listed in Tables 6.4 and 6.5, respectively. Peptides with mass < 600 u are not listed and the sequence coverage from the tryptic digest was 82%. The 4 missing peptides include a peptide containing Cys $\beta$ 125 (E<sub>121</sub>FTPCAQAAFQK<sub>132</sub>, M<sub>r</sub> 1339.623 u) (Table 6.4). The Cys-containing tryptic peptides from the Hb-NEM and (Hb-SNO)-NEM digests (Table 6.6) reveal that no labels were detected on peptide F<sub>100</sub>LSHCLLVTLACHHPGDFTPAMHASLDK<sub>127</sub> (M<sub>r</sub> 3060.477 u) indicating that Cys $\alpha$ 104 and Cys $\alpha$ 111 are unreactive towards both GSNO and NEM. Peptide N<sub>12</sub>CWGGK<sub>16</sub> (M<sub>r</sub> 606.258 u) was singly NEM labelled in both the Hb-NEM and (Hb-SNO)-NEM fingerprints indicating that Cys $\alpha$ 13 was not *S*-nitrosated by GSNO consistent with the results shown in Figure 6.12B. Likewise, peptide G<sub>83</sub>TFAHLSELHCDK<sub>95</sub> (M<sub>r</sub> 1456.677 u) was singly NEM-labelled in the Hb-NEM and (Hb-SNO)-NEM fingerprints indicating that Cys $\beta$ 93 was not *S*-nitrosated or *S*-thiolated by GSNO. Although tryptic peptide E<sub>121</sub>FTPCAQAAFQK<sub>132</sub> was not detected in the mass fingerprint of the  $\beta$ -chain1, singly-NO and GS-labelled derivatives were observed in the spectra of intact Hb-SNO (Figure 6.12A) and (Hb-SNO)-NEM (Figure 6.12B), and Cys $\beta$ 125 is considered the likely site of *S*-nitrosation and *S*-glutathiolation.

**Table 6.6 MALDI-MS analysis of Cys-containing tryptic peptides of rat Hb-NEM and (Hb-SNO)-NEM<sup>a</sup>**

Chain	Peptide sequence <sup>b</sup> (residue number)	Calc MH <sup>+</sup> <sup>c</sup>	Observed MH <sup>+</sup> <sup>d</sup>		$\Delta m$	Assigned modification
$\alpha 1 \& \alpha 2$	NCWGK (12–16)	607.258	Hb-NEM	732.18	125	NEM
			(Hb-SNO)-NEM	732.06	125	NEM
$\alpha 1 \& \alpha 2$	FLSH <u>C</u> LLVTLA <u>C</u> HHPGDFT PAMHASLDK (100–127)	3061.477	Hb-NEM	3061.45	0	none
			(Hb-SNO)-NEM	3061.45		
$\beta 1 \& \beta 2$	GTFAHLSELH <u>C</u> DK(8395)	1457.677	Hb-NEM	1583.01	126	NEM
			(Hb-SNO)-NEM	1582.68	125	NEM
$\beta 1$	EFTP <u>C</u> AQAAFQK(121–132)	1340.623	Hb-NEM	ND	--	--
			(Hb-SNO)-NEM	ND	--	--

<sup>a</sup>Proteins (3–4.6  $\mu\text{g}/\mu\text{L}$ ) in 100 mM  $\text{NH}_4\text{HCO}_3$  buffer (pH ~8.5) were incubated with trypsin (40:1, w/w) at 37°C overnight. Preparation of the Hb-NEM and (Hb-SNO)-NEM samples is described in the legends of Figures 6.7B and 6.12B, respectively. <sup>b</sup>Cys-containing peptides from the Hb digests; Cys residues are in bold underlined font. <sup>c</sup>Calculated monoisotopic masses of the singly protonated ions ( $\text{MH}^+$ ) of the tryptic peptides. <sup>d</sup>Observed monoisotopic masses of the  $\text{MH}^+$  ions.

To further identify the reaction sites of rat oxyHb with GSNO, Glu-C was used to digest the protein (Table 6.5). The sequence coverage was ~82% with two missing peptides ( $M_r > 7000$  u). Table 6.7 lists the Cys-containing peptides detected in the MALDI mass fingerprints of the  $\alpha$ - and  $\beta$ -chains from the Glu-C digests of native rat Hb and its derivatives.

The Cys $\alpha 13$ -containing peptides in  $\alpha$ -chain1 and  $\alpha$ -chain2 as well as the Cys $\beta 93$ -containing peptide were found to be singly NEM-labelled in both the Hb-NEM and (Hb-SNO)-NEM fingerprints (Table 6.7). However, partially *S*-glutathiolated Cys $\beta 93$  was detected in the Hb-SNO and (Hb-SNO)-NEM fingerprints (Table 6.7), suggesting that this residue reacts to some extent with GSNO before incubation with

**Table 6.7 MALDI-MS analysis of the Cys-containing Glu-C peptides from rat oxyHb and its derivatives**

Sample <sup>a</sup>		Peptide Sequence <sup>b</sup> (residue numbers)	Calc MH <sup>+c</sup>	Observed MH <sup>+d</sup>	Δm	Label
Hb	α1	VLSADDK <b>T</b> NIK <b>N</b> CWGKI GGHGGE (1-23)	2399.17	2399.21	0.04	none
Hb-SNO	α1			2398.77	-0.40	none
Hb-NEM	α1			2524.39	125.22	NEM
(Hb-SNO)-NEM	α1			2523.59	124.42	NEM
Hb	α2	VLSAADK <b>T</b> NIK <b>N</b> CWGKI GGHGGE (1-23)	2355.18	2355.25	0.07	none
Hb-SNO	α2			2354.76	-0.42	none
Hb-NEM	α2			2480.38	125.20	NEM
(Hb-SNO)-NEM	α2			2479.59	124.41	NEM
Hb	β1&β2	LH <b>C</b> DKLHVDPE (91-101)	1305.62	1305.68	0.06	none
Hb-SNO	β1&β2			1305.47	-0.15	none
				610.50	304.88	GS
Hb-NEM	β1&β2			1430.80	125.18	NEM
(Hb-SNO)-NEM	β1&β2			1430.43	124.81	NEM
				1610.42	304.80	GS
Hb	β1	FTP <b>C</b> AQA <b>F</b> QKV <b>V</b> AGVA SALAHKYH (122-146)	2615.35	2615.39	0.04	none
Hb-SNO	β1			2614.86	-0.49	none
				2919.89	304.54	GS
Hb-NEM	β1			2740.62	125.27	NEM
(Hb-SNO)-NEM	β1			2614.72	-0.63	none
				2920.63	305.28	GS

<sup>a</sup>Hb, Hb-NEM, Hb-SNO, and (Hb-SNO)-NEM samples from Figures 6.7A, 6.7B, 6.12A, and 6.12B, respectively. Proteins were desalted on a NAP-5 column and concentrated by ultrafiltration (12,000 rpm, 8 min, Ultrafree-0.5, Millipore). Endoproteinase Glu-C digestion was carried out in 50 mM ammonium acetate (pH 4.0) at 35°C for 2-4 h at a Hb/Glu-C ratio of 20/1(w/w), ~1  $\mu$ L of the digests was mixed with 9  $\mu$ L of matrix solution (10 mg/ml  $\alpha$ -CHCA in 2:1 acetonitrile/0.1%TFA), 1  $\mu$ L of the mixture was spotted onto a 100-well MALDI plate and air-dried. <sup>b</sup>Sequences from the NCBI protein database (<http://www.ncbi.nlm.nih.gov>) (Table 6.2); Cys residues are in bold underlined font. <sup>c</sup>Calculated monoisotopic masses of the singly protonated ions (MH<sup>+</sup>) of the Glu-C peptides. <sup>d</sup>Observed monoisotopic masses of the MH<sup>+</sup> ions

NEM. NEM-labelled Cys $\beta$ 125 peptide was not found in the (Hb-SNO)-NEM fingerprint of isoform1 but was present in the Hb-NEM fingerprint (Figure 6.12). Also, this peptide

was found to be *S*-glutathiolated in Hb-SNO from the Hb/GSNO and (Hb-SNO)/NEM incubations indicating that Cys $\beta$ 125 is *S*-nitrosated and *S*-glutathiolated at a GSNO/Hb ratio of 10:1 (Figures 6.10 and 6.12).

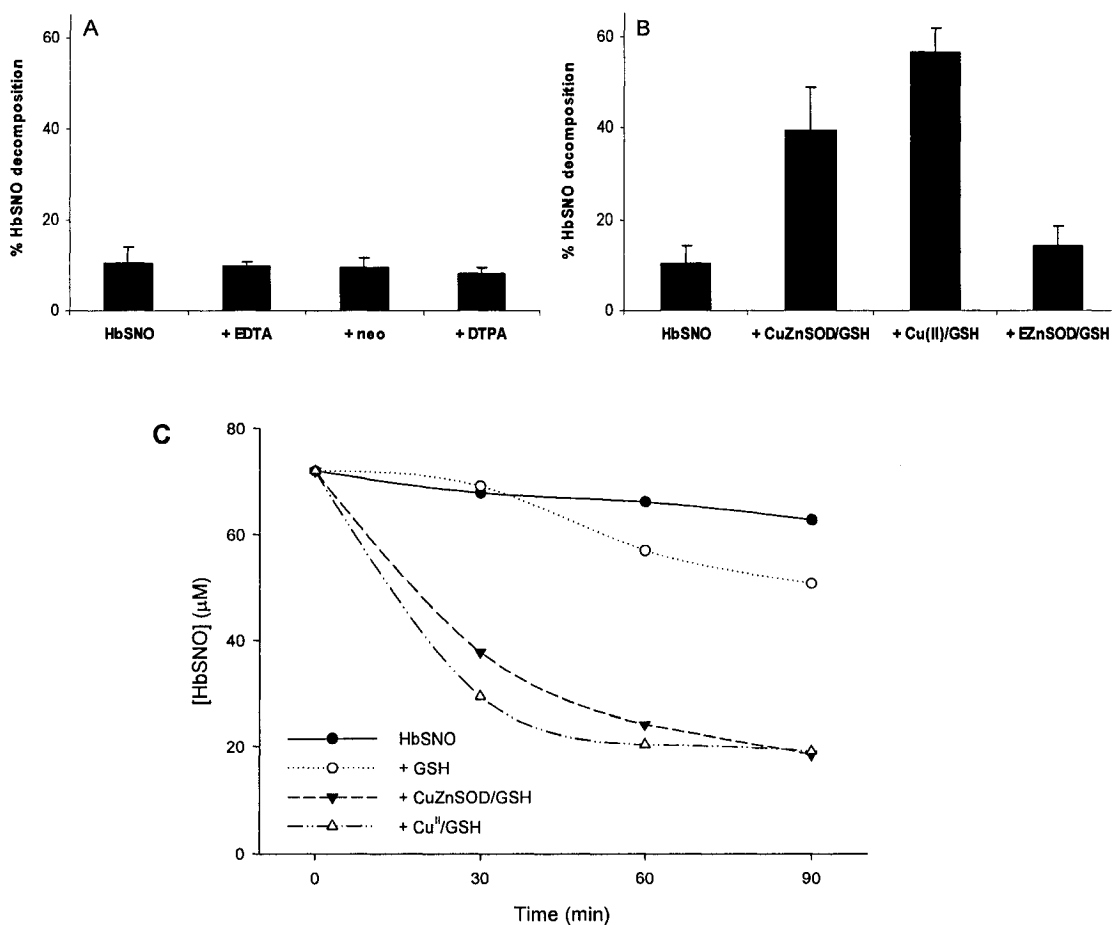


**Figure 6.13 Effects of GSH, chelators, CuSO<sub>4</sub>, and BCuZnSOD on NO release from Sigma rat metHb-SNO.** The %Hb-SNO decomposition in incubations of 40–72 μM metHb-SNO with (A) 10 mM PBS only, plus 200 μM EDTA, 200 μM DTPA, 500 μM neocuproine, (B) 125 μM GSH plus 5 μM CuSO<sub>4</sub>, 10 μM BCuZnSOD, 20 μM BEZnSOD. (C) [Hb-SNO] vs time of the samples in B was measured by the Saville assay after incubation at 37°C for 0–90 min. Experimental procedures: Sigma rat oxyHb was prepared as described in Section 6.3.2.1. Hb-SNO was prepared by incubating oxyHb (200–300 μM) with CysNO at RT for 30 min in 10 mM PBS (pH 7.2) as described in Section 6.3.2.4. The %Hb-SNO breakdown was calculated from the SNO concentration determined by the Saville assay before and after 30-min incubation with the reagents indicated in the figure. The results are the averages of 1–4 measurements.

#### 6.4.5 Determination of NO release from Sigma rat Hb-SNO

Hb-SNO was prepared by incubation of 180  $\mu\text{M}$  Sigma rat oxyHb with 70-fold molar excess of CysNO at room temperature for 30 min. After desalting on a NAP-10 G-25 column, the *S*-nitroso content was determined by the Saville assay, and the NO released from 40–70  $\mu\text{M}$  Hb-SNO were examined. As indicated in the figure legends, the solutions also contained 125  $\mu\text{M}$  GSH, 10  $\mu\text{M}$  BCuZnSOD, 5  $\mu\text{M}$   $\text{Cu}^{2+}$ , 200  $\mu\text{M}$  EDTA, 200  $\mu\text{M}$  DTPA, or 500  $\mu\text{M}$  neocuproine, and the *S*-nitroso content before and after 30 min incubation at 37°C was determined.

***Effect of metal chelators on NO release from Hb-SNO*** ~10% Hb-SNO was decomposed over 30 min incubation at 37°C. Decomposition was inhibited by ~5–22% in the presence of the chelators (Figure 6.13A), with DTPA being more effective than the others.

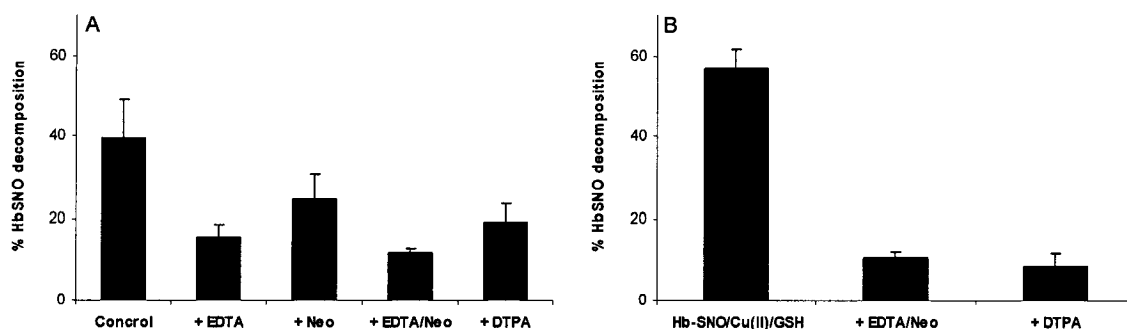


Figure 6.14 Effects of EDTA, DTPA, and neocuproine on (A) BCuZnSOD- and (B)  $\text{CuSO}_4$ -catalyzed NO release from Sigma rat methHb-SNO. The chelators (200–500  $\mu\text{M}$ ) were added to the incubations and the experimental procedures are given in the legend of Figure 6.13. “Control” in (A) denotes the Hb-SNO/BCuZnSOD/GSH incubation.

#### ***Effects of added free copper and BCuZnSOD on NO release from Hb-SNO.***

Samples containing 40–75  $\mu\text{M}$  rat methHb-SNO with/without 5  $\mu\text{M}$   $\text{CuSO}_4$  or 10  $\mu\text{M}$

BCuZnSOD dimer were incubated with 125  $\mu$ M GSH in 10 mM PBS buffer (pH 7.2) at 37°C for 30 min. Breakdown of  $39.33 \pm 9.46\%$  and  $56.32 \pm 5.44\%$  Hb-SNO occurred in the presence of BCuZnSOD and  $\text{Cu}^{\text{II}}$ , respectively, compared to  $10.25 \pm 3.74\%$  in GSH only and  $14 \pm 4.42\%$  in the presence of copper-free enzyme (EZnSOD) (Figure 6.14). These results reveal the significant role of free copper and active-site copper in the modulation of NO release from rat metHb-SNO *in vitro*.

***Effects of chelators on free copper- and BCuZnSOD-catalyzed NO release from Hb-SNO.*** Figure 6.14A shows that the %Hb-SNO decomposition in metHb-SNO/GSH/BCuZnSOD was  $15.2 \pm 3.25\%$ ,  $19.2 \pm 4.99\%$ ,  $24.9 \pm 6.05\%$ , and  $11.4 \pm 1.29\%$  in the presence of EDTA, DTPA, neocuproine, and EDTA + neocuproine, respectively. Thus, the chelators inhibit CuZnSOD-catalyzed decomposition of metHb-SNO in addition to inhibiting GSNO breakdown (Chapter 2.0, Figure 2.5). Free-copper-catalyzed decomposition of metHb-SNO was also inhibited by the chelators (Figure 6.14B). Both DTPA and EDTA/neocuproine (200–500  $\mu$ M) are effective inhibitors of  $\text{CuSO}_4$ -catalyzed Hb-SNO decomposition decreasing breakdown from 56% to 10%.

## 6.5 Discussion

### 6.5.1 Comparison of Cys reactivity in rat and human Hbs

Hb is a tetrameric protein composed of two  $\alpha$ - and two  $\beta$ -chains and each chain contains a heme group. Cys residues in Hb from different species are not identical but Cys $\beta$ 93 is highly conserved. Human adult Hb (HbA) contains three pairs of Cys residues, Cys $\beta$ 93, Cys $\beta$ 112, and Cys $\alpha$ 104. Rat Hbs are unusually heterogeneous with two  $\alpha$ -chains and at least three  $\beta$ -chains that are structurally different (272, 281-285). The



primary structure of the major  $\beta$ -chain and the partial sequences of two  $\alpha$ -chains have been reported (282, 283). The Cys residues in the  $\alpha$ -chain at positions 13, 104, and 111 (283, 286), and in the major  $\beta$ -chain at positions 93 and 125 (282) have been characterized.

It has been demonstrated that Cys $\beta$ 125 and Cys $\alpha$ 13 are more reactive than Cys $\beta$ 93 of human Hb. The remarkable reactivity of Cys $\beta$ 125 is due to its low  $pK_a$  ( $\sim 6.9$ ) and its high accessibility, which leads to its various reactions (29, 79, 83, 271-273, 287-289). For example, mixed disulfides formed with GSH (HbSSG) when rat but not human RBCs were treated with the intracellular thiol-oxidizing diazenes (diazenedicarboxylic acid *bis-N,N*-dimethylamide and diazenedicarboxylic acid *bis-N'*-ethylpiperazine) (287). Rossi *et al.* (273) confirmed that diamide and other oxidizing agents such as hydrogen peroxide, *tert*-butyl hydroperoxide, and menadione were more reactive with one of the thiol groups in rat Hb than with GSH. *S*-Conjugation of DTNB to Cys $\beta$ 125 ( $2.94 \times 10^4 \text{ M}^{-1}\text{s}^{-1}$ ) (83) is faster than with any previously characterized protein thiol, and an order of magnitude faster than with GSH ( $2.6 \times 10^3 \text{ M}^{-1}\text{s}^{-1}$ ) (83). Also, DTNB conjugation is independent of oxygen binding to rat Hb.

Two isoforms of the  $\alpha$ -chain with masses of 15,197 u ( $\alpha$ -chain1) and 15,153 u ( $\alpha$ -chain2) were detected in the ESI mass spectra of Hb from rat RBCs and from Sigma (Figures 6.7A and 6.8A) in agreement with the literature report (283). Consistent with the presence of Cys $\alpha$ 13, Cys $\alpha$ 104 and Cys $\alpha$ 111 (286), up to three NEM-labels were observed in the major  $\alpha$ -chain1 but only two in the minor  $\alpha$ -chain2 (Figure 6.7C) indicating that the Cys residues in two different isoforms of rat Hb have different reactivity. At low NEM/Hb ratios, only a single adduct was observed (Figures 6.7B and

6.8B) suggesting that one of the three Cys residues in the  $\alpha$ -chains is more reactive than the other two. Tryptic peptide mass fingerprinting of the Hb-NEM digest revealed that Cys $\alpha$ 13 of both  $\alpha$ -chains was NEM-labelled (Table 6.6) indicating that this Cys residue is far more reactive than Cys $\alpha$ 104 or Cys $\alpha$ 111. This is in agreement with the literature data that Cys $\alpha$ 104 and Cys $\alpha$ 111 are masked sulfhydryl groups located at the  $\alpha_1\beta_1$  interface and that their reactivity is controlled by the tetramer dissociation beyond the dimer stage (83, 290). An important role for Cys $\alpha$ 13 in the crystallization of rat Hb has been reported by Chua *et al.* (286), who found that the protein crystallized rapidly at low pH but this is prevented by Cys $\alpha$ 13 ionization on raising the pH to 8.6. The ionized side chain presumably swings to the exterior of the molecule, and this can be suppressed by alkylation with iodoacetamide (286).

Two  $\alpha$ - and four  $\beta$ -chains have been characterized by reversed-phase HPLC of Hb from Sprague-Dawley rats (272). Cys $\beta$ 93 is present in all four  $\beta$ -chain isoforms but Cys $\beta$ 125 exists in three of the four isoforms (83, 272, 282, 285). In the present study, only two  $\beta$ -isoforms with masses of 15,848 u ( $\beta$ -chain1) and 15,861 u ( $\beta$ -chain2) were detected in Hb from Sprague-Dawley rat RBCs (Figure 6.7A). Sigma Hb also possessed two  $\beta$ -isoforms with masses of 15,927 u ( $\beta$ -chain1) and 15,862 u ( $\beta$ -chain2) (Figure 6.8A). While the  $\beta$ -chain1 isoforms have different masses ( $\Delta m = 79$  u),  $\beta$ -chain2 from the two Hb samples was identical in mass and contained one reactive Cys residue (Figures 6.7B&C and 6.8B). As shown in Figures 6.7B,C vs 6.8B, singly and doubly NEM-labelled  $\beta$ -chain1 was observed in the rat Hb samples from Sigma and RBCs, respectively, suggesting that Cys $\beta$ 125 was not present in the Sigma protein. The observed

$\Delta m$  suggests that the  $\beta$ -chain1 in the Sigma and RBC rat Hbs used here may be different isoforms.

DTNB titrations were also carried out to determine the reactive Cys residues in Hb from various sources. Over 30-min incubation,  $3.97 \pm 0.30$  Cys residues in rat RBC oxyHb, and  $2.28 \pm 0.13$  Cys residues in Sigma rat Hb were titrated by DTNB (Figures 6.5 and 6.5) revealing double the number of reactive Cys residues in the former. The fast titration of RBC Hb vs Sigma Hb (solid circles, Figures 6.5 vs 6.6) suggests that Cys $\beta$ 125 is absent from the Sigma protein, consistent with the mass spectral results. In contrast to rat Hb, only  $0.72 \pm 0.04$  Cys residues were titrated by DTNB under the same conditions in human HbA. Thus, in addition to the presence of highly reactive Cys $\beta$ 125, it is possible that Cys $\beta$ 93 is more reactive in rat vs human Hb. Clearly, *S*-nitrosation and *S*-glutathiolation are expected to differ considerably in the rat and human proteins as reported (29, 273)

### 6.5.2 *S*-Nitrosation of rat vs human Hbs

The mechanism by which Hb-SNO is formed *in vivo* and the route by which the NO moiety is released are not clear. To elucidate possible mechanisms underlying these processes, formation of Hb-SNO by incubation of oxyHb with the low-molecular-weight RSNOs, GSNO and CysNO, as well as dissociation of NO from Hb-SNO *via* a thiol-dependent mechanism were investigated (72). The present Saville assay data (Table 6.3) indicating that ~1–4 Cys residues are *S*-nitrosated in the Sigma rat oxyHb incubations with 10–100-fold molar excess CysNO are in close agreement with the Saville assay and LC-MS results of Wolzt *et al.* (72). They found that 0.69 Cys residues on the  $\beta$ -chain are *S*-nitrosated in a 1:4 human oxyHb/CysNO incubation whereas 2.34 Cys residues are

modified in a 1:40 human oxyHb/CysNO incubation (72). Singly and doubly *S*-nitrosated Cys residues on the  $\beta$ -chain account for most of the NO adducts but the  $\alpha$ -chain thiols also formed NO adducts. Our data (Table 6.3) and that of Wolzt *et al.* (72) clearly indicate that Cys $\beta$ 93 is not the only *S*-nitrosated residue when oxyHb is exposed to high concentrations of CysNO (CysNO/oxyHb, 40:1) (72). Thus, *S*-nitrosation of human and rat Hb is similar when Cys $\beta$ 125 is absent from the protein such as in the case for Sigma Hb.

However, our data for rat Hb containing the highly reactive Cys $\beta$ 125 with GSNO as NO donor are not consistent with the published data for human Hb (57, 72). In contrast to the report from Woltz *et al.* that a single NO-adduct (43%) and a single GS-adduct (28%) formed on the  $\beta$ -chain (most likely at Cys $\beta$ 93) in 1:40 (but not 1:4) human oxyHb/GSNO incubations (72), peaks corresponding to single and double NO adducts, single and double GS adducts, and NO/GS mixed adducts of the  $\beta$ -chain were detected here (Figure 6.10). In addition, a low abundant NO-adduct on the  $\alpha$ -chain was detected revealing that the Cys residues in rat Hb are more susceptible to *S*-nitrosation using GSNO as a donor.

### **6.5.3 Role of CuZnSOD**

A role for CuZnSOD in the *S*-nitrosation of Cys residues, especially Cys $\beta$ 93 in human Hb was reported by Gow *et al.* (64) and a possible mechanism was proposed by Romeo *et al.* (Reactions 1.19–1.20) (57). An attempt was made here to evaluate the amount of CuZnSOD in rat RBCs and, by introducing BCuZnSOD into the reaction mixtures, to explore the role of CuZnSOD in the *S*-nitrosation and denitrosation of rat Hb. We found  $\sim 5 \mu\text{M}$  CuZnSOD dimer in rat RBCs which is close to the reported copper

concentration (5 – 10  $\mu$ M) in human erythrocytes (60) but inconsistent with a previous report (59) that CuZnSOD level are higher in rat than in human RBCs (Table 1.2).

No significant difference in the *S*-nitrosation of oxyHb from rat RBCs by 10-fold excess GSNO was observed in the presence and absence of 20  $\mu$ M BCuZnSOD (Figure 6.10A vs B). Peaks corresponding to one or two NO-adducts on the  $\beta$ -chain1 and one NO-adduct on the  $\beta$ -chain2 were detected in both incubations consistent with two and one reactive Cys residues in isoforms 1 and 2, respectively (Figures 6.7B and C). Cys $\beta$ 125 and/or Cys $\beta$ 93 appear to be susceptible to *S*-nitrosation by a copper-independent mechanism suggesting that CuZnSOD may play a minimal role in the *S*-nitrosation of Hb from rat RBCs. Peptide mass fingerprinting of the singly *S*-nitrosated  $\beta$ -chain1 (Figure 6.12) confirmed the literature report that Cys $\beta$ 125 is the most reactive thiol in rat Hb (83, 271), and the data shown in Tables 6.6 and 6.7 indicate that NO is targeted to Cys $\beta$ 125 rather than Cys $\beta$ 93.

#### 6.5.4 *Trans-S*-nitrosation and *S*-thiolation of rat RBC Hb

NO-group transfer between *S*-nitrosothiols and thiols *via trans-S*-nitrosation ( $\text{RSNO} + \text{R'SH} \rightleftharpoons \text{RSH} + \text{R'SNO}$ ) has been proposed (29, 31, 291-293). This reaction is considered to be important under physiological conditions and closely related to the biological effects of Hb-SNO (26, 293, 294). Literature data suggest that this reaction occurs *via* the thiolate anion since the rate constants are pH dependent (291). Moreover, the reaction is more favored for thiols with low  $\text{p}K_a$  and high accessibility (31, 291). Our results suggest that *S*-nitrosation of Cys residues in rat oxyHb occurs *via trans-S*-nitrosation (Reaction 1.4). Cys $\beta$ 125 has an apparent  $\text{p}K_a$  of 6.89, which is lower than of GSH ( $\text{p}K_a = 8.9$ ) and of other protein thiols plus its large solvent exposure (83, 271)

support Cys $\beta$ 125 being the major target site for NO transfer from GSNO (Tables 6.6 and 6.7).

Our hypothesis that RBC CuZnSOD likely plays a role in channeling NO from GSNO to Cys $\beta$ 93 of human oxyHb stems from observations made at physiological concentrations of the protein (57). For example, in a solution containing 3.75 mM oxyHb (15 mM heme, 7.5 mM Cys $\beta$ 93) with 3.75 mM or 7.5 mM GSNO (57), one or both Cys $\beta$ 93 residues were *S*-nitrosated and no methHb formation caused by NO depletion (Reaction 1.14) was observed. The data observed here for rat Hb do not support our hypothesis derived from studies on human Hb (57). This might be due to species differences in thiol reactivity, the lower physiological Hb concentrations and the large excess of GSNO used in the rat Hb experiments. As the rat oxyHb concentration was < 1 mM and the Cys $\beta$ 93/GSNO ratio was 1:5, Hb-SNO was not the exclusive product. MetHb was detected in the reaction mixture (Figure 6.11) similar to the observations at low concentrations of human oxyHb (57). The rat oxyHb reaction should be investigated at high Hb concentrations and in the presence of chelators to eliminate the effects of trace copper in the reagents. However, the gradients in circulating Hb-SNO in rodents (70–800 nM) compared to humans (< 1 nM) Hb (79) support marked differences in the reactivity and mechanism toward NO donors between human and rat Hb. As discussed in Section 1.5.4 and repeated here (Figure 6.5 and 6.6), rat Hb possesses four reactive Cys residues vs 0.7 in human Hb.

*S*-Glutathiolation by GSNO has been reported for several proteins, including glycogen phosphorylase b, H-ras, carbonic anhydrase III, recombinant human brain calbindin D<sub>28K</sub> (rHCBP), glyceraldehyde-3-phosphate dehydrogenase (GAPDH), and

human CuZnSOD (213, 295). Tao *et al.* (213) and Ji *et al.* (295) reported more effective *S*-glutathiolation in decomposed vs fresh GSNO solutions due to the presence of higher amount of GS(O)SG (glutathione disulfide *S*-oxide), which is a potent *S*-glutathiolation agent (213). However, the reactivity and environment of thiols in proteins is controlled by several factors that can result in either *S*-nitrosation or *S*-thiolation. For example, *S*-glutathiolated H-ras and carbonic anhydrase III have been detected in freshly prepared solution of GSNO (295). One of the five Cys residues in rHCaBP is susceptible to *S*-glutathiolation (213) as in Cys $\beta$ 93 of human oxyHb (72). The latter was *S*-glutathiolated on incubation of human oxyHb with 40-fold excess GSNO (72). Two Cys residues in the  $\beta$ -chain1 of rat Hb are readily *S*-glutathiolated on incubation with 10-fold excess GSNO (Figures 6.10A and B, Table 6.7). Clearly, the existence of fast reacting Cys residues in rat but not in human Hb will influence the biochemical, pharmacological, and toxicological activity of many drugs (83, 273).

### 6.5.5 Hb-SNO denitrosation

The mechanism of NO release from Hb-SNO, which is required for vasodilation, is incompletely understood. Hb-SNO dilates blood vessels and inhibits platelets under conditions that promote its T structure, but not under conditions that promote its R structure (16, 19, 62). It has been demonstrated that free Cu<sup>I</sup> and Cu<sup>I</sup>ZnSOD catalyze the reductive decomposition of RSNOs (Reactions 1.7 and 1.11) (33-35, 56, 97) and the activity of CuZnSOD as a GSNO-reductase is attenuated by copper chelators (Chapter 2). In this chapter, we report that the Hb-SNO is relatively stable at 37°C over 30 min (Figure 6.13A) since the extent of its decomposition both in buffer only and in the presence of the chelators, EDTA, DTPA, and neo, is  $\leq 10\%$ . Both free

copper and the active-site copper of BCuZnSOD exhibit Cu<sup>I</sup>-dependent catalysis of release NO from Hb-SNO in the presence of GSH (56% vs 39% after 30 min at 37°C) (Figure 6.13B). The lower Hb-SNO decomposition in the reaction with the copper-free enzyme, EZnSOD, provides further support that the active-site copper catalyzes NO release.

Interestingly, 5 μM free copper is a more efficient catalyst than 10 μM BCuZnSOD (equivalent to 20 μM copper) as shown in Figure 6.13C. However, they reach the same decomposition levels over 90 min incubation at 37°C, suggesting that steric effects likely hinder the accessibility of GSH and Hb-SNO to the active-copper of CuZnSOD. In agreement with observations in Chapters 2 and 3, CuZnSOD-catalyzed protein-SNO bond decomposition was inhibited by the chelators (Figure 6.14A). As the affinity of the chelators for free copper is stronger than for enzyme bound copper (Table 2.3), the free-copper-catalyzed Hb-SNO decomposition is inhibited more strongly than CuZnSOD-catalyzed decomposition (Figure 6.14B vs A).

## 6.6 Conclusions

The differences in the *S*-thiolation and *S*-nitrosation/denitrosation reactions of rat and human Hb are critical since a rat model is frequently used in studies of NO biochemistry and pharmacology. We demonstrated here that rat Hb containing fast-reacting thiols (Cysβ125) and slow-reacting thiols (Cysβ93 and Cysα13) does not share the same mechanism of *S*-nitrosation as human Hb with GSNO as a NO donor. Significant differences in *S*-thiolation of the two Cys residues on the β-chain of human and rat Hb were also observed. This could significantly influence the biochemical,



pharmacological, and toxicological effects of some drugs (273). CuZnSOD is hypothesized to be an important catalyst involved in RSNO-mediated control of basal blood flow in human blood. Its SNO-reductase activity towards high-molecular-weight substrates, such as rat Hb-SNO, with GSH as an electron donor was identified. Full characterization of Cu<sup>I</sup>ZnSOD-catalyzed Hb-SNO decomposition will shed light on such controversial questions as the mechanism of NO release in the reductive environment of the RBC cytoplasm and its modulation by the ligation state of Hb.

## 7.0 Conclusions and Suggestions for Future Work

### 7.1 Chapters 2 and 3

From the data presented in these two chapters, the GSNO-reductase and SOD activities of CuZnSOD are affected by the commonly used polyaminocarboxylate chelators, EDTA and DTPA, the copper colorimetric reagents, cuprizone and DDC, and the specific  $\text{Cu}^{\text{I}}$  chelator, neocuproine, *via* two mechanisms: (1) inhibition of both activities by removal of the active-site copper from CuZnSOD (e.g., DDC), and (2) inhibition of the GSNO-reductase but not the SOD activity by chelators that associate strongly with the active-site copper and interfere with access of large substrates to the active site (e.g., EDTA, DTPA, and neo). Chelators such as cuprizone that interact weakly with the active-site copper inhibit neither the GSNO-reductase activity nor the SOD activity of CuZnSOD.

It was demonstrated spectrophotometrically that EDTA and DTPA decrease the  $\text{Cu}^{\text{II}}$  *d-d* absorption, decelerate the reduction of  $\text{Cu}^{\text{II}}$  to  $\text{Cu}^{\text{I}}$ , and decelerate GSNO degradation. The oxyMb NO scavenging assay provided further evidence that NO release from GSNO was slowed down by the two chelators. Consistent with no loss of SOD activity, the copper and zinc loading of the enzyme following incubation with EDTA and DTPA was unaltered as determined by ICP-MS. EDTA and DTPA inhibit the GSNO-reductase activity of CuZnSOD due to their ability to enter the active-site channel. This was demonstrated by the protection they provided against PGO-induced inactivation of SOD activity. Furthermore, these chelators associate with a single copper per homodimer as revealed by isothermal calorimetric titration (ITC). Computational modeling indicated

that one of the carboxylic groups can access the active-site copper when EDTA is docked into the active-site channel of CuZnSOD. From the data presented, EDTA and DTPA are proposed to bind to the solvent-exposed active-site copper of one subunit of the CuZnSOD homodimer without removing the metal and this induces a conformational change at the second active site that inhibits the GSNO-reductase but not the SOD activity of the enzyme (Chapter 2).

All three copper colorimetric reagents examined, DDC, cuprizone, and neocuproine, combine to varying degrees with the active-site copper of CuZnSOD. ICP-MS analysis revealed that 77% copper and 44% zinc were removed from CuZnSOD on its incubation with DDC, which is the key reason that DDC is a highly efficient inhibitor of both the GSNO-reductase and SOD activities of CuZnSOD. Neocuproine associated with the active-site copper and, like EDTA and DTPA, it did not remove any metal from the enzyme. However, unlike the polyaminocarboxylates, neocuproine did not protect Arg141, a key residue for SOD activity in the active-site channel, from PGO modification. The data presented in Chapter 3 support the literature report that neocuproine inhibits the GSNO-reductase but not the SOD activity of CuZnSOD (56). However, neocuproine was a poorer inhibitor than reported (56), and this was attributed to the higher concentrations of GSSG formed in the present work which would compete with neocuproine as an inhibitor of the GSNO-reductase activity of CuZnSOD. In agreement with the literature data (56), cuprizone has little effect on GSNO-reductase activity and no effect on the SOD activity of CuZnSOD. The high sensitivity and selectivity of cuprizone in the determination of trace cupric ion is well established (152, 173, 296), but its interaction with active-site copper is weak over the pH range 7.0–9.0.

The accessibility of cuprizone to the active-site of CuZnSOD may be prevented by its hydrophobic property (Chapter 3).

Amyotrophic lateral sclerosis (ALS) is a familial neurodegenerative disease associated with mutations in CuZnSOD (297, 298). It has been reported that the increased GSNO-reductase activity of SOD1 mutants contributes to motor neuron death in ALS (299). Our results raise the possibility that drugs, for example, dexrazoxane (300), that can penetrate into the cells to give EDTA- and DTPA-like compounds, may bind to the active-site copper of CuZnSOD. Such binding could have therapeutic efficacy in ALS by inhibiting the GSNO reductase but not the SOD activity of CuZnSOD mutants (99, 299).

## **7.2 Chapter 4**

Both the SOD and the GSNO-reductase activity of CuZnSOD require redox turnover of the active-site copper. Also, Arg141 was shown to be required for SOD activity. Thus, chemical modification of Arg141 was attempted to establish the relative importance of this residue in the GSNO-reductase vs the SOD activity of the enzyme. A literature procedure (55) reported to specifically target PGO to Arg141 was followed but mass spectrometric analysis revealed three of the four Arg residues of BCuZnSOD were singly labelled by PGO. To re-evaluate PGO as an Arg-specific reagent, its reactions with peptides containing Arg (the tripeptide MRF and porcine rennin substrate fragment), both Arg and Lys (adrenocorticotrophic hormone fragment), and Cys (reduced glutathione, GSH) were examined. The PGO-modified peptides and BCuZnSOD were characterized by ESI mass spectrometry, site(s) of PGO labelling were determined by MS/MS and by peptide mass fingerprints, and free amino groups following PGO-exposure were probed

by acetylation. We demonstrated that PGO has high specificity for Arg residues, which is supported by the observations that it modified no Lys residues or  $\alpha$ -amino groups. Of the four Arg residues in BCuZnSOD (Arg77, Arg113, Arg141, and Arg126), the most reactive is likely Arg126 based on the crystal structure (107, 140) and the lossing trend of SOD activity but not Arg141 as reported (55).

We also found that PGO can react with the thiol group of GSH to produce not only the addition adduct reported previously (187) but also multi-PGO-labelled condensation products. Similar to buried Arg113, the buried Cys6 in BCuZnSOD was not labelled by PGO. A significant difference between PGO-labelling of the peptides and BCuZnSOD is that in the latter the modified Arg residues were singly PGO-labelled but mainly doubly PGO-labelled in the peptides. Since modification of Arg residues in BCuZnSOD by PGO is time- and concentration-dependent, to obtain enzyme selectively modified at Arg141 would require extensive purification of BCuZnSOD(PGO)<sub>x</sub> (x = 1–3) derivatives.

### 7.3 Chapter 5

Since PGO-labelling results in multiple BCuZnSOD derivatives, site-directed mutagenesis was considered a better approach than chemical modification. Two systems were set up for wild-type hSOD1 expression. The YEp351-hSOD1 plasmid was introduced into *S. cerevisiae* strain BY4742 but the yield of expressed hSOD1 was below 2% of the total cellular protein. To raise the protein expression level, the hSOD1 gene was transferred from YEp351 to pET-22b(+) and the protein was expressed in

BL21(DE3) *E. coli* host cells. Purification by gel-filtration and anion-exchange chromatography was evaluated.

#### 7.4 Chapter 6

The level of CuZnSOD in rat RBCs was measured and found to be similar to that in human RBCs. In agreement with the literature data (83), we demonstrated that Cys $\beta$ 125 and Cys $\beta$ 93 in rat Hb are more reactive than Cys $\beta$ 93 in human Hb. NEM reacts readily with both  $\beta$ Cys residues, and one of the three  $\alpha$ Cys residues in the major isoform of rat Hb from RBCs is also NEM-labelled. Hb-SNO formation in rat vs human Hb was compared. In accordance with their Cys reactivity, we demonstrated that GSNO more readily *S*-nitrosates rat oxyHb than human oxyHb even when Cys $\beta$ 125 is absent from the rat protein. Also, unlike human Hb, Cys $\beta$ 125 and Cys $\beta$ 93 are *S*-nitrosated and *S*-glutathiolated in the absence of added CuZnSOD, and Cys $\beta$ 93 is not selectively *S*-nitrosated in presence of CuZnSOD. It is possible that the GSNO-transferase activity of CuZnSOD competes poorly with direct *trans*-*S*-nitrosation when proteins possess highly reactive thiols such as Cys $\beta$ 125 of rat Hb.

The rat Hb-SNO-reductase activity of BCuZnSOD was compared to that of free copper ions. As expected, both free and protein-bound copper effectively catalyze the reductive denitrosation of rat Hb-SNO with free copper giving rise to faster decomposition than BCuZnSOD. As demonstrated for GSNO in Chapter 2, free copper- and CuZnSOD-catalyzed NO release from rat Hb-SNO was retarded by the copper chelators.

## 7.5 Suggestions for Future Work

- (1) The role of zinc and the interaction of chelators with zinc in the GSNO-reductase activity of CuZnSOD should be further investigated.
- (2) To probe the interaction of chelators with the active-site Arg and to explore its role in the GSNO-reductase of CuZnSOD, wild-type recombinant hSOD1 and its Arg143 mutants should be characterized.
- (3) The therapeutic potential of compounds that inhibit the GSNO-reductase but not the SOD activities of CuZnSOD should be investigated for ALS and other diseases.
- (4) The interaction of GSSG with the active-site copper and its shielding of the active-site channel to prevent the GSNO-reductase activity of CuZnSOD should be studied.
- (5) S-Nitrosation of rat Hb should be examined in the presence of copper chelators to eliminate possible copper-catalyzed side reactions.
- (6) S-Nitrosation of rat Hb should be carried out under the same conditions used for human Hb to evaluate the GSNO-transferase activity of CuZnSOD with Hb from different species. Rat Hb with free and blocked Cys $\beta$ 125 should be used in these studies as well as CuZnSOD from different species.
- (7) The degradation of rat Hb-SNO under aerobic and anaerobic conditions should be examined to determine if the allosteric transition of rat Hb controls NO release.
- (8) 2,3-DPG and IHP are important modulators of the O<sub>2</sub> affinity of Hb in RBCs (301). 2,3-DPG is a highly charged anion and it interacts electrostatically with positively charged groups on the Hb molecule (70). The interaction of 2,3-DPG

and IHP with the positively charged groups in the active-site channel of CuZnSOD should be tested. Also, the function of these modulators in controlling the GSNO-reductase activity of CuZnSOD should be investigated.


- (9) hSOD1 expression in yeast should be carried out in selective medium to increase protein expression.



## References

1. Kerwin, J. F., Jr., Lancaster, J. R., Jr., and Feldman, P. L. (1995) Nitric oxide: a new paradigm for second messengers, *J Med Chem* 38, 4343-4362.
2. Moncada, S., Palmer, R. M., and Higgs, E. A. (1991) Nitric oxide: physiology, pathophysiology, and pharmacology, *Pharmacol Rev* 43, 109-142.
3. Ignarro, L. J., and Kadowitz, P. J. (1985) The pharmacological and physiological role of cyclic GMP in vascular smooth muscle relaxation, *Annual review of pharmacology and toxicology* 25, 171-191.
4. Ignarro, L. J. (1990) Haem-dependent activation of guanylate cyclase and cyclic GMP formation by endogenous nitric oxide: a unique transduction mechanism for transcellular signaling, *Pharmacology & toxicology* 67, 1-7.
5. Butler, A. R., Flitney, F. W., and Williams, D. L. (1995) NO, nitrosonium ions, nitroxide ions, nitrosothiols and iron-nitrosyls in biology: a chemist's perspective, *Trends in pharmacological sciences* 16, 18-22.
6. Borland, C. (1991) Endothelium in control, *British heart journal* 66, 405.
7. Liu, X., Miller, M. J., Joshi, M. S., Sadowska-Krowicka, H., Clark, D. A., and Lancaster, J. R., Jr. (1998) Diffusion-limited reaction of free nitric oxide with erythrocytes, *The Journal of biological chemistry* 273, 18709-18713.
8. Vaughn, M. W., Huang, K. T., Kuo, L., and Liao, J. C. (2000) Erythrocytes possess an intrinsic barrier to nitric oxide consumption, *The Journal of biological chemistry* 275, 2342-2348.
9. Gally, J. A., Montague, P. R., Reeke, G. N., Jr., and Edelman, G. M. (1990) The NO hypothesis: possible effects of a short-lived, rapidly diffusible signal in the

- development and function of the nervous system, *Proc. Natl. Acad. Sci. USA* 87, 3547-3551.
10. Girard, P., and Potier, P. (1993) NO, thiols and disulfides, *FEBS letters* 320, 7-8.
  11. Rassaf, T., Preik, M., Kleinbongard, P., Lauer, T., Heiss, C., Strauer, B. E., Feelisch, M., and Kelm, M. (2002) Evidence for in vivo transport of bioactive nitric oxide in human plasma, *The Journal of clinical investigation* 109, 1241-1248.
  12. Rassaf, T., Kleinbongard, P., Preik, M., Dejam, A., Gharini, P., Lauer, T., Erckenbrecht, J., Duschin, A., Schulz, R., Heusch, G., Feelisch, M., and Kelm, M. (2002) Plasma nitrosothiols contribute to the systemic vasodilator effects of intravenously applied NO: experimental and clinical Study on the fate of NO in human blood, *Circulation research* 91, 470-477.
  13. Stamler, J. S., Simon, D. I., Osborne, J. A., Mullins, M. E., Jaraki, O., Michel, T., Singel, D. J., and Loscalzo, J. (1992) S-nitrosylation of proteins with nitric oxide: synthesis and characterization of biologically active compounds, *Proceedings of the National Academy of Sciences of the United States of America* 89, 444-448.
  14. Stamler, J. S., Jaraki, O., Osborne, J., Simon, D. I., Keaney, J., Vita, J., Singel, D., Valeri, C. R., and Loscalzo, J. (1992) Nitric oxide circulates in mammalian plasma primarily as an S-nitroso adduct of serum albumin, *Proceedings of the National Academy of Sciences of the United States of America* 89, 7674-7677.
  15. Richardson, G., and Benjamin, N. (2002) Potential therapeutic uses for S-nitrosothiols, *Clinical science (London, England)* 102, 99-105.

- 
16. Pawloski, J. R., Swaminathan, R. V., and Stamler, J. S. (1998) Cell-free and erythrocytic S-nitrosohemoglobin inhibits human platelet aggregation, *Circulation* 97, 263-267.
  17. Ignarro, L. J., and Gruetter, C. A. (1980) Requirement of thiols for activation of coronary arterial guanylate cyclase by glyceryl trinitrate and sodium nitrite: possible involvement of S-nitrosothiols, *Biochimica et biophysica acta* 631, 221-231.
  18. Ignarro, L. J., Lippton, H., Edwards, J. C., Baricos, W. H., Hyman, A. L., Kadowitz, P. J., and Gruetter, C. A. (1981) Mechanism of vascular smooth muscle relaxation by organic nitrates, nitrites, nitroprusside and nitric oxide: evidence for the involvement of S-nitrosothiols as active intermediates, *The Journal of pharmacology and experimental therapeutics* 218, 739-749.
  19. Jia, L., Bonaventura, C., Bonaventura, J., and Stamler, J. S. (1996) S-nitrosohaemoglobin: a dynamic activity of blood involved in vascular control, *Nature* 380, 221-226.
  20. Myers, P. R., Minor, R. L., Jr., Guerra, R., Jr., Bates, J. N., and Harrison, D. G. (1990) Vasorelaxant properties of the endothelium-derived relaxing factor more closely resemble S-nitrosocysteine than nitric oxide, *Nature* 345, 161-163.
  21. Gaston, B., Reilly, J., Drazen, J. M., Fackler, J., Ramdev, P., Arnette, D., Mullins, M. E., Sugarbaker, D. J., Chee, C., Singel, D. J., and et al. (1993) Endogenous nitrogen oxides and bronchodilator S-nitrosothiols in human airways, *Proceedings of the National Academy of Sciences of the United States of America* 90, 10957-10961.

22. Clancy, R. M., Levartovsky, D., Leszczynska-Piziak, J., Yegudin, J., and Abramson, S. B. (1994) Nitric oxide reacts with intracellular glutathione and activates the hexose monophosphate shunt in human neutrophils: evidence for S-nitrosoglutathione as a bioactive intermediary, *Proceedings of the National Academy of Sciences of the United States of America* 91, 3680-3684.
23. Giustarini, D., Milzani, A., Colombo, R., Dalle-Donne, I., and Rossi, R. (2003) Nitric oxide and S-nitrosothiols in human blood, *Clin Chim Acta* 330, 85-98.
24. William A. Pryor, D. F. C., C. K. Govindan, and George Crank. (1982) Oxidation of thiols by nitric oxide and nitrogen dioxide: synthetic utility and toxicological implications, *J Org Chem* 47, 156 - 159.
25. Hogg, N., Singh, R. J., and Kalyanaraman, B. (1996) The role of glutathione in the transport and catabolism of nitric oxide, *FEBS Lett* 382, 223-228.
26. Stamler, J. S., Singel, D. J., and Loscalzo, J. (1992) Biochemistry of nitric oxide and its redox-activated forms, *Science* 258, 1898-1902.
27. Stubauer, G., Giuffre, A., and Sarti, P. (1999) Mechanism of S-nitrosothiol formation and degradation mediated by copper ions, *J Biol Chem* 274, 28128-28133.
28. Williams, D. L. (1997) Nitrosating agents: is peroxynitrite a likely candidate?, *Nitric oxide* 1, 522-527.
29. Rossi, R., Lusini, L., Giannerini, F., Giustarini, D., Lungarella, G., and Di Simplicio, P. (1997) A method to study kinetics of transnitrosation with nitrosoglutathione: reactions with hemoglobin and other thiols, *Analytical biochemistry* 254, 215-220.

30. Hogg, N. (2002) The biochemistry and physiology of S-nitrosothiols, *Annual review of pharmacology and toxicology* 42, 585-600.
31. Liu, Z., Rudd, M. A., Freedman, J. E., and Loscalzo, J. (1998) S-Transnitrosation reactions are involved in the metabolic fate and biological actions of nitric oxide, *The Journal of pharmacology and experimental therapeutics* 284, 526-534.
32. Kluge, I., Gutteck-Amsler, U., Zollinger, M., and Do, K. Q. (1997) S-nitrosoglutathione in rat cerebellum: identification and quantification by liquid chromatography-mass spectrometry, *Journal of neurochemistry* 69, 2599-2607.
33. Singh, R. J., Hogg, N., Joseph, J., and Kalyanaraman, B. (1996) Mechanism of nitric oxide release from S-nitrosothiols, *J Biol Chem* 271, 18596-18603.
34. Noble, D. R. S., Helen R.; Williams, D. Lyn H. (1999) Nitric oxide release from S-nitrosoglutathione (GSNO). *Chem comm (Cambridge)*, 2317-2318.
35. Burg, A., Cohen, H., and Meyerstein, D. (2000) The reaction mechanism of nitrosothiols with copper(I), *J Biol Inorg Chem* 5, 213-217.
36. Radomski, M. W., Rees, D. D., Dutra, A., and Moncada, S. (1992) S-nitroso-glutathione inhibits platelet activation in vitro and in vivo, *Br J Pharmacol* 107, 745-749.
37. MacAllister, R. J., Calver, A. L., Riezebos, J., Collier, J., and Vallance, P. (1995) Relative potency and arteriovenous selectivity of nitrovasodilators on human blood vessels: an insight into the targeting of nitric oxide delivery, *The Journal of pharmacology and experimental therapeutics* 273, 154-160.
38. de Belder, A. J., MacAllister, R., Radomski, M. W., Moncada, S., and Vallance, P. J. (1994) Effects of S-nitroso-glutathione in the human forearm circulation:

- evidence for selective inhibition of platelet activation, *Cardiovascular research* 28, 691-694.
39. Baker, J. E., Holman, P., Kalyanaraman, B., Griffith, O. W., and Pritchard, K. A., Jr. (1999) Adaptation to chronic hypoxia confers tolerance to subsequent myocardial ischemia by increased nitric oxide production, *Annals of the New York Academy of Sciences* 874, 236-253.
  40. Ma, X. L., Gao, F., Liu, G. L., Lopez, B. L., Christopher, T. A., Fukuto, J. M., Wink, D. A., and Feelisch, M. (1999) Opposite effects of nitric oxide and nitroxyl on postischemic myocardial injury, *Proceedings of the National Academy of Sciences of the United States of America* 96, 14617-14622.
  41. Singh, R. J., Hogg, N., Goss, S. P., Antholine, W. E., and Kalyanaraman, B. (1999) Mechanism of superoxide dismutase/H<sub>2</sub>O<sub>2</sub>-mediated nitric oxide release from S-nitrosoglutathione--role of glutamate, *Arch Biochem Biophys* 372, 8-15.
  42. Kashiba-Iwatsuki, M., Yamaguchi, M., and Inoue, M. (1996) Role of ascorbic acid in the metabolism of S-nitroso-glutathione, *FEBS letters* 389, 149-152.
  43. Scorza, G., Pietraforte, D., and Minetti, M. (1997) Role of ascorbate and protein thiols in the release of nitric oxide from S-nitroso-albumin and S-nitroso-glutathione in human plasma, *Free radical biology & medicine* 22, 633-642.
  44. Arnette, D. R., and Stamler, J. S. (1995) NO<sup>+</sup>, NO, and NO<sup>-</sup> donation by S-nitrosothiols: implications for regulation of physiological functions by S-nitrosylation and acceleration of disulfide formation, *Arch Biochem Biophys* 318, 279-285.

45. Mathews, W. R., and Kerr, S. W. (1993) Biological activity of S-nitrosothiols: the role of nitric oxide, *The Journal of pharmacology and experimental therapeutics* 267, 1529-1537.
46. Stuesse, D. C., Giraud, G. D., Vlessis, A. A., Starr, A., and Trunkey, D. D. (2001) Hemodynamic effects of S-nitrosocysteine, an intravenous regional vasodilator, *The Journal of thoracic and cardiovascular surgery* 122, 371-377.
47. McCord, J. M., and Fridovich, I. (1969) Superoxide dismutase. An enzymic function for erythrocuprein (hemocuprein), *J Biol Chem* 244, 6049-6055.
48. Marmocchi, F., Argese, E., Rigo, A., Mavelli, I., Rossi, L., and Rotilio, G. (1983) A comparative study of bovine, porcine and yeast superoxide dismutases, *Mol Cell Biochem* 51, 161-164.
49. Tainer, J. A., Getzoff, E. D., Richardson, J. S., and Richardson, D. C. (1983) Structure and mechanism of copper, zinc superoxide dismutase, *Nature* 306, 284-287.
50. Cudd, A., and Fridovich, I. (1982) Electrostatic interactions in the reaction mechanism of bovine erythrocyte superoxide dismutase, *J Biol Chem* 257, 11443-11447.
51. Fridovich, I. (1979) Superoxide and superoxide dismutase, in *Advances in inorganic biochemistry* (Eichhorn, G., Marzilli, LG, Ed.), pp 67-90, Elsevier/North-Holland, New York.
52. Klug, D., Rabani, J., and Fridovich, I. (1972) A direct demonstration of the catalytic action of superoxide dismutase through the use of pulse radiolysis, *J Biol Chem* 247, 4839-4842.

53. Rotilio, G., Bray, R. C., and Fielden, E. M. (1972) A pulse radiolysis study of superoxide dismutase, *Biochim Biophys Acta* 268, 605-609.
54. Klug-Roth, D., Fridovich, I., and Rabani, J. (1973) Pulse radiolytic investigations of superoxide catalyzed disproportionation. Mechanism for bovine superoxide dismutase, *Journal of the American Chemical Society* 95, 2786-2790.
55. Malinowski, D. P., and Fridovich, I. (1979) Chemical modification of arginine at the active site of the bovine erythrocyte superoxide dismutase, *Biochemistry* 18, 5909-5917.
56. Jourde'heuil, D., Laroux, F. S., Miles, A. M., Wink, D. A., and Grisham, M. B. (1999) Effect of superoxide dismutase on the stability of S-nitrosothiols, *Arch Biochem Biophys* 361, 323-330.
57. Romeo, A. A., Capobianco, J. A., and English, A. M. (2003) Superoxide dismutase targets NO from GSNO to Cysbeta93 of oxyhemoglobin in concentrated but not dilute solutions of the protein, *J Am Chem Soc* 125, 14370-14378.
58. Mota de Freitas, D., and Valentine, J. S. (1984) Phosphate is an inhibitor of copper-zinc superoxide dismutase, *Biochemistry* 23, 2079-2082.
59. Nebot, C., Moutet, M., Huet, P., Xu, J. Z., Yadan, J. C., and Chaudiere, J. (1993) Spectrophotometric assay of superoxide dismutase activity based on the activated autoxidation of a tetracyclic catechol, *Analytical biochemistry* 214, 442-451.
60. Gartner, A., and Weser, U. (1983) Erythrocuprein (Cu<sub>2</sub>Zn<sub>2</sub> superoxide dismutase) is the major copper protein of the red blood cell, *FEBS letters* 155, 15-18.



61. McMahon, T. J., Moon, R. E., Luschinger, B. P., Carraway, M. S., Stone, A. E., Stolp, B. W., Gow, A. J., Pawloski, J. R., Watke, P., Singel, D. J., Piantadosi, C. A., and Stamler, J. S. (2002) Nitric oxide in the human respiratory cycle, *Nature medicine* 8, 711-717.
62. Stamler, J. S., Jia, L., Eu, J. P., McMahon, T. J., Demchenko, I. T., Bonaventura, J., Gernert, K., and Piantadosi, C. A. (1997) Blood flow regulation by S-nitrosohemoglobin in the physiological oxygen gradient, *Science* 276, 2034-2037.
63. Gow, A. J., and Stamler, J. S. (1998) Reactions between nitric oxide and haemoglobin under physiological conditions, *Nature* 391, 169-173.
64. Gow, A. J., Luchsinger, B. P., Pawloski, J. R., Singel, D. J., and Stamler, J. S. (1999) The oxyhemoglobin reaction of nitric oxide, *Proceedings of the National Academy of Sciences of the United States of America* 96, 9027-9032.
65. McMahon, T. J., Exton Stone, A., Bonaventura, J., Singel, D. J., and Solomon Stamler, J. (2000) Functional coupling of oxygen binding and vasoactivity in S-nitrosohemoglobin, *The Journal of biological chemistry* 275, 16738-16745.
66. Pawloski, J. R., Hess, D. T., and Stamler, J. S. (2001) Export by red blood cells of nitric oxide bioactivity, *Nature* 409, 622-626.
67. Joshi, M. S., Ferguson, T. B., Jr., Han, T. H., Hyduke, D. R., Liao, J. C., Rassaf, T., Bryan, N., Feelisch, M., and Lancaster, J. R., Jr. (2002) Nitric oxide is consumed, rather than conserved, by reaction with oxyhemoglobin under physiological conditions, *Proceedings of the National Academy of Sciences of the United States of America* 99, 10341-10346.

68. Eich, R. F., Li, T., Lemon, D. D., Doherty, D. H., Curry, S. R., Aitken, J. F., Mathews, A. J., Johnson, K. A., Smith, R. D., Phillips, G. N., Jr., and Olson, J. S. (1996) Mechanism of NO-induced oxidation of myoglobin and hemoglobin, *Biochemistry* 35, 6976-6983.
69. Hobbs, A. J., Gladwin, M. T., Patel, R. P., Williams, D. L., and Butler, A. R. (2002) Haemoglobin: NO transporter, NO inactivator or NO one of the above?, *Trends in pharmacological sciences* 23, 406-411.
70. Lancaster, J. R., Jr. (1994) Simulation of the diffusion and reaction of endogenously produced nitric oxide, *Proceedings of the National Academy of Sciences of the United States of America* 91, 8137-8141.
71. Olson, J. S. (1981) Stopped-flow, rapid mixing measurements of ligand binding to hemoglobin and red cells., *Methods Enzymol.* 76, 631-651.
72. Wolzt, M., MacAllister, R. J., Davis, D., Feelisch, M., Moncada, S., Vallance, P., and Hobbs, A. J. (1999) Biochemical characterization of S-nitrosohemoglobin. Mechanisms underlying synthesis, no release, and biological activity, *The Journal of biological chemistry* 274, 28983-28990.
73. Pagliaro, P. (2003) Differential biological effects of products of nitric oxide (NO) synthase: it is not enough to say NO, *Life sciences* 73, 2137-2149.
74. Kelm, M., and Schrader, J. (1990) Control of coronary vascular tone by nitric oxide, *Circulation research* 66, 1561-1575.
75. Mellion, B. T., Ignarro, L. J., Myers, C. B., Ohlstein, E. H., Ballot, B. A., Hyman, A. L., and Kadowitz, P. J. (1983) Inhibition of human platelet aggregation by S-

- nitrosothiols. Heme-dependent activation of soluble guanylate cyclase and stimulation of cyclic GMP accumulation, *Molecular pharmacology* 23, 653-664.
76. Cosby, K., Partovi, K. S., Crawford, J. H., Patel, R. P., Reiter, C. D., Martyr, S., Yang, B. K., Wacławiw, M. A., Zalos, G., Xu, X., Huang, K. T., Shields, H., Kim-Shapiro, D. B., Schechter, A. N., Cannon, R. O., 3rd, and Gladwin, M. T. (2003) Nitrite reduction to nitric oxide by deoxyhemoglobin vasodilates the human circulation, *Nat Med* 9, 1498-1505.
77. Nagababu, E., Ramasamy, S., Abernethy, D. R., and Rifkind, J. M. (2003) Active nitric oxide produced in the red cell under hypoxic conditions by deoxyhemoglobin-mediated nitrite reduction, *The Journal of biological chemistry* 278, 46349-46356.
78. Luchsinger, B. P., Rich, E. N., Gow, A. J., Williams, E. M., Stamler, J. S., and Singel, D. J. (2003) Routes to S-nitroso-hemoglobin formation with heme redox and preferential reactivity in the beta subunits, *Proceedings of the National Academy of Sciences of the United States of America* 100, 461-466.
79. Bryan, N. S., Rassaf, T., Rodriguez, J., and Feelisch, M. (2004) Bound NO in human red blood cells: fact or artifact?, *Nitric oxide* 10, 221-228.
80. Lundberg, J. O., and Weitzberg, E. (2005) NO generation from nitrite and its role in vascular control, *Arteriosclerosis, thrombosis, and vascular biology* 25, 915-922.
81. Luchsinger, B. P., Rich, E. N., Yan, Y., Williams, E. M., Stamler, J. S., and Singel, D. J. (2005) Assessments of the chemistry and vasodilatory activity of

- nitrite with hemoglobin under physiologically relevant conditions, *Journal of inorganic biochemistry* 99, 912-921.
82. Tao, L., and English, A. M. (2003) Mechanism of S-nitrosation of recombinant human brain calbindin D28K, *Biochemistry* 42, 3326-3334.
  83. Rossi, R., Barra, D., Bellelli, A., Boumis, G., Canofeni, S., Di Simplicio, P., Lusini, L., Pascarella, S., and Amiconi, G. (1998) Fast-reacting thiols in rat hemoglobins can intercept damaging species in erythrocytes more efficiently than glutathione, *The Journal of biological chemistry* 273, 19198-19206.
  84. Gladwin, M. T., Wang, X., Reiter, C. D., Yang, B. K., Vivas, E. X., Bonaventura, C., and Schechter, A. N. (2002) S-Nitrosohemoglobin is unstable in the reductive erythrocyte environment and lacks O<sub>2</sub>/NO-linked allosteric function, *The Journal of biological chemistry* 277, 27818-27828.
  85. Gladwin, M. T., Shelhamer, J. H., Schechter, A. N., Pease-Fye, M. E., Wacławiw, M. A., Panza, J. A., Ognibene, F. P., and Cannon, R. O., 3rd. (2000) Role of circulating nitrite and S-nitrosohemoglobin in the regulation of regional blood flow in humans, *Proceedings of the National Academy of Sciences of the United States of America* 97, 11482-11487.
  86. Gladwin, M. T., Ognibene, F. P., Pannell, L. K., Nichols, J. S., Pease-Fye, M. E., Shelhamer, J. H., and Schechter, A. N. (2000) Relative role of heme nitrosylation and beta-cysteine 93 nitrosation in the transport and metabolism of nitric oxide by hemoglobin in the human circulation, *Proceedings of the National Academy of Sciences of the United States of America* 97, 9943-9948.

87. Patel, R. P., Hogg, N., Spencer, N. Y., Kalyanaraman, B., Matalon, S., and Darley-Usmar, V. M. (1999) Biochemical characterization of human S-nitrosohemoglobin. Effects on oxygen binding and transnitrosation, *The Journal of biological chemistry* 274, 15487-15492.
88. Bonaventura, C., Ferruzzi, G., Tesh, S., and Stevens, R. D. (1999) Effects of S-nitrosation on oxygen binding by normal and sickle cell hemoglobin, *The Journal of biological chemistry* 274, 24742-24748.
89. Chan, N. L., Rogers, P. H., and Arnone, A. (1998) Crystal structure of the S-nitroso form of liganded human hemoglobin, *Biochemistry* 37, 16459-16464.
90. Pezacki, J. P., Ship, N. J., and Kluger, R. (2001) Release of nitric oxide from S-nitrosohemoglobin. Electron transfer as a response to deoxygenation, *Journal of the American Chemical Society* 123, 4615-4616.
91. Ship, N. J., Pezacki, J. P., and Kluger, R. (2003) Rates of release of nitric oxide from HbSNO and internal electron transfer, *Bioorg Chem* 31, 3-10.
92. Singel, D. J., and Stamler, J. S. (2005) Chemical physiology of blood flow regulation by red blood cells: the role of nitric oxide and S-nitrosohemoglobin, *Annu Rev Physiol* 67, 99-145.
93. McMahon, T. J., and Stamler, J. S. (1999) Concerted nitric oxide/oxygen delivery by hemoglobin, *Methods Enzymol.* 301, 99-114.
94. May, J. M. (1998) Ascorbate function and metabolism in the human erythrocyte, *Frontiers in bioscience* 3, d1-10.
95. K. Fukunaga, N. N. a. M. Y. (1998) Determination of reduced-form glutathione and total glutathione in blood and plasma by high performance liquid

- chromatography with on-column fluorescence derivatization, *Chromatographia* 48, 690-694.
96. Gorren, A. C., Schrammel, A., Schmidt, K., and Mayer, B. (1996) Decomposition of S-nitrosoglutathione in the presence of copper ions and glutathione, *Arch Biochem Biophys* 330, 219-228.
  97. Noble, D. R., and Williams, D. L. (2000) Structure-reactivity studies of the Cu(2+)-catalyzed decomposition of four S-nitrosothiols based around the S-Nitrosocysteine/S-nitrosoglutathione structures, *Nitric Oxide* 4, 392-398.
  98. Dicks, A. P., and Williams, D. L. (1996) Generation of nitric oxide from S-nitrosothiols using protein-bound Cu<sup>2+</sup> sources, *Chem Biol* 3, 655-659.
  99. Johnson, M. A., Macdonald, T. L., Mannick, J. B., Conaway, M. R., and Gaston, B. (2001) Accelerated s-nitrosothiol breakdown by amyotrophic lateral sclerosis mutant copper,zinc-superoxide dismutase, *J Biol Chem* 276, 39872-39878.
  100. Rae, T. D., Schmidt, P. J., Pufahl, R. A., Culotta, V. C., and O'Halloran, T. V. (1999) Undetectable intracellular free copper: the requirement of a copper chaperone for superoxide dismutase, *Science* 284, 805-808.
  101. Romeo, A. A., Capobianco, J. A., and English, A. M. (2002) Heme nitrosylation of deoxyhemoglobin by s-nitrosoglutathione requires copper, *J Biol Chem* 277, 24135-24141.
  102. Fridovich, I. (1983) Superoxide radical: an endogenous toxicant, *Annu Rev Pharmacol Toxicol* 23, 239-257.
  103. Fridovich, I. (1986) Superoxide dismutases, *Adv Enzymol Relat Areas Mol Biol* 58, 61-97.

104. Christine C. Winterbourn, A. V. P., and Helena N. Parsons-Mair. (2002) Thiol Oxidase Activity of Copper,Zinc Superoxide Dismutase, *THE JOURNAL OF BIOLOGICAL CHEMISTRY* 277, 1906-1911.
105. Marklund, S., and Marklund, G. (1974) Involvement of the superoxide anion radical in the autoxidation of pyrogallol and a convenient assay for superoxide dismutase, *Eur J Biochem* 47, 469-474.
106. Bryan, N. S., Rassaf, T., Maloney, R. E., Rodriguez, C. M., Saijo, F., Rodriguez, J. R., and Feelisch, M. (2004) Cellular targets and mechanisms of nitros(yl)ation: an insight into their nature and kinetics in vivo, *Proc Natl Acad Sci U S A* 101, 4308-4313.
107. Tainer, J. A., Getzoff, E. D., Beem, K. M., Richardson, J. S., and Richardson, D. C. (1982) Determination and analysis of the 2 A-structure of copper, zinc superoxide dismutase, *J Mol Biol* 160, 181-217.
108. Beyer, W. F., Jr., Fridovich, I., Mullenbach, G. T., and Hallewell, R. (1987) Examination of the role of arginine-143 in the human copper and zinc superoxide dismutase by site-specific mutagenesis, *J Biol Chem* 262, 11182-11187.
109. Fisher, C. L., Cabelli, D. E., Tainer, J. A., Hallewell, R. A., and Getzoff, E. D. (1994) The role of arginine 143 in the electrostatics and mechanism of Cu,Zn superoxide dismutase: computational and experimental evaluation by mutational analysis, *Proteins* 19, 24-34.
110. Bertini, I., A. Lepori, C. Luchinat, P. Turano. (1991) Role of Arg-143 in human Cu<sub>2</sub>Zn<sub>2</sub>SOD studied through anion binding., *Inorg. Chem.* 30, 3363-3364.

111. Getzoff, E. D., Tainer, J. A., Weiner, P. K., Kollman, P. A., Richardson, J. S., and Richardson, D. C. (1983) Electrostatic recognition between superoxide and copper, zinc superoxide dismutase, *Nature* 306, 287-290.
112. Bermingham-McDonogh, O., Mota de Freitas, D., Kumamoto, A., Saunders, J. E., Blech, D. M., Borders, C. L., Jr., and Valentine, J. S. (1982) Reduced anion-binding affinity of Cu,Zn superoxide dismutases chemically modified at arginine, *Biochem Biophys Res Commun* 108, 1376-1382.
113. Fee, J. A. (1973) Studies on the reconstitution of bovine erythrocyte superoxide dismutase. IV. Preparation and some properties of the enzyme in which Co(II) is substituted for Zn(II), *J Biol Chem* 248, 4229-4234.
114. Carrico, R. J., and Deutsch, H. F. (1970) The presence of zinc in human cytocuprein and some properties of the apoprotein, *J Biol Chem* 245, 723-727.
115. Weser, U., Barth, G., Djerassi, C., Hartmann, H. J., Krauss, P., Voelcker, G., Voelter, W., and Voetsch, W. (1972) A study on purified apo-erythrocuprein, *Biochim Biophys Acta* 278, 28-44.
116. Konorev, E. A., Tarpey, M. M., Joseph, J., Baker, J. E., and Kalyanaraman, B. (1995) S-nitrosoglutathione improves functional recovery in the isolated rat heart after cardioplegic ischemic arrest-evidence for a cardioprotective effect of nitric oxide, *J Pharmacol Exp Ther* 274, 200-206.
117. Rauhala, P., Lin, A. M., and Chiueh, C. C. (1998) Neuroprotection by S-nitrosoglutathione of brain dopamine neurons from oxidative stress, *Faseb J* 12, 165-173.



118. Padgett, C. M., and Whorton, A. R. (1998) Cellular responses to nitric oxide: role of protein S-thiolation/dethiolation, *Arch Biochem Biophys* 358, 232-242.
119. Takahashi, K. (1977) The reactions of phenylglyoxal and related reagents with amino acids, *J Biochem (Tokyo)* 81, 395-402.
120. Cocco, D., Calabrese, L., Rigo, A., Argese, E., and Rotilio, G. (1981) Re-examination of the reaction of diethyldithiocarbamate with the copper of superoxide dismutase, *J Biol Chem* 256, 8983-8986.
121. Abbyad, P. T., John; Lam, Joseph; Salin, Eric. (2001) Optimization of the technique of standard additions for inductively coupled plasma mass spectrometry., *Journal of Analytical Atomic Spectrometry* 16, 464-469.
122. Fee, J. A., and Gaber, B. P. (1972) Anion binding to bovine erythrocyte superoxide dismutase. Evidence for multiple binding sites with qualitatively different properties, *J Biol Chem* 247, 60-65.
123. Fee, J. A., and DiCorleto, P. E. (1973) Observations on the oxidation-reduction properties of bovine erythrocyte superoxide dismutase, *Biochemistry* 12, 4893-4899.
124. Misra, H. P. (1979) Reaction of copper-zinc superoxide dismutase with diethyldithiocarbamate, *J Biol Chem* 254, 11623-11628.
125. Lawrence, G. D., and Sawyer, D. T. (1979) Potentiometric titrations and oxidation-reduction potentials of manganese and copper-zinc superoxide dismutases, *Biochemistry* 18, 3045-3050.
126. McCord, J. M., and Fridovich, I. (1968) The reduction of cytochrome c by milk xanthine oxidase, *J Biol Chem* 243, 5753-5760.

127. Flohe, L., and Otting, F. (1984) Superoxide dismutase assays, *Methods Enzymol* 105, 93-104.
128. Butler, J., Koppenol, W. H., and Margoliash, E. (1982) Kinetics and mechanism of the reduction of ferricytochrome c by the superoxide anion, *J Biol Chem* 257, 10747-10750.
129. Incorporated, M. (1998) ITC Data Analysis in Origin Tutorial Guide, Version 5.0.9.
130. E. D. Getzoff, R. A. H., and J. A. Tainer (1986) *Protein engineering: Applications in science, medicine and industry.*, Academic Press, Orlando, Fla.
131. Rypniewski, W. R., Mangani, S., Bruni, B., Orioli, P. L., Casati, M., and Wilson, K. S. (1995) Crystal Structure of Reduced Bovine Erythrocyte Superoxide Dismutase at 1.9 Å Resolution, *Journal of Molecular Biology* 251, 282-296.
132. Dolinsky, T. J., Nielsen, J. E., McCammon, J. A., and Baker, N. A. (2004) PDB2PQR: an automated pipeline for the setup of Poisson-Boltzmann electrostatics calculations, *Nucl. Acids Res.* 32, W665-667.
133. Baker, N. A., Sept, D., Joseph, S., Holst, M. J., and McCammon, J. A. (2001) Electrostatics of nanosystems: Application to microtubules and the ribosome, *PNAS* 98, 10037-10041.
134. DeLano, W. L. (2002) *The PyMOL Molecular Graphics System*, <http://www.pymol.org>, DeLano Scientific, San Carlos, CA.
135. Carugo, K. D., Battistoni, A., Carri, M. T., Polticelli, F., Desideri, A., Rotilio, G., Coda, A., and Bolognesi, M. (1994) Crystal structure of the cyanide-inhibited *Xenopus laevis* Cu,Zn superoxide dismutase at 98 K, *FEBS letters* 349, 93-98.

136. L. Banci, I. B., C. Luchinat, R. Monnanni, and A. Scozzafava. (1987) Characterization of the cobalt(II)-substituted superoxide dismutase-phosphate systems, *Inorganic Chemistry* 26, 153-156.
137. S. Chaberek, A. E. F., M. A. Doran and N. J. Bicknell. (1959) Interaction of some divalent metal ions with diethylenetriaminepentaacetic acid, *Journal of Inorganic and Nuclear Chemistry* 11, 184-196.
138. Cocco, D., Calabrese, L., Rigo, A., Marmocchi, F., and Rotilio, G. (1981) Preparation of selectively metal-free and metal-substituted derivatives by reaction of Cu--Zn superoxide dismutase with diethyldithiocarbamate, *Biochem J* 199, 675-680.
139. Sette, M., Paci, M., Desideri, A., and Rotilio, G. (1992) Formate as an NMR probe of anion binding to Cu,Zn and Cu,Co bovine erythrocyte superoxide dismutases, *Biochemistry* 31, 12410-12415.
140. Richardson, J., Thomas, K. A., Rubin, B. H., and Richardson, D. C. (1975) Crystal structure of bovine Cu,Zn superoxide dismutase at 3 Å resolution: chain tracing and metal ligands, *Proceedings of the National Academy of Sciences of the United States of America* 72, 1349-1353.
141. Polticelli, F., Battistoni, A., O'Neill, P., Rotilio, G., and Desideri, A. (1998) Role of the electrostatic loop charged residues in Cu,Zn superoxide dismutase, *Protein Sci* 7, 2354-2358.
142. Pantoliano, M. W., Valentine, J. S., Burger, A. R., and Lippard, S. J. (1982) A pH-dependent superoxide dismutase activity for zinc-free bovine erythrocyte superoxide dismutase.

- Reexamination of the role of zinc in the holoprotein, *J Inorg Biochem* 17, 325-341.
143. Takahashi, M., and Asada, K. (1982) A flash-photometric method for determination of reactivity of superoxide: application to superoxide dismutase assay, *J Biochem (Tokyo)* 91, 889-896.
  144. Fersht, A. R., Mulvey, R. S., and Koch, G. L. (1975) Ligand binding and enzymic catalysis coupled through subunits in tyrosyl-tRNA synthetase, *Biochemistry* 14, 13-18.
  145. Wiback, S. J., and Palsson, B. O. (2002) Extreme pathway analysis of human red blood cell metabolism, *Biophys J* 83, 808-818.
  146. Fee, J. A. (1973) Studies on the reconstitution of bovine erythrocyte superoxide dismutase. I. The presence of four divalent metal-binding sites on the apo protein which are different from the native sites, *Biochim Biophys Acta* 295, 87-95.
  147. Fielden, E. M., Roberts, P. B., Bray, R. C., Lowe, D. J., Mautner, G. N., Rotilio, G., and Calabrese, L. (1974) The mechanism of action of superoxide dismutase from pulse radiolysis and electron paramagnetic resonance. Evidence that only half the active sites function in catalysis, *Biochem J* 139, 49-60.
  148. R LaCoste, M. E., S Wiberley. (1951) Colorimetric Estimation of Various Metal Derivatives of Sodium Diethyldithiocarbamate, *Anal. Chem.* 23, 871-874.
  149. G. F. Smith, W. H. M., , Jr. (1952) 2,9-Dimethyl-1,10-phenanthroline, *Anal. Chem.* 24, 371-373.
  150. Kuang Lu Cheng, R. H. B. (1953) Two Specific Methods of Determining Copper in Soil and in Plant Material, *Anal. Chem.* 25, 655-659.

151. GAHLER, A. R. (1954) Colorimetric Determination of Copper with Neocuproine, *Analytical Chemistry* 26, 577 - 579.
152. R. E. Peterson, M. E. B. (1955) Spectrophotometric Determination of Serum Copper with Biscyclohexanoneoxalyldihydrazone, *Anal. Chem.* 27, 1195-1197.
153. Borchers, R. (1959) Spectrophotometric Determination of Amino Acids. Alkaline Copper Salt Method Using Cuprizone, Biscyclohexanoneoxalyldihydrazone, *Anal. Chem.* 31, 1179-1180.
154. NEBESAR, B. (1964) Spectrophotometric Determination of Copper in Tellurium and Related Thermoelectric Compounds of the Bismuth Telluride Type with 2,9-Dimethyl-1,10-phenanthroline., *Anal. Chem.*; 36, 1961-1965.
155. Tompsett, S. L. (1934) The copper content of blood, *The Biochemical journal* 28, 1544-1549.
156. McFarlane, W. D. (1932) Application of the sodium diethyldithiocarbamate reaction to the micro-colorimetric determination of copper in organic substances, *The Biochemical journal* 26, 1022-1033.
157. Thomas Callan M.Sc., P. D., F.I.C. and J. A. Russell Henderson D.Sc. (1929) A new reagent for the colorimetric determination of minute amounts of copper, *Analyst* 54, 650 - 653.
158. George E. Cartwright, P. J. J., and Maxwell M. Wintrobe. (1945) A METHOD FOR THE DETERMINATION OF COPPER IN BLOOD SERUM, *J. Biol. Chem.* 160, 593-600.

159. Heikkila, R. E., Cabbat, F. S., and Cohen, G. (1976) In vivo inhibition of superoxide dismutase in mice by diethyldithiocarbamate, *The Journal of biological chemistry* 251, 2182-2185.
160. Sinet, P. M., Garber, P., and Jerome, H. (1982) H<sub>2</sub>O<sub>2</sub> production, modification of the glutathione status and methemoglobin formation in red blood cells exposed to diethyldithiocarbamate in vitro, *Biochemical pharmacology* 31, 521-525.
161. Kelner, M. J., and Alexander, N. M. (1986) Inhibition of erythrocyte superoxide dismutase by diethyldithiocarbamate also results in oxyhemoglobin-catalyzed glutathione depletion and methemoglobin production, *The Journal of biological chemistry* 261, 1636-1641.
162. Kobayashi, Y., Okahata, S., and Usui, T. (1979) Hemolysis of human erythrocytes by paraquat in relation to superoxide dismutase activity, *Biochemical and biophysical research communications* 91, 1288-1294.
163. Goldberg, B., and Stern, A. (1976) Superoxide anion as a mediator of drug-induced oxidative hemolysis, *The Journal of biological chemistry* 251, 6468-6470.
164. Lilley, E., and Gibson, A. (1995) Inhibition of relaxations to nitrergic stimulation of the mouse anococcygeus by duroquinone, *British journal of pharmacology* 116, 3231-3236.
165. De Man, J. G., De Winter, B. Y., Boeckxstaens, G. E., Herman, A. G., and Pelckmans, P. A. (1996) Effect of thiol modulators and Cu/Zn superoxide dismutase inhibition on nitrergic relaxations in the rat gastric fundus, *British journal of pharmacology* 119, 1022-1028.

166. al., K. e. (1991) *Jap Analyt Sci* 7, 913-917.
167. C. L. Luke, M. E. C. (1953) Determination of Impurities in Germanium and Silicon, *Anal. Chem.* 25, 1588-1593.
168. Diehl, H. a. S., G. F. *The Copper Reagents: Cuproine, neocuproine, bathocuproine, 2nd Ed.*, G.F. Smith Chemical Co; 2nd ed edition (January 1, 1972).
169. Anson, Y. L. a. F. C. (1995) Dynamics of the Coordination Equilibria in Solutions Containing Copper(II), Copper(I), and 2,9-Dimethyl-1,10-phenanthroline and Their Effect on the Reduction of O<sub>2</sub> by Cu(I), *Inorg. cChem.* 34, 1083-1089.
170. James, B. R. W., R. J. P. (1961) The Oxidation-Reduction Potentials of Some copper complexes, *J. Chem. Soc.*, 2007-2019.
171. Jour'dheuil, D., Mai, C. T., Laroux, F. S., Wink, D. A., and Grisham, M. B. (1998) The reaction of S-nitrosoglutathione with superoxide, *Biochemical and biophysical research communications* 244, 525-530.
172. Gocmen, C., Gokturk, H. S., Ertug, P. U., Onder, S., Dikmen, A., and Baysal, F. (2000) Effect of neocuproine, a selective Cu(I) chelator, on nitregric relaxations in the mouse corpus cavernosum, *European journal of pharmacology* 406, 293-300.
173. Nilsson, G. (1950) *Acta Chem. Scand.* 4, 205.
174. Rotilio, G., Calabrese, L., Bossa, F., Barra, D., Agro, A. F., and Mondovi, B. (1972) Properties of the apoprotein and role of copper and zinc in protein conformation and enzyme activity of bovine superoxide dismutase, *Biochemistry* 11, 2182-2187.

175. Diehl, H. a. S., G. F. *The Copper Reagents: Cuproine, neocuproine, bathocuproine.*, 2nd Ed ed.
176. Valentine, J. S., Pantoliano, M. W., (Ed.) (1981) *The Copper Protein*.
177. Simonian, M. A., and Nalbandian, R. M. (1975) [Preparation of electrophoretically homogeneous erythrocuprein and its thermodenaturation], *Biokhimiia* 40, 726-732.
178. Forman, H. J., and Fridovich, I. (1973) On the stability of bovine superoxide dismutase. The effects of metals, *J Biol Chem* 248, 2645-2649.
179. Rigo, A., Viglino, P., Bonori, M., Cocco, D., Calabrese, L., and Rotilio, G. (1978) The binding of copper ions to copper-free bovine superoxide dismutase. Kinetic aspects, *The Biochemical journal* 169, 277-280.
180. Rigo, A., Terenzi, M., Viglino, P., Calabrese, L., Cocco, D., and Rotilio, G. (1977) The binding of copper ions to copper-free bovine superoxide dismutase. Properties of the protein recombined with increasing amounts of copper ions, *The Biochemical journal* 161, 31-35.
181. Rigo, A., Viglino, P., Calabrese, L., Cocco, D., and Rotilio, G. (1977) The binding of copper ions to copper-free bovine superoxide dismutase. Copper distribution in protein samples recombined with less than stoichiometric copper ion/protein ratios, *The Biochemical journal* 161, 27-30.
182. Heikkila, R. E., Cabbat, F. S., and Cohen, G. (1978) Inactivation of superoxide dismutase by several thiocarbamic acid derivatives, *Experientia* 34, 1553-1554.



183. Abernethy, J. L., Steinman, H. M., and Hill, R. L. (1974) Bovine erythrocyte superoxide dismutase. Subunit structure and sequence location of the intrasubunit disulfide bond, *The Journal of biological chemistry* 249, 7339-7347.
184. St. Clair, C. S. G., Harry B.; Valentine, Joan Selverstone. (1992) Spectroelectrochemistry of copper-zinc superoxide dismutase., *Inorganic Chemistry* 31, 925-927.
185. Ciriolo, M. R., Desideri, A., Paci, M., and Rotilio, G. (1990) Reconstitution of Cu,Zn-superoxide dismutase by the Cu(I).glutathione complex, *The Journal of biological chemistry* 265, 11030-11034.
186. Takahashi, K. (1968) The reaction of phenylglyoxal with arginine residues in proteins, *J Biol Chem* 243, 6171-6179.
187. Schubert, M. P. (1935) COMBINATION OF THIOL ACIDS WITH METHYLGLYOXAL, *J Biol Chem* 111, 671-678.
188. Delomenie, C., Goodfellow, G. H., Krishnamoorthy, R., Grant, D. M., and Dupret, J. M. (1997) Study of the role of the highly conserved residues Arg9 and Arg64 in the catalytic function of human N-acetyltransferases NAT1 and NAT2 by site-directed mutagenesis, *Biochem J* 323 ( Pt 1), 207-215.
189. Boivin, D., Lin, W., and Beliveau, R. (1997) Essential arginine residues in isoprenylcysteine protein carboxyl methyltransferase, *Biochem Cell Biol* 75, 63-69.
190. Harris, M. N., Bertolucci, C. M., and Ming, L. J. (2002) Paramagnetic cobalt(II) as a probe for kinetic and NMR relaxation studies of phosphate binding and the

- catalytic mechanism of *Streptomyces* dinuclear aminopeptidase, *Inorg Chem* 41, 5582-5588.
191. Kanaani, J., Maltby, D., Somoza, J. R., and Wang, C. C. (1997) Inactivation of *Trichomonas foetus* and *Schistosoma mansoni* purine phosphoribosyltransferases by arginine-specific reagents, *Eur J Biochem* 244, 810-817.
  192. Watanabe, K., and Funatsu, G. (1986) Involvement of arginine residues in inhibition of protein synthesis by ricin A-chain, *FEBS Lett* 204, 219-222.
  193. Mizohata, E., Anwaruzzaman, M., Okuno, H., Tomizawa, K., Shigeoka, S., Kai, Y., and Yokota, A. (2003) Chemical modification of arginine alleviates the decline in activity during catalysis of spinach Rubisco, *Biochem Biophys Res Commun* 301, 591-597.
  194. Smith, E. L. (1977) Reversible blocking at arginine by cyclohexanedione, *Methods in enzymology* 47, 156-161.
  195. King, T. P. (1966) Selective chemical modification of arginyl residues, *Biochemistry* 5, 3454-3459.
  196. Yankeelov, J. A., Jr., Mitchell, C. D., and Crawford, T. H. (1968) A simple trimerization of 2,3-butanedione yielding a selective reagent for the modification of arginine in proteins, *J Am Chem Soc* 90, 1664-1666.
  197. Yankeelov, J. A., Jr., Kochert, M., Page, J. and, and Westphal, A. (1966) *Fed. Proc.* 25, 590.
  198. SHRINER, R. L., AND NEUMAN, FRED. W. (1944) THE CHEMISTRY OF THE AMIDINES, *Chem. Rev.* 35, 351-425.

199. HOFMANN, K. (1953) *The chemistry of heterocyclic compounds, imidazole and its derivatives, Part I*, Interscience Publishers, Inc., New York.
200. Riordan, J. F. (1979) Arginyl residues and anion binding sites in proteins, *Molecular and cellular biochemistry* 26, 71-92.
201. L. I. Moukhametova, R. B. A., G. Yu. Lomakina, and S. D. Varfolomeev. (2002) Properties of the Urokinase-Type Plasminogen Activator Modified with Phenylglyoxal, *Russian Journal of Bioorganic Chemistry* 28, 278-283.
202. Pierce. INSTRUCTIONS: Sulfo-NHS Acetate.
203. Thornalley, P. J. (2003) Glyoxalase I--structure, function and a critical role in the enzymatic defence against glycation, *Biochem Soc Trans* 31, 1343-1348.
204. <http://www.answers.com/topic/thioacetal>
205. Beyer, W. F., Jr., Wang, Y., and Fridovich, I. (1986) Phosphate inhibition of the copper- and zinc-containing superoxide dismutase: a reexamination, *Biochemistry* 25, 6084-6088.
206. Polticelli, F., Bottaro, G., Battistoni, A., Carri, M. T., Djinovic-Carugo, K., Bolognesi, M., O'Neill, P., Rotilio, G., and Desideri, A. (1995) Modulation of the catalytic rate of Cu,Zn superoxide dismutase in single and double mutants of conserved positively and negatively charged residues, *Biochemistry* 34, 6043-6049.
207. Creighton, T. E. (1993) *Proteins: Structure and Molecular Properties*.
208. Tsugita, A., and Scheffler, J. J. (1982) A rapid method for acid hydrolysis of protein with a mixture of trifluoroacetic acid and hydrochloric acid, *Eur J Biochem* 124, 585-588.

209. M. Kinter, N. E. S. (2001) *Protein Sequencing and Identification Using Tandem Mass Spectrometry*, Wiley-Interscience.
210. Paul, R. G., Avery, N. C., Slatter, D. A., Sims, T. J., and Bailey, A. J. (1998) Isolation and characterization of advanced glycation end products derived from the in vitro reaction of ribose and collagen, *The Biochemical journal* 330 ( Pt 3), 1241-1248.
211. Westwood, M. E., Argirov, O. K., Abordo, E. A., and Thornalley, P. J. (1997) Methylglyoxal-modified arginine residues--a signal for receptor-mediated endocytosis and degradation of proteins by monocytic THP-1 cells, *Biochimica et biophysica acta* 1356, 84-94.
212. Saraiva, M. A., Borges, C. M., and Florencio, M. H. (2006) Non-enzymatic model glycation reactions--a comprehensive study of the reactivity of a modified arginine with aldehydic and diketonic dicarbonyl compounds by electrospray mass spectrometry, *Journal of mass spectrometry* 41, 755-770.
213. Tao, L., and English, A. M. (2004) Protein S-glutathiolation triggered by decomposed S-nitrosoglutathione, *Biochemistry* 43, 4028-4038.
214. Kurahashi, T., Miyazaki, A., Suwan, S., and Isobe, M. (2001) Extensive investigations on oxidized amino acid residues in H<sub>2</sub>O<sub>2</sub>-treated Cu,Zn-SOD protein with LC-ESI-Q-TOF-MS, MS/MS for the determination of the copper-binding site, *J Am Chem Soc* 123, 9268-9278.
215. Antonella Badia, R. C., Arthur Fernandez, Fernando Battaglini, Susan R. Mikkelsen, and Ann M. English. (1993) Intramolecular electron-transfer rates in

- ferrocene-derivatized glucose oxidase, *Journal of the American Chemical Society* 115, 7053 - 7060.
216. de Beus, M. D., Chung, J., and Colon, W. (2004) Modification of cysteine 111 in Cu/Zn superoxide dismutase results in altered spectroscopic and biophysical properties, *Protein science* 13, 1347-1355.
  217. Yamasaki, R. B., Vega, A., and Feeney, R. E. (1980) Modification of available arginine residues in proteins by p-hydroxyphenylglyoxal, *Analytical biochemistry* 109, 32-40.
  218. Harris, G. W., Pickersgill, R. W., Howlin, B., and Moss, D. S. (1992) The segmented anisotropic refinement of monoclinic papain by the application of the rigid-body TLS model and comparison to bovine ribonuclease A, *Acta crystallographica* 48 ( Pt 1), 67-75.
  219. McRee, D. E., Redford, S. M., Getzoff, E. D., Lepock, J. R., Hallewell, R. A., and Tainer, J. A. (1990) Changes in crystallographic structure and thermostability of a Cu,Zn superoxide dismutase mutant resulting from the removal of a buried cysteine, *J Biol Chem* 265, 14234-14241.
  220. Polevoda, B., and Sherman, F. (2000) Nalpha -terminal acetylation of eukaryotic proteins, *The Journal of biological chemistry* 275, 36479-36482.
  221. Driessen, H. P., de Jong, W. W., Tesser, G. I., and Bloemendal, H. (1985) The mechanism of N-terminal acetylation of proteins, *CRC critical reviews in biochemistry* 18, 281-325.
  222. Kendall, R. L., Yamada, R., and Bradshaw, R. A. (1990) Cotranslational amino-terminal processing, *Methods in enzymology* 185, 398-407.

223. Wold, F. (1981) In vivo chemical modification of proteins (post-translational modification), *Annual review of biochemistry* 50, 783-814.
224. Fields, H. B. F. D. a. R. (1972) Specific modification of NH<sub>2</sub>-terminal residues by transamination, *Methods in Enzymology, Part B: Enzyme Structure* 25, 409-419.
225. Ye, M., and English, A. M. (2006) Binding of polyaminocarboxylate chelators to the active-site copper inhibits the GSNO-reductase activity but not the superoxide dismutase activity of Cu,Zn-superoxide dismutase, *Biochemistry* 45, 12723-12732.
226. Alfred R. Fratzke, P. J. R. (1986) Thermodynamic and kinetic analysis of the dimerization of aqueous glyoxal, *International Journal of Chemical Kinetics* 18, 775-789.
227. <http://www.inchem.org/documents/sids/sids/107222.pdf>
228. <http://pubchem.ncbi.nlm.nih.gov/summary/summary.cgi?cid=92988>
229. Bannister, J. V., Bannister, W. H., and Rotilio, G. (1987) Aspects of the structure, function, and applications of superoxide dismutase, *CRC Crit Rev Biochem* 22, 111-180.
230. Rotilio, G., Morpurgo, L., Giovagnoli, C., Calabrese, L., and Mondovi, B. (1972) Studies of the metal sites of copper proteins. Symmetry of copper in bovine superoxide dismutase and its functional significance, *Biochemistry* 11, 2187-2192.
231. Lepock, J. R., Arnold, L. D., Torrie, B. H., Andrews, B., and Kruuv, J. (1985) Structural analyses of various Cu<sup>2+</sup>, Zn<sup>2+</sup>-superoxide dismutases by differential

- scanning calorimetry and Raman spectroscopy, *Archives of biochemistry and biophysics* 241, 243-251.
232. Roe, J. A., Butler, A., Scholler, D. M., Valentine, J. S., Marky, L., and Breslauer, K. J. (1988) Differential scanning calorimetry of Cu,Zn-superoxide dismutase, the apoprotein, and its zinc-substituted derivatives, *Biochemistry* 27, 950-958.
  233. Steinman, H. M., Naik, V. R., Abernethy, J. L., and Hill, R. L. (1974) Bovine erythrocyte superoxide dismutase. Complete amino acid sequence, *The Journal of biological chemistry* 249, 7326-7338.
  234. McCord, J. M., and Day, E. D., Jr. (1978) Superoxide-dependent production of hydroxyl radical catalyzed by iron-EDTA complex, *FEBS Lett* 86, 139-142.
  235. Borders, C. L., Jr., and Johansen, J. T. (1980) Identification of Arg-143 as the essential arginyl residue in yeast Cu,Zn superoxide dismutase by use of a chromophoric arginine reagent, *Biochemical and biophysical research communications* 96, 1071-1078.
  236. Borders, C. L., Jr., Saunders, J. E., Blech, D. M., and Fridovich, I. (1985) Essentiality of the active-site arginine residue for the normal catalytic activity of Cu,Zn superoxide dismutase, *The Biochemical journal* 230, 771-776.
  237. Lucia Banci, I. B., Claudio Luchinat, and Robert A. Hallewell. (1988) An investigation of superoxide dismutase Lys-143, Ile-143, and Glu-143 mutants: Cu<sub>2</sub>Co<sub>2</sub>SOD derivatives, *J. Am. Chem. SOC.* 110, 3629-3633.
  238. Ciriolo, M. R., Battistoni, A., Falconi, M., Filomeni, G., and Rotilio, G. (2001) Role of the electrostatic loop of Cu,Zn superoxide dismutase in the copper uptake process, *Eur J Biochem* 268, 737-742.

- intermediacy of tryptophan-derived oxidation products, *The Journal of biological chemistry* 278, 24078-24089.
252. Heikkila, R. E., and Cabbat, F. (1976) A sensitive assay for superoxide dismutase based on the autoxidation of 6-hydroxydopamine, *Analytical biochemistry* 75, 356-362.
  253. Nishida, C. R., Gralla, E. B., and Valentine, J. S. (1994) Characterization of three yeast copper-zinc superoxide dismutase mutants analogous to those coded for in familial amyotrophic lateral sclerosis, *Proceedings of the National Academy of Sciences of the United States of America* 91, 9906-9910.
  254. Hart, P. J., Balbirnie, M. M., Ogihara, N. L., Nersissian, A. M., Weiss, M. S., Valentine, J. S., and Eisenberg, D. (1999) A structure-based mechanism for copper-zinc superoxide dismutase, *Biochemistry* 38, 2167-2178.
  255. Shi Huijuan, F. L., Chen Changhua. (1999) Cloning, expressing, Fermentation and purification of human copper/zinc-superoxide dismutase cDNA, *CHINESE PHARMACEUTICAL JOURNAL* 34, 340-342.
  256. Lyons, T. J., Liu, H., Goto, J. J., Nersissian, A., Roe, J. A., Graden, J. A., Cafe, C., Ellerby, L. M., Bredesen, D. E., Gralla, E. B., and Valentine, J. S. (1996) Mutations in copper-zinc superoxide dismutase that cause amyotrophic lateral sclerosis alter the zinc binding site and the redox behavior of the protein, *Proc Natl Acad Sci U S A* 93, 12240-12244.
  257. Novagen. pET System Manual, 11 ed.
  258. Retallack, D. M., Schneider, J. C., Mitchell, J., Chew, L., and Liu, H. (2007) Transport of heterologous proteins to the periplasmic space of *Pseudomonas*



- fluorescens using a variety of native signal sequences, *Biotechnology letters* 29, 1483-1491.
259. Sonveaux, P., Kaz, A. M., Snyder, S. A., Richardson, R. A., Cardenas-Navia, L. I., Braun, R. D., Pawloski, J. R., Tozer, G. M., Bonaventura, J., McMahon, T. J., Stamler, J. S., and Dewhirst, M. W. (2005) Oxygen regulation of tumor perfusion by S-nitrosohemoglobin reveals a pressor activity of nitric oxide, *Circ Res* 96, 1119-1126.
  260. Nakai, K., Sakuma, I., Togashi, H., Yoshioka, M., Sugawara, T., Satoh, H., and Kitabatake, A. (2003) S-nitrosylated polyethylene glycol-conjugated hemoglobin derivative as a candidate material for oxygen therapeutics, *Advances in experimental medicine and biology* 519, 207-216.
  261. Doyle, M. P., and Hoekstra, J. W. (1981) Oxidation of nitrogen oxides by bound dioxygen in hemoproteins, *Journal of inorganic biochemistry* 14, 351-358.
  262. Cassoly, R., and Gibson, Q. (1975) Conformation, co-operativity and ligand binding in human hemoglobin, *Journal of molecular biology* 91, 301-313.
  263. Ferranti, P., Malorni, A., Mamone, G., Sannolo, N., and Marino, G. (1997) Characterisation of S-nitrosohaemoglobin by mass spectrometry, *FEBS letters* 400, 19-24.
  264. Romeo, A. A., Filosa, A., Capobianco, J. A., and English, A. M. (2001) Metal chelators inhibit S-nitrosation of Cys beta 93 in oxyhemoglobin, *J Am Chem Soc* 123, 1782-1783.

239. Basch, R. O. a. H. (1984) On the Mechanism of Action of Superoxide Dismutase: A Theoretical Study, *J. Am. Chem. Soc.* 106, 5710-5714.
240. M. Rosi, A. S., F. Tarantelli, I. Bertini, and C. Luchinat. (1986) Ab initio calculations of the copper(2+)-O<sub>2</sub><sup>-</sup> interaction as a model for the mechanism of copper/zinc superoxide dismutase, *Inorg. Chem.* 25, 1005-1008.
241. M. Rosi, A. S. a. F. T. B. a. C. L. (1985) A theoretical investigation of the copper-super-oxide system. A model for the mechanism of copper-zinc superoxide dismutase, *Inorganica Chimica Acta* 107, L21-L22.
242. Hill, J. E., Myers, A. M., Koerner, T. J., and Tzagoloff, A. (1986) Yeast/E. coli shuttle vectors with multiple unique restriction sites, *Yeast (Chichester, England)* 2, 163-167.
243. Rabizadeh, S., Gralla, E. B., Borchelt, D. R., Gwinn, R., Valentine, J. S., Sisodia, S., Wong, P., Lee, M., Hahn, H., and Bredesen, D. E. (1995) Mutations associated with amyotrophic lateral sclerosis convert superoxide dismutase from an antiapoptotic gene to a proapoptotic gene: studies in yeast and neural cells, *Proceedings of the National Academy of Sciences of the United States of America* 92, 3024-3028.
244. Gietz, R. D. a. R. A. W. (2002) TRANSFORMATION OF YEAST BY THE Liac/SS CARRIER DNA/PEG METHOD., *Methods in Enzymology* 350, 87-96.
245. Hough, M. A., Grossmann, J. G., Antonyuk, S. V., Strange, R. W., Doucette, P. A., Rodriguez, J. A., Whitson, L. J., Hart, P. J., Hayward, L. J., Valentine, J. S., and Hasnain, S. S. (2004) Dimer destabilization in superoxide dismutase may result in disease-causing properties: structures of motor neuron disease mutants,

*Proceedings of the National Academy of Sciences of the United States of America* 101, 5976-5981.

246. Thulin, E., and Linse, S. (1999) Expression and purification of human calbindin D28k, *Protein expression and purification* 15, 265-270.
247. Hayward, L. J., Rodriguez, J. A., Kim, J. W., Tiwari, A., Goto, J. J., Cabelli, D. E., Valentine, J. S., and Brown, R. H., Jr. (2002) Decreased metallation and activity in subsets of mutant superoxide dismutases associated with familial amyotrophic lateral sclerosis, *The Journal of biological chemistry* 277, 15923-15931.
248. Yoo, H. Y., Kim, S. S., and Rho, H. M. (1999) Overexpression and simple purification of human superoxide dismutase (SOD1) in yeast and its resistance to oxidative stress, *Journal of biotechnology* 68, 29-35.
249. Hartman, J. R., Geller, T., Yavin, Z., Bartfeld, D., Kanner, D., Aviv, H., and Gorecki, M. (1986) High-level expression of enzymatically active human Cu/Zn superoxide dismutase in Escherichia coli, *Proceedings of the National Academy of Sciences of the United States of America* 83, 7142-7146.
250. Francis, J. W., Hosler, B. A., Brown, R. H., Jr., and Fishman, P. S. (1995) CuZn superoxide dismutase (SOD-1):tetanus toxin fragment C hybrid protein for targeted delivery of SOD-1 to neuronal cells, *The Journal of biological chemistry* 270, 15434-15442.
251. Zhang, H., Andrekopoulos, C., Joseph, J., Chandran, K., Karoui, H., Crow, J. P., and Kalyanaraman, B. (2003) Bicarbonate-dependent peroxidase activity of human Cu,Zn-superoxide dismutase induces covalent aggregation of protein:

265. Chan, N. L., Kavanaugh, J. S., Rogers, P. H., and Arnone, A. (2004) Crystallographic analysis of the interaction of nitric oxide with quaternary-T human hemoglobin, *Biochemistry* 43, 118-132.
266. Datta, B., Tufnell-Barrett, T., Bleasdale, R. A., Jones, C. J., Beeton, I., Paul, V., Frenneaux, M., and James, P. (2004) Red blood cell nitric oxide as an endocrine vasoregulator: a potential role in congestive heart failure, *Circulation* 109, 1339-1342.
267. Doctor, A., Platt, R., Sheram, M. L., Eischeid, A., McMahon, T., Maxey, T., Doherty, J., Axelrod, M., Kline, J., Gurka, M., Gow, A., and Gaston, B. (2005) Hemoglobin conformation couples erythrocyte S-nitrosothiol content to O<sub>2</sub> gradients, *Proceedings of the National Academy of Sciences of the United States of America* 102, 5709-5714.
268. Funai, E. F., Davidson, A., Seligman, S. P., and Finlay, T. H. (1997) S-nitrosohemoglobin in the fetal circulation may represent a cycle for blood pressure regulation, *Biochemical and biophysical research communications* 239, 875-877.
269. Rassaf, T., Bryan, N. S., Maloney, R. E., Specian, V., Kelm, M., Kalyanaraman, B., Rodriguez, J., and Feelisch, M. (2003) NO adducts in mammalian red blood cells: too much or too little?, *Nature medicine* 9, 481-482; author reply 482-483.
270. McMahon, T. J., Pawloski, J. R., Hess, D. T., Piantadosi, C. A., Luchsinger, B. P., Singel, D. J., and Stamler, J. S. (2003) S-nitrosohemoglobin is distinguished from other nitrovasodilators by unique oxygen-dependent responses that support an allosteric mechanism of action, *Blood* 102, 410-411; author reply 412-413.

271. Miranda, J. J. (2000) Highly reactive cysteine residues in rodent hemoglobins, *Biochemical and biophysical research communications* 275, 517-523.
272. Ferranti, P., Carbone, V., Sannolo, N., Fiume, I., and Malorni, A. (1993) Mass spectrometric analysis of rat hemoglobin by FAB-overlapping. Primary structure of the alpha-major and of four beta constitutive chains, *The International journal of biochemistry* 25, 1943-1950.
273. Rossi, R., Milzani, A., Dalle-Donne, I., Giannerini, F., Giustarini, D., Lusini, L., Colombo, R., and Di Simplicio, P. (2001) Different metabolizing ability of thiol reactants in human and rat blood: biochemical and pharmacological implications, *The Journal of biological chemistry* 276, 7004-7010.
274. Coletta, M., Angeletti, M., Ascone, I., Boumis, G., Castellano, A. C., Dell'Araccia, M., Della Longa, S., De Sanctis, G., Priori, A. M., Santucci, R., Feis, A., and Amiconi, G. (1999) Heterotropic effectors exert more significant strain on monoligated than on unligated hemoglobin, *Biophysical journal* 76, 1532-1536.
275. <http://www.sigmaaldrich.com/sigma/datasheet/d5941dat.pdf>.
276. Ellman, G. L. (1959) Tissue sulfhydryl groups, *Archives of biochemistry and biophysics* 82, 70-77.
277. A., H. A. F. S. (1972) *Methods in Enzymology* 25, 457-464.
278. Saville, B. (1958) A scheme for the colorimetric determination of microgram amounts of thiols, *Analyst* (993), 670-672.
279. Zhang, Y. Y., Xu, A. M., Nomen, M., Walsh, M., Keaney, J. F., Jr., and Loscalzo, J. (1996) Nitrosation of tryptophan residue(s) in serum albumin and model

- dipeptides. Biochemical characterization and bioactivity, *The Journal of biological chemistry* 271, 14271-14279.
280. Amiconi, G. A., Eraldo; Brunori, Maurizio; Nason, Alvin; Wyman, Jeffries. (1971) Functional Properties of Human Hemoglobin Treated with 5, 5'-Dithiobis, 3,3'-Nitrobenzoic Acid, *European Journal of Biochemistry* 22, 321-326.
  281. Condo, S. G., Giardina, B., Barra, D., Gill, S. J., and Brunori, M. (1981) Purification and functional properties of the hemoglobin components from the rat (Wistar), *European journal of biochemistry / FEBS* 116, 243-247.
  282. Garrick, L. M., Sloan, R. L., Ryan, T. W., Klonowski, T. J., and Garrick, M. D. (1978) Primary structure of the major beta-chain of rat haemoglobins, *The Biochemical journal* 173, 321-330.
  283. Garrick, L. M., Sharma, V. S., McDonald, M. J., and Ranney, H. M. (1975) Rat haemoglobin heterogeneity. Two structurally distinct alpha chains and functional behaviour of selected components, *The Biochemical journal* 149, 245-258.
  284. Stein, S., Cherian, M. G., and Mazur, A. (1971) Preparation and properties of six rat hemoglobins. Nonuniform biosynthesis in marrow erythroid cells, *The Journal of biological chemistry* 246, 5287-5293.
  285. Datta, M. C., and Gilman, J. G. (1981) Rat hemoglobin heterogeneity: postnatal changes in proportions of multiple components and effects of erythropoietin on marrow cell cultures, *Hemoglobin* 5, 701-714.
  286. Chua, C. G., Carrell, R. W., and Howard, B. H. (1975) The amino acid sequence of the alpha chain of the major haemoglobin of the rat (*Rattus norvegicus*), *The Biochemical journal* 149, 259-269.

287. Kosower, N. S., Kosower, E. M., and Koppel, R. L. (1977) Sensitivity of hemoglobin thiol groups within red blood cells of rat during oxidation of glutathione, *European journal of biochemistry / FEBS* 77, 529-534.
288. John C. L. Erve, O. N. J., Holly S. Valentine, Venkataraman Amarnath, and William M. Valentine. (2000) Disulfiram Generates a Stable N,N-Diethylcarbamoyl Adduct on Cys-125 of Rat Hemoglobin b-Chains in Vivo, *Chem. Res. Toxicol.* 13, 237-244.
289. Di Simplicio, P., Lupis, E., and Rossi, R. (1996) Different mechanisms of formation of glutathione-protein mixed disulfides of diamide and tert-butyl hydroperoxide in rat blood, *Biochimica et biophysica acta* 1289, 252-260.
290. Chiancone, E., Currell, D. L., Vecchini, P., Antonini, E., and Wyman, J. (1970) Kinetics of the reaction of the "masked" and "free" sulfhydryl groups of human hemoglobin with p-mercuribenzoate, *The Journal of biological chemistry* 245, 4105-4111.
291. D. Jonathan Barnett, A. R. a. D. L. H. W. (1995) NO-Group transfer (transnitrosation) between S-nitrosothiols and thiols. Part 2, *J. Chem. Soc., Perkin Trans. 2*, 1279 - 1282.
292. Scharfstein, J. S., Keaney, J. F., Jr., Slivka, A., Welch, G. N., Vita, J. A., Stamler, J. S., and Loscalzo, J. (1994) In vivo transfer of nitric oxide between a plasma protein-bound reservoir and low molecular weight thiols, *The Journal of clinical investigation* 94, 1432-1439.

293. Park, J. W., Billman, G. E., and Means, G. E. (1993) Transnitrosation as a predominant mechanism in the hypotensive effect of S-nitrosoglutathione, *Biochemistry and molecular biology international* 30, 885-891.
294. Stamler, J. S., Simon, D. I., Jaraki, O., Osborne, J. A., Francis, S., Mullins, M., Singel, D., and Loscalzo, J. (1992) S-nitrosylation of tissue-type plasminogen activator confers vasodilatory and antiplatelet properties on the enzyme, *Proceedings of the National Academy of Sciences of the United States of America* 89, 8087-8091.
295. Ji, Y., Akerboom, T. P., Sies, H., and Thomas, J. A. (1999) S-nitrosylation and S-glutathiolation of protein sulfhydryls by S-nitroso glutathione, *Archives of biochemistry and biophysics* 362, 67-78.
296. Taylor, C. E. L. a. W. V. (1968) Determination of trace copper in petroleum middle distillates with cuprizone, *Analytical Chemistry* 40, 2196-2197.
297. Rosen, D. R., Siddique, T., Patterson, D., Figlewicz, D. A., Sapp, P., Hentati, A., Donaldson, D., Goto, J., O'Regan, J. P., Deng, H. X., and et al. (1993) Mutations in Cu/Zn superoxide dismutase gene are associated with familial amyotrophic lateral sclerosis, *Nature* 362, 59-62.
298. Rowland, L. P., and Shneider, N. A. (2001) Amyotrophic lateral sclerosis, *The New England journal of medicine* 344, 1688-1700.
299. Schonhoff, C. M., Matsuoka, M., Tummala, H., Johnson, M. A., Estevez, A. G., Wu, R., Kamaid, A., Ricart, K. C., Hashimoto, Y., Gaston, B., Macdonald, T. L., Xu, Z., and Mannick, J. B. (2006) S-nitrosothiol depletion in amyotrophic lateral



sclerosis, *Proceedings of the National Academy of Sciences of the United States of America* 103, 2404-2409.

300. Weiss, G., Loyevsky, M., and Gordeuk, V. R. (1999) Dexrazoxane (ICRF-187), *General pharmacology* 32, 155-158.
301. Bunn H. F., F. B. G., and Ranney H. M. (1977) *Human Hemoglobins*, W. B. Saunders Company.